

École Doctorale “Sciences fondamentales et appliquées”
et



UNIVERSITÀ DEGLI STUDI DI GENOVA
FACOLTÀ DI SCIENZE M.F.N.
Dipartimento di Fisica

THÈSE

Présentée pour obtenir le titre de

Docteur en SCIENCES

Spécialité: Physique
par

Alberto Puliafito

Dynamics and statistics of single polymer and polymer solutions

Soutenue publiquement le 10 juillet 2006 devant le jury composé de:

A. Celani	<i>Directeur</i>
A. Mazzino	<i>Co-directeur</i>
C. M. Casciola	<i>Rapporteur</i>
H. Kellay	<i>Rapporteur</i>
R. Rolandi	<i>Examineur</i>
O. Cadot	<i>Examineur</i>
V. Steinberg	<i>Invité</i>
N. Zanghí	<i>Invité</i>
A. Pumir	<i>Invité</i>



TESI

presentata per il conseguimento del titolo di
Dottore di Ricerca in Fisica

da

Alberto Puliafito

Dynamics and statistics of single polymer and polymer solutions

Discussa di fronte alla commissione composta da:

A. Celani	<i>Direttore</i>
A. Mazzino	<i>Co-direttore</i>
C. M. Casciola	<i>Lettore esterno</i>
H. Kellay	<i>Lettore esterno</i>
R. Rolandi	<i>Commissario</i>
O. Cadot	<i>Commissario</i>
V. Steinberg	<i>Invitato</i>
N. Zanghì	<i>Invitato</i>
A. Pumir	<i>Invitato</i>

to my families

Acknowledgments

I must first express my heartfelt gratitude towards my advisor, Antonio Celani. His leadership, support, attention to detail, hard work, and scholarship have set an example I hope to match some day. His patience and endless supply have helped me in entering the world of research.

I would like to express my sincere thanks to my co-advisor Andrea Mazzino for sharing his passion for research and for advising me whenever I needed it.

I am sincerely grateful to the members of the committee, and in particular to Carlo Casciola and Hamid Kellay for their careful revision of the thesis, and to Olivier Cadot and Ranieri Rolandi for coming all the way from to serve as my external examiners. Special thanks must be addressed to Alain Pumir and Nino Zanghi for their support and interest in my work.

I am deeply grateful to Victor Steinberg and Misha Chertkov for their valuable advice and support, and for the high quality science they proposed me.

I would like to thank the many colleagues I have worked with: Andrea Bistagnino, Konstantin Turitsyn, Massimo Vergassola, and Dario Vincenzi who helped and supported me in many difficult moments.

I would like to especially thank Augusto Destrero, Benedetta Montanari, Matteo Noceti, Agnese Seminara, Alberto Sorrentino and Andrea Vassallo for their precious esteem and friendship, and I am grateful to Julien Barré and Magali Ribot for their support and sincere affection.

Finally, I thank my parents and my sister Elisa for instilling in me confidence and a drive for pursuing my PhD, and for the one who has made the many hours spent in my office (and in my car between Nice and Genoa) seem worthwhile after all, Federica.

Abstract

Résumé

Cette thèse regroupe des travaux numériques et théoriques s'inscrivant dans le cadre général de la dynamique des polymères en écoulement. La première partie est dédiée à l'étude de la dynamique de molécules isolées dans des écoulements, situation d'intérêt pour la rhéologie et la biophysique. Le mouvement individuel d'une molécule a été analysé en détail grâce à des méthodes stochastiques et à de nouveaux algorithmes numériques. Ces études ont permis d'obtenir les distributions de probabilité de l'élongation et de l'orientation des molécules et de caractériser les temps dynamiques du système dans des écoulements laminaires et aléatoires.

La deuxième partie de la thèse porte sur les solutions diluées de polymères, qui jouent un rôle essentiel dans les applications industrielles et pour l'étude de la dynamique des fluides complexes en général. La stabilité de l'écoulement de Kolmogorov viscoélastique a été étudiée à l'aide d'une approche perturbative multi-échelles. On a ainsi montré que les polymères peuvent stabiliser l'écoulement mais aussi générer des instabilités purement élastiques. L'état turbulent correspondant a été analysé par des simulations numériques, qui mettent en évidence les différences entre les cas viscoélastique et newtonien.

Sinossi

Questa tesi contiene uno studio teorico e numerico della dinamica di polimeri in flussi. La prima parte è dedicata allo studio del moto di un singolo polimero in flussi esterni, argomento di interesse nella caratterizzazione delle proprietà meccaniche di biomolecole e in reologia. Il moto di una singola molecola e le quantità statistiche relative sono state analizzate in dettaglio grazie a metodi stocastici e a nuovi algoritmi numerici. Tali strumenti permettono di accedere alla distribuzione di probabilità della lunghezza e dell'orientamento della molecola e di studiare i tempi dinamici del problema in flussi laminari e aleatori.

Nella seconda parte della tesi affronterò il problema della dinamica di soluzioni diluite di polimeri, tematica di grande interesse per le sue applicazioni industriali nonché nello studio della meccanica di fluidi complessi in generale. Ho studiato la stabilità del flusso di

Kolmogorov di una soluzione polimerica con metodi perturbativi a scale multiple. La presenza di polimeri può aumentare la stabilità, ma può dare anche luogo a instabilità di tipo puramente elastico. Ho analizzato il corrispondente regime turbolento per mezzo di simulazioni numeriche, che mettono in evidenza come tale stato sia differente dal caso newtoniano.

Abstract

This thesis encompasses numerical and theoretical work within the general framework of polymers in fluid flows. The first part concerns the study of single polymer dynamics and statistics, a subject of interest in the research on mechanical properties of biomolecules and in rheology. By means of stochastic methods and of new numerical algorithms the motion of a single molecule in an external flow has been analyzed in detail, and its statistics has been studied. In particular the probability distribution functions of extension and orientation of the molecule, as well as the dynamical timescales of the system, can be derived both in laminar and random flows.

The second part of the thesis refers to the dynamics of dilute polymer solutions which appears in technological and industrial applications as well as in complex fluid dynamics. The stability properties of a polymer solution in a Kolmogorov flow have been inferred by means of multiple-scale perturbation techniques. The presence of polymers results in a stabilization of the flow, but can also generate purely elastic instabilities. The corresponding turbulent dynamics is analyzed via direct numerical simulations, and the viscoelastic and the Newtonian cases are compared.

Publications list

Published or submitted papers related to the thesis

Part I

- p. 45 A. Celani, A. Puliafito and K. Turitsyn, *Polymers in linear shear flow: a numerical study*, Europhys. Lett., **70**, 464, (2005)
- p. 52 A. Puliafito and K. Turitsyn, *Numerical study of polymer tumbling in linear shear flows*, Physica D, **211**, 9, (2005)
- p. 77 A. Celani, A. Puliafito, D. Vincenzi, *Dynamical slowdown of polymers in laminar and random flows*, submitted to Phys. Rev. Lett., (2006)

Part II

- p. 115 G. Boffetta, A. Celani, A. Mazzino, A. Puliafito and M. Vergassola, *The viscoelastic Kolmogorov flow: eddy viscosity and stability analysis*, J. Fluid Mech., **523**, 161-170, (2005)
- p. 133 A. Bistagnino, A. Boffetta, A. Celani, A. Mazzino, A. Puliafito and M. Vergassola, *Nonlinear stability analysis of the viscoelastic Kolmogorov flow*, submitted to J. Fluid Mech., (2006)
- p. 167 G. Boffetta, A. Celani, A. Mazzino and A. Puliafito, *Drag reduction without boundaries: the viscoelastic turbulent Kolmogorov flow*, Advances in Turbulence X, pp. 649–652, (2004)

In preparation

1. M. Chertkov, A. Puliafito and K. Turitsyn, *Statistics of work done by flow on a polymer*, in preparation, (2006)
2. M. Chertkov, A. Puliafito and K. Turitsyn, *Lyapunov spectrum in time irreversible flows*, in preparation, (2006)
3. A. Celani, A. Puliafito and K. Turitsyn, *Shape dynamics of polymers in linear shear flow*, in preparation, (2006)

Contents

Abstract	i
Français	i
Italiano	i
English	i
Publications list	iii
Polymer dynamics in fluid flows: from single molecules to complex fluids	ix
I Single polymer dynamics and statistics	1
Introduction	3
1 Single polymer dynamics in fluid flows	5
1.1 Coil-stretch transition in elongational flows	5
1.2 Hysteresis in elongational flows	8
1.3 Shape dynamics and tumbling in shear flows	10
1.4 Single polymer dynamics in random flows	12
2 Polymer models	17
2.1 The freely jointed chain	18
2.2 Excluded-volume effects	20
2.3 The Rouse and Zimm models	21
2.4 The dumbbell model	24
2.4.1 Nonlinear elasticity	26
2.5 PDF for the polymer extension	26
3 Tumbling dynamics in shear flows	29
3.1 Tumbling dynamics in laminar shear flows	30
3.1.1 Elongation statistics	31

3.1.2	Orientation statistics	33
3.1.3	Tumbling statistics	35
3.1.4	Comparison with experimental data	36
3.2	Tumbling in shear flows with weak superposed velocity fluctuations	38
3.2.1	Orientation statistics	40
3.2.2	Elongation statistics	41
3.2.3	Tumbling dynamics	42
3.3	Perspectives	44
	Paper: <i>Polymers in a linear shear flow: A numerical study</i> .	45
	Paper: <i>Numerical study of polymer tumbling in linear shear flows</i>	53
4	Relaxation and conformation dynamics in elongational and random flows	67
4.1	Relaxation dynamics in external flows	68
4.2	Shape effects on relaxation dynamics	68
4.3	Dynamical slowdown in random and elongational flows	70
4.4	Perspectives	76
	Paper: <i>Dynamical slowdown of polymers in laminar and random flows</i>	77
	Bibliography to Part I	84
II	Dynamics of dilute polymer solutions	85
	Introduction	87
5	Dynamics of polymer solutions	89
5.1	Flow stability analysis	89
5.1.1	The Newtonian case	89
5.1.2	The viscoelastic case	92
5.2	Elastic turbulence	93
5.3	The drag reduction phenomenon	95
6	Viscoelastic fluid models	97
6.1	Constitutive equations for viscoelastic fluids	97
6.1.1	The Maxwell model	99
6.1.2	The Oldroyd-B model	100
6.1.3	The Giesekus model	101
6.2	From the dumbbell to the constitutive equation	102

6.2.1	Evolution equations for the Oldroyd-B model	103
6.2.2	The FENE-P models	104
7	Linear stability analysis of the viscoelastic Kolmogorov flow	105
7.1	The Newtonian case	106
7.2	The viscoelastic case	109
7.3	The validity of the scale separation hypothesis	111
7.4	Generalization to finite Schmidt numbers	112
7.5	Perspectives	114
	Paper: <i>The viscoelastic Kolmogorov flow: eddy viscosity and linear stability</i>	115
8	Nonlinear stability analysis of the viscoelastic Kolmogorov flow	125
8.1	Weakly nonlinear analysis: the standard Cahn-Hilliard dynamics	126
8.2	A novel Cahn-Hilliard dynamics	129
8.3	Numerical simulations	131
8.4	Perspectives	132
	Paper: <i>Nonlinear dynamics of the viscoelastic Kolmogorov flow</i>	133
9	The viscoelastic turbulent Kolmogorov flow	159
9.1	The Newtonian case	159
9.2	The viscoelastic case	161
9.2.1	Oldroyd-B model	161
9.2.2	Uniaxial model	163
9.3	Perspectives	166
	Paper: <i>Drag reduction without boundaries: the viscoelastic turbulent Kolmogorov flow</i>	167
	Bibliography to Part II	176

Polymer dynamics in fluid flows: from single molecules to complex fluids

Polymers are molecules of high molecular mass, structurally composed by repeated units derived from molecules of low relative molecular mass. There are both natural and synthetic polymers: among naturally occurring polymers are DNA, proteins, starches, cellulose, and latex. Synthetic polymers are produced commercially on a very large scale and have a wide range of properties and uses. For example the materials commonly called plastics are all synthetic polymers.

Polymers are formed by chemical reactions where the repeating units, called monomers, are joined sequentially, forming a chain. In many polymers, only one type of monomer is used. In others, two or three different monomers may be combined.

Natural polymers began to be chemically modified during the 18th century to produce many materials. The first industrial use goes back to the first half of the 19th century: in 1834 Ludersdorf and Hayward discovered that adding sulfur to raw rubber helped preventing the rubber from becoming sticky. In 1839 Goodyear accidentally dropped a mixture of rubber latex, sulfur, and white lead on a hot stove-top. The result was a rubber that was more resistant to temperature extremes. Goodyear named the process vulcanization, and vulcanized rubber became the wonder material of the 1800s. The first theories on polymer aggregates appear at the end of 19th century but most of the knowledge about polymers has been gleaned during the past century.

In this thesis I will present the research I performed during

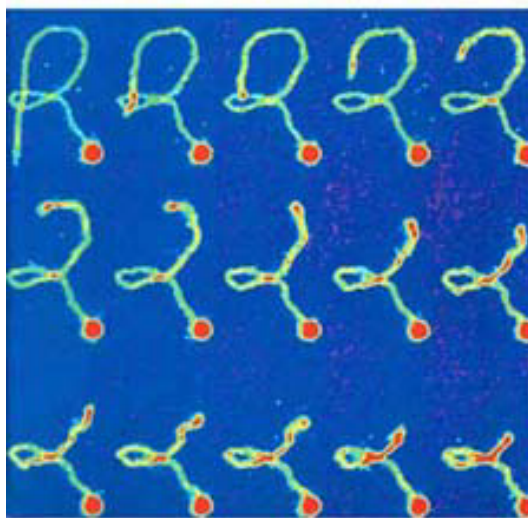


Figure 1: In this experiment by Chu and coworkers [1] a bead is attached to one end of a single DNA molecule and is pulled to form different pathways. The snapshots of the molecule are obtained by fluorescence microscopy.

my PhD. The thesis is subdivided into two parts, introduced hereafter. Each part aims at introducing the fundamental concepts and models, and at reporting the results I obtained. Chapters are followed by the corresponding research articles.

Each part, including the introduction, has its own bibliography.

Part I: Single polymer dynamics and statistics

Until about fifteen years ago, measurements of polymer properties were taken in 'bulk' experiments. Typically, macroscopic properties of a solution were measured and the result was connected with properties of single molecules. Thanks to the extraordinary technological progresses and to the development of novel experimental techniques it is nowadays possible to have direct access to microscopic observables, such as extension, orientation or conformation of a single molecule. In particular, a macromolecule can be directly manipulated and its mechanical properties can be studied in great detail (see for example figs. 1 and 2). Furthermore, by means of fluorescence microscopy, also the dynamics of a single polymer can be tracked in time and analyzed directly.

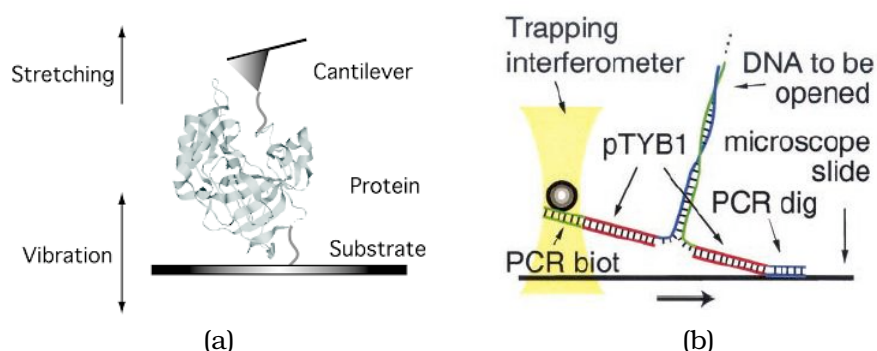
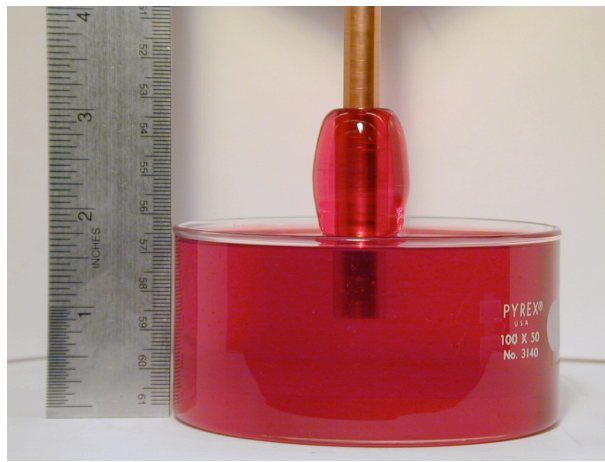


Figure 2: (a) A sketch of an experiment where a protein is stretched by an atomic force microscopy. The cantilever of the microscope is attached to one end of the molecule, and its other end is attached to the substrate. Mechanical properties of the molecule can be determined by measuring the deviation of the cantilever or by inducing vibrations of the substrate. (b) In this experiment, a double stranded DNA is unzipped. One end of the molecule is pulled by interferometric techniques. In this way the forces in molecular reactions where DNA opens its strands can be measured in detail.

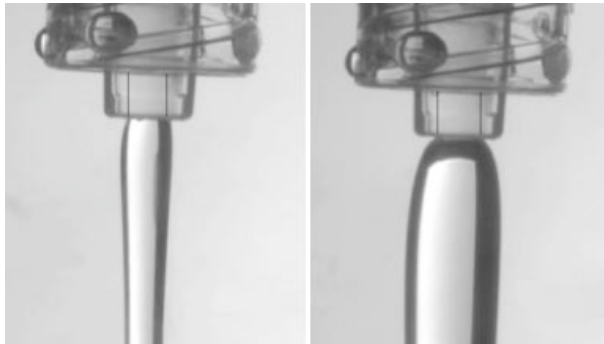
A large number of experiments have been performed in the past decade to exploit the accessibility of the microscopic properties of these macromolecules (including very important biomolecules such as DNA). As a result many of the theoretical polymer models proposed in the past fifty years have been verified and refined. Phenomenological models predicting elasticity of macromolecules have been confirmed by some very nice experiments between 1991 and 1997 (see ref. [2] and references therein).

Due to the applicability of these techniques to biomolecules, many experiments have been performed to investigate the forces involving DNA in biological reaction or the variation of mechanical properties of DNA-protein complexes (see ref. [2] and references therein).

Finally, numerous efforts have been devoted to the detailed analysis of the motion of macromolecules in fluid flows. These experiments have a twofold aim: they attempt on the one hand to refine the accepted polymer models and to identify the fundamental elasticity-related physical mechanisms (see for example [3] for a recent review), and on the other hand to study the complicated dynamics of a polymer in external velocity fields such as conformation hysteresis in elongational flows [4, 5], coil-stretch transition in deterministic and turbulent flows [6, 7], tumbling dynamics in shear flows [8–10].



(a)



(b)

Figure 3: (a) The Weissenberg effect. (b) The die swell effect: on the left the Newtonian case and on the right the viscoelastic case. Pictures taken from web.mit.edu.

This first part of the thesis is dedicated to new results in single polymer dynamics: I will give a brief description of the phenomenology of single polymers dynamics in external flows, introduce a few widely accepted models and show how, in spite of their simplicity, they can be very useful to understand the basic physics of single polymer motion in external flows.

Part II: Dynamics of dilute polymer solutions

It is known since the end of the 40s that the addition of polymer additives into a fluid can dramatically change its properties. The



Figure 4: Two squads of firemen using a water cannon carrying pure water (right) and a dilute polymer solution (left). It has been noted that besides the fact that pure water covers a smaller distance (starting with the same pressure) the cannon with the polymer solution exerts also weaker recoil forces.

mechanical response of a fluid is defined by a so called “constitutive equation” which links the deformation rate to the stresses in the flow. The fluids for which there is proportionality between the two are called Newtonian fluids, the constant being the viscosity. A dilute solution of a Newtonian fluid and soluble polymers is a viscoelastic fluid, as it behaves both like viscous and elastic materials. Among the large number of notable phenomena which are known to appear when dealing with viscoelastic fluids there are the entanglement, the die swell effect, the Weissenberg effect and the *turbulent drag reduction*.

To have a flavor of how a polymer solution can show very interesting properties a simple experiment can be performed. Using a saturated solution of water and cornstarch, it can be clearly seen that depending on the external solicitation the solution reacts in different ways. If a weak stress is imposed (for example by slowly stirring the mixture with a teaspoon) the fluid reacts as a liquid. If the external solicitation is strong (take the tea spoon and abruptly dip it or extract it from the mixture) the fluid reacts as a solid. This is a typical example of entanglement: the cornstarch is a polymer (a complex carbohydrate), and its concentration in this solution is very large. When the external stress is low, polymers can slide past each other, whereas when the stress is large they tend to tangle on each other and this causes a rigidity of the mixture.

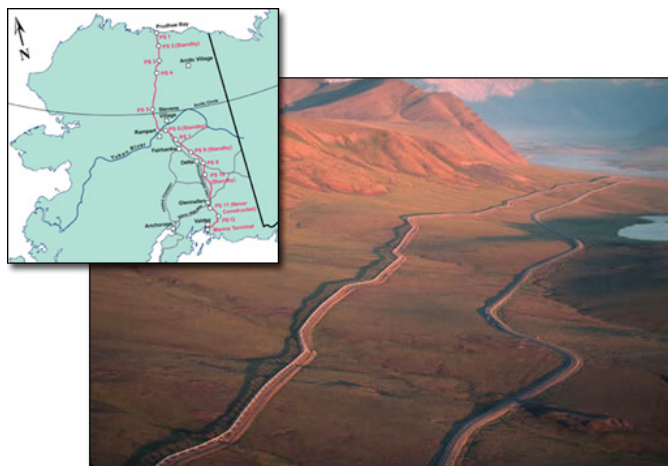


Figure 5: A picture of the Trans Alaska Pipelines. 800 miles of pipe cross all Alaska, carrying roughly 1 million of barrels per day. A drag reducing agent is used since the middle of the 70s to reduce the pressure drop between the starting point and the final point of the pipe. The pumping stations have been reduced from 11 to 7 thanks to the drag reduction phenomenon.

A striking behavior of viscoelastic fluids can be observed in an experiment called rod-climbing or Weissenberg effect [11]. The free surface of a Newtonian fluid put in rotation inside a tank takes the typical shape of a paraboloid, whereas some viscoelastic fluids tend to climb the rod, as in fig. 3a.

Analyzing the motion of a fluid coming out from a capillary, a big difference can be observed between a Newtonian fluid and a viscoelastic fluid, as shown in fig. 3b. For fully developed flow of a viscoelastic fluid in the tube, a tension along the streamlines is present. When the fluid exits the tube, it relaxes the tension along the streamlines by contracting in a longitudinal direction. For an incompressible liquid, this results in a lateral expansion, giving rise to the die-swell phenomenon [12].

Finally, when fully developed turbulence is achieved, a viscoelastic fluid can show a very interesting behavior from a practical point of view. The addition of a small amount of long-chain polymers to a Newtonian fluid flowing in a pipe can display a dramatic reduction of the skin friction between the walls of the pipe and the fluid. This effect has been first reported by the British chemist Toms [13] but it was probably already discovered during the Second World War by the US army, and kept in secrecy. Drag reduction by polymer ad-

ditives has been studied for more than half a century [14–17], and it has been used in a variety of different applications (see fig. 4 and fig. 5). Nevertheless a commonly accepted explanation still does not exist.

This part of the thesis concerns the results I obtained in the analysis of dilute polymer solutions dynamics. I will briefly review the physics of polymer solutions and describe the stability properties of a flow. I will present the most used models of polymer solutions and introduce and explain in detail the results on the stability of polymer solutions and on the study of the drag reduction phenomenon in the context of the viscoelastic Kolmogorov flow.

Bibliography

- [1] Perkins T.-T., Quake S.-R., Smith D.-E., Chu S., *Relaxation of a single DNA molecule observed with optical microscopy*, *Science*, **264**, (1994), 822.
- [2] Bustamante C., Smith S.-B., Liphardt J., Smith D., *Single-molecule studies of DNA mechanics*, *Current opinion in structural biology*, **10**, (2000), 279–285.
- [3] Shaqfeh E.-S.-G., *The dynamics of single-molecule DNA in flow*, *J. Non-Newtonian Fluid Mech.*, **130**, (2005), 1–28.
- [4] de Gennes P.-G., *Coil-stretch-transition of dilute flexible polymers under ultra-high velocity gradients*, *J. Chem. Phys.*, **60**, (1974), 5030.
- [5] Schroeder C.-M., Babcock H.-P., Shaqfeh E.-S.-G., Chu S., *Observation of polymer conformation hysteresis in extensional flow*, *Science*, **301**, (2003), 1515–1519.
- [6] Perkins T.-T., Smith D.-E., Chu S., *Single polymer dynamics in an elongational flow*, *Science*, **276**, (1997), 2016–2021.
- [7] Gerashchenko S., Chevillard C., Steinberg V., *Single-polymer dynamics: Coil-stretch transition in a random flow*, *Europhys. Lett.*, **71**, (2005), 221.
- [8] Smith D.-E., Babcock H.-P., Chu S., *Single polymer dynamics in steady shear flow*, *Science*, **283**, (1999), 1724.
- [9] Gerashchenko S., Steinberg V., *Statistics of tumbling of a single polymer molecule in shear flow*, *Phys. Rev. Lett.*, **96**, (2006), 038304.

- [10] Schroeder C.-M., Teixeira R.-E., Shaqfeh E.-S.-G., Chu S., *Characteristic periodic motion of polymers in shear flow*, Phys. Rev. Lett., **95**, (2005), 018301.
- [11] Bird R.-B., Armstrong R.-C., Hassager O., Curtiss C.-F. *Dynamics of polymeric liquids*. John Wiley, 1987.
- [12] Joseph D.-D., Matta J.-E., Chen K., *Delayed die swell*, J. Non Newtonian Fluid Mech., **24**, (1987), 31–65.
- [13] Toms B.-A. *Observation on the flow of linear polymer solutions through straight tubes at large reynolds numbers*. In *Proc. 1st International Congress on Rheology*, 1949.
- [14] Virk P.-S., *Drag reduction fundamentals*, AiChe J., **21 (4)**, (1975), 625.
- [15] Lumley J.-J., *Drag reduction by additives*, Ann. Rev. Fluid Mech., **1**, (1969), 367–383.
- [16] Tabor M., de Gennes P.-G., *A cascade theory of drag reduction*, Europhys. Lett., **2**, (1986), 519.
- [17] Sreenivasan K.-R., White C.-M., *The onset of drag reduction by polymer additives, and the maximum drag reduction asymptote*, J. Fluid Mech., **409**, (2000), 149–164.

Part I

**Single polymer dynamics and
statistics**

Introduction

The dynamics of polymers in fluid flows has been investigated for more than half a century, due to the rich phenomenology and wide applications of polymer solutions. The rheological properties of dilute and concentrated solutions of polymers are of paramount importance in polymer processing. For example in industrial processing of plastic materials a polymer melt is formed by a prestretching process occurring in a flow. Another very important application of polymers is the use of polymer additives to accelerate the motion of a fluid through a pipe system (see part II).

The direct access to microscopic observables in the study of the motion of polymers in fluid flows has been a motivation to deepen the understanding of phenomena which had been observed several years ago.

In the first chapter I will present the phenomenology of the dynamics of a single molecule in a fluid flow, referring to recent experiments in the field that represent some of the major accomplishments of single molecule techniques. The coil-stretch transition and the conformation hysteresis appearing in the laminar elongational flow will be reviewed and the motion of a polymer in a linear shear flow will be described, addressing the problem of shape dynamics. Recent observations of coil-stretch transition and single polymer dynamics in random flows will be also presented.

In chapter 2 I will introduce the most common polymer models, focusing on the appropriate approximations and on the known drawbacks.

The following chapters are devoted to present my research results. Chapter 3 is dedicated to the analysis of the tumbling motion in a linear shear flow. Due to the particular alternation between regions where the flow is weak compared to fluctuations and to regions where it is dominating, a typical flipping motion occurs, that can be studied and explained by means of theoretical analysis and numerical simulations.

In chapter 4 I will present the results of a theoretical and numerical analysis of the influence of an external flow on the relaxational dynamics of a single polymer. This study aims at explaining in detail how polymer-flow interactions can dramatically change the typical dynamical timescales compared to the case where the flow is absent.

Chapter 1

Single polymer dynamics in fluid flows

1.1 Coil-stretch transition in elongational flows

It is known since the end of the '50s that a polymer in a fluid flow can be strongly deformed by the interaction with the velocity field. A polymer in a fluid at rest typically resembles a spongy ball. A homo-polymer (i.e. a polymer with a unique monomer repeated many times) is like a wire that coils up due to hits with the molecules of the solvent. In principle all the configurations are permitted (even the fully stretched one) but in probabilistic terms highly coiled configurations are much more probable. Conversely, when intense velocity gradients are imposed across a polymer, stretched states occur with large probabilities.

The entropic tendency to recover a coiled state is indicated by an intrinsic parameter of the polymer, which is the time needed by the molecule to reach the steady state, in the absence of flow, starting from a non-coiled configuration. This time is called *relaxation time* or Zimm's time and depends on the temperature and viscosity of the solvent, on the number of monomers in the molecule (and hence on the molecular weight) and on the effective length of the bonds between monomers.

Clearly the stretching rate of a given velocity field must be compared to the relaxation time of the molecule. If the velocity field is weak the recalling force prevails and the molecule is not stretched. On the contrary, if it is sufficiently strong the polymer will be

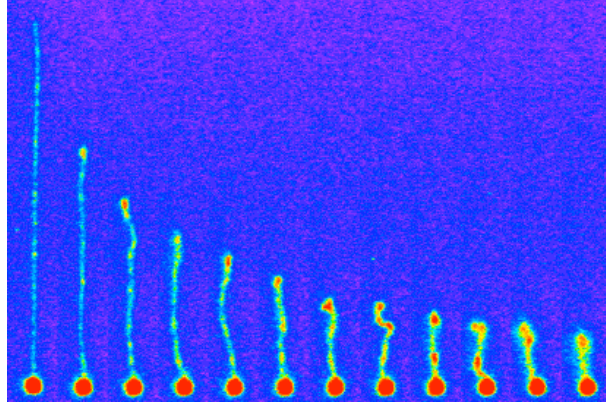


Figure 1.1: Snapshots of a single DNA molecule relaxing to a coiled state [1]. In this experiment a bead is attached to an end of the molecule and is tethered. The molecule is stretched by a uniform flow and once the molecule is fully elongated the flow is switched off and the relaxation of the molecule is measured at different times.

stretched.

This concept can be quantified in terms of the non-dimensional Weissenberg number (from the German physicist Karl Weissenberg):

$$Wi = \|\nabla v\|_t \tau \quad (1.1)$$

where $\|\nabla v\|_t$ stands for the typical velocity gradient across the molecule and τ is the Zimm's time. $Wi \ll 1$ corresponds to a relaxation-dominated dynamics and hence to substantially coiled molecules, while $Wi \gg 1$ corresponds to a dynamics entirely dominated by the stretching, and therefore to highly stretched molecules.

The natural question that arises is: what happens when stretching and relaxation are competing with each other, i.e. for $Wi \sim 1$?

De Gennes and Hinch were the first to address this question [2, 3], claiming that a sharp transition exists between relaxation-dominated states and stretching-dominated states in strong flows. This transition has been called *coil-stretch transition* (see fig. 1.2). A typical example cited by de Gennes where the transition is expected is the elongational flow (see fig. 1.3a). A quite trivial observation is that if we imagine that the molecule is linearly stretched by the velocity field there will be a value of Wi above which the length of the polymer would grow indefinitely because stretching would prevail

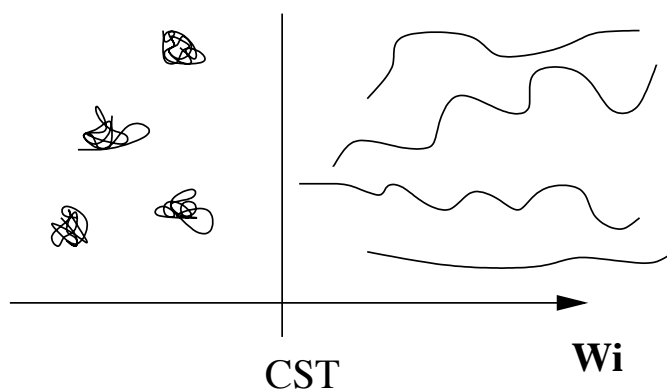


Figure 1.2: A sketch of the coil-stretch transition. In a probabilistic sense below the critical Wi the molecule is coiled, and above it is substantially stretched.

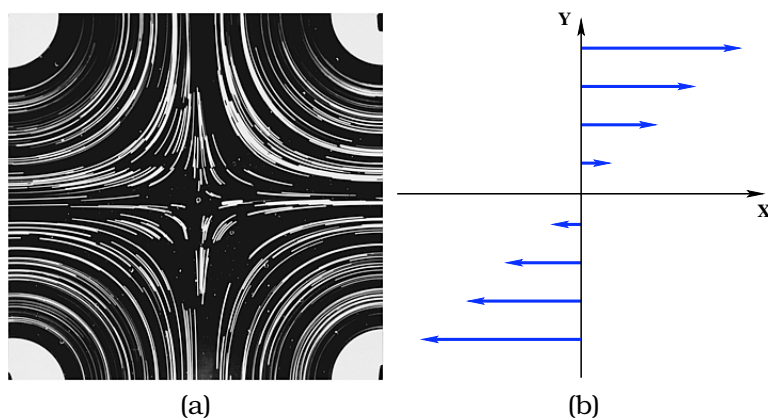


Figure 1.3: (a) Streamlines of an elongational flow. (b) Sketch of a linear shear flow.

on relaxation. In fact, polymer recalling forces are nonlinear, so that the length of a polymer stretched by a velocity field saturates to the fully extended length for large enough values of Wi .

The coil-stretch transition has been observed in a bulk experiment by Leal and collaborators [4, 5] by means of birefringence methods, by measuring the optical properties as a function of the orientation of molecules in a two-dimensional flow. One of the first experiments where single molecule measurements of the coil-stretch transition were taken has been performed by Chu and coworkers [6], where a linear mixed flow was generated by moving rods. With real-time imaging fluorescence microscopy, the conformation of molecules was observed (see fig. 1.4). More recently the coil-stretch transition has been observed also in random flows (see

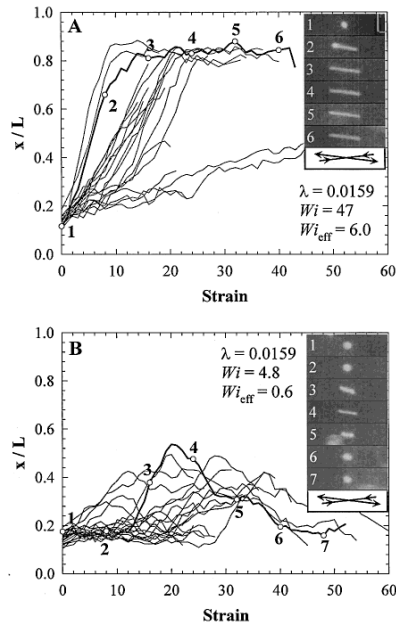


Figure 1.4: In the two pictures are displayed the average molecular extensions as a function of time rescaled with the flow intensity for different Wi numbers [6]. On the top, the one above the coil-stretch transition and, on the bottom, the one below. Qualitatively it is clear that above the coil-stretch transition the polymers are elongated in average, whereas below the transition molecules have a smaller fractional extension. In the insets the corresponding typical conformations are shown: “dumbbell” conformations are typically observed above the transition, and coiled or “hairpin” conformations are found below the transition.

ref. [7] and sec. 1.4).

1.2 Conformation hysteresis in elongational flows

In the same papers by Hinch and de Gennes reporting the observation on the coil-stretch transition [2, 3], another important phenomenon is predicted: the conformation hysteresis. In these seminal papers is argued that the interactions between the different parts of the molecule must be included in the modelization of polymers in fluid flows. Every segment of the molecule feels a velocity field which is modified by the remaining segments of the polymer. These hydrodynamic interactions decay with the distance

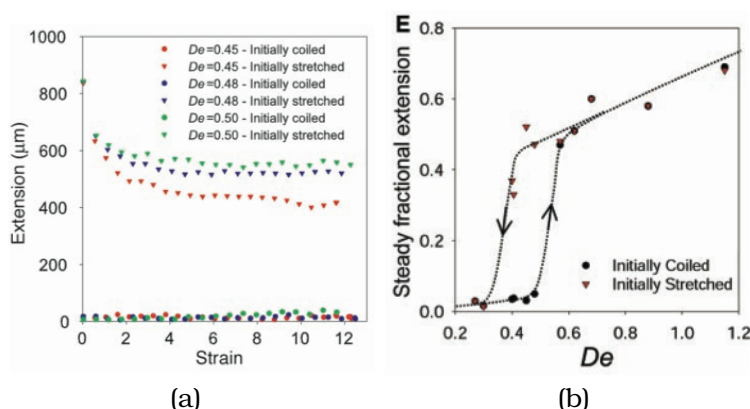


Figure 1.5: (a) The values of the fractional extension measured for different values of De number (identical to the Weissenberg number) and different initial states [8]. (b) The average fractional extension for coiled and stretched initial conditions as a function of De . The diagram shows the hysteretic behavior.

between the different segments. It is thus evident that coiled configurations are characterized by strong hydrodynamic interactions, while in stretched configurations hydrodynamic interactions decrease. Nevertheless in a coiled state only the outer segments of the “spongy ball” are exposed to the flow, while in a stretched state all segments are exposed, and longer molecules are consequently more affected. This observation leads naturally to think that the relaxation process is not independent on the configuration. The relaxation from a fully stretched state is hindered with respect to a moderately stretched state.

This conclusion suggests that the relaxation process of a polymer which is initially very stretched can be quite slow. This effect takes place only when stretching and relaxation are comparable, thus around the coil-stretch transition, and is more pronounced for those polymers showing a big difference between coiled and stretched states. When these conditions are met, hysteresis is expected: if we measure the mean extension of two identical molecules near the coil-stretch transition, one starting near the maximum extension and the other starting in a coiled configuration we expect two different typical extensions.

This phenomenon has been recently observed by Chu and coworkers [8] in a plane elongational flow. This flow has a stagnation point where the molecule can be kept at rest and where real-time imaging can be performed. The main results of this experiment are shown in fig. 1.5.

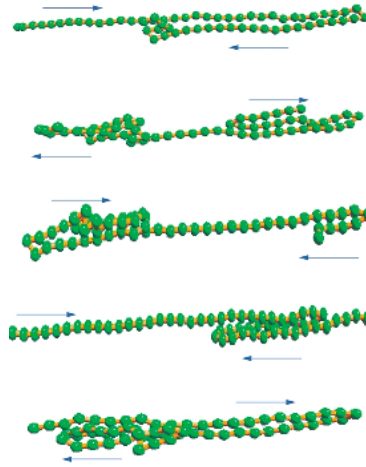


Figure 1.6: A sketch of the tumbling motion extracted from numerical simulations [9].

As already noticed the effect is supposed to be evident for very long molecules: in ref. [8] these are DNA molecules for which the ratio of the maximum length to the length of the polymer at rest is about a thousand (for comparison, in common synthetic polymers this ratio ranges between 50 and 100).

1.3 Shape dynamics and tumbling in shear flows

One of the most interesting aspects of polymer dynamics in fluid flows is the description of the wide variety of configurations dynamically occurring in the molecule motion. Both the coil-stretch transition and the conformation hysteresis can be described simply in terms of the length of the molecule (this concept will become more clear in the next chapter). Nonetheless, focusing on the sequence of conformations bringing the polymer from a coiled to a stretched state (or vice-versa) we can easily argue that there are preferred conformation pathways, or simply that the probability to find the polymer in a given conformation is larger than for the other conformations. In a sufficiently long polymer for example there will be knots whose formation and disentanglement can be studied.

The dynamics of a single polymer in a shear flow (see fig. 1.3b) is particularly interesting from this point of view. The shear flow has

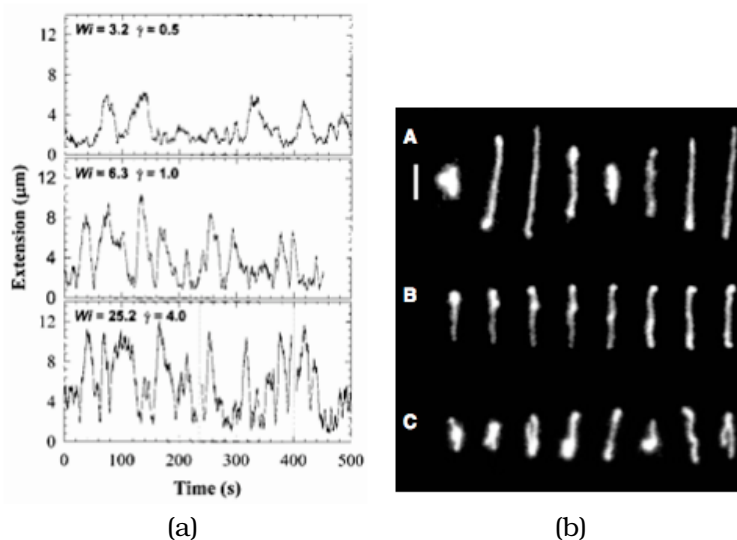


Figure 1.7: (a) Typical time dependence of the fractional extension of a single polymer in a shear flow. (b) Typical conformations of polymers in a shear flow (see ref. [10]).

a stagnation line (the line $y = 0$ in fig. 1.3b). For a rigid rod in a pure linear shear flow the (unstable) equilibrium configurations are those where the rod is aligned along the x axis. In the presence of thermal noise, the motion through regions with weak flow (near the line $y = 0$) and regions with strong flow yields the so called tumbling motion, i.e. the polymer initially aligned along the x axis flips and ends up aligned in the opposite direction. A typical sketch of this motion is depicted in fig. 1.6.

Let's consider a polymer which is initially stretched along the y axis. The shear flow would induce a rotation bringing the polymer aligned along the x axis. There, as already said, the velocity field is negligible, hence the polymer motion is fully dominated by thermal fluctuations. When a realization of these fluctuations brings a part of the polymer out of the weak flow region, the shear flow becomes again important, and it induces a flip. This phenomenon can happen through very different pathways, depending on which is the initial part of the polymer starting the rotation, and it is aperiodic. The dynamics of a single polymer in shear flows has been investigated in detail once more by Chu and coworkers [10]. A shear flow is generated as a superposition of an elongational flow and a pure rotational flow. The probability density function (PDF) of the extension can be extracted from this experiment, and shows similar

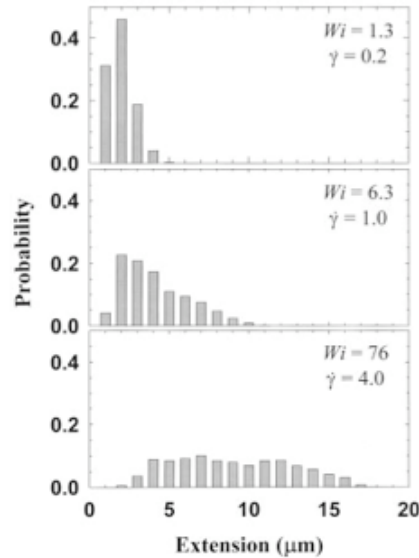


Figure 1.8: Probability density function of the fractional extension for different Wi numbers [10]. Smaller Wi correspond to a PDF which is more peaked around small extensions (below transition) whereas larger Wi correspond to large extensions (above transition).

features to the elongational flow (see fig. 1.8), and different conformations can be observed such as “dumbbell”, “half-dumbbell”, “kinked” and “folded” (see fig. 1.7b).

In another recent experiment Steinberg and collaborators [11] investigated the orientation of polymers in a shear flow, confirming the picture drawn by Chu and extending further the experimental investigations of the theories, measuring the PDFs of the orientation of the polymer and the distribution of tumbling times, i.e. the time between two subsequent flips (see fig. 1.9).

1.4 Single polymer dynamics in random flows

The majority of flows occurring at macroscopic scales are turbulent, i.e. essentially random in nature. At the level of polymer motion these flows are characterized by a smooth dependence on space and an irregular behavior in time. Recently it has been discovered that a random flow can be generated by exciting a fluid in the “elastic turbulence” state (see for example [12, 13] and part II).

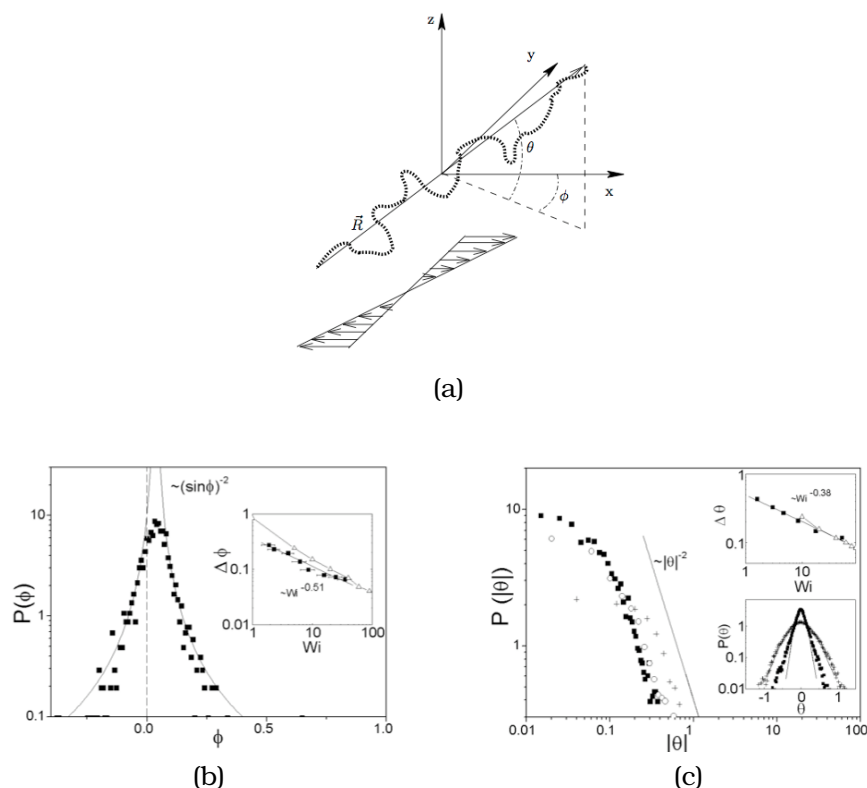


Figure 1.9: (a) The geometry of polymer orientation in a shear flow, with the definition of azimuthal and polar angle. (b) The PDF of angle ϕ . The PDF is centered at $\phi = 0, \pi$, i.e. the polymer spends most of the time aligned in the x direction. (c) The PDF of angle θ . It is centered around 0.

In an experiment performed by Steinberg and coworkers [7], single polymer dynamics is studied in such random flow. The stretching properties of the flow are measured and, averaging over different molecules, the probability density function (PDF) of the elongation of the molecule is reconstructed (see fig. 1.10).

In the random flow, as well as in the elongational flow, the coil-stretch transition is observed, confirming the qualitative picture of de Gennes and Hinch [2, 3], as shown in fig. 1.11.

The sharpness of the transition depends on the stretching properties of the flow. Heuristically we could say that in the elongational flow the transition occurs much more abruptly than in the random flow, because the random flow has a fluctuating extension rate, resulting in a broader distribution of polymer elongations.

It is worth noticing that the value of Wi for which the transition

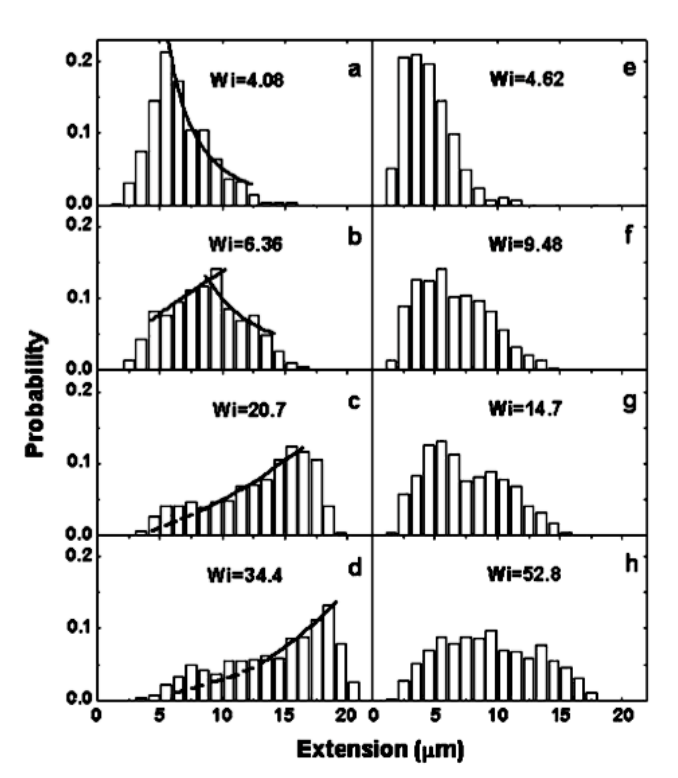


Figure 1.10: Probability density function of polymer elongation [7]. On the left (a, b, c, d): PDFs for random flow; on the right (e, f, g, h) PDFs for laminar shear flow. For small Wi the distribution is peaked around small values of the extension; the contrary holds for large Wi .

occurs depend on the flow details and on the molecule properties, but the transition occurs always at $Wi \sim 1$, when stretching effects and relaxation become comparable in magnitude.

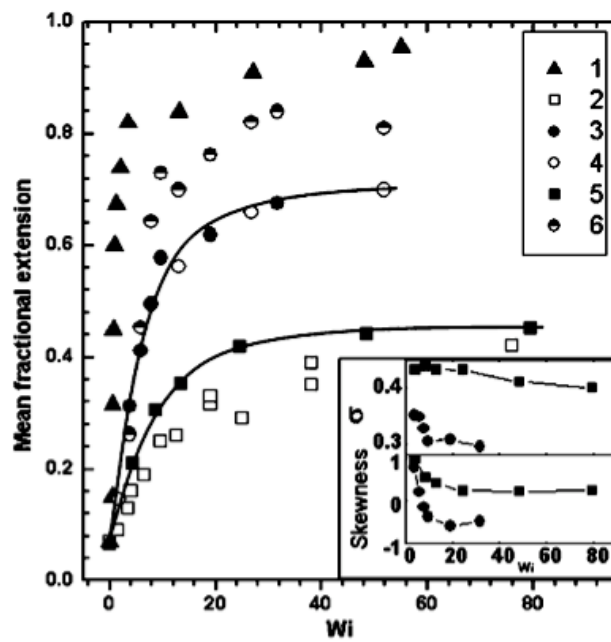


Figure 1.11: The mean fractional extension plotted as a function of Wi in different flows reported in ref. [7]: 1) elongational flow from ref. [14]; 2) plane shear from ref. [10]; 3) random flow generated in a λ -DNA solution; 4) random flow generated in a Polyacrylamide solution; 5) laminar shear flow in both solutions; 6) more frequent values of fractional extension extracted from the probability density functions in both solutions.

Chapter 2

Polymer models

In this chapter I will briefly review the most common polymer models, trying to address their specificity and generality. Furthermore I will try to focus on the ability of these models to reproduce experimental observations and measurements. I will describe only those models that apply to polymers with the following properties:

- long polymers: the number of repeating units M is typically much larger than one. M is also called degree of polymerization, and can reach in certain cases 10^5 .
- flexible polymers: the angle formed by a bond between two monomers is fixed. This means that at the scale of the monomers a polymer is rigid. However if we look at the molecule at a typical length-scale ℓ_p we see a flexible coil. ℓ_p is called the persistence length. When the persistence length is much smaller than the total length of the polymer, the molecule is highly flexible.
- homo-polymers: in general a polymer can have different repeating units. We will consider only macromolecules formed by only one kind of monomer.
- no branching: we will consider only single chain molecules, even if in general there exists molecules formed by several branches.

The dynamical properties of the polymer that we want to take into account are the following:

- at rest the polymer assumes a random coil configuration whose radius is connected with the thermal energy. Experimental

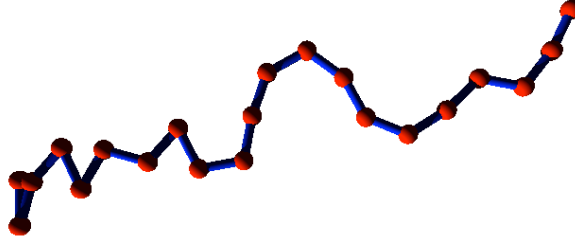


Figure 2.1: A sketch of a freely jointed chain.

measurements of the typical dependence of the radius of the coil on the degree of polymerization give typically scalings between $R \sim M^{0.55}$ and $R \sim M^{0.6}$.

- once elongated the polymer relaxes asymptotically with a typical relaxation time τ
- for relatively small extensions, the polymer opposes to a constant elongation force a recalling force which is proportional to its extension.

Given these phenomenological observations we can introduce briefly some of the most known polymer models.

2.1 The freely jointed chain

A freely jointed chain is formed by M rods of length b_0 each, connected one to another, and free to point in any direction independently of each other. Each node is characterized by a vector \vec{P}^n in space, where n stands for bond index $n = 1, \dots, M$. We can simply construct the bond vectors \vec{r}^n as:

$$\vec{r}^n = \vec{P}^n - \vec{P}^{n-1} \quad (2.1)$$

The characteristic size of the chain is given by:

$$\langle R^2 \rangle^{\frac{1}{2}} = \left\langle \left(\sum_{n=1}^M \vec{r}^n \right)^2 \right\rangle^{\frac{1}{2}} = \left\langle \sum_{n=1}^M \|\vec{r}^n\|^2 \right\rangle^{\frac{1}{2}} + \left\langle 2 \sum_{n>m}^M \vec{r}^n \cdot \vec{r}^m \right\rangle^{\frac{1}{2}} \quad (2.2)$$

Segments are oriented independently so that:

$$\langle \vec{r}^n \cdot \vec{r}^m \rangle = \begin{cases} \langle \|\vec{r}^n\|^2 \rangle = b_0^2 & \text{for } n = m \\ \langle \vec{r}^n \cdot \vec{r}^m \rangle = \langle \vec{r}^n \rangle \cdot \langle \vec{r}^m \rangle = 0 & \text{for } n \neq m \end{cases} \quad (2.3)$$

Hence we obtain:

$$\langle R^2 \rangle^{\frac{1}{2}} = \sqrt{M} b_0 \quad (2.4)$$

Even if the freely jointed chain is a very simple model, this scaling holds also for more general models. If we keep fixed the angle θ between two successive bonds we obtain for example:

$$\langle R^2 \rangle^{\frac{1}{2}} = \sqrt{M} b_0 \sqrt{\frac{1 + \cos \theta}{1 - \cos \theta}} \quad (2.5)$$

A quantity very often used to describe polymer elongation at rest is the radius of gyration, defined as:

$$R_g^2 = \left\langle \frac{1}{2M^2} \left(\sum_{n=1}^M \sum_{m=1}^M (\vec{P}^n - \vec{P}^m)^2 \right) \right\rangle \quad (2.6)$$

For flexible polymers we have:

$$R_g = \frac{\langle R^2 \rangle^{\frac{1}{2}}}{\sqrt{6}} \quad (2.7)$$

Introducing the maximum extension (the contour length) $L = Mb_0$ of a polymer we have:

$$\langle R^2 \rangle = L b_0 \quad (2.8)$$

The freely jointed chain is completely equivalent to a diffusion process: a particle following the path formed by the bonds performs a random walk. By the central limit theorem, the probability density function of the extension is given (in the limit of large M) by:

$$P_M(\vec{R}) = \left(\frac{3}{2\pi M b_0^2} \right)^{\frac{3}{2}} e^{-\frac{3R^2}{2M b_0^2}} \quad (2.9)$$

This PDF gives the entropic force that restores the coiled configuration starting from a stretched one; we can write the free energy of the chain in terms of the partition function $\mathcal{Z} \propto P_M$:

$$\mathcal{F} = -k_B T \ln \mathcal{Z} = \frac{3k_B T R^2}{2Lb_0} + \text{const} \quad (2.10)$$

Thus the variation of the energy due to a variation of the end-to-end elongation of the chain is

$$f = \frac{\partial \mathcal{F}}{\partial R} = \frac{3k_B T}{Lb_0} R \quad (2.11)$$

which means that the polymer as a whole behaves like a spring with elastic constant $H = \frac{3k_B T}{Lb_0}$.

2.2 Excluded-volume effects

Experimental measurements give evidence that the ingredients of the freely jointed chain are not sufficient to describe the microscopic dependence of the radius of gyration on the polymer parameters. Precisely, the scaling behavior of the radius of gyration as a function of the degree of polymerization is $R_g \sim M^\nu$ where the scaling exponent ν is between 0.55 and 0.6.

Within this model the chain is a phantom chain. In other words crossing and superposition of segments are allowed. This results in an overestimation of the number of permitted configurations, and in a wrong exponent ν , which for a freely jointed chain is $\nu = 1/2$. A better approximation of the dynamics of the chain is a self-avoiding random walk, that is a random-walk that cannot intersect itself. While the theory of random walk is quite simple, the treatment of the self-avoiding walk is more difficult. A theoretical estimation of the scaling exponent ν has been given by Flory [15] in dimension $d \leq 4$:

$$\nu = \frac{3}{d+2} \quad (2.12)$$

which is exactly 0.6 for the case $d = 3$. It is worth noticing that a “real” chain recovers an ideal chain ($\nu = 1/2$) for $d \geq 4$, which means that the repulsions due to excluded-volume interactions become negligible when the polymer has “enough room” to avoid the other segments of the chain.

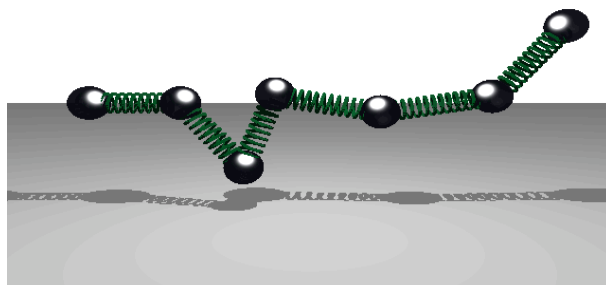


Figure 2.2: A sketch of Rouse and Zimm chains.

2.3 The Rouse and Zimm models

To describe the dynamics of a polymer in a solution it is convenient to resort to a simpler view of the problem. In the Rouse model each segment of the molecule can be represented as a spring containing all the microscopic informations of the molecule: it is an over-damped oscillator with a relaxation time τ_r , it has a linear response to external forces (i.e. it is a Hookean spring), and in the absence of the flow the spring relaxes to an equilibrium elongation given by the thermal noise. The only prescription on the “coarse-graining” of a segment into a spring is that the segment be long enough to have Gaussian statistics, i.e. the response to a constant elongation force is linear in the polymer extension. The nodes connecting two different springs can be represented by beads which interact with the flow with a Stokes friction coefficient:

$$\zeta = 6\pi\eta a \quad (2.13)$$

where η is the dynamic viscosity of the solvent and a is the bead radius. The most important approximations of the Rouse model are [16]:

- the beads do not interact with each other (i.e. the hydrodynamic interactions are negligible)
- the chain is a phantom chain (i.e. excluded-volume interactions are negligible)
- inertial effects due to the mass of the beads are negligible (i.e. the mass of the beads is virtually zero)

With these assumptions each bead experiences two forces arising from the two neighboring springs, the thermal motion and the external velocity field.

It is justified to assume that the velocity field is smooth at the length scales of the polymer. In other words, the difference between two velocities computed in two different points \vec{x}_1 and \vec{x}_2 is simply proportional to the velocity gradient which is independent of the position:

$$\vec{v}(\vec{x}_2, t) - \vec{v}(\vec{x}_1, t) \simeq \vec{\nabla} \vec{v}(t) \cdot (\vec{x}_2 - \vec{x}_1) \quad (2.14)$$

Within this approximation we can write the Newton equations for the N beads, and successively for the $N - 1$ vectors describing the springs, obtaining (see for example [17–20]):

$$\dot{r}_\alpha^n = (\partial_\beta v_\alpha) r_\beta^n - \frac{1}{\tau_r} \sum_{m=1}^{N-1} A^{nk} r_\alpha^k + \sqrt{\frac{2R_{eqs}^2}{\tau_r}} (\eta_\alpha^{n+1}(t) - \eta_\alpha^n(t)) \quad (2.15)$$

where Latin indices stand for bead indices and Greek indices stand for vector indices, R_{eqs} represents the equilibrium length of the springs¹ and is proportional to the thermal energy $k_B T$, τ_r is the relaxation time of the springs and $\eta^n(t)$ is a Gaussian white noise modeling the thermal noise, characterized by the correlation:

$$\langle \eta_\alpha^l(t) \eta_\beta^k(t') \rangle = \delta^{lk} \delta_{\alpha\beta} \delta(t - t') \quad (2.16)$$

The matrix A is called the Rouse matrix and is defined as:

$$A^{nk} = \begin{cases} 2 & \text{if } |n - k| = 0 \\ -1 & \text{if } |n - k| = 1 \\ 0 & \text{in all other cases} \end{cases} \quad (2.17)$$

This system can be treated via a normal modes expansion, and the end-to-end length at rest can be computed as well as the slowest relaxation time of the molecule:

$$\langle R^2 \rangle = NR_{eqs}^2 \sum_{m:odd} \frac{8}{m^2 \pi^2} = NMb^2 \sum_{m:odd} \frac{8}{m^2 \pi^2} \quad (2.18)$$

$$\tau = \frac{\zeta N^2 R_{eqs}^2}{3\pi^2 k_B T} = \frac{\zeta N^2 M b^2}{3\pi^2 k_B T} \quad (2.19)$$

¹For a freely jointed chain this is given by $\sqrt{M}b_0$, where M is the number of stiff segments of the sub-chain that can be considered as a freely jointed chain.

The obvious critiques to the Rouse model are the absence of hydrodynamics interactions and excluded-volume interactions. The first drawback is addressed within the Zimm model [21]. If we consider N identical spherical particles in a solvent we can describe how the velocity field experienced by a particle is distorted by the presence of other particles by the Oseen tensor \mathcal{H} . The velocity $\dot{\vec{x}}$ of a particle k is given by:

$$\dot{x}_\alpha^k = \sum_{m=1}^N \mathcal{H}_{\alpha\beta}^{km} F_\beta^m \quad (2.20)$$

$$\mathcal{H}_{\alpha\beta}^{km} = \begin{cases} \delta^{km} \delta_{\alpha\beta} & \text{for } k = m \\ \frac{1}{8\pi\eta r^{mk}} (\delta_{\alpha\beta} - \hat{r}_\alpha^{mk} \hat{r}_\beta^{mk}) & \end{cases} \quad (2.21)$$

where \vec{F}^m is the net force acting on particle m , \vec{r}^{mk} is the vector joining the particles m and k , r^{mk} is its modulus and $\hat{r}_\alpha^{mk} = r_\alpha^{mk}/r^{mk}$. With simple algebra we could in principle describe the evolution of a Zimm chain in terms of the vectors \vec{r}^n . The obvious problem that arises is that the equivalent of eq. (2.15) accounting for hydrodynamic interactions is nonlinear. Zimm [21] suggested to preaverage the different components of the Oseen tensor over the statistics at equilibrium. This yields:

$$\mathcal{H}^{km} \rightarrow \langle \mathcal{H}^{km} \rangle_{eq} = \int \prod_{k=1}^N d\vec{r}^k \mathcal{H}^{km} \mathcal{P}_{eq}(\vec{r}^k, t) \quad (2.22)$$

where $\mathcal{P}_{eq}(\vec{r}^k, t)$ is the probability density function (PDF) of the vector \vec{r}^k at time t . With this procedure the evolution equations for the vectors describing the elongation and orientation of the springs become again linear and we can compute the leading relaxation time:

$$\tau = \frac{\eta_s N^{\frac{3}{2}} R_{eqs}^3}{\sqrt{3\pi} k_B T} \quad (2.23)$$

These two models are quite accurate even when compared with experiments. Nevertheless very few analytical calculations can be performed within these multi-bead models, and from a computational point of view they can be quite expensive. Furthermore there are physical situations that do not require so many degrees of freedom. The next section is dedicated to a very simple, yet reliable model that bypasses such difficulties.

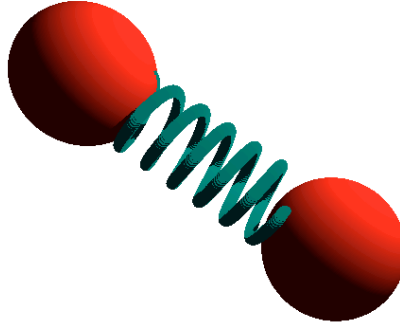


Figure 2.3: A sketch of a dumbbell.

2.4 The dumbbell model

A model which is very often used for its simplicity is the dumbbell model [18]. The basic ingredients of the model are:

- there is only one relaxation time (the longest time of the Rouse model), which determines asymptotically the relaxation properties of a polymer
- the end-to-end vector is described by an entropic force trying to restore an equilibrium length at rest, and opposing a Hookean force to an external stretching
- the velocity gradient is homogeneous in space as in previous models

With these simple assumptions we can now build a “dumbbell” with two beads of radius a , negligible mass, and density much larger than the one of the solvent, connected by a spring with elastic constant $H = \frac{3k_B T}{Lb_0}$. Such a spring has the same properties of an entire freely jointed chain (see sec. 2.1). On each bead acts an elastic force, the thermal noise and the extension forces of the velocity gradient. The evolution equation for the end-to-end vector is:

$$\dot{R}_\alpha = R_\beta \partial_\beta v_\alpha - \frac{1}{2\tau} R_\alpha + \sqrt{\frac{R_0^2}{\tau}} \xi_\alpha(t) \quad (2.24)$$

where ξ_α are Gaussian white noises modeling the thermal fluctuations, $\frac{\zeta}{4H} = \tau$ and $R_0^2 = \frac{k_B T}{H}$. With these definitions the scaling of the

equilibrium length R_0 is $R_0 \sim Mb_0^2$ as predicted by the freely jointed chain model and by the Rouse and Zimm models. The scaling of the relaxation time is the following:

$$\tau \sim \frac{\zeta Mb^2}{k_B T} \quad (2.25)$$

To compare directly this scaling with the one of the Rouse model we should reformulate the problem in terms of the number of bonds: a Rouse chain is a coarse-graining of several freely jointed chains of M links, in a chain of N springs (each containing Q links). For the equilibrium value R_{eqs} then holds $R_{eqs} = Qb^2$. From eq. (2.19) we obtain

$$\tau_R \sim \frac{\zeta N M b^2}{k_B T} \quad (2.26)$$

This means that to recover the “right” scaling we must increase the friction coefficient ζ by a factor N , i.e. the radius a of the beads must be N times larger than in the Rouse model. This condition is reasonable, since we are concentrating the friction into two beads instead of N .

The entropic dynamics of the polymer relaxation is embedded in the dependence of the elastic constant H on the thermal energy of the solvent. At high temperatures the relaxation to the equilibrium length is faster. As for the equilibrium length, the higher is the thermal energy of the solvent, the bigger is the coil formed by the polymer at rest (the length R_0 of the spring in the dumbbell language).

The equilibrium properties in the absence of external flows of such a polymer can be computed analytically. In particular we can compute the moments $\langle R^n \rangle$ for $n = 1$ and $n = 2$:

$$\langle R_\alpha \rangle = 0 \quad (2.27)$$

$$\langle R_\alpha^2 \rangle = R_0^2 \quad (2.28)$$

$$\langle R^2 \rangle = 3R_0^2 \quad (2.29)$$

The dynamics of an initially stretched polymer can also be computed yielding:

$$\langle R^2(t) \rangle = 3R_0^2 + (R^2(0) - 3R_0^2) e^{-\frac{t}{\tau}} \quad (2.30)$$

The introduction of a velocity gradient (except for a very few cases) hinders most of analytical calculation and often makes numerical simulations of eq. (2.24) a suitable approach to the problem.

2.4.1 Nonlinear elasticity

The approximation of linear elasticity is no longer valid when the end-to-end extension approaches the contour length L . This fact is also experimentally very well confirmed by recent experiments on DNA (see [22] for a recent review). It is reasonable to expect that molecules that have different structures and properties will have different elasticities. The two most commonly accepted models in the literature are the finitely extensible nonlinear elastic model and the Marko-Siggia model, which refer to synthetic polymers and biopolymers respectively.

To take into account the nonlinearity of polymers we must add a term in eq. (2.24) which modifies the restoring force:

$$\dot{R}_\alpha = -\frac{f(R)}{2\tau}R_\alpha + R_\beta\partial_\beta v_\alpha + \sqrt{\frac{R_0^2}{\tau}}\xi_\alpha(t) \quad (2.31)$$

where $f(R)$ must be specified according to the phenomenology. The first model I will consider has been introduced by Warner [23], and it is known as the FENE model (finitely extensible nonlinear elastic). It consists in the introduction of the following nonlinearity in the restoring force:

$$f(R) = \frac{1}{1 - \frac{R^2}{L^2}} \quad (2.32)$$

This simple law works particularly well in the case of synthetic polymers (such as PolyEthileneOxide and PolyAcrylaMide). The other common model of nonlinearity has been introduced more recently by Marko and Siggia [24], and is obtained directly by measuring the stretching of a DNA molecule:

$$f(R) = \frac{2}{3} - \frac{L}{6R} + \frac{L}{6R(1 - R/L)^2} \quad (2.33)$$

Both the Marko-Siggia force and the Warner force reduce to the linear case for small extensions $R \ll L$ (see fig. 2.4).

2.5 Probability density function for the polymer extension

A differential equation for the probability density function $\mathcal{P}(\vec{R})$, i.e. the probability to find a polymer described by the end-to-end

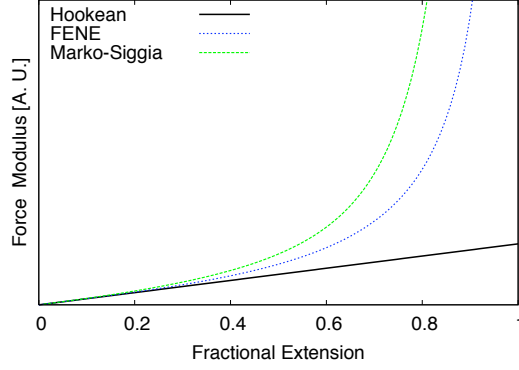


Figure 2.4: The three different forces plotted as a function of the fractional extension (the end-to-end elongation rescaled with the contour length).

vector \vec{R} is associated to the stochastic differential equation (2.31). This equation is called (depending on the context) Fokker-Planck equation, Kolmogorov equation or Smoluchowsky equation. In the absence of the flow we have:

$$\partial_t \mathcal{P}(\vec{R}) = -\partial_{R_\alpha} \left(-f(R) \frac{R_\alpha}{2\tau} \mathcal{P}(\vec{R}) \right) + \frac{R_0^2}{2\tau} \partial_{R_\alpha} \partial_{R_\alpha} \mathcal{P}(\vec{R}) \quad (2.34)$$

The stationary solution of eq. (2.34) can be written in terms of a potential Φ :

$$\mathcal{P}_{st} = e^{-\frac{\Phi}{k_B T}} \quad (2.35)$$

where:

$$\Phi(\vec{R}) = -k_B T \frac{2\tau}{R_0^2} \int^{R_\alpha} d\rho_\alpha \left(-\frac{f(\rho)}{2\tau} \rho_\alpha \right) \quad (2.36)$$

We can now compute the marginal probability density function $p(R)$:

$$p(R) = \int d\Omega R^2 \mathcal{P}(R) \quad (2.37)$$

with the normalization condition $\int p(R) dR = 1$.

In the FENE case we have:

$$\frac{\Phi}{k_B T} = -\frac{L^2}{2R_0^2} \ln \left(1 - \frac{R^2}{L^2} \right) \quad (2.38)$$

$$p(R) = \mathcal{N}_1 4\pi R^2 \left(1 - \frac{R^2}{L^2} \right)^{\frac{L^2}{2R_0^2}} \quad (2.39)$$

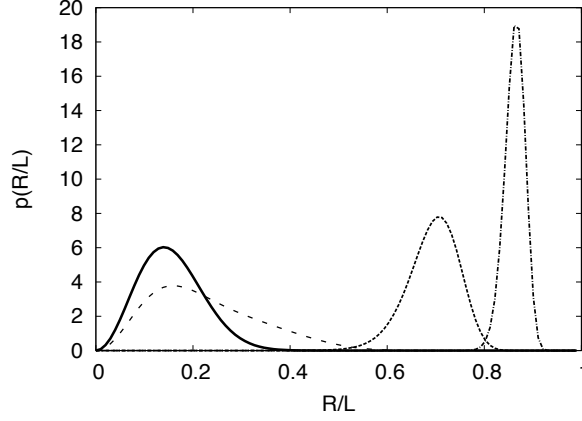


Figure 2.5: The probability density function of elongation of a FENE polymer in an elongational flow for $Wi = 0$ (solid line), $Wi = 1$ (long-dashed line), $Wi = 2$ (short-dashed line), $Wi = 4$ (dot-dashed line). It is evident that for large Wi the probability to find states for which $R \sim L$ is almost one, while the probability to find coiled polymers is nearly zero.

where \mathcal{N}_1 is set by the normalization condition.

Adding an external elongational flow stretching in the x direction we have:

$$\frac{\Phi}{k_B T} = Wi \frac{R_x^2 - R_y^2}{R_0^2} - \frac{L^2}{2R_0^2} \ln \left(1 - \frac{R^2}{L^2} \right) \quad (2.40)$$

$$p(R) = \mathcal{N}_2 \int d\phi \int d\theta \sin \theta R^2 \left(1 - \frac{R^2}{L^2} \right)^{\frac{L^2}{2R_0^2}} e^{\frac{1}{2} Wi \frac{R^2}{R_0^2} \cos 2\phi \sin \theta} \quad (2.41)$$

where \mathcal{N}_2 is set by the normalization condition. The PDF is shown in fig. 2.5.

Chapter 3

Tumbling dynamics in shear flows

In this chapter I will present an investigation on single polymer dynamics in a shear flow. Theoretical predictions are supported by Brownian Dynamics simulations.

The typical rotation motion of non spherical particles in a shear flow is called “tumbling”. This problem has been first addressed by Hinch and Leal [25] who studied the dynamics of non spherical rigid Brownian particles in a shear flow. Examples of tumbling motion can be found in many situations in nature: red blood cells can rotate suddenly due to the local shear flow in vessels [26]; tumbling dynamics has been studied in detail for vesicles in shear flows where the membrane can be considered elastic or rigid [27–29], depending on the ratio between internal and external viscosity.

I will describe the dynamics of a single polymer in two different situations:

- linear shear flow with thermal noise
- linear shear flow with weak superimposed random velocity fluctuations.

Even if analytical calculations are not possible, it has been possible to deduce the fundamental physical laws of tumbling in shear flow, following Chertkov *et al.* [30]. Hereafter I will present the theoretical predictions and numerical simulations I performed to confirm the theory. I will show the probability distributions for the orientation and elongation of the polymer and the statistics of the

tumbling times, i.e. the time between two subsequent flips. The theoretical and numerical results of the case of linear shear with thermal noise will be also compared with a recent experiment by Steinberg and coworkers. This comparison shows that the non-linear dumbbell model, in spite of its simplicity, is very effective in reproducing experimental data and scaling laws.

3.1 Tumbling dynamics in laminar shear flows

A pure shear flow (or linear shear flow) can be obtained by a superposition of a pure elongational flow and a pure rotation flow, and is defined by:

$$\vec{v} = (sy, 0, 0) \quad (3.1)$$

$$\hat{\partial}v = \begin{pmatrix} 0 & s & 0 \\ 0 & 0 & 0 \\ 0 & 0 & 0 \end{pmatrix} = \underbrace{\begin{pmatrix} 0 & \frac{s}{2} & 0 \\ \frac{s}{2} & 0 & 0 \\ 0 & 0 & 0 \end{pmatrix}}_{\text{elongation}} + \underbrace{\begin{pmatrix} 0 & \frac{s}{2} & 0 \\ -\frac{s}{2} & 0 & 0 \\ 0 & 0 & 0 \end{pmatrix}}_{\text{rotation}} \quad (3.2)$$

A sketch of a linear shear flow is depicted in fig. 1.3b. This flow is weak in the region near the xz plane, while is strong far from it. When the polymer is elongated, and its ends are in the region of strong flow, elongation and rotation both occur. The polymer is thus stretched and rotates clockwise until it is aligned along the x axis. At this point it is in a region of weak flow, where the dynamics is dominated by the thermal noise. In this state the polymer remains elongated and fluctuates, until a sequence of thermal fluctuations brings it in a region where the flow is not negligible anymore. Then the polymer flips clockwise (tumbles). When it approaches the x axis (in the opposite direction) it is stretched again and the process starts over.

To describe polymer dynamics we use the dumbbell model with a choice of parameters corresponding to the experimental values of ref. [11]. The dynamics of a dumbbell in a shear flow is described

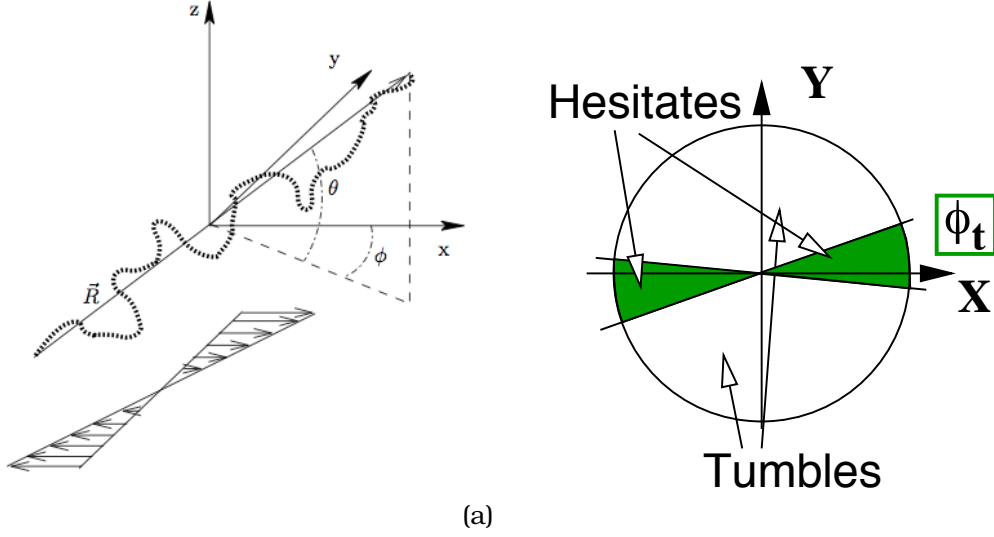


Figure 3.1: (a) The angles ϕ and θ describe respectively the dynamics in the shear plane and off the shear plane. (b) A two-dimensional projection of the system: the region defined by the angle ϕ_t is the region where the polymer waits for a typical time τ_t before rotating and tumbling.

by the equations:

$$\begin{aligned}
 \dot{R}_x &= sR_y - \frac{f(R)}{2\tau}R_x + \sqrt{\frac{R_0^2}{\tau}}\xi_x(t) \\
 \dot{R}_y &= -\frac{f(R)}{2\tau}R_y + \sqrt{\frac{R_0^2}{\tau}}\xi_y(t) \\
 \dot{R}_z &= -\frac{f(R)}{2\tau}R_z + \sqrt{\frac{R_0^2}{\tau}}\xi_z(t)
 \end{aligned} \tag{3.3}$$

where $f(R)$ can be 1 in the Hookean case or $1/(1 - R^2/L^2)$ in the FENE case.

3.1.1 Elongation statistics

The PDF of the vector \vec{R} in the statistically stationary state can be computed analytically, whereas the PDF of the elongation R has a closed expression only in the two opposite limits of very small shear rates and very high shear rates. In terms of the Weissenberg number $Wi = s\tau$, these limits correspond respectively to $Wi \ll 1$ and $Wi \gg 1$.

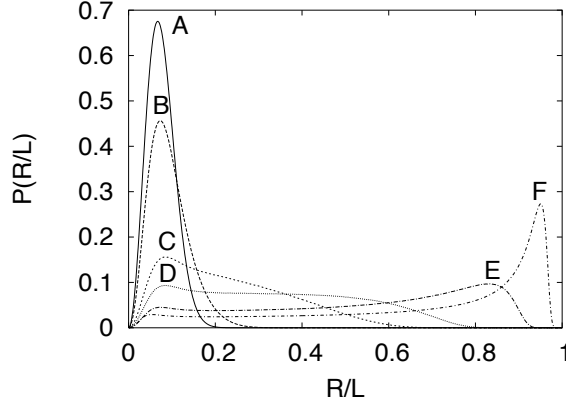


Figure 3.2: The probability density function of the fractional extension for $Wi = 0, 1, 5, 10, 40, 200$ from A to F extracted from numerical simulations of FENE polymers in shear flows.

For linear dumbbells the probability density functions of \vec{R} is Gaussian, as well as the marginal PDFs. For the mean values we have:

$$\langle R_x \rangle = \langle R_y \rangle = \langle R_z \rangle = 0 \quad (3.4)$$

and for the variances:

$$\langle R_y^2 \rangle = \langle R_z^2 \rangle = R_0^2 \quad \langle R_x^2 \rangle = R_0^2(1 + 2Wi^2) \quad (3.5)$$

For small Wi the polymer elongation is completely determined by the balance between thermal fluctuations and relaxation. For large Wi the same holds for R_y and R_z , while R_x is strongly enhanced by the flow, yielding a proportionality between the extension of the polymer and the relative strength of the flow:

$$R \sim \langle R_x^2 \rangle^{\frac{1}{2}} \sim R_0 Wi \quad (3.6)$$

Thus the polymer is linearly extended by the shear flow.

For high shear rates the linear dumbbell model fails so that it is necessary to switch to nonlinear models. In the FENE case the PDF in the absence of flow can be computed quite easily [31], but analytical calculations are not possible in the general case, and the probability density function must be extracted from numerical simulations. As shown in fig. 3.2 for small Wi we recover the linear case, whereas for large Wi the typical value of the elongation approaches the maximum length $R \sim L$.

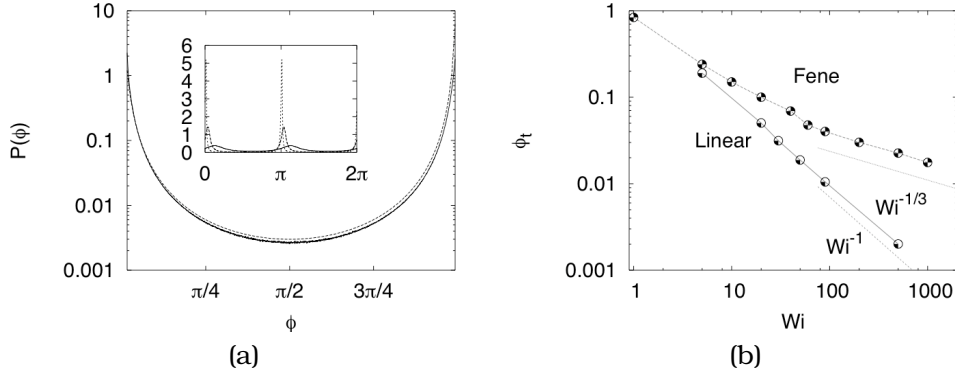


Figure 3.3: Data extracted from numerical simulations. (a) The PDF of the angle ϕ , plotted against $\sin^{-2} \phi$; in the inset the whole PDF in linear scale. (b) The width at half height of the PDF, ϕ_t , as a function of Wi .

3.1.2 Orientation statistics

The orientation dynamics of rigid non spherical particles in a shear flow has been previously investigated by Jeffery [32] and by Hinch and Leal [25]. As for polymers, in a recent work Chertkov and coworkers [30] have investigated the dynamics and statistics of polymer in a shear flow.

An evolution equation for the angle ϕ can be derived from eqs. (3.3), yielding:

$$\partial_t \phi = -s \sin^2 \phi + \xi_\phi \quad \langle \xi_\phi(t) \xi_\phi(t') \rangle \propto \frac{R_0^2}{\tau R^2} \delta(t - t') \quad (3.7)$$

The boundary between weak and strong flow regions is by definition where the flow and the thermal noise are comparable. This portion corresponds to a small angle ϕ_t . For $\phi \lesssim \phi_t$ we are in the weak flow region, whereas for $\phi \gtrsim \phi_t$ we are in the strong flow region. From eq. (3.7) we can estimate ϕ_t by the balance $s \phi_t^2 \simeq \xi_\phi$, yielding:

$$\phi_t \sim \left(\frac{R_0^2}{Wi R^2} \right)^{\frac{1}{3}} \quad (3.8)$$

As the polymer spends most of the time aligned along the x axis, the most probable value for the probability density function of ϕ are $0, \pi$, and the width of the peaks is proportional to ϕ_t^1 . The dependence of ϕ_t on Wi can be derived immediately by recalling the expression of the extension in the linear and nonlinear cases,

¹The PDF of \vec{R} can be determined in this case, and can be integrated over the

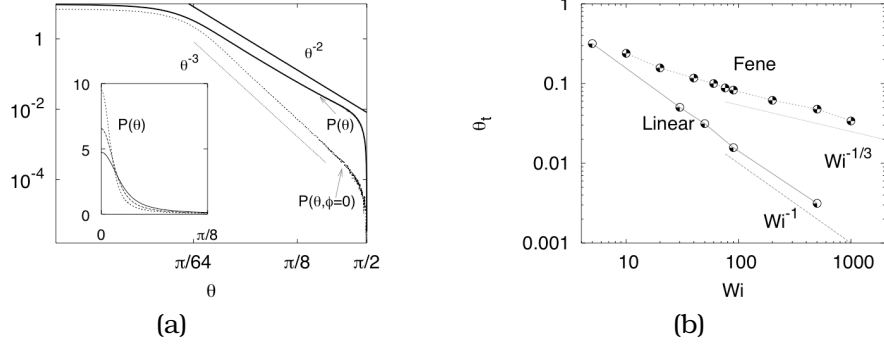


Figure 3.4: Numerical simulations of a single polymer in a linear shear flow. (a) The PDF of the angle θ and the plot of the marginal PDF taken around $\phi = 0$, showing a power law tail θ^{-3} ; in the inset the whole PDF in linear scale for different Wi . (b) The width θ_t at half height of the PDF, as a function of Wi .

$R \sim R_0 Wi$ and $R \sim L$ respectively. These estimates, plugged into eq. (3.8), give the scaling laws:

$$\text{Linear} \quad \phi_t \sim Wi^{-1} \quad (3.10)$$

$$\text{Nonlinear} \quad \phi_t \sim Wi^{-\frac{1}{3}} \quad (3.11)$$

As for the dynamics of θ another equation can be derived:

$$\partial_t \theta = -s \frac{\sin 2\phi \sin 2\theta}{4} + \xi_\theta \quad \langle \xi_\theta(t) \xi_\theta(t') \rangle \propto \frac{R_0^2}{\tau R^2} \delta(t - t') \quad (3.12)$$

The symmetry with respect to the xy plane implies that the probability density function for the angle θ is symmetric with respect to $\theta = 0$ (see fig. 3.4a). The most probable value for this PDF is $\theta = 0$, and its width can be estimated as $\theta_t \sim \phi_t$, thus decreasing with Wi as:

$$\text{Linear} \quad \theta_t \sim Wi^{-1} \quad (3.13)$$

$$\text{Nonlinear} \quad \theta_t \sim Wi^{-\frac{1}{3}} \quad (3.14)$$

elongation R giving:

$$\mathcal{P}(\phi, \theta) \propto \frac{\cos \theta}{\left\{ 1 - \frac{\cos^2 \theta}{4 + Wi^2} [Wi^2 \cos(2\phi) + 2Wi \sin(2\phi)] \right\}^{3/2}}. \quad (3.9)$$

The marginal PDF of each angle cannot be calculated analytically and must be integrated numerically.

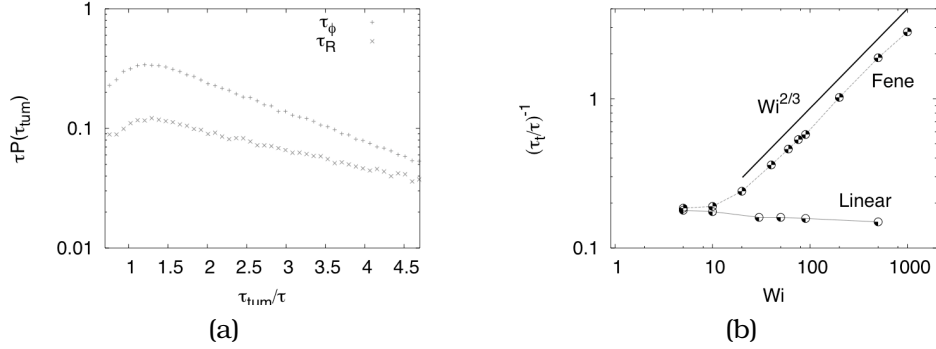


Figure 3.5: Numerical simulations of a single polymer in a linear shear flow. (a) The PDF of the tumbling time τ_{tum} rescaled with the relaxation time of the polymer, shown for two different definitions of tumbling time: τ_ϕ and τ_R (see the text for details). The peak at $\tau_{tum} \sim \tau_t$ and the exponential tail $\sim \exp(-\tau_{tum}/\tau_t)$ are evident. (b) The typical tumbling time τ_t as a function of Wi .

As the flow strength grows (together with the typical elongation), large off-shear-plane angular fluctuations becomes less probable. It can be shown that when $\theta_t \lesssim \theta \ll 1$ the PDF decays as a power law θ^{-2} , and that in the range $\phi \sim \phi_t$ the whole PDF follows a power law $p(\theta, \phi \sim \phi_t) \sim \theta^\alpha$ where $\alpha > 2$.

3.1.3 Tumbling statistics

The tumbling time is defined as the time elapsed between two successive flips. Tumbling occurs as follows: if we start from a stretched configuration there will be a typical time τ_{res} of residence in the region defined by ϕ_t , then suddenly a flip occurs, and the polymer rotates around its center of mass in a typical time s^{-1} , and then the process starts over. The total duration of a tumbling event is given by:

$$\tau_t \sim \tau_{res} + s^{-1} \quad (3.15)$$

For small Wi the contribution s^{-1} of the rotation itself is more relevant, while for large Wi the tumbling time is essentially determined by the time of residence in the region $\phi \sim \phi_t$. This can be estimated by a simple physical argument. In the region $\phi \sim \phi_t$ the dynamics is dominated by the thermal noise. Hence the time of residence is the exit-time of a diffusive process:

$$\tau_{res} \sim \frac{\phi_t^2}{D} \quad (3.16)$$

where \mathcal{D} is the diffusion coefficient associated with the evolution equation (3.7), i.e. $\mathcal{D} = \frac{R_0^2}{\tau R^2}$. Substituting the typical values for the extension in the linear ($R \sim R_0 \text{Wi}$) and nonlinear case ($R \sim L$) we have:

$$\text{Linear} \quad \tau_t \sim \tau \quad (3.17)$$

$$\text{Nonlinear} \quad \tau_t \sim \tau \text{Wi}^{-\frac{2}{3}} \quad (3.18)$$

showing how the typical tumbling time is affected by the nonlinear elasticity of the polymer at large Wi .

The probability density function of the tumbling time cannot be computed analytically. However, since the exit-process is a Poisson process, as the polymer tries a large number of times to exit the “hesitation region”, the tail of the PDF should be exponential (see fig. 3.5), with a typical tumbling time τ_t .

There are two ways to give an operational definition of the tumbling time, one referring to the angle ϕ and the other to the elongation (τ_ϕ and τ_R , respectively, of fig. 3.5a). The first one is the following: a tumbling event starts when the polymer crosses the line $\phi = \pi/2$, and ends when the polymer crosses it again. The second way is to define a certain appropriate threshold R_{th} and to identify a tumbling event as the sequence of consecutive crossings of the plane $R = R_{th}$ in the phase space (R, θ, ϕ) . This means that a tumbling event is a sequence of consecutive coiled-stretched-coiled states. It is worth noticing that for small Wi the tumbling time is difficult to measure in experiments, because of the very high resolution needed.

3.1.4 Comparison with experimental data

This subsection is devoted to show how the dumbbell model compares well with experimental results on the dynamics of polymers in a linear shear flow.

In the experiment by Steinberg and Geraschenko [11] a single DNA molecule is observed with microscopy techniques in two different flows: one generated by a rotating cylinder, and a Poiseuille flow in a microchannel. Both these flows are locally linear shear flows. By averaging over several molecules in time, the PDFs of the orientation angles can be extracted, as well as the PDFs of the tumbling times. Furthermore scaling laws for ϕ_t , θ_t and τ_t are obtained in the measured range of Wi .

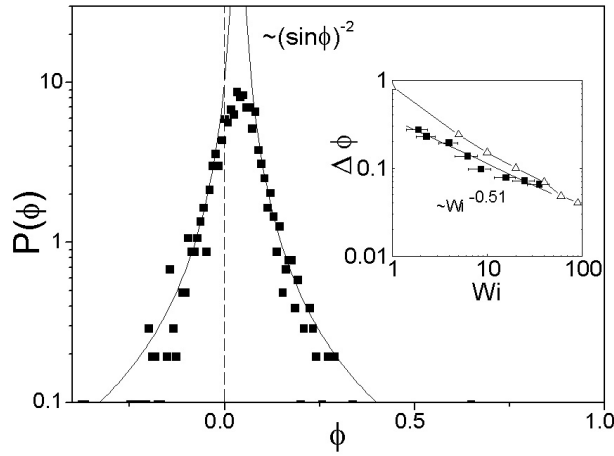


Figure 3.6: Data extracted from experiments [11]. The PDF of ϕ is shown against $\sin^{-2} \phi$. In the inset ϕ_t as a function of Wi with an effective scaling $Wi^{-0.51}$. The black squares represent experimental measurements, while white triangles represent our numerical data.

Angle ϕ

The probability density function is measured in the vicinity of $\phi = 0$ and is shown in fig. 3.6. It is peaked around $\phi = 0$ as predicted, and decays as $\sin^{-2} \phi$, as in the results of numerical simulations shown in fig. 3.3a.

In the inset are plotted the experimental data of the measured width of the peak of the PDF as a function of Wi . The exponent -0.51 is extracted from a fit, and interpolates between the two asymptotics Wi^{-1} and $Wi^{-1/3}$. As shown in fig. 3.3b, the exponent reaches the value $-1/3$ after $Wi \sim 100$ whereas in experimental measurements the maximum value is $Wi \sim 50$.

Angle θ

The probability density function of the angle θ is shown in fig. 3.7. As predicted it is symmetric with respect to $\theta = 0$ and it is peaked around $\theta = 0$. The scaling θ^{-2} is clear for $\theta > 0$.

The upper inset of fig. 3.7 shows the width of the PDF as a function of Wi . The exponent is in good agreement with the theoretical and numerical predictions.

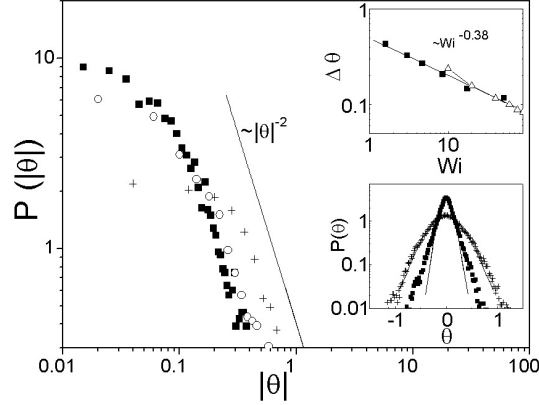


Figure 3.7: Data extracted from experiments [11]. The PDF of θ is shown, with the clear scaling θ^{-2} . In the upper inset θ_t as a function of Wi , showing the exponent -0.38 . The black squares represent experimental measurements, while white triangles represent our numerical data. In the lower inset the PDFs in linear scale for two different values of Wi .

Tumbling times

The PDFs of the tumbling times measured in the experiment by Steinberg and coworkers are shown in fig. 3.8a, and are exponential. In fig. 3.8b is shown the typical tumbling time τ_t plotted as a function of Wi at different relaxation times and shear rates. The comparison between the numerical data and the experimental data shows a good agreement. The difference in the prefactor is due to the different criterion used to define a tumbling event. In the experiment the definition τ_R is used, as well as for the numerical data of the picture, but the threshold values are different: this explains the overall multiplicative factor between the two curves.

3.2 Tumbling in shear flows with weak superposed velocity fluctuations

In this section I will present the results of the study of tumbling in a turbulent flow, modeled by a random flow superposed to a strong linear shear. This condition is met whenever a polymer is in a strong vortex and senses small velocity fluctuations or when single polymer dynamics is studied in elastic turbulence (see sec. 5.2). The velocity gradient in this case is decomposed into a deterministic part and a stochastic part. The deterministic part is a lin-

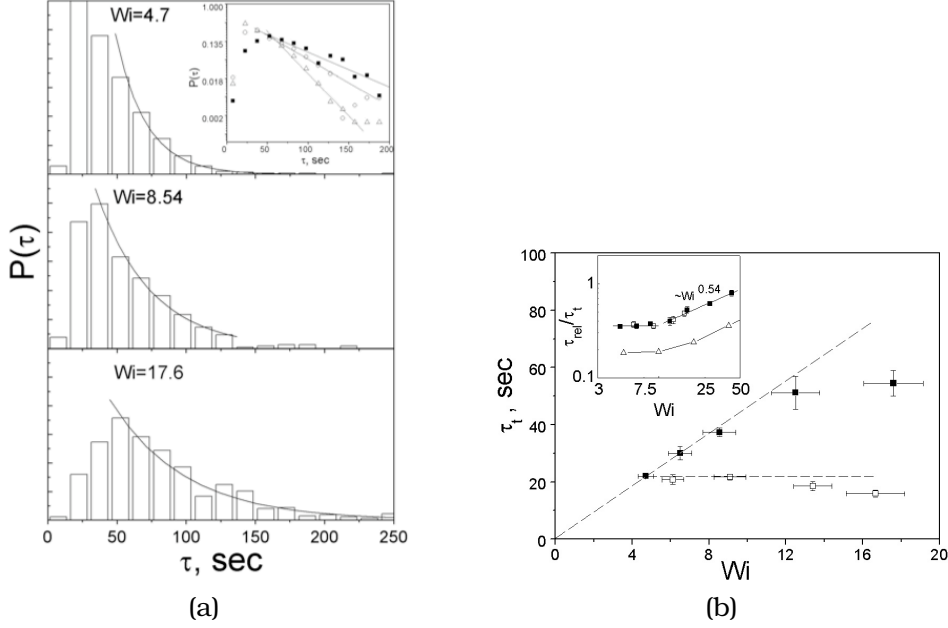


Figure 3.8: Data extracted from experiments [11]. (a) PDF of tumbling times measured in the experiment. (b) The typical tumbling time τ_t as a function of Wi : full squares are taken at constant shear rate and varying the relaxation time, while open squares are taken at constant relaxation times and varying the shear rate. In the inset: the relaxation time over the typical tumbling time. Black squares are the experimental measurements while white triangles are numerical data.

ear shear flow of the form: $\vec{v} = (sy, 0, 0)$. The stochastic part is a Gaussian random field, white in time, statistically isotropic, homogeneous and parity invariant:

$$\langle \sigma_{ij}(t) \rangle = 0 \quad (3.19)$$

$$\langle \sigma_{ij}(t) \sigma_{kl}(t') \rangle = D \delta(t - t') (4\delta_{ik}\delta_{jl} - \delta_{il}\delta_{kj} - \delta_{ij}\delta_{kl}). \quad (3.20)$$

This is called a Kraichnan-Batchelor field [33]. Here thermal fluctuations are negligible so that the evolution equation of the dumbbell reads:

$$\dot{R}_\alpha = R_\beta \partial_\beta v_\alpha - \frac{R_\alpha}{2\tau} \quad (3.21)$$

There is a region (as in the previous section) where velocity fluctuations govern the dynamics and a region where the shear flow is dominating. The former region is defined by an angular width ϕ_t . As in the case of pure linear shear flow, the polymer hesitates in the weak flow region, then suddenly flips, and is realigned along the x axis.

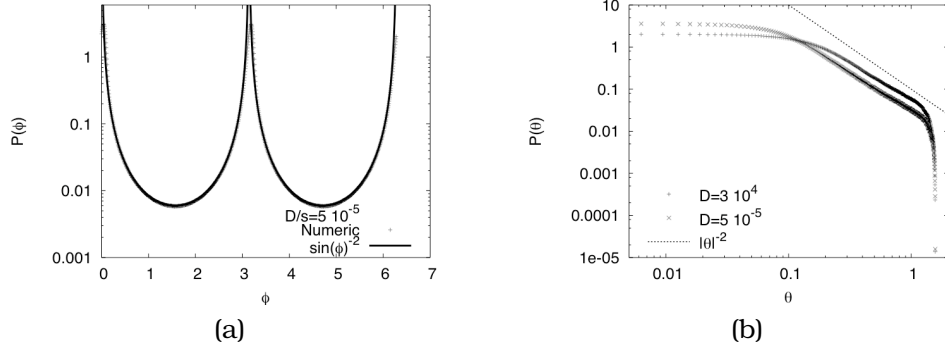


Figure 3.9: Data extracted from numerical simulations of polymers in linear shear flow with weak velocity fluctuations. (a) The PDF of the angle ϕ plotted against the function $\sin^{-2} \phi$. (b) The PDF of the angle θ with the power law θ^{-2} .

3.2.1 Orientation statistics

For the angle ϕ an evolution equation can be derived, as in the previous section:

$$\dot{\phi} = -s \sin^2 \phi + \xi_\phi \quad \langle \xi_\phi(t) \xi_\phi(t') \rangle = \frac{4D}{\cos^2 \theta} \delta(t - t') \quad (3.22)$$

where the term proportional to s represents the effect of the shear flow and the noise represents the effect of the weak velocity fluctuations. The angular amplitude ϕ_t can be estimated by imposing that these two effects are comparable, yielding:

$$\phi_t \sim \left(\frac{D}{s}\right)^{\frac{1}{3}} \quad (3.23)$$

The PDF is peaked in the vicinity of $0, \pi$ as in the case of the thermal noise, and decays as $\sin^{-2} \phi$, as shown in fig. 3.9a.

An evolution equation for the angle θ can be derived in a similar way:

$$\dot{\theta} = -s \frac{\sin(2\phi)}{2} \sin \theta \cos \theta + \xi_\theta \quad \langle \xi_\theta(t) \xi_\theta(t') \rangle = 4D \delta(t - t') \quad (3.24)$$

The width of the PDF of θ can be estimated as for ϕ , yielding $\theta_t \sim \phi_t$, it is symmetric with respect to $\theta = 0$ as fluctuations are isotropic and the shear flow is in the xy plane, and decays as a power law for $\theta \gtrsim \theta_t$, as shown in fig. 3.9b.

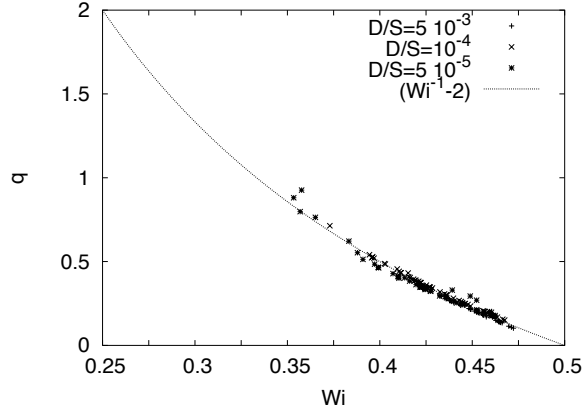


Figure 3.10: The exponent of the probability density function of the elongation for $Wi < 0.5$, plotted for different ratios D/S .

3.2.2 Elongation statistics

From eq. (3.21) we can derive an evolution equation for the end-to-end extension R :

$$\partial_t \ln \frac{R}{R_0} = -\frac{1}{2\tau} + \frac{s}{2} \cos^2 \theta \sin 2\phi + 6D + \eta, \quad (3.25)$$

where $\langle \eta(t)\eta(t') \rangle = 2D\delta(t - t')$. The corresponding Fokker-Planck equation is quite complicated. Yet, below the coil-stretch transition, the properties of the probability density function of the elongation can be derived. In particular in this regime the polymer spends most of the time in the coiled state, but rare events lead to a large polymer stretching, when the flow becomes strong enough. It can be shown, that the right tail of the polymer elongation PDF is a power law $p(R) \propto R^{-1-q}$ [31, 34–38], where the exponent q depends on the parameters of the flow. For example in the case of pure Kraichnan-Batchelor field we have that the exponent q is smaller than 0 for $Wi < 0.5$, i.e. below the coil-stretch transition. Above the transition, strong elongation events are more probable yielding a non-normalizable PDF, and nonlinear elasticity has to be accounted for. The numerical measurements of the exponent q as a function of Wi below the coil-stretch transition are shown in fig. 3.10, and compare well to those found in refs. [31, 38]

Here the Wi number is defined as the product of the relaxation time and the largest Lyapunov exponent of the flow. The Lyapunov exponent is the rate of divergence of two initially close Lagrangian

trajectories in the flow, and is defined as:

$$\lambda = \lim_{T \rightarrow \infty} \lambda_T = \lim_{T \rightarrow \infty} \ln \left\langle \frac{R(T)}{R(0)} \right\rangle \quad (3.26)$$

where λ_T is called finite-time Lyapunov exponent. For the Kraichnan-Batchelor flow the Lyapunov exponent can be calculated exactly and we have $\lambda = 3D$. For nonzero shear rates the Lyapunov exponent can be estimated as follows: for two points in the flow the equation describing the divergence of trajectories is:

$$\partial_t \ln \frac{R}{R_0} = \frac{s}{2} \cos^2 \theta \sin 2\phi + 6D + \eta, \quad (3.27)$$

The maximum rate of divergence is in the x direction, for $\theta, \phi \ll 1$. As $s\phi \gg \eta, D$ we have [30]:

$$\partial_t \ln \frac{R}{R_0} \sim s\phi \quad (3.28)$$

and on average $\lambda \sim s\phi_t \sim (Ds^2)^{1/3}$.

The numerical measurements of the Lyapunov exponent are shown in fig. 3.11a. A more refined characterization of the statistics of the flow is given by the Cramèr function, or entropy function S , which is related to the so called finite-time Lyapunov exponent. In particular this relation holds:

$$P(\lambda_T) \sim e^{-\lambda T S(\frac{\lambda T}{\lambda})} \quad (3.29)$$

where S is the Cramèr function, that has a quadratic minimum at $\lambda_T = \lambda$. This function can be found explicitly only in few cases: in the particular case $s = 0$ (Kraichnan-Batchelor flow) it can be shown that S is exactly quadratic. The Cramèr function gives the details of the statistics of convergence of the stretching rate of the flow. For this flow it is shown in fig. 3.11b.

3.2.3 Tumbling dynamics

The tumbling time τ_{tum} is determined by the time of residence in the region $\phi \lesssim \phi_t$ and by the duration of the flip s^{-1} . Here the time of residence is set by the relevant timescale of the flow λ^{-1} : for high Wi a tumbling event duration is determined only by the residence time. The dependence of the typical tumbling time on the

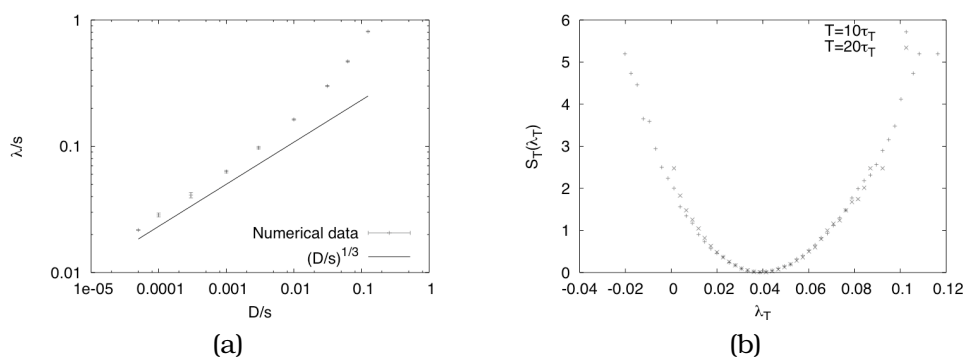


Figure 3.11: (a) Measured largest Lyapunov exponent of the flow. The line represents the theoretical prediction and is a guide to the eye. (b) The Cramèr function of the finite-time Lyapunov exponent for this flow.

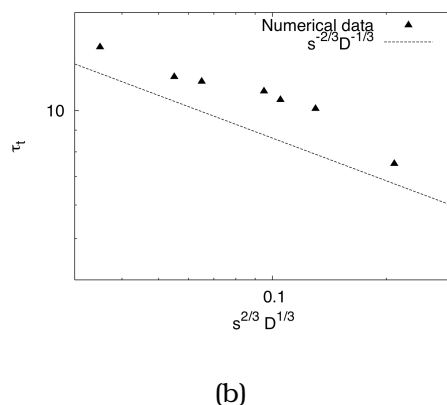
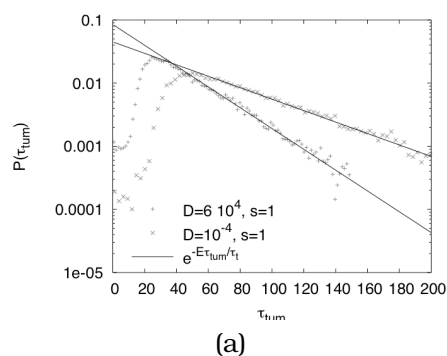


Figure 3.12: Data extracted from numerical simulations. (a) Probability density function of the tumbling time, plotted against the theoretical calculations. (b) The typical tumbling time τ_t as a function of the Lyapunov exponent.

Lyapunov exponent extracted from numerical simulations is shown in fig. 3.12a. The probability of long tumbling events is determined

by the Poisson distribution, resulting in an exponential tail for the probability density function, as shown in fig. 3.12a:

$$P(\tau_{tum}) \sim e^{-E \frac{\tau_{tum}}{\tau_t}}, \tau_{tum} \gg \tau_t \quad (3.30)$$

The prefactor E can be computed analytically, and the theoretical calculations are compared with numerical results in fig. 3.12a.

3.3 Perspectives

A tumbling event can take place through very different sequences of conformations. These cannot be described within the dumbbell model. Thus a future task would be to study tumbling by means of multi-bead models. Starting from a trimer (a three-bead chain), it would be interesting to study the probability to find the polymer in a given configuration, which, in this case, is simply given by the probability density function of the angle between the two vectors joining the beads (see for example ref. [39]). The latter is also connected to another interesting quantity: the probability that a tumbling event occurs starting from a given conformation.

This analysis would be a first step toward the investigation of the shape dynamics of a N -bead Rouse or nonlinear Rouse chain in shear flows. In the case $N \gg 1$ it is necessary to analyze more complex quantities. For example it is possible to characterize the shapes by means of the statistics of the number of folds of the chain in the direction of the mean shear. The average number of folds can be computed analytically in the case of the Rouse model for a large number of beads. The analytical calculations become difficult when nonlinear elasticity is considered and in this case numerical simulations are a suitable approach.

Polymers in linear shear flow: A numerical study

A. CELANI¹, A. PULIAFITO^{1,3} and K. TURITSYN^{1,2,3}

¹ *Institut Non Linéaire de Nice - UMR 6618 CNRS*
1361 route des Lucioles, 06560 Valbonne, France

² *Landau Institute for Theoretical Physics - Kosygina 2, Moscow 119334, Russia*

³ *CNLS, Theoretical Division, Los Alamos National Laboratory*
Los Alamos, NM 87545, USA

received 27 January 2005; accepted in final form 22 March 2005

published online 15 April 2005

PACS. 36.20.-r – Macromolecules and polymer molecules.

PACS. 47.55.Kf – Multiphase and particle-laden flows.

PACS. 82.35.Lr – Physical properties of polymers.

Abstract. – We study the dynamics of a single polymer subject to thermal fluctuations in a linear shear flow. The polymer is modeled as a finitely extendable nonlinear elastic (FENE) dumbbell. Both orientation and elongation dynamics are investigated numerically as a function of the shear strength, by means of a new efficient integration algorithm. The results are in agreement with recent experiments.

Introduction. – Nowadays, thanks to the development of effective experimental techniques, it is possible to follow the motion of a single macromolecule in a flow, either laminar or turbulent [1–16]. This is of crucial importance for applications in polymer processing [17] and biophysics [1]. Dynamical properties of biomolecules have been explored in detail (see, *e.g.*, [1–5, 9–12] for DNA and [13] for chromatin) and protein-macromolecule interactions have been studied [14–16].

The formulation of theoretical models (see, *e.g.*, [17]) able to reproduce qualitatively and quantitatively these measurements represents an important step towards the understanding of single-molecule biophysics. An extensive analysis of single polymer dynamics in simple flows has been conducted in a series of papers by Chu and coworkers, Larson and coworkers and Shaqfeh and coworkers (see [1–8] and references therein). Here we mention in particular two recent papers where the statistics of orientation and conformation of long-chain molecules in linear shear flows has been studied in great detail, with a direct comparison with numerical models [18, 19]. An intrinsic difficulty is represented by the large number of degrees of freedom required to describe the polymer conformation, and thus its dynamics. Nonetheless, nontrivial aspects of polymer-fluid interactions may be accounted for and even explained at a semi-quantitative level by means of simple, few-degrees-of-freedom models. One of the simplest, yet reliable, model is the finitely extendable nonlinear elastic dumbbell (FENE) [17]. The polymer is described by its end-to-end distance vector \mathbf{R} and the microphysical properties are essentially dumped into two parameters: $1/\gamma$, the longest elastic relaxation time of the

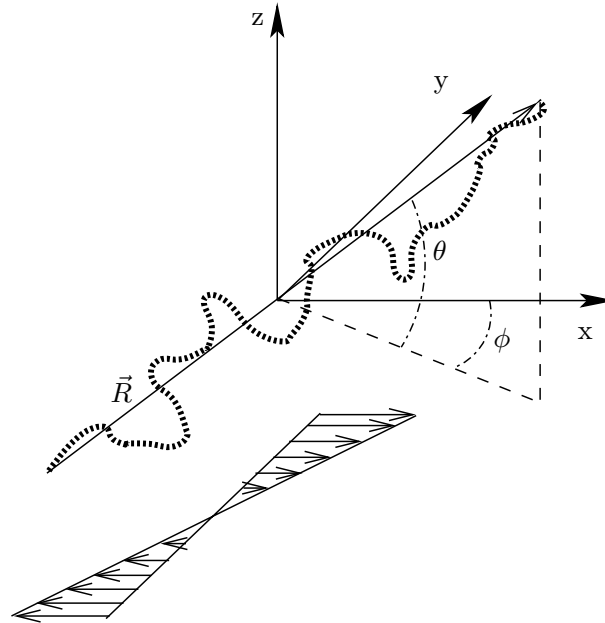


Fig. 1 – A sketch of the geometry of polymer motion in a linear shear flow.

macromolecule, and ζ , its friction coefficient with the surrounding solvent. Nonlinear elastic effects must be accounted for whenever the polymer is considerably stretched, as is the case of shear flows [4]. The geometry of this problem is depicted in fig. 1. The polymer spends a large fraction of time in elongated configurations along the shear direction. In the following we will present numerical results about end-to-end orientation, elongation and about the statistics of tumbling times. The latter is defined as the time spent between two successive “flips” of the polymer ends (see fig. 2). Tumbling can occur via different pathways, *e.g.* passing by a coiled state or through folded configurations: those details cannot be addressed within the single-dumbbell model and will be the subject of future study.

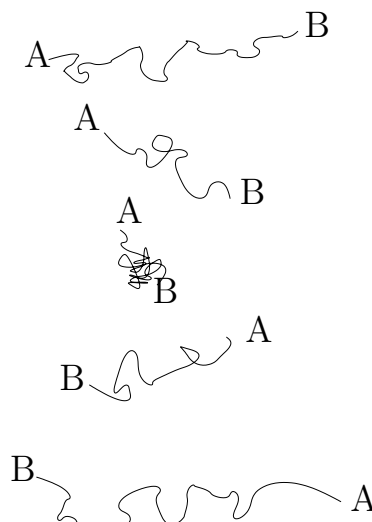


Fig. 2 – Four possible stages of a tumbling event.

From experiments to numerics. – Single polymer orientation and tumbling dynamics was recently studied experimentally by Steinberg *et al.* [10] with a 10^{-3} ppm solution of λ -DNA molecules labeled with fluorescence methods (but see also the experiments presented in [18, 19]). To resolve the angular dynamics two different flow configurations were used: one was generated by two discs one of which was rotating with uniform angular velocity Ω and the other flow was obtained by a boundary layer in a micro-channel produced with the soft lithography method (see [10] and references therein for details).

To reproduce the physical situation of [10] we studied a FENE dumbbell in a simple shear flow $\vec{v} = (sy, 0, 0)$, sensing thermal fluctuations (see fig. 1). The equation describing the evolution of the end-to-end vector of the polymer is

$$\dot{R}_i = s \delta_{ix} R_y - \frac{\gamma R_i}{2} (1 - R^2/R_m^2)^{-1} + \sqrt{\gamma R_0^2} \eta_i(t), \quad (1)$$

where $R_0 = K_B T/H$, $\gamma = 4H/\zeta$, $\boldsymbol{\eta}$ is a three-dimensional white noise with zero mean and correlation $\langle \eta_i(t) \eta_j(t') \rangle = \delta_{ij} \delta(t - t')$, R_m is the maximum length of the polymer, K_B is the Boltzmann constant, T is the temperature, ζ is the isotropic drag coefficient, and H the spring constant.

Even if the single-FENE-dumbbell model does not reproduce precisely the behavior of real molecules [8], we can set the parameters of our model, R_0 , R_m , γ , as close as possible to their corresponding experimental values [4, 10]: we choose $R_0 \simeq 1 \mu\text{m}$, $R_m/R_0 \simeq 21$, $\gamma \simeq 0.01 \text{ s}^{-1}$.

The orientation dynamics has been investigated for rigid spheroid by Hinch and Leal [20]. As for polymers, at large Weissenberg numbers $Wi = s/\gamma$, where s is the shear rate, the basic ingredients of the polymer dynamics can be summarized as follows [7, 20–25]: due to the shear flow the polymer tends to reach the unstable equilibrium configuration where it is fully extended along the shear direction. In polar coordinates $(R, \theta, \phi) = (R_m, 0, 0 \text{ or } \pi)$. The effect of thermal noise is to drive the polymer away from this configuration. The most probable value of θ is zero, due to the symmetry of the dynamics along the z -axis. However, large fluctuations in the off-shear-plane angle can occur. The most probable value for ϕ will be slightly larger than 0, or π : the symmetry-breaking effect of shear causes the polymers to “hesitate” for some time before crossing the x -axis and then give rise to a tumbling event. Few results can be obtained analytically for this model, except for the linear case where $R_m/R_0 \rightarrow \infty$.

Numerical algorithm. – Several numerical methods have been proposed to simulate polymer dynamics (see, for example, [26]). A commonly encountered problem with nonlinear elastic models is the loss of accuracy close to the singularity $R \rightarrow R_m$. In order to overcome this problem, it is possible to perform a change of variables in the vicinity of R_m that removes the singularity and allows to use a straightforward time-marching scheme. This method can be easily extended to other nonlinear models [27] as well as to other flows.

Equation (1) can be solved by any stochastic discretization scheme (Euler-Itô in our case) in the region $R < R_{thr}$, where R_{thr} is a fraction of R_m , say $0.5R_m$. Whenever R exceeds the threshold we switch to polar variables $(R, \hat{\mathbf{n}})$, where $\hat{\mathbf{n}}$ is the unity vector describing the orientation of the polymer $\hat{n}_i = R_i/R$, and then to the new variables $(z, \hat{\mathbf{n}})$, where

$$z = -\frac{R_m}{2} \left(1 - \frac{R}{R_m} \right)^2. \quad (2)$$

This relation can be easily inverted to give R as a function of z . After computing all the

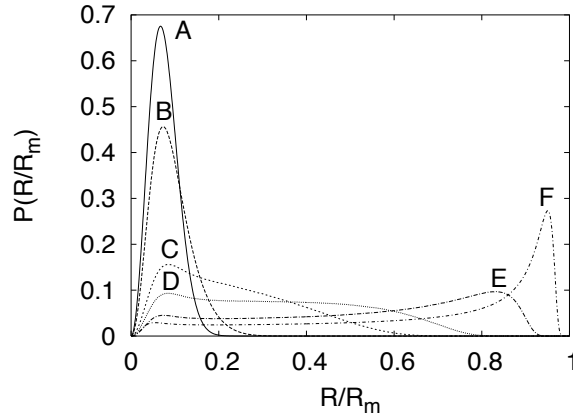


Fig. 3 – The PDF of elongation plotted for $Wi = 0, 1, 5, 10, 40, 200$ (from A to F).

contact terms in the Itô convention we have the following equations for $(z, \hat{\mathbf{n}})$:

$$\partial_t z = -\gamma R \left(1 + \frac{R}{R_m}\right)^{-1} - \frac{\gamma R_0^2}{2} \frac{1}{R_m} + \left(1 - \frac{R}{R_m}\right) \left(s \hat{n}_x \hat{n}_y R + \frac{\gamma R_0^2}{R} + \sqrt{\gamma R_0^2} \hat{n}_i \eta_i(t) \right), \quad (3)$$

$$\partial_t \hat{n}_i = s (\hat{n}_y - \hat{n}_y \hat{n}_x^2) \delta_{ix} - \frac{\gamma R_0^2}{R^2} \left(1 - \frac{R}{R_m}\right)^2 \hat{n}_i + \frac{\sqrt{\gamma R_0^2}}{R} (\eta_i(t) - \eta_j(t) \hat{n}_j \hat{n}_i). \quad (4)$$

which is regular in the neighborhood of $R = R_m$, *i.e.* $z = 0$.

Results. – The Probability Density Function (PDF) of the modulus of the conformation vector depends strongly on Wi . At sufficiently small $Wi \approx 1$, the statistics does not differ much from the linear elastic case, since $R \ll R_m$. The PDF in the FENE case can be computed analytically only in asymptotic regimes [25, 28]. The numerical result is shown in fig. 3 for several Weissenberg numbers. At very large Wi the elongation PDF presents a peak with height scaling as $Wi^{2/3}$ and width as $Wi^{-2/3}$ (not shown). This result is in agreement with the predictions of ref. [23]. As a side remark we notice that experimental measurements of the elongation PDF at Wi as large as $Wi = 76$ do not display a peak near R_m (see [8] and fig. 5 of [4]) as well as numerical results of multi-beads models (see figs. 4, 5 in [8] and the discussion therein).

The orientation of polymers follows the qualitative picture drawn in the linear elastic case [24, 25], even though there appear important quantitative differences. The PDF of the in-shear-plane angle ϕ is shown in fig. 4. The probability is concentrated in the vicinity of $\phi = 0, \pi$ with a peak width at half height ϕ_t , whose dependency on Wi is shown in fig. 5. The case of a linear elastic dumbbell $R_m = \infty$ is shown for comparison. The angle ϕ_t decreases with Wi in both cases, *i.e.* the larger is Wi the narrower is the region around the x -axis where the polymer spends most of its time. The scaling can be derived by simple physical arguments: following Chertkov *et al.* [22], the evolution equation for ϕ in the region $\phi \ll 1$ is approximated by $\partial_t \phi = -s \phi^2 + \sqrt{\gamma R_0^2 / R^2} \eta_\phi$, where η_ϕ is a white noise. Thus ϕ_t can be estimated balancing shear and noise terms in the right-hand side terms, *i.e.* $\phi_t \sim Wi^{-1/3} (R_0/R)^{2/3}$. At large Wi , for a linear elastic dumbbell one has $R \propto Wi$, yielding $\phi_t \sim Wi^{-1}$, whereas for a nonlinear elastic force one estimates $R \sim R_m$ to find $\phi_t \sim Wi^{-1/3}$. The tails of the PDF follow closely the distribution $\sin^{-2} \phi$ dictated by the shear (see fig. 4).

The agreement with the experiments is very good [10]: the scaling in the tail follows

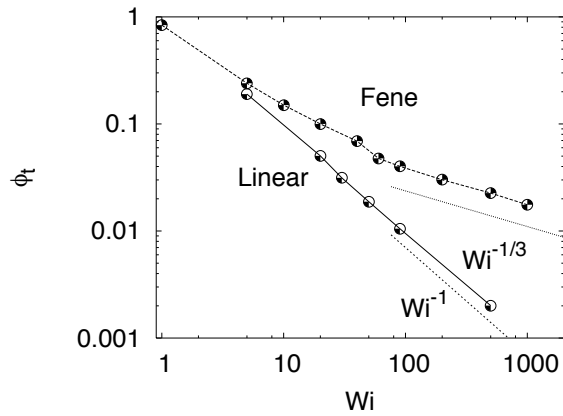
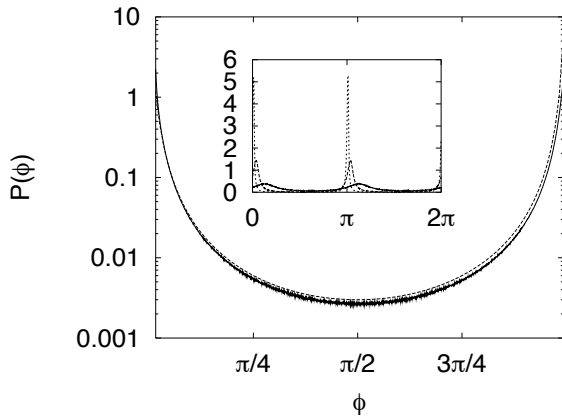


Fig. 4

Fig. 5

Fig. 4 – The PDF of the angle ϕ plotted with $\sin^{-2} \phi$. In the inset the PDF in linear scale plotted for $Wi = 1, 5, 40$.

Fig. 5 – The behavior of ϕ_t as a function of Wi .

$\sin^{-2} \phi$, and the dependence of ϕ_t on Wi is close to the theoretical prediction already for $Wi = 25$.

The marginal PDF of the angle θ is presented in fig. 6. The tails decay as θ^{-2} , with a scaling range increasing with Wi . The algebraic behavior has been observed in [10] for $Wi = 17.6$, and even if Wi is not very high the agreement is remarkable. The probability density of θ for small angles $\phi \sim \phi_t$, or equivalently the joint PDF $P(\theta, \phi = 0)$, shows a neat power law close to θ^{-3} for $\theta \gg \theta_t$. This nontrivial scaling behavior has been predicted theoretically and observed numerically for the linear elastic case in refs. [22,24,25]. The width of the peak of the $P(\theta)$ at half height, θ_t , decays as $Wi^{-1/3}$ for the nonlinear elastic case (see fig. 7). The agreement with experimental data is perfect [10].

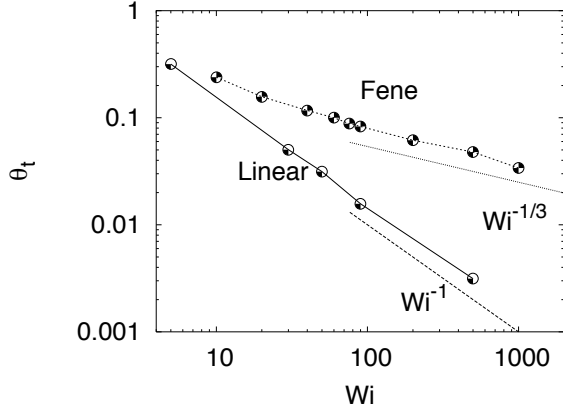
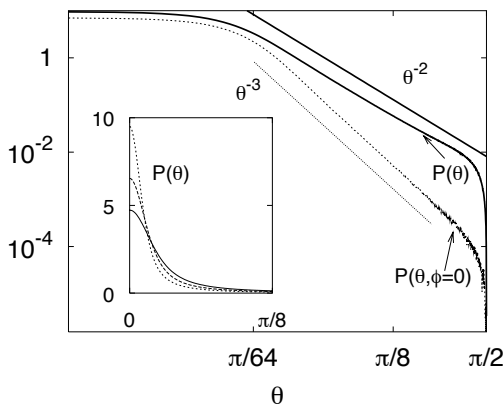


Fig. 6

Fig. 7

Fig. 6 – The PDF of the angle θ plotted against θ^{-2} . In the inset the PDF in linear scale for $Wi = 20, 40, 100$.

Fig. 7 – The behavior of θ_t as a function of Wi .

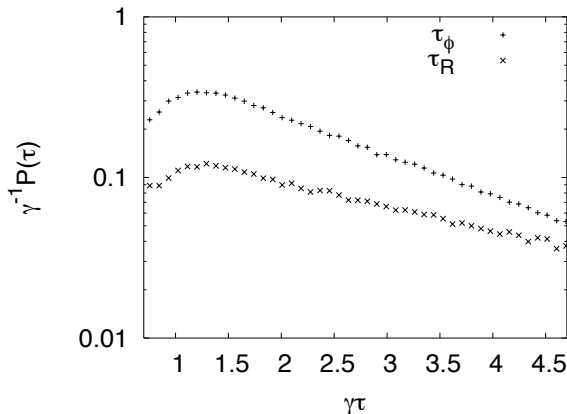


Fig. 8

Fig. 8 – The PDF of tumbling times: τ_R is the time elapsed between two nonadjacent coiled states, defined as the states where R is smaller than λR_0 ($\lambda = 1.5$ in this figure); τ_ϕ is defined as the time between two rotations of π in the angle ϕ . Here, $Wi = 76$.

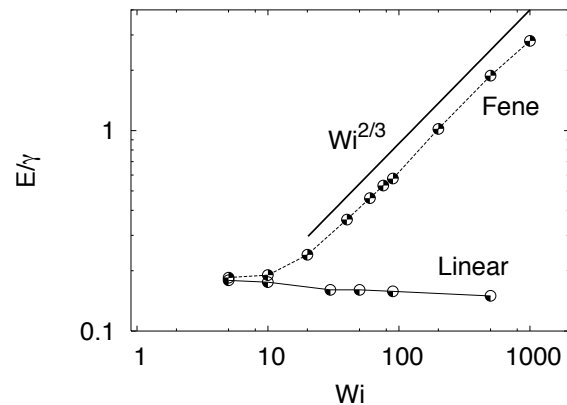


Fig. 9

Fig. 9 – The exponent E rescaled with the relaxation time as a function of Wi in the linear case and in the FENE case.

Note that the crossover between the linear elastic case $\phi_t \sim \theta_t \sim Wi^{-1}$ and the FENE case $\phi_t \sim \theta_t \sim Wi^{-1/3}$ occurs at $Wi \sim 1$, as measured experimentally.

For what concerns the tumbling times statistics there are two possible definitions [25]: i) given an appropriate threshold value in R that defines the coiled state for the polymer, one can compute the time spent during two successive coiled states [10]. ii) One can consider the time between two subsequent crossings of the plane $\phi = \pi/2$.

Both definitions are ambiguous for small values of Wi , *i.e.* when the polymer spends most of its time in a coiled state. For large tumbling times the PDF is exponential for both definitions of τ , $P(\tau) \sim \exp[-E\tau]$ (see fig. 8). This is a robust feature of this phenomenon [10, 22]. Experimental measurements of the tumbling time are possible only following the first definition, due to lack of angular resolution [10].

The exponent E of the tail in the linear elastic case is inversely proportional to the relaxation time of the polymer γ^{-1} . In the FENE case there is a nontrivial dependence on Wi , as shown in fig. 9. The scaling of the typical tumbling time $\tau_t \sim E^{-1}$ can be estimated at large Wi as follows: the angular motion in the region $\phi \sim \phi_t$ is driven by the thermal noise and is therefore diffusive. The diffusion coefficient is $D = \gamma(R_0/R)^2$ and therefore $\tau_t \sim \phi_t^2/D$. Substituting $R \propto R_0 Wi$ for the linear spring model and $R \sim R_m$ for the FENE model one obtains for E/γ the scalings Wi^0 and $Wi^{2/3}$, respectively.

The behavior of the PDF at $\tau \ll \tau_t$ is model dependent and should not be considered as relevant (see, *e.g.*, [25]). In experiments [10] the exponential tail of the PDF is observed and the dependence of τ_t on Wi is in accordance with theoretical arguments and numerical results.

Conclusions. – We studied the dynamics of a single FENE polymer immersed in a simple shear flow with thermal noise. The statistics of orientation, elongation and tumbling of the polymer have been analyzed in comparison with experimental measurements [10], previous numerical simulations [8, 25], and theoretical expectations [22–24]. Even if the large variety of conformations of real polymers cannot be explored within such a simple model, single-FENE-dumbbell can reproduce semiquantitatively several aspects of the behavior of real polymers.

* * *

We acknowledge innumerable inspiring discussions with M. CHERTKOV, V. LEBEDEV and V. STEINBERG. This work was supported by EU network HPRN-CT-2002-00300, and by the PROCOPE grant No. 07574. AP and KT acknowledge CNLS at Los Alamos National Laboratory for hospitality and support. KT was also supported by RFBR grant 04-02-16520a.

REFERENCES

- [1] CHU S., *Philos. Trans. R. Soc. London, Ser. A*, **361** (2003) 689.
- [2] PERKINS T. T., SMITH D. E. and CHU S., *Science*, **276** (1997) 2016.
- [3] SMITH D. E. and CHU S., *Science*, **281** (1998) 1335.
- [4] SMITH D. E., BABCOCK H. P. and CHU S., *Science*, **283** (1999) 1724.
- [5] HUR J. S., SHAQFEH E., BABCOCK H. P., SMITH D. E. and CHU S., *J. Rheol.*, **45** (2001) 421.
- [6] LI L., LARSON R. G. and SRIDHAR T., *J. Rheol.*, **44** (2000) 291.
- [7] DOYLE P. S., SHAQFEH E. S. G. and GAST A. P., *J. Fluid Mech.*, **334** (1997) 251.
- [8] HUR J. S., SHAQFEH E. and LARSON R. G., *J. Rheol.*, **44** (2000) 713.
- [9] GERASHCHENKO S., CHEVALLARD C. and STEINBERG V., *Single polymer dynamics: coil-stretch transition in a random flow*, submitted to *Phys. Rev. Lett.* (see also nlin.CD/0404045).
- [10] GERASHCHENKO S. and STEINBERG V., *Statistics of tumbling of a single polymer molecule in shear flow*, submitted to *Phys. Rev. Lett.* (see also nlin.CD/0503028).
- [11] LADOUX B., QUIVY J., DOYLE P. S., AMOUZNI G. and VIOVY J., *Science Prog.*, **84** (2001) 267.
- [12] MANNEVILLE S., CLUZEL P., VIOVY J.-L., CHATENAY D. and CARON F., *Europhys. Lett.*, **36** (1996) 413.
- [13] CUI Y. and BUSTAMANTE C., *Proc. Natl. Acad. Sci. U.S.A.*, **97** (2000) 127.
- [14] HEGNER M., SMITH S. B. and BUSTAMANTE C., *Proc. Natl. Acad. Sci.*, **96** (1999) 10109.
- [15] YIN H., WANG M. D., SVOBODA K., LANDICK R., BLOCK S. M. and GELLES J., *Science*, **270** (1995) 1653.
- [16] WUITE G. J., SMITH S. B., YOUNG M., KELLER D. and BUSTAMANTE C., *Nature*, **404** (2000) 103.
- [17] BIRD R. B., CURTISS C. F., ARMSTRONG R. C. and HASSAGER O., *Dynamics of Polymeric Liquids*, Vol. **II** (Wiley, New York) 1987.
- [18] SCHROEDER C. M., TEIXEIRA R. E., SHAQFEH E. S. G. and CHU S., *Macromolecules*, **38** (2005) 1967.
- [19] TEIXEIRA R. E., BABCOCK H. P., SHAQFEH E. and CHU S., *Macromolecules*, **38** (2005) 581.
- [20] HINCH E. J. and LEAL L. G., *J. Fluid Mech.*, **52** (1972) 683.
- [21] LIU T. W., *J. Chem. Phys.*, **90** (1989) 5826.
- [22] CHERTKOV M., KOLOKOLOV I., LEBEDEV V. and TURITSYN K., *J. Fluid Mech.*, **531** (2005) 251.
- [23] CHERTKOV M., KOLOKOLOV I., LEBEDEV V. and TURITSYN K., *Statistics of polymer extension in random flow with mean shear*, cond-mat/0411705.
- [24] TURITSYN K., *Polymer dynamics in chaotic flows with strong shear component*, submitted to *Phys. Rev. E* (see also nlin.CD/0501025).
- [25] PULIAFITO A. and TURITSYN K., *Numerical study of polymer tumbling in linear shear flows*, submitted to *Physica D*.
- [26] ÖTTINGER H. C., *Stochastic Processes in Polymeric Liquids* (Springer, Berlin) 1995.
- [27] MARKO J. F. and SIGGIA E. D., *Macromolecules*, **28** (1995) 8759.
- [28] VINCENZI D. and AFONSO M. M., *Nonlinear elastic polymers in random flow*, submitted to *J. Fluid Mech.*



Numerical study of polymer tumbling in linear shear flows

A. Puliafito^{a,c,*}, K. Turitsyn^{a,b,c}

^a INLN, UMR 6618 CNRS, 1361, Route des Lucioles, 06560 Valbonne, France

^b Landau Institute for Theoretical Physics, Kosygina 2, Moscow 119334, Russia

^c CNLS, Theoretical Division, Los Alamos National Laboratory, Los Alamos, NM 87545, USA

Received 18 March 2005; received in revised form 27 July 2005; accepted 27 July 2005

Available online 16 August 2005

Communicated by M. Vergassola

Abstract

We investigate numerically the dynamics of a single polymer in a linear shear flow. The effects of thermal fluctuations and randomly fluctuating velocity gradients are both analyzed. Angular, elongation and tumbling time statistics are measured numerically. We perform analytical calculations and numerical simulations for a linear single-dumbbell polymer model comparing the results with previous theoretical and experimental studies. For thermally driven polymers the balance between relaxation and thermal fluctuations plays a fundamental role, whereas for random velocity gradients the ratio between the intensity of the random part and the mean shear is the most relevant quantity. In the low-noise limit, many universal aspects of the motion of a polymer in a shear flow can be understood in this simplified framework.

© 2005 Elsevier B.V. All rights reserved.

Keywords: Fluid dynamics; Single polymer dynamics

1. Introduction

Thanks to recent improvements in experimental techniques it is nowadays possible to follow the motion of individual molecules in solvents [1–9]. The characterization of polymer dynamics at the level of a single molecule is a first step towards the understanding of mechanical interactions between biomolecules (see, e.g. [10–17]), of the fundamental rheology of polymer solutions, and of the viscoelastic properties of more complex flows (see, for example [18], and references therein for elastic turbulence).

Recently measurements of elongation and orientation with respect to simple external flows have been performed [7,9] in order to analyze how the conformation of a single molecule can be modified by an external field.

* Corresponding author. Tel.: +33 4 92 96 73 35; fax: +33 4 93 65 25 17.

E-mail address: alberto.puliafito@inln.cnrs.fr (A. Puliafito).

As the number of degrees of freedom needed to fully describe a macromolecule is extremely high it is necessary to formulate theoretical models, to verify them with numerical simulations, to simplify the problem, and to understand which observables play a key role.

Large numbers of papers have been written on the subject of single polymer dynamics in shear flows from experimental, numerical and theoretical viewpoint by Chu, Larson, Shaqfeh and their respective collaborators.

A polymer molecule in a plane, linear, steady shear flow is oriented in the flow direction by the velocity field. As the rotational motion of the polymer is determined only by the velocity difference in the space points, when it is aligned along the shear direction the external flow effect becomes negligible, and the thermal noise is the most relevant external force. Thermal fluctuations can push the polymer to regions where the external flow is relevant again. In these cases the shear flow can induce a fast rotation and align the polymer again along the (reverse) flow direction, i.e. the polymer tumbles [21,3,4,8,9,7].

This phenomenon can happen via several conformational pathways due to the complexity of the motion of a polymer molecule (see, for example [8,9]), and can be fully described only by taking into account all the degrees of freedom of the polymer. Unfortunately in the framework of these complex polymer models it is very difficult to obtain analytical results.

The main goal of our paper is to test numerically the predictions of recent theoretical and experimental studies [20,7] in a framework in which analytical results can be obtained [23], and to analyze the statistics of the tumbling times, i.e. the time between two subsequent flips of the polymer [21,3,7]. The simplest model that reproduces qualitatively the behavior of polymers is the dumbbell model [22]. This model allows one to carry out some analytical calculations in the case which we analyze [19,20,24,23], it is very easy and fast to simulate numerically (see Section 2 and [25]) and reproduces qualitatively recent experimental results [3,7].

The paper is organized as follows: in Section 2, the evolution equation of the polymer and the numerical methods are briefly explained. Section 3 is devoted to the analysis of the statistics of thermal fluctuations of a flexible polymer placed into a linear shear flow. In our work we present the analysis of the stationary distribution of the polymer end-to-end vector and we study the distribution function of the polymer tumbling time, which can be measured experimentally. In Section 4, we study the angular dynamics of strongly elongated polymers, for which the size fluctuations are negligible. Finally, in Section 5, we study the elongation statistical properties of the end-to-end vector in a random flow with a large mean shear.

2. Basic relations and numerical analysis

We wish to analyze the behavior of a polymer in a generic simple shear flow experiencing the Langevin force [19]. In general there are two effects of the velocity field on a polymer molecule: the Lagrangian advection of the polymer and the elongation/relaxation dynamics due to velocity gradients. In all the cases discussed in this paper we disregard the Lagrangian dynamics by staying in the reference frame of the polymer center of mass. For the internal degrees of freedom of the polymer we use the simple dumbbell model [22], leaving the analysis of more realistic models for future studies [26]. In this case the basic equation describing the evolution of the polymer end-to-end vector \mathbf{R} has the following form:

$$\dot{R}_i = \sigma_{ij} R_j - \gamma R_i + \sqrt{\frac{2\gamma R_0^2}{3}} \xi_i, \quad (1)$$

where $\sigma_{ij} = \partial_j v_i$ is the velocity gradient matrix, γ the polymer relaxation rate, ξ the thermal noise term, which has white-noise statistics: $\langle \xi_i(t) \xi_j(t') \rangle = \delta_{ij} \delta(t - t')$, and R_0 is the equilibrium length in the absence of an external field.

For incompressible flows there is no ambiguity in the discretization of the stochastic differential equation (1), and no additional contact term must be taken into account, so we resort to the Euler–Itô scheme without any loss of generality.

When the gradient σ contains only a steady linear shear contribution we can write down the formal solution of (1) as:

$$\dot{R}_i(t) = R_i(0)e^{-\gamma t} + e^{-\gamma t} \int_0^t e^{\gamma t'} s_{ij} R_j(t') \delta_{ix} \delta_{jy} dt' - \gamma e^{-\gamma t} \int_0^t e^{\gamma t'} R_i(t') dt' + \sqrt{\frac{2\gamma R_0^2}{3}} e^{-\gamma t} \int_0^t e^{\gamma t'} \xi_i(t') dt'. \quad (2)$$

This equation can be discretized, and the terms containing the thermal noise can be rewritten as new gaussian variables with amplitudes that can be computed directly, so that the final solution reads:

$$R_x^{k+1} = R_x^k e^{-\gamma \Delta t} + \sqrt{\frac{R_0^2}{3}} (1 - e^{-2\gamma \Delta t}) \eta_x^k + s \Delta t e^{-\gamma \Delta t} R_y^k + s \frac{R_0}{\sqrt{3}} \eta_y^k \\ \times \sqrt{\left[\frac{1}{2\gamma^2} (1 - e^{-2\gamma \Delta t}) - \frac{1}{\gamma} \Delta t e^{-2\gamma \Delta t} - \Delta t^2 e^{-2\gamma \Delta t} \right]} \quad (3)$$

$$R_i^{k+1} = R_i^k e^{-\gamma \Delta t} + \sqrt{\frac{R_0^2}{3}} (1 - e^{-2\gamma \Delta t}) \eta_i^k, \quad i = y, z \quad (4)$$

where $\langle \eta_i^k \eta_j^l \rangle = \delta_{ij} \delta^{kl}$. The subscripts stand for the cartesian coordinates while the superscripts stand for the discretized time. As expected in the limit $\Delta t \rightarrow 0$ there is no contribution of η_y in the first equation and the amplitudes are the same as in Eq. (1).

In the case of a random velocity gradient, w_{ij} , we have to generate the variables w_{ij}^k such that they have the prescribed correlation function:

$$\langle \sigma_{ij}(t) \sigma_{kl}(t') \rangle = D \delta(t - t') (4\delta_{ik} \delta_{jl} - \delta_{il} \delta_{kj} - \delta_{ij} \delta_{kl}), \quad (5)$$

where again the Dirac delta function is substituted by a Kronecker symbol. In this case the modulus of the vector \mathbf{R} grows indefinitely so that we can normalize it at each time step. In order to describe the elongation properties we can compute the maximum Lyapunov exponent λ and the corresponding finite time Lyapunov exponent λ_T [27].

3. Thermally driven polymers

In this section we will examine the case of a linear steady shear flow in the plane XY : $\sigma_{ij} = s \delta_{ix} \delta_{jy}$, where s is the shear rate. Eq. (1) has an explicit solution of the following form:

$$R_i(t) = \exp(-\gamma t) W_{ij}(t) R_j(0) + \int_0^t dt' \exp[-\gamma(t - t')] W_{ij}(t - t') \xi_j(t'), \quad (6)$$

where $W(t) = \exp(t\sigma)$. At large times the initial polymer elongation is forgotten and after averaging over the thermal fluctuations ξ one can easily obtain the following distribution function:

$$P(\mathbf{R}) = (2\pi)^{-3/2} (\det I)^{-1/2} \exp \left[-\frac{1}{2} \mathbf{R}^T I^{-1} \mathbf{R} \right] \quad (7)$$

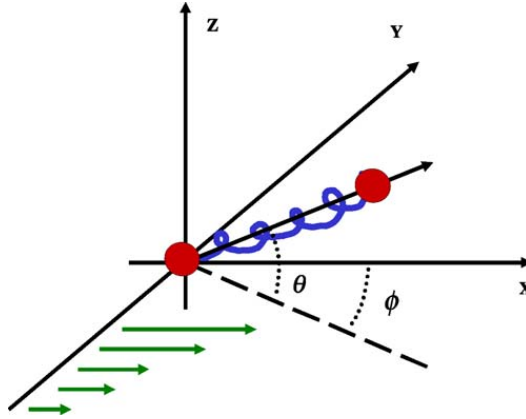


Fig. 1. Schematic figure explaining polymer orientation geometry.

$$I = \frac{2\gamma R_0^2}{3} \int_0^\infty \exp(-2\gamma t) W(t) W^T(t). \quad (8)$$

The probability density function (PDF) (7) is valid for any velocity gradient. In the particular case of a steady shear flow in the XY plane, as shown in Fig. 1, the matrices can be found explicitly:

$$W(t) = \begin{pmatrix} 1 & st & 0 \\ 0 & 1 & 0 \\ 0 & 0 & 1 \end{pmatrix}, \quad I = \frac{R_0^2}{3} \begin{pmatrix} 1 + \frac{s^2}{2\gamma^2} & \frac{s}{2\gamma} & 0 \\ \frac{s}{2\gamma} & 1 & 0 \\ 0 & 0 & 1 \end{pmatrix}, \quad (9)$$

where the axis are sorted in the order X – Z . One can see that for large Weissenberg numbers $Wi = s/\gamma \gg 1$, the mean polymer elongation in the X -direction is much larger than in transversal directions.

3.1. Elongation PDF

The PDF of elongation can be easily computed from (7): the elongation in the y - and z -direction are independent of Wi and the two marginal PDFs are gaussian with zero mean value and variance $\langle R_y^2 \rangle = \langle R_z^2 \rangle = R_0^2/3$, while in the mean flow direction the variance is $\langle R_x^2 \rangle = (R_0^2/3) (1 + (1/2)Wi^2)$ (Fig. 2).

The distribution function of \mathbf{R} cannot be obtained analytically for an arbitrary value of Wi , but one can study its behavior in two limiting cases. For $Wi \ll 1$ the effect of the shear flow can be neglected, and we have the simple thermally driven polymer with linear relaxation force. The distribution function of its elongation has a simple gaussian form [22]:

$$P(R) = \sqrt{\frac{2}{\pi}} \frac{R^2}{R_0^3} \exp \left[-\frac{R^2}{2R_0^2} \right]. \quad (10)$$

In the opposite case $Wi \gg 1$ the system is strongly anisotropic and the main contribution to the polymer elongation comes from the X component. This fact allows one to obtain the right tail of the elongation PDF. For $R \gg R_0$ one has

$$P(R) = \sqrt{\frac{12}{\pi(2 + Wi^2)}} \frac{1}{R_0} \exp \left[-\frac{3R^2}{(2 + Wi^2)R_0^2} \right]. \quad (11)$$

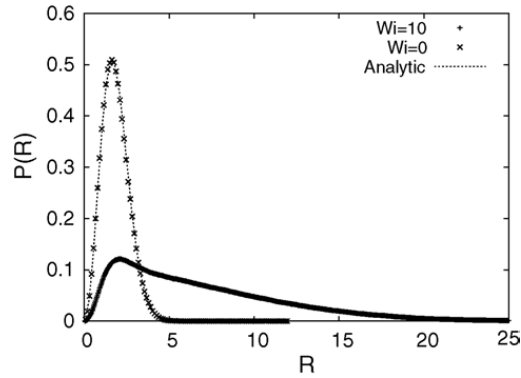


Fig. 2. The PDF of the modulus of the end-to-end vector R for different Wi numbers. While for $Wi = 0$ the PDF is concentrated around the radius of equilibrium, for higher values of Wi it is broader and the high elongation configurations become more and more probable.

3.2. Angular PDF

Next we are interested in the orientation of the polymer. The angular distribution function will allow us to show that for large Wi the polymer spends most of the time aligned to the X -axis, while for $Wi \ll 1$ the orientation distribution is almost isotropic. In order to parameterize the orientation of the polymer we introduce the angles ϕ and θ as shown in Fig. 1. The angle ϕ represents the deviation of the polymer end-to-end vector from the X -axis in the shear velocity plane XY while the angle θ gives us the polymer deviation in the transversal direction Z . Switching to spherical coordinates we have $R_x = R \cos \theta \cos \phi$, $R_y = R \cos \theta \sin \phi$, $R_z = R \sin \theta$. After integrating over the polymer elongation in Eq. (7) one immediately obtains the angular PDF:

$$\mathcal{P}(\phi, \theta) \propto \frac{\cos \theta}{\{1 - (\cos^2 \theta / (4 + Wi^2)) [Wi^2 \cos(2\phi) + 2Wi \sin(2\phi)]\}^{3/2}}. \quad (12)$$

The calculation of the two marginal PDFs is not possible in general, and we have to integrate Eq. (12) numerically (Figs. 3(a) and 4).

As one can see in Fig. 4, the PDF of θ decays as a power law (asymptotically $\mathcal{P}(\theta) \sim \theta^{-2}$ in the region $\phi_t \ll \theta \ll 1$), and is symmetric about $\theta = 0$. The higher the value of Wi , the wider is the power law region.

In principle, if the polymer tumbles in the shear plane, we should consider a time-dependent PDF of ϕ on a unbounded domain. However, if we consider ϕ to be between 0 and 2π one arrives at a stationary PDF, peaked in

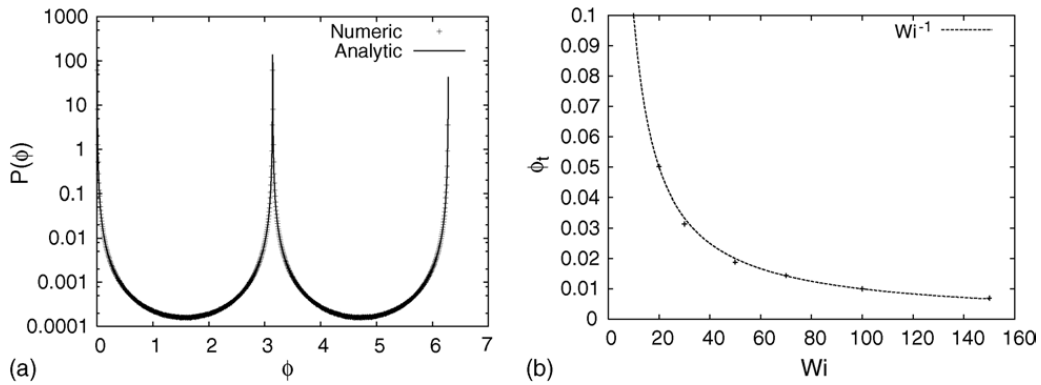


Fig. 3. The PDF of the angle ϕ . (a) The analytic PDF is the numerical integration of (12), while the dots come from the numerical simulations. (b) The amplitude of the PDF's peak ϕ_t as a function of Wi .

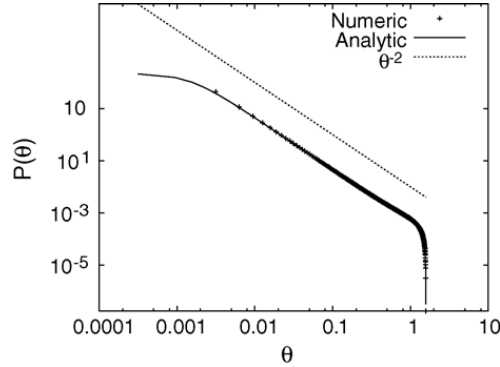


Fig. 4. The PDF of the angle θ is symmetric with respect to $\theta = 0$ and can be described by a power law relationship over a wide range of values of θ .

the regions $\phi = k\pi + \phi_t$, $k = 0-2$ (Fig. 3(a)), where $\phi_t \sim 1/Wi$ as shown in Fig. 3(b). In the region where $\phi \gg \phi_t$ we have $\mathcal{P}(\phi) \sim \sin^{-2} \phi$.

The angular PDFs tell us that any fluctuations in θ are not relevant to the tumbling dynamics, and that for the angle θ there is no relevant scale. The fact that increasing Wi the power law region becomes wider and wider means that when the shear is much stronger than the relaxation the polymer is nearly aligned with the X -axis. The PDF of the angle ϕ expresses the fact that the polymer spends most of the time in the vicinity of $\phi = 0$, $\phi = \pi$, $\phi = 2\pi$. The polymer is aligned in the X -direction as a result of the shear flow, it fluctuates for a certain time in the region $\phi \sim \phi_t$, where the shape effects are strong. When thermally activated it goes beyond the region $\phi \gtrsim \phi_t$ and the shear becomes more important and induces a fast rotation of $\Delta\phi \simeq \pi$ or multiples thereof, that is the polymer tumbles.

3.3. Tumbling time distributions

In the previous two sections we have studied the stationary distribution functions which can be measured experimentally by averaging the polymer elongation and orientation over large time periods. However, as described in the introduction and in [20,23] the dynamics of the polymer is non-stationary, due to continuous tumbling. The natural question which arises is whether there are some quantities, which would allow experimental observation and quantitative description of the tumbling process. In the recent papers by Chu et al. [3,5], the different time correlation functions of the polymer elongation were studied, and it has been shown that they can have different forms in the presence of shear. Here we introduce the tumbling time, which can be measured experimentally [7] and used to describe the tumbling process. As described above the most striking difference between the tumbling dynamics of the polymer in a shear flow and spinning in a rotational flow is the a-periodicity of the tumbling process. Due to the stochastic nature of tumbling, the tumbling time, i.e. time between subsequent flips of the polymer, is a random variable with relatively large fluctuations. Our task is now to study the distribution function of the tumbling time and to give some theoretical and numerical predictions of its dependence on the Weissenberg number (Fig. 5.).

In the case of the dumbbell model, we can define tumbling as a flip of the polymer induced by the thermal noise. When the polymer is in an unstable equilibrium configuration $\phi = k\pi$, $k = 0-2$ the thermal noise can bring the polymer out of the region $\phi \sim \phi_t$, and this induces a fast rotation which takes a time of the order of s^{-1} . We define the tumbling time τ_ϕ as the interval between two subsequent flips. This is typically the time between subsequent crossings of the lines $\phi = (k + 1/2)\pi$. For $Wi \gg 1$, as shown in the previous section (see Fig. 3(a)), the polymer spends only a small fraction of the total time far from the shear direction, and therefore the exact value of the angular threshold defining the tumbling time is not very important. Indeed this time is made up of two contributions: the time spent in the region $\phi \sim \phi_t$ and the duration of the rotation of order s^{-1} . The latter can be neglected for large Wi .

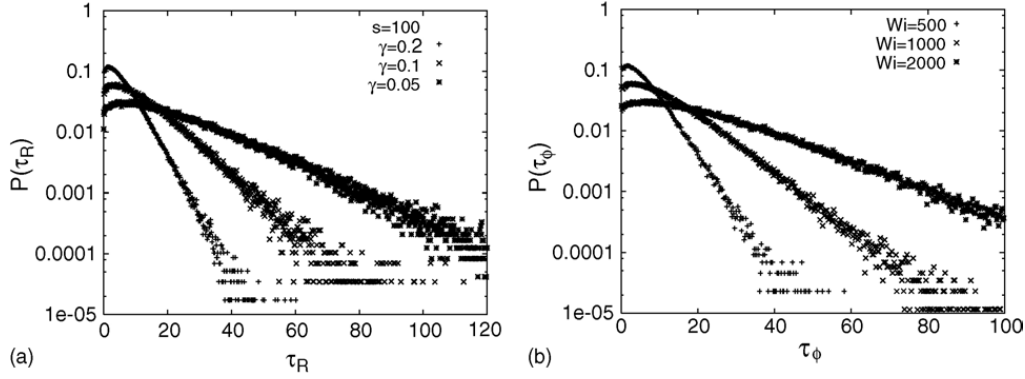


Fig. 5. The two different tumbling time PDFs. (a) The elongation-based tumbling time PDF. (b) The angle-based tumbling time PDF.

Experimental techniques do not always allow the polymer orientation angle ϕ to be resolved and therefore it is convenient to introduce another definition of the tumbling time (τ_R). This quantity measures the interval between subsequent changes between stretched and coiled polymer conformations. In other words, we start measuring when the length of the polymer exceeds a certain threshold value and we stop when it again becomes smaller than this threshold value.

While τ_ϕ is the most natural definition it can be difficult to measure experimentally. On the other hand, the PDF of τ_R depends in a non-universal way on the threshold, but experimental techniques allows it to be measured when the polymer is sufficiently stretched.

In order to analyze the behavior of the tumbling time PDFs at large Weissenberg numbers we should analyze the dynamics of the polymer elongation projected onto the X -axis (R_x). Indeed, the angle-based tumbling time τ_ϕ measures the time intervals between subsequent events when $R_x = 0$, while the elongation based tumbling time τ_R corresponds to the time intervals between crossings of a threshold value $R_x = R_{TH}$. In order to find how the shape of the tumbling time PDF changes with increasing Wi number, we can rescale the time and the polymer size in the following way: $R_x = xR_0 Wi$, $R_y = yR_0$, $t = \gamma^{-1}\tau$, which leads to the following equations:

$$\dot{x} = -x + y \quad (13)$$

$$\dot{y} = -y + \sqrt{\frac{2}{3}}\zeta_y \quad (14)$$

$$\langle \zeta_y(0)\zeta_y(\tau) \rangle = \delta(\tau). \quad (15)$$

In Eq. (13), we have omitted the term corresponding to ξ_x because it is negligible in the large Weissenberg number regime compared to the other terms. Note that these equations do not depend on the Weissenberg number, and it enters the problem only through the threshold R_{TH} . In our simulations we choose $R_{TH} = \sqrt{3}\langle R^2 \rangle \propto R_0 Wi$, so that in the dimensionless variables we have $x_{TH} = 1/\sqrt{2}$ which does not depend on Weissenberg number either. From this analysis we conclude that the tumbling time PDF at large Weissenberg numbers approaches some universal form: its peak is positioned at characteristic time scale of order γ^{-1} , and as γ increases the peak moves towards the origin. The problem of finding the exact form of this function is equivalent to the problem of finding the PDF of persistence times of a non-Markovian random process $x(\tau)$. This problem has recently attracted a lot of attention (see, e.g. ref. [28]), however no explicit solution is known for a general random process. Still it is possible to make some predictions on the PDF: the right tail of the PDF τ_R , $\tau_\phi \gg \gamma^{-1}$ is exponential and has the form $P(\tau_R) \propto \exp[-c_R\gamma\tau_R]$, $P(\tau_\phi) \propto \exp[-c_\phi\gamma\tau_\phi]$ because large tumbling times correspond to a large number $\gamma\tau \gg 1$ of unsuccessful attempts to cross the threshold. The correlation time of our stochastic process $R_x(t)$ is of order γ^{-1} , and therefore these attempts to cross the threshold are almost independent, and one should take the product of their probabilities, which leads to the above exponential laws. Both the PDFs of τ_ϕ and τ_R are not well

defined for $\tau_\phi \sim 0$, $\tau_R \sim 0$ since they are sensitive to brownian noise discretization: it is possible to tumble very rapidly when the polymer is coiled, and this is why the probability of measuring a tumbling time much smaller than s^{-1} is not zero. Both the tumbling time definitions do not work very well in the case of small Wi experimentally because of the high resolution needed, and numerically because of the discretization procedure.

4. Strongly elongated and rigid molecules

Another physical situation we are interested in is the dynamics of strongly elongated polymers in random flows. In this model, described in detail in [20,24,23], the polymer is placed into a random flow above the coil-stretch transition, where the effect of the thermal fluctuations can be neglected. In this case the orientational dynamics of the polymer are decoupled from the evolution of the elongation, so that we can introduce the unit vector $n_i = R_i/R$, obeying the following evolution equation:

$$\dot{n}_i = n_j(\delta_{ik} - n_i n_k) \nabla_j v_k. \quad (16)$$

The velocity gradient consists of a regular shear part (as in the previous section), and an isotropic incompressible random part. The polymer size in the experiments is always much smaller than the characteristic viscous scale of the velocity field which allows us to assume smoothness of the velocity field. We will also assume short-correlated velocity field which corresponds to the so called Kraichnan–Batchelor model, which has been extensively studied in recent years [29]. In the framework of this model the velocity gradient matrix $\sigma_{ij} = \nabla_j v_i$ in the Lagrangian frame is described by a gaussian process with the following pair-correlation function [30]:

$$\langle \sigma_{ij}(t) \sigma_{kl}(t') \rangle = D \delta(t - t') (4\delta_{ik} \delta_{jl} - \delta_{il} \delta_{kj} - \delta_{ij} \delta_{kl}), \quad (17)$$

where σ_{ij} is the gradient matrix of the random velocity component. Using the same notations as in the previous sections one arrives at the following dynamical equation for the angles:

$$\dot{\phi} = -s \sin^2 \phi + \xi_\phi, \quad (18)$$

$$\dot{\theta} = -s \frac{\sin(2\phi)}{2} \sin \theta \cos \theta + \xi_\theta, \quad (19)$$

where ξ_ϕ and ξ_θ are zero mean random variables related to the fluctuating components of the velocity gradient. The statistics of both ξ_ϕ and ξ_θ can be obtained from the correlation function (17):

$$\langle \xi_\theta(t) \xi_\theta(t') \rangle = 4D \delta(t - t') \quad (20)$$

$$\langle \xi_\phi(t) \xi_\phi(t') \rangle = \frac{4D}{\cos^2 \theta} \delta(t - t'). \quad (21)$$

Note that the measure of configurations with $\theta \sim \pi/2$ is small, thus making the formal singularity in Eq. (21) not essential. From Eq. (18) it turns out that the polymer experiences constant a-periodic tumbling in the XY plane [20,24,23].

4.1. Stationary angular PDF

From a dimensional analysis it can be shown that for $s \ll D$ the characteristic values of the angles ϕ , θ will be of order $(D/s)^{1/3} \ll 1$. In this region one can set $\cos \theta = 1$ in the expression (21) so that Eq. (18) becomes completely independent of θ . Hence in this limit one derives:

$$P_{st}(\varphi) = \frac{\omega}{D} \int_0^\infty d\phi \exp \left[-\frac{s}{8D} \phi(\phi - 2\varphi)^2 - \frac{s\phi^3}{24D} \right], \quad (22)$$

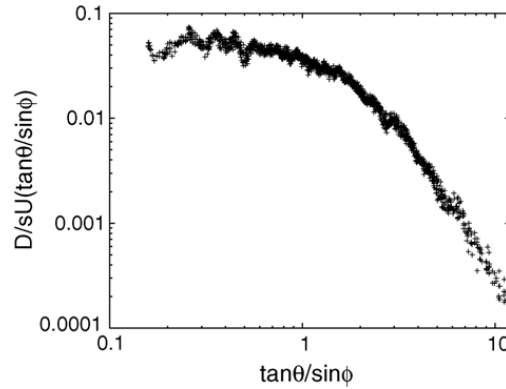


Fig. 6. The function $U(x)$, where $x = \tan \theta / \sin \phi$.

where ω is the mean rotation frequency of the polymer, which is determined from the normalization condition $\int_0^\pi P_{st}(\phi) d\phi = 1$ and is given by

$$\omega = \frac{(Ds^2)^{1/3}}{4 \times 3^{1/6} \Gamma(7/6) \sqrt{\pi}}. \quad (23)$$

The explicit form of the joint angular PDF is hard to compute analytically. However, one can obtain the expression for the tails of the PDF $\phi, \theta \gg (D/s)^{1/3}$ [24,19]:

$$P(\phi, \theta) = \frac{U(\tan \theta / \sin \phi)}{\sin^3 \phi \cos^2 \theta}, \quad (24)$$

where $U(x)$ is an unknown function with an universal argument. Numerical simulations confirms this prediction, as shown in Fig. 6.

The two marginal PDFs obtained by numerical simulations show a behavior similar to that of thermally driven polymers. Also the phenomenology of the systems are similar, but now all the quantities depend on the ratio between the amplitude of the random velocity gradient and the mean shear. The PDF of the angle ϕ has peaks at $\phi \sim \phi_t + k\pi, k = 0-2$, where $\phi_t \sim (D/s)^{1/3}$ and the PDF of θ has an algebraic core $\mathcal{P}(\theta) \sim \theta^{-2}$ for $(D/s) \ll 1$ (see Fig. 7).

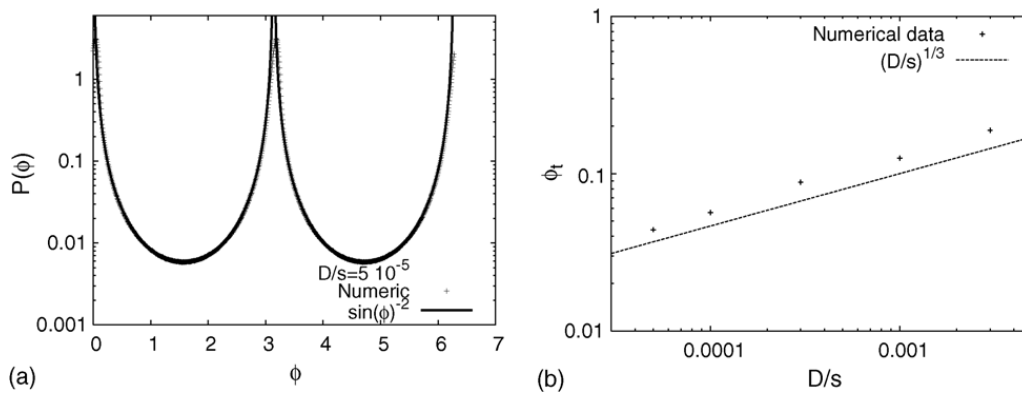


Fig. 7. The PDF of the angle ϕ . (a) The agreement between the PDF and $\sin^{-2} \phi$ is good in the region $\phi \gg \phi_t + k\pi, k = 0-2$. (b) The behavior of ϕ_t as a function of D/s , with the dotted line shown as a guide only.

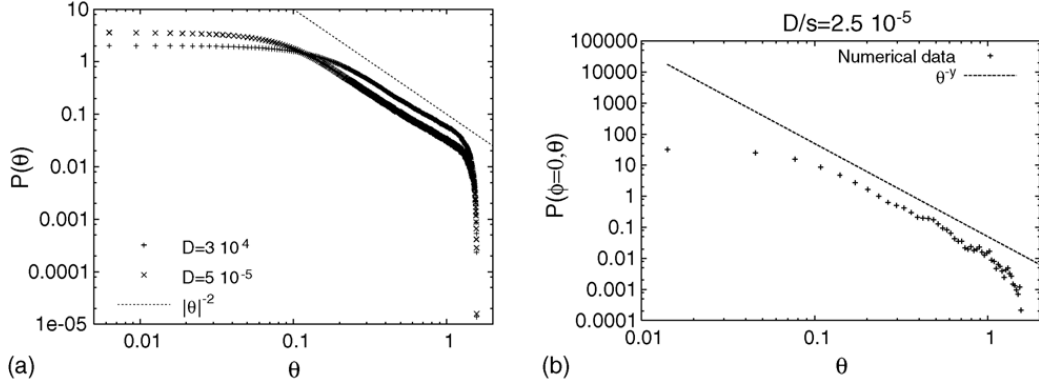


Fig. 8. The PDF of the angle θ . (a) The PDF of the angle θ is symmetric with respect to $\theta = 0$ and can be expressed by a power law in a wide range of θ . (b) The power law for the core region $\phi \sim 0$. For this case $y \sim 3$.

In the stochastic region $|\phi| \lesssim \phi_t$ the tails of the θ -angle PDF $P(\theta)$ are also algebraic $P(\phi = 0, \theta) \propto \theta^{-y}$, but the exponent y is non-universal and depends on the statistical properties of the random velocity gradient (see Fig. 8). It has been shown in [23] that a simple relation exists between the exponent y and the entropy Cramèr function $S(x)$ of the Lyapunov exponent of the system (see Section 5). For the non-universal exponent y the relation $y = S'(x)$ holds, where x is the solution of the equation $xS'(x) = S(x)$. Numerical simulations show that in the case of an isotropic, short correlated, random velocity, the value of the exponent is approximately $y \approx 3$, as shown in Fig. 8. This implies that it is subdominant on the background of the θ^{-2} tail coming from the regular dynamics region $|\phi| \gtrsim \phi_t$. However, in the general case of a finite-correlated and non-gaussian velocity field, one can imagine a situation where the non-universal exponent y becomes smaller than the universal one $y < 2$, and in this case the θ -angle distribution becomes non-universal.

4.2. Tumbling time distribution

For rigid polymers with a fixed size the tumbling time can be defined only through the angular dynamics and therefore we will refer only to τ_ϕ . The evolution time of this system is $\tau_t \sim (s\phi_t)^{-1}$ so we expect that both the width and the maximum of the tumbling time distribution are τ_t . The tails are related to the probability of passing (clock-wise) the angle ϕ_t after a large amount of independent attempts, and can be estimated as $\mathcal{P}(\tau) \sim e^{-E(Ds^2)^{1/3}\tau}$ [20]. In [23], it has been shown that the constant E is connected with the ground state energy value of a one-dimensional quantum-mechanical system and can be estimated with simple numerical analysis ($E \simeq 0.45$). It is possible to analyze the left tail of the tumbling time PDF:

$$p(\tau) \propto \exp \left[-\frac{2K^4(1/2)}{3Ds^2\tau^3} \right], \quad s^{-1} \ll \tau \ll (Ds^2)^{-1/3}, \quad (25)$$

where $K(x)$ is an elliptical integral of the first kind, and also to give an exact expression for the tail $\tau \ll s^{-1}$ of the PDF. For large values of s/D this tail can be barely observed experimentally or numerically, and the structure of the tail strongly depends on the statistics of the chaotic flow, and is therefore non-universal (see Fig. 9).

5. Polymer elongation in chaotic flows

In this final section we will study elongation statistics of the polymer in the case of random velocity plus mean shear. The polymer is not strongly elongated and can be treated as a linear dumbbell, as in Section 3. Such a situation

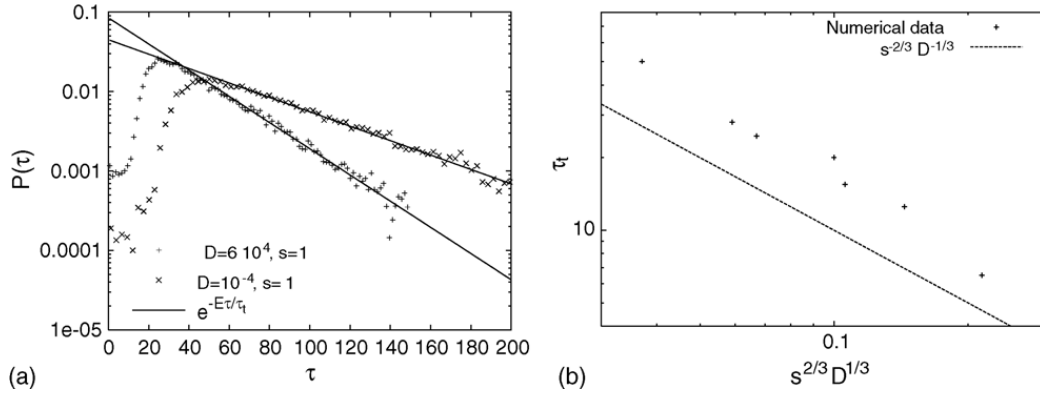


Fig. 9. The PDF of the tumbling time τ . (a) The exponential tail of the PDF. (b) The behavior of τ_t as a function of $s^2 D$.

corresponds to a flexible polymer in a chaotic flow below the coil-stretch transition[31]. Formally, this is the case when the maximum Lyapunov exponent is smaller than the inverse relaxation time $\lambda < \gamma$, where the Lyapunov exponent is the rate of divergence or convergence of two neighboring trajectories.

The equation governing the system is again Eq. (1) where the gradient of the velocity is decomposed into a regular shear part and a chaotic part. We can switch to spherical coordinates obtaining an evolution equation for the angles (as in Eqs. (18) and (19)) and an evolution equation for the modulus of the elongation vector [24,23]:

$$\partial_t \ln R = -\gamma + \frac{1}{2}s \cos^2 \theta \sin 2\phi + 6D + \eta, \quad (26)$$

where in our model we assume $\langle \eta(t)\eta(t') \rangle = 2D\delta(t - t')$. Dimensional arguments show that the Lyapunov exponent should be proportional to $(Ds^2)^{1/3}$ (see Fig. 10).

In this situation the polymer spends most of the time in the coiled state, but rare events lead to a large polymer stretching, when the flow becomes strong enough. It can be shown, that the right tails of polymer elongation PDF have the algebraic form $P(R) \propto R^{-1-q}$ [32,23], where the exponent q depends on the parameters of the system. While in the thermal noise case the tails were Gaussian, here the probability of observing the polymer stretched is strongly enhanced. The algebraic behavior of the tail can be easily explained: the probability of having a local stretching rate $\lambda > \gamma$ for a large time t decays exponentially with t , and during such events the polymer is stretched by a factor which grows exponentially with the time t .

It has been shown in [32,23] that the exponent q is related with the Cramèr function of the Lyapunov exponent of the flow [29]. This function can be found explicitly only in few cases, hence the main aim of this section is to

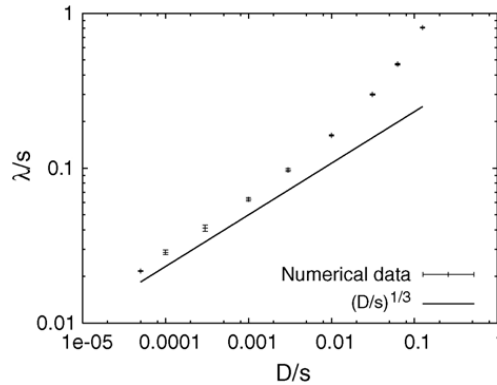


Fig. 10. The behavior of the Lyapunov exponent as a function of D/s .

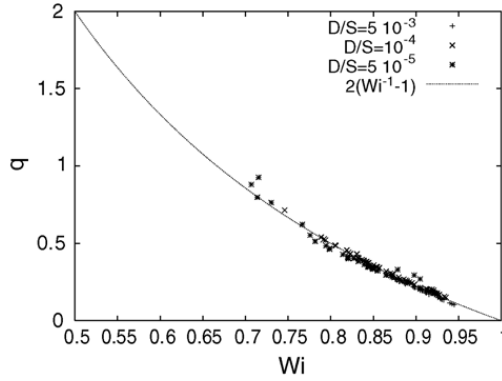


Fig. 11. The exponent of the elongation PDF as a function of Wi .

present numerical measurements of the Cramèr function and of the dependence of the exponent q on the Weissenberg number $Wi_\lambda = \lambda/\gamma$ below the coil-stretch transition (i.e. $Wi_\lambda < 1$). As shown in [23] the large deviation theory predicts that for large averaging times $T \gg (Ds^2)^{-1/3} \equiv \tau_T$ the PDF of the Lyapunov exponent is:

$$P(\lambda_T) \sim \exp\left(-\frac{T}{\tau_T} S(\lambda_T \tau_T)\right), \quad T \gg \tau_T, \quad (27)$$

where the function $S(x)$ is the Cramèr function. Note that for large but finite values of T/τ_T the measured Cramèr function $S_T(x) = -(\tau_T/T) \log P_T(x/\tau_T)$ depends on the time T , but the difference between $S_T(x)$ and $S(x)$ is significant only in the region $|x| \gtrsim T/\tau_T \gg 1$. Therefore in order to calculate the core of the Cramèr function we can use the finite time approximation. In our simulations we considered the ratio T/τ_T from 10 up to 280.

In order to connect the Cramèr function with the exponent q in the elongation PDF we need to use the Legendre transform (see refs. [32,23] for details):

$$S(x) - xS'(x) + \gamma\tau_T S'(x) = 0 \quad (28)$$

$$q = S'(x). \quad (29)$$

In [32,33], the behavior of q in the case of zero mean shear has been computed, and the calculations leads to:

$$q = \frac{2}{\Delta} (\gamma - \lambda), \quad (30)$$

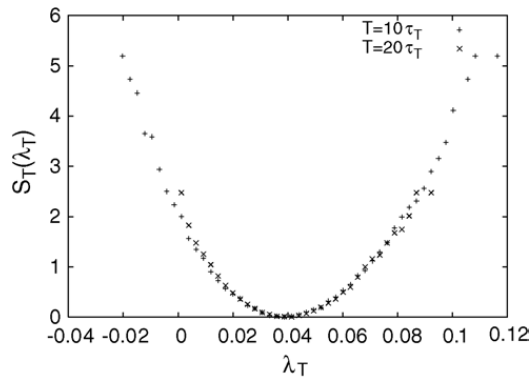


Fig. 12. The Cramèr function for two different times.

where Δ is the variance of the Lyapunov exponent distribution. In the case of Kraichnan field without mean shear the ratio Δ is proportional to λ (see ref. [29] for details), so that q becomes proportional to $Wi_\lambda^{-1} - 1$. In [34], the case of shear turbulence has been analyzed and the scaling is the same as in Eq. (30).

The exponent q extracted from numerical simulations is plotted in Fig. 11. The convergence of the Lyapunov exponent, given by the Cramèr function, is shown in Fig. 12.

6. Conclusions

The tumbling phenomenon [21,3,20,7] has been studied in the framework of the linear dumbbell model, and some universal features of this motion are derived and numerically verified.

Three different examples of polymers in a linear, steady, plane, shear flow have been studied: (i) a flexible polymer experiencing thermal noise, (ii) a rigid polymer in a smooth random velocity gradient above the coil-stretch transition [31,32,6]), and (iii) a flexible polymer in a smooth random velocity gradient below the coil-stretch transition.

In all three cases, the polymer tumbles aperiodically and the probability density function of the time between two successive tumbling events is exponential. While in the case of pure thermal noise, the typical tumbling time is determined only by the relaxation process, in the cases of random velocity gradient, the typical rate of divergence of two initially close lagrangian trajectories is the most important time scale.

The analysis of the statistics of orientation leads one to conclude that the phenomenology of these three situations is very similar: in the plane formed by the polymer end-to-end vector and the Z-axis there are no relevant scales and the polymer spends most of the time in the shear plane. In the shear plane, the dynamics is determined by the balance between the shear and the thermal fluctuations. The majority of time is spent nearly aligned to the velocity field. Aperiodically the shear induces a tumbling event.

The elongation dynamics is determined only by the balance between the relaxation and the stretching due to the shear flow in the thermal noise case. In the other two cases stretching is determined by the presence of a positive Lyapunov exponent. In the case below the coil-stretch transition the tail of the PDF can be determined by measuring the statistics of the Lyapunov exponent.

Acknowledgements

We would like to thank A. Celani, M. Chertkov, I. Kolokolov and V. Lebedev for many fruitful and inspiring discussions and S. Geraschenko and V. Steinberg for many useful comments and interest in our work. We are grateful to Chris Carr and Colm Connaughton who helped us to develop the final form of this paper. We acknowledge hospitality of CNLS at Los Alamos National Laboratory where this work was partially done. KT was supported by RFBR grant 04-02-16520a and INTAS grant Nr 04-83-2922.

References

- [1] T.T. Perkins, D.E. Smith, S. Chu, Single polymer dynamics in an elongational flow, *Science* 276 2016 (1997).
- [2] D.E. Smith, S. Chu, Response of flexible polymers to a sudden elongational flow, *Science* 281 (1998) 1335.
- [3] D.E. Smith, H.P. Babcock, S. Chu, Single polymer dynamics in steady shear flow, *Science* 283 (1999) 1724.
- [4] J.S. Hur, E.S.G. Shaqfeh, R.G. Larson, Brownian dynamics simulations of single DNA molecules in shear flow, *J. Rheol.* 44 (2000) 713.
- [5] J.S. Hur, E. Shaqfeh, H.P. Babcock, D.E. Smith, S. Chu, Dynamics of dilute and semidilute DNA solutions in the start-up of shear flow, *J. Rheol.* 45 (2001) 421.
- [6] S. Gerashchenko, C. Chevillard, V. Steinberg, Single polymer dynamics: coil-stretch transition in a random flow, *Europhys. Lett.* 71 (2) (2005) 221–227.

- [7] S. Gerashchenko and V. Steinberg, Statistics of tumbling of a single polymer molecule in shear flow, *Phys. Rev. Lett.*, submitted for publication (see also nlin.CD/0503028).
- [8] R.E. Teixeira, H.P. Babcock, E. Shaqfeh, S. Chu, Shear thinning and tumbling dynamics of single polymers in the flow-gradient plane, *Macromolecules* 38 (2005) 581–592.
- [9] C.M. Schroeder, R.E. Teixeira, E.S.G. Shaqfeh, S. Chu, Dynamics of DNA in the flow-gradient plane of steady shear flow: observations and simulations, *Macromolecules* 38 (2005) 1967–1978.
- [10] B. Ladoux, J. Quivy, P.S. Doyle, G. Amouzni, J. Viovy, Direct imaging of single molecules: from dynamics of a single DNA chain to the study of complex DNA–protein interactions, *Sci. Prog.* 84 (4) (2001) 267.
- [11] S. Chu, Biology and polymer physics at the single-molecule level, *Phil. Trans. R. Soc. Lond. A* 361 689–698 6 (2003).
- [12] S. Manneville, P. Cluzel, J.L. Viovy, D. Chatenay, F. Caron, Evidence for the universal scaling behaviour of a freely relaxing DNA molecule, *Europhys. Lett.* 36 (1996) 413.
- [13] R.G. Larson, T.T. Perkins, D.E. Smith, S. Chu, Hydrodynamics of a DNA molecule in a flow field, *Phys. Rev. E* 55 (1997) 1794.
- [14] Y. Cui, C. Bustamante, Pulling a single chromatin fiber reveals the forces that maintain its higher-order structure, *Proc. Natl. Acad. Sci.* 97 (2000) 127.
- [15] M. Hegner, S.B. Smith, C. Bustamante, Polymerisation and mechanical properties of single RecA-DNA filaments, *Proc. Natl. Acad. Sci.* 96 (1999) 10109.
- [16] H. Yin, M.D. Wang, K. Svoboda, R. Landick, S.M. Block, J. Gelles, Transcription against an applied force, *Science* 270 (1995) 1653.
- [17] G.J. Wuite, S.B. Smith, M. Young, D. Keller, C. Bustamante, Single molecule studies of the effect of template tension on T7 DNA polymerase activity, *Nature* 404 (2000) 103.
- [18] A. Groisman, V. Steinberg, Elastic turbulence in curvilinear flows of polymer solutions, *New J. Phys.* 6 (2004) 29.
- [19] E.J. Hinch, L.G. Leal, The effect of Brownian motion on the rheological properties of a suspension of non-spherical particles, *J. Fluid Mech.* 52 (1972) 634.
- [20] M. Chertkov, I. Kolokolov, V. Lebedev and K. Turitsyn, Tumbling of polymers in random flow with mean shear, *J. Fluid Mech.*, submitted for publication.
- [21] T.W. Liu, Flexible polymer chain dynamics and rheological properties in steady flows, *J. Chem. Phys.* 90 (1989) 5826.
- [22] R.B. Bird, C.F. Curtiss, R.C. Armstrong, O. Hassager, *Dynamics of Polymeric Liquids*, Wiley, New York, 1987.
- [23] K. Turitsyn, Polymer dynamics in chaotic flows with strong shear component, Submitted to *Phys. Rev. E* (see also nlin.CD/0501025).
- [24] M. Chertkov, I. Kolokolov, V. Lebedev, K. Turitsyn, Polymer statistics in a random flow with mean shear, *J. Fluid Mech.* 531 (2005) 251–260.
- [25] H.C. Ottinger, *Stochastic Processes in Polymeric Liquids*, Springer, Berlin, 1995.
- [26] A. Celani, A. Puliafito, K. Turitsyn, Polymers in linear shear flow: a numerical study, *EuroPhys. Lett.* 70 (2005) 464.
- [27] G. Benettin, L. Galgani, A. Giorgilli, J.-M. Strelcyn, Lyapunov exponents for smooth dynamical systems and for Hamiltonian systems; a method for computing all of them, *Meccanica* 15 (1980) 9–30.
- [28] S.N. Majumdar, C. Sire, Survival probability of a Gaussian non-Markovian process: application to the $T = 0$ dynamics of the Ising model, *Phys. Rev. Lett.* 77 (1996) 1420.
- [29] G. Falkovich, C. Gawedzky, M. Vergassola, Particles and fields in fluid turbulence, *Rev. Mod. Phys.* 73 (4) (2001) 913–975.
- [30] R.H. Kraichnan, Small-scale structure of a scalar field convected by turbulence, *Phys. Fluids* 11 (1968) 945–963.
- [31] P.G. De Gennes, Coil-stretch-transition of dilute flexible polymers under ultra-high velocity gradients, *J. Chem Phys* 60 (1974) 5030.
- [32] E. Balkovsky, A. Fouxon, V. Lebedev, Turbulent dynamics of polymer solutions, *Phys. Rev. Lett.* 84 (2000) 4765;
E. Balkovsky, A. Fouxon, V. Lebedev, Turbulent dynamics of polymer solutions, *Phys. Rev. E* 64 (2001) 056301.
- [33] A. Celani, S. Musacchio, D. Vincenzi, Polymer transport in random flow, *J. Stat. Phys.* 118 (2005) 529–552.
- [34] B. Eckhardt, J. Kronjager, J. Schumacher, Stretching of polymers in a turbulent environment, *Comp. Phys. Commun.* 147 (2002) 538.

Chapter 4

Relaxation and conformation dynamics in elongational and random flows

One of the most important observables in polymer dynamics is the Zimm's relaxation time. The Zimm's relaxation time is the time needed by the polymer to reach the equilibrium configuration, starting from a given initial condition. In principle there exists a whole spectrum of relaxation times (see chapter 2). Nevertheless the relaxation dynamics is determined asymptotically by the largest time in the spectrum, which depends on the thermal energy of the solvent, on the viscosity, and on the length of the polymer. In this chapter I will show that in the presence of an external flow, the relaxation process may be significantly different from the thermal equilibrium situation. The external flow introduces dynamical timescales that interfere with the relaxation process, resulting in a strong slowdown around the coil-stretch transition. This phenomenon is present even in simple flows such as the elongational flow and the random flow, where a full or semi-analytical approach is permitted.

The model I will use is the dumbbell model with nonlinear elasticity. The evolution equations are:

$$\dot{R}_\alpha = R_\beta \partial_\beta v_\alpha - \frac{f(R)}{2\tau} R_\alpha + \sqrt{\frac{R_0^2}{\tau}} \xi_\alpha(t) \quad (4.1)$$

4.1 Relaxation dynamics in external flows

The relaxation in an external flow is the process bringing the polymer from a given initial condition to the stationary state. Formally, the time-dependent Fokker-Planck equation associated with eq. (4.1) can be expanded in eigenfunctions:

$$P(\vec{R}, t) = P_{st}(\vec{R}) + \sum_{k=1}^{\infty} a_k p_k(\vec{R}) e^{-\frac{t}{T_k}} \quad (4.2)$$

where P_{st} is the stationary-state PDF, the coefficients a_k depend on $P(\vec{R}, 0)$, the functions p_k are eigenfunctions of the Fokker-Planck operator and T_k are the inverse of the eigenvalues. The relaxation time to the stationary state is the largest value $T = \max_k \{T_k\}$.

An operative way to measure the time of convergence to the stationary state of a polymer in a fluid flow is to measure the rate of convergence of the moments. Suppose to be able to measure, for a single molecule, the function $R^2(t)$ for a sufficiently long time (several Zimm's relaxation times) starting from a given initial condition, and to repeat the measure on several molecules. The average of $R^2(t)$ over the ensemble of polymer trajectories tends to a constant value with increasing t . From the behavior of the second order moment of the extension we can thus extract the relaxation time to the steady state. It is possible to show that the convergence times of the moments are the same as the relaxation time of the whole PDF.

4.2 Shape effects on relaxation dynamics

As observed by de Gennes [2] a fundamental feature to include in a polymer model is the conformation dependent drag: the related effects become crucial as the polymer length increases. The observation by de Gennes is based simply on the fact that in the coiled state a polymer can be considered as a ball of radius R_0 and typically offers a resistance proportional to the gyration radius ($R_g \sim 1\mu m$), given by the Stokes law, i.e.:

$$\zeta_c = 6\pi\eta_s R_0 \quad (4.3)$$

In the stretched state the polymer resembles much more a slender cylinder than a sphere, resulting in a resistance which is very different from the one in the coiled state [17]. For a polymer of length

Polymer	$R_g[\mu m]$	$L[\mu m]$
PEO	0.4	40
PAM	0.5	77
<i>E. Coli</i> DNA	3	1300
λ DNA	0.71	21
7λ DNA	1.82	150

Table 4.1: Indicative gyration radii and contour lengths of common polymers.

L we have indeed:

$$\zeta_s = \frac{2\pi L\eta_s}{\ln \frac{L}{d}} \quad (4.4)$$

where d is the cross sectional area of the polymer. For very long polymers the ratio between the two can be as large as 10 and cannot be neglected.

A first approximation is to consider that the effective drag experienced by a polymer can be linearly interpolated between the drag of a slender cylinder of length L (the contour length) and the one of a coiled polymer [40, 41] (obtained within the Zimm model) [17]:

$$\zeta_c = \frac{3}{8}\sqrt{(6\pi^3)\eta_s R_0} \quad (4.5)$$

$$\frac{\zeta(R)}{\zeta_c} = 1 + \left(\frac{\zeta_c}{\zeta_s} - 1\right)\frac{R}{L} \quad (4.6)$$

Note that the drag coefficient enters the dumbbell model in the relaxation time, so that formally the introduction of a conformation dependent drag corresponds to the introduction of a variable relaxation time: stretched conformations are slower to relax than coiled ones. Thus we have:

$$\dot{R}_\alpha = R_\beta \partial_\beta v_\alpha - \frac{f(R)}{2\tau(R)} R_\alpha + \sqrt{\frac{R_0^2}{\tau(R)}} \xi_\alpha(t) \quad (4.7)$$

$$\tau(R) = \tau \frac{\zeta_c}{\zeta(R)} \quad (4.8)$$

Hereafter I will refer to the FENE model for constant relaxation times τ and to FENE-CD (FENE corrected drag) when conformation effects will be accounted for. The values of the characteristic parameters for the most commonly used polymers are given in table 4.1.

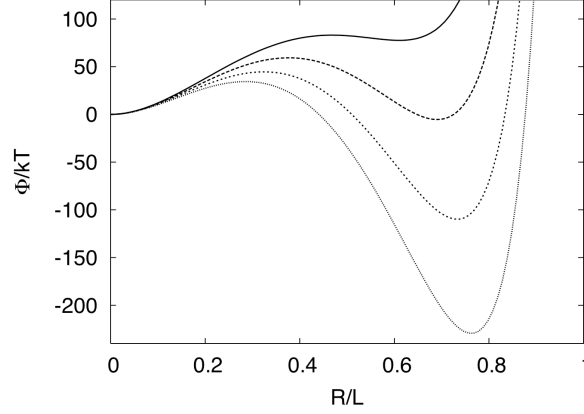


Figure 4.1: Elongational flow: the potential associated with the stationary state of polymer elongation for a dumbbell with nonlinear elasticity and conformation dependent drag for (from top to bottom) $Wi = 0.125$, $Wi = 0.135$, $Wi = 0.145$, $Wi = 0.155$. Here $\zeta_s/\zeta_c = 6.87$. Hysteresis is found in the vicinity of the coil-stretch transition. The values of Wi for which hysteresis can be found depend on the ratio ζ_s/ζ_c . Note also that when this ratio is high, the transition occurs for smaller critical Wi .

4.3 Dynamical slowdown in random and elongational flows

Elongational flow

The elongational flow is defined by the velocity gradient:

$$\hat{\partial}v = \begin{pmatrix} \lambda & 0 & 0 \\ 0 & -\lambda & 0 \\ 0 & 0 & 0 \end{pmatrix} \quad (4.9)$$

The potential associated with the stationary PDF of a dumbbell in an elongational flow can be computed analytically both in the FENE model and in the FENE-CD model and is shown in fig. 4.1 for the conformation dependent drag:

$$\frac{\Phi}{k_B T} = b \left(Wi \frac{R^2}{L^2} + \frac{2}{3} Wi \left(\frac{\zeta_s}{\zeta_c} - 1 \right) \frac{R^3}{L^3} + \frac{1}{2} \ln \left(1 - \frac{R^2}{L^2} \right) \right) \quad (4.10)$$

$$p_{st}(R) = \mathcal{N} R^2 e^{-\frac{\Phi}{k_B T}} \quad (4.11)$$

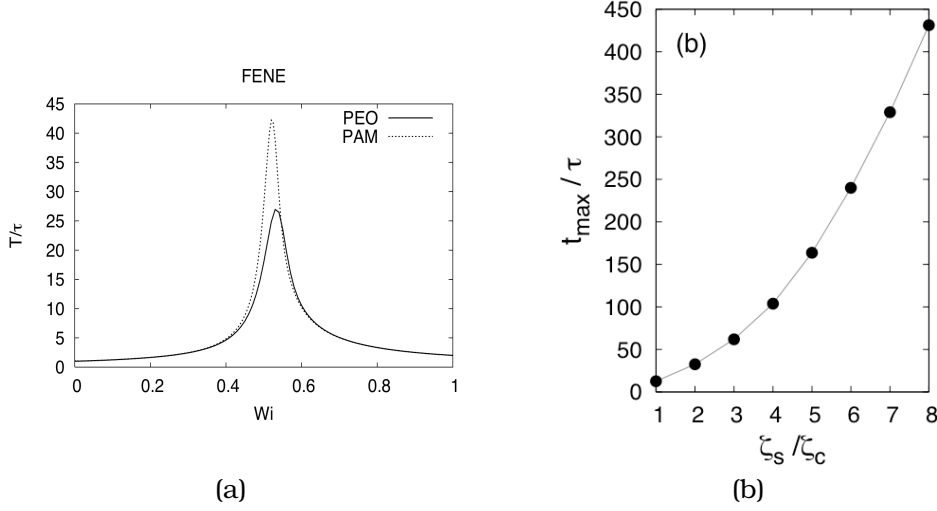


Figure 4.2: Elongational flow: (a) the largest relaxation time rescaled with the Zimm's time plotted as a function of Wi for two different FENE polymers: PEO is poly-ethylene-oxyde and PAM is poly-acrylamyde. These two polymers differ (from a macroscopic point of view) only for the different characteristic lengths: PAM is longer than PEO. (b) The peak value of the relaxation time plotted as a function of the ratio ζ_s/ζ_c (FENE-CD model).

where $b = L^2/R_0^2$ is called the extensibility parameter, $Wi = \lambda\tau$ and \mathcal{N} is set by the normalization condition for $p(R)$. Conformation hysteresis occurs for the FENE-CD model because of the deep double well structure of the potential and consequently of the double peak of the PDF. A polymer starting from a coiled configuration will spend a long time in a coiled configuration before reaching the steady average extension. Conversely, an initially prestretched polymer will stay stretched for a long time. It is worth noticing that for the FENE model ($\zeta_s/\zeta_c = 1$) the potential does not show a double well structure, thus the presence of conformation dependent drag in the model is essential for the observation of hysteresis.

The slowdown corresponding to hysteresis can be expressed in terms of the dynamical relaxation times to the stationary state, which can be computed semi-analytically (see eq. (4.2)), and are shown in fig. 4.2. The relaxation time as a function of Wi shows that a strong slowdown occurs in correspondence of the coil-stretch transition (see fig. 4.2a). Near $Wi = 0$ the dynamics is dominated by the Brownian nature of the system, resulting in $T = \tau$. For very large Wi the flow timescales are dominating: the relaxation

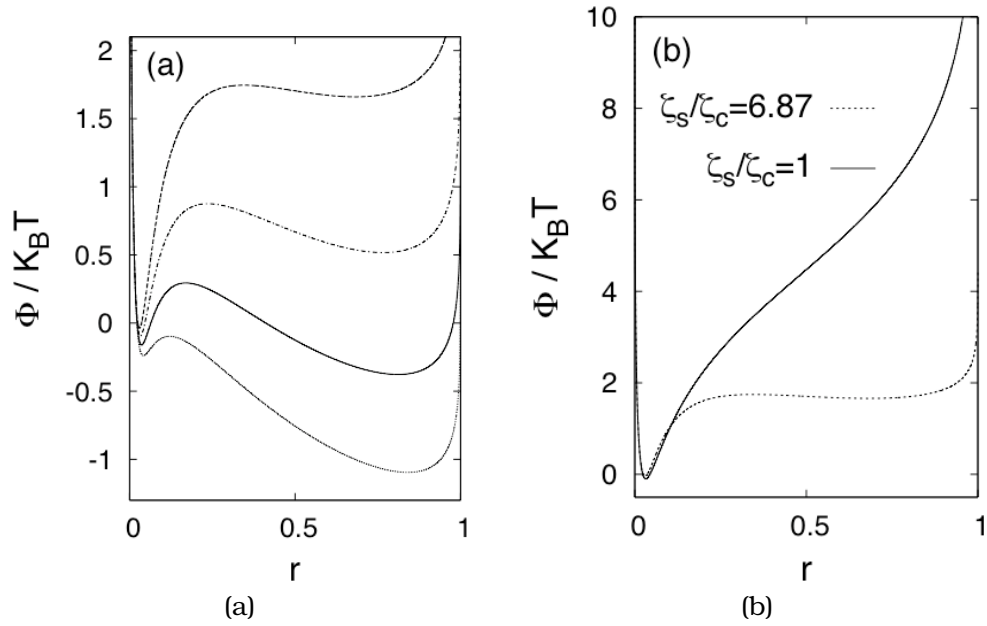


Figure 4.3: Random flow: (a) effective energy for a FENE-CD PAM as a function of the fractional extension. From top to bottom: $Wi = 0.28, 0.33, 0.38, 0.43$; (b) Comparison with a FENE dumbbell polymer with same extensibility parameter b .

dynamics due to the elasticity of the polymer is negligible, yielding $T \sim \lambda^{-1}$.

The noticeable slowdown occurring around the transition is due to a critical competition between the entropic relaxation and the stretching due to the velocity field. Note that this critical slowdown can occur also without the appearance of conformation hysteresis. The introduction of a conformation dependent Zimm's time increases further the slowdown, as shown in fig. 4.2b, whereas it does not affect the regimes $Wi \ll 1$ and $Wi \gg 1$. The value t_{max} of the relaxation time at the peak increases with the ratio ζ_s / ζ_c , i.e. increasing the length of the polymer (fig. 4.2b). Finite time hysteresis is more evident as the length of the polymer increases.

Random flows

Another interesting case are random flows. These flows are irregular in space and time and are thus relevant to the study of turbulence of polymer solutions. Single molecule measurements in a random flow have been performed in elastic turbulence [12, 13, 42]. Here we model the random flow with the Kraichnan-Batchelor flow

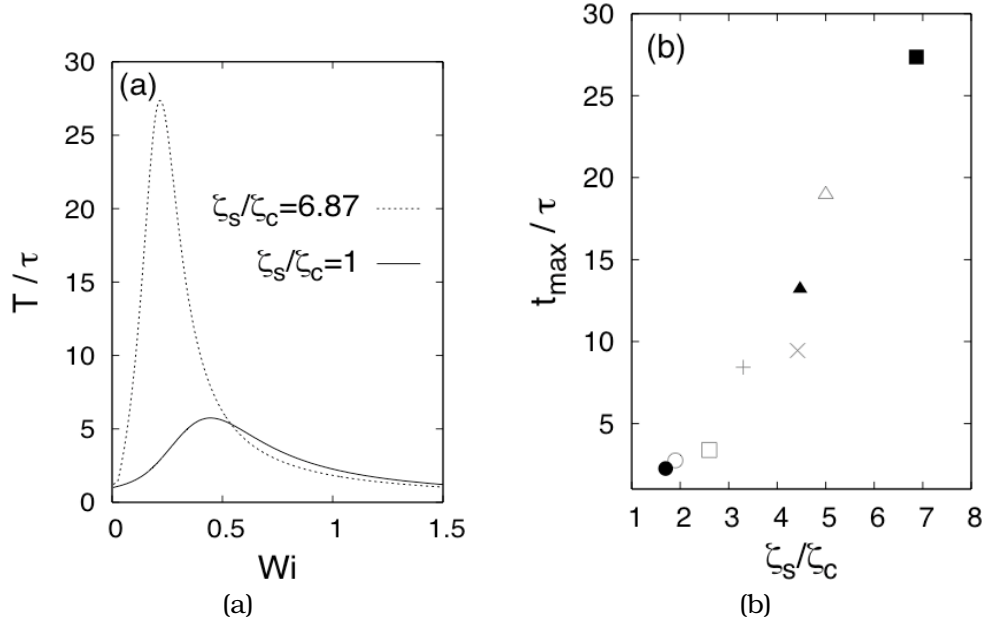


Figure 4.4: Random flow: (a) the largest relaxation time rescaled with the Zimm's time plotted as a function of Wi for a FENE and a FENE-CD PAM polymer. (b) The peak value of the computed relaxation time plotted as a function of Wi for different polymer lengths extracted from refs [8, 41, 44, 45].

introduced in sec. 3.2. This flow permits also to carry on analytical calculations (see e.g. [31, 43]).

The stationary PDF (and the potential) can be calculated exactly for $\zeta_s = \zeta_c$:

$$p_{st}(R) = \mathcal{N} R^2 \left(1 + \frac{Wi}{6} \frac{R^2}{R_0^2}\right)^{-h} \left(1 - \frac{R^2}{L^2}\right)^h \quad (4.12)$$

$$h = \frac{1}{2 \left(\frac{1}{b} + \frac{Wi}{4}\right)} \quad (4.13)$$

where $Wi = \lambda\tau$ (see chapter 3). The potential is shown in fig 4.3a, and has a double well structure near the coil-stretch transition. However the depth is smaller or comparable with $k_B T$, therefore hysteresis does not take place in the random flow. The effect of the conformation dependent drag is to flatten the potential (see fig. 4.3b), leading to a broader distribution of elongations.

The relaxation times to the stationary states can be computed analytically, and the results are shown in fig. 4.4a. Even though no hysteresis is present, the relaxation dynamics is similar to the case of the elongational flow. The fact that the peak is less pronounced

and broader can be explained by the stretching properties of the random flow, where there are large fluctuations around the average stretching rate or Lyapunov exponent. As with the elongational flow, the peak t_{max} of the relaxation time increases with the length of the polymers (see fig. 4.3b).

These results are a clear indication that in a random flow the dynamics of polymer near the coil-stretch transition can be significantly slowed down. This applies also to other flows than the Kraichnan-Batchelor one. We have studied the following flow (introduced first in ref. [46]), decomposed into a strain and a rotational part :

$$\partial_\alpha v_\beta = \mathcal{S}_{\alpha\beta} + \mathcal{R}_{\alpha\beta} \quad (4.14)$$

where each component has Gaussian statistics and a finite correlation time (τ_S and τ_R , respectively):

$$\langle \mathcal{S}_{\alpha\beta}(t) \mathcal{S}_{\gamma\delta}(t') \rangle = S_{\alpha\beta\gamma\delta} \frac{1}{\tau_\eta \tau_S} e^{-\frac{|t-t'|}{\tau_S}} \quad (4.15)$$

$$\langle \mathcal{R}_{\alpha\beta}(t) \mathcal{R}_{\gamma\delta}(t') \rangle = R_{\alpha\beta\gamma\delta} \frac{1}{\tau_\eta \tau_R} e^{-\frac{|t-t'|}{\tau_R}}, \quad (4.16)$$

where τ_η is the Kolmogorov timescale and $S_{\alpha\beta\gamma\delta}$ and $R_{\alpha\beta\gamma\delta}$ are fourth-order tensors which ensure incompressibility and isotropy:

$$S_{\alpha\beta\gamma\delta} = \frac{1}{20} [\delta_{\alpha\gamma} \delta_{\beta\delta} + \delta_{\alpha\delta} \delta_{\beta\gamma} - \frac{2}{3} \delta_{\alpha\beta} \delta_{\gamma\delta}] \quad (4.17)$$

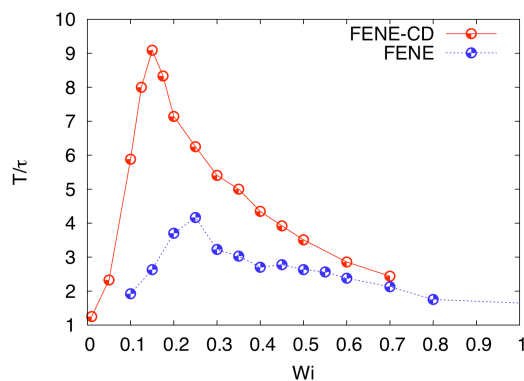
$$R_{\alpha\beta\gamma\delta} = \frac{1}{12} [\delta_{\alpha\gamma} \delta_{\beta\delta} - \delta_{\alpha\delta} \delta_{\beta\gamma}] \quad (4.18)$$

The correlation times of each component are set to be $\tau_S = 2.3\tau_\eta$, and $\tau_R = 7.2\tau_\eta$ [46], and the Lyapunov exponent is $\lambda \sim 10\tau_\eta^{-1}$. In the limit $\tau_\eta \rightarrow 0$ we recover the Kraichnan-Batchelor flow.

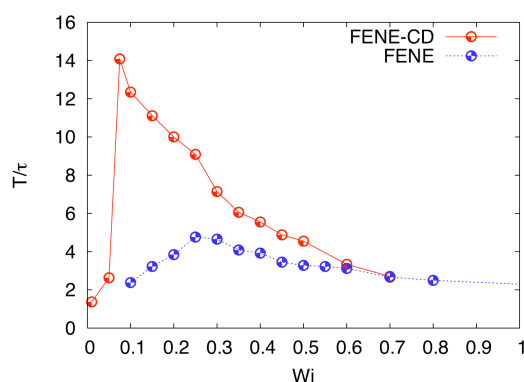
We have simulated numerically the evolution equation for a dumbbell with nonlinear elasticity and conformation dependent drag, and we have collected statistics over the realizations of the thermal noise and of the velocity field. The relaxation times are obtained from the rate of convergence of the moments:

$$\langle \frac{R^n(t)}{L^n} \rangle - \langle \frac{R^n}{L^n} \rangle_{st} \propto e^{-\frac{t}{T}} \quad \text{for } t \rightarrow \infty \quad (4.19)$$

The results of the simulations are shown in fig. 4.5. The phe-



(a)



(b)

Figure 4.5: Results of numerical simulations of the flow introduced in ref. [46]: the relaxation times to the stationary states for a FENE and FENE-CD (a) PEO and (b) PAM molecules.

nomenology is exactly the same as in the Kraichnan-Batchelor flow: the relaxation time T to the stationary state is equal to the Zimm's time for small Wi , it is proportional to the inverse Lyapunov exponent for large Wi , whereas it is larger than the Zimm's time in the vicinity of the coil-stretch transition. The effect of the conformation dependent drag is to further increase the peak, as in the Kraichnan-Batchelor flow.

4.4 Perspectives

A first natural extension to the case of single polymer in random flows is the addition of a mean shear. This flow is more similar to those flows where drag reduction is observed (see part II). As shown in chapter 3, this would change the dependence of the Lyapunov exponent on the flow parameter but the dynamics should remain unchanged, and a dynamical slowdown should occur, as in the case of pure random flow.

It would be interesting to measure the relaxation times to the stationary state in external flows within a multi-bead model with hydrodynamic interactions. In this context it would be interesting to perform a detailed measurement of the effective drag coefficient of the polymer as a function of the conformation, namely the function $\nu(R)$. Indeed the linear interpolation between the drag of a coil and a cylinder has been proposed for the elongational flow, where the most probable configurations are either coiled or fully extended ones. In the random flow conformation fluctuations can be larger, leading to a heterogeneity of configurations and, possibly, to a different functional form of the effective drag.

Dynamical slowdown of polymers in laminar and random flows

A. Celani,¹ A. Puliafito,¹ and D. Vincenzi^{2,3}

¹*CNRS-INLN, 1361 Route des Lucioles, 06560 Valbonne, France*

²*Max-Planck-Institut für Dynamik und Selbstorganisation, Busenstr. 10, 37073 Göttingen, Germany*

³*Laboratory for Atomic and Solid State Physics, Cornell University, Ithaca, NY 14853*

(Dated: March 6, 2006)

The influence of an external flow on the relaxation dynamics of a single polymer is investigated theoretically and numerically. We show that a pronounced dynamical slowdown occurs in the vicinity of the coil-stretch transition, especially when the dependence on polymer conformation of the drag is accounted for. For the elongational flow, relaxation times are exceedingly larger than the typical relaxation times, resulting in the observation of conformation hysteresis. For random smooth flows hysteresis is not present. Yet, relaxation dynamics is significantly slowed down because of the large variety of accessible polymer configurations. The implications of these results for the modeling of dilute polymer solutions in turbulent flows are addressed.

PACS numbers: 47.57.Ng, 47.27.-i

The dynamics of an isolated polymer in a flow field forms the basis of constitutive models for dilute polymer solutions [1–3]. The modeling of drag-reducing flows, for instance, requires an appropriate description of single polymer deformation in turbulent velocity fields [4]. In the last decade, major advances in fluorescence microscopy offered the possibility of tracking isolated polymers both in laminar [3] and random flows [5]. The dynamics of a polymer in thermal equilibrium with the surrounding solvent is commonly described in terms of normal modes and relaxation times associated with them. The analytical form of the relaxation spectrum was first obtained by Rouse under the assumption that the polymer could be described as a series of beads connected by Hookean springs [6]. The Rouse model was subsequently improved by Zimm to include hydrodynamical interactions between segments of the polymer [7]. In Zimm’s formulation, the equations of motion are decoupled into a normal mode structure by preaveraging the distances between the beads over the distribution of polymer configurations. The relaxation time associated with the fundamental mode, τ , determines the typical time that it takes for a deformed polymer to recover the equilibrium configuration in a solvent. The normal mode theory was confirmed by the analysis of the oscillatory motion of a DNA molecule immersed in a solvent and held in a partially extended state by means of optical tweezers [8]. An alternative approach to examine polymer relaxation consists in stretching a tethered DNA molecule in a flow and measuring its relaxation after cessation of the flow [9, 10]. The theoretical predictions for these experimental conditions are provided by the scaling theory [11] and the static dynamics formalism [12].

The aforementioned studies all consider the internal dynamics of a polymer floating in a solvent under the influence of thermal noise only — the interaction of the polymer with an external flow is not taken into account. One of the aspects highlighted by experiments is that

polymer dynamics in a moving fluid is strongly influenced by the carrier velocity field. The coil–stretch transition is the most noticeable example: as the strain rate exceeds a threshold value, the polymer undergoes a transition from the coiled, equilibrium configuration to an almost fully extended one [13]. Therefore, when a polymer is freely transported by a nonhomogeneous flow, we expect that the time scales describing its dynamics may be significantly different from the Zimm time τ . Simple models for polymer stretching indeed suggest deviations from Zimm’s theory near the coil–stretch transition [14–16]. Discrepancies in the definition of the correct relaxation time are also encountered in drop formation experiments [17].

In this Letter we investigate polymer relaxation dynamics both in elongational and random smooth flows. Our analysis brings to evidence an important slowdown of dynamics with respect to the Zimm timescales, in the vicinity of the coil–stretch transition. For the elongational flow, this is related to conformation hysteresis [18]. For random flows, we show that hysteresis is not present. Nonetheless, the amplification of the relaxation time persists, albeit to a lesser extent, due to the large heterogeneity of polymer configurations. In both cases, the dependence of the drag force on the polymer configuration plays a prominent role. This suggests the necessity of improving current models of polymer solutions in turbulent flows to account for such effect.

The dumbbell approximation is the basis of the most common models of single polymer dynamics and viscoelastic models of dilute polymer solutions [19]. Its validity relies on the fact that the slowest deformational mode of the polymer is the most influential in producing viscoelasticity [4]. However, when attention is directed to non-equilibrium dynamics it is often too crude to assume that τ is independent of the conformation of the molecule [20]. Therefore, following de Gennes and Hinch’s approach [13, 21], we consider a model where

the polymer is described as two beads connected by an elastic spring, and the separation vector of the ends of the molecule, \mathbf{R} , satisfies the stochastic differential equation (in the Stratonovich sense):

$$\dot{\mathbf{R}} = \nabla \mathbf{v}(t) \cdot \mathbf{R} - \frac{f(R)}{2\tau\nu(R)} \mathbf{R} + \sqrt{\frac{R_0^2}{\tau\nu(R)}} \boldsymbol{\xi}(t), \quad (1)$$

where \mathbf{v} is the velocity field, R_0 is the mean extension at thermal equilibrium, $R = |\mathbf{R}|$, and $\boldsymbol{\xi}(t)$ is a three-dimensional white noise modeling the thermal fluctuations of the solvent. The function $f(R)$ defines the entropic force restoring stretched molecules into the coiled configuration. Synthetic polymers are properly described by the Warner law, $f(R) = 1/(1 - R^2/L^2)$, where L is the contour length of the polymer. Biological macromolecules are better characterized by the Marko-Siggia law, $f(R) = 2/3 - L/(6R) + L/[6R(1 - R/L)^2]$ [2]. The function $\nu(R)$ encodes for the dependence on the polymer conformation of the drag exerted by the fluid: a thick coil offers a larger resistance with respect to a long thin rod-like configuration. We utilize the expression $\nu(R) = 1 + (\zeta_s/\zeta_c - 1)R/L$ that interpolates linearly between these extremes (see Refs. [22, 23]). Here, $\zeta_c = 3\sqrt{6\pi^3}R_0/(8\eta_s)$ and $\zeta_s = 2\pi L\eta_s/\ln(L/\ell)$ are the friction coefficients for the coiled and the stretched configuration, respectively, η_s is the solvent viscosity and ℓ is the diameter of the molecule. The flow strength relative to the polymer tendency to recoil is expressed by the Weissenberg number Wi , defined as the product of the Zimm time τ by a characteristic extension rate of the flow.

In order to define the relaxation time in presence of an arbitrary external flow, we consider the probability density function of the rescaled extension, $P(r, t)$ with $r = R/L$, and identify the dynamical relaxation time of the polymer, t_{rel} , as the characteristic time needed for $P(r, t)$ to attain its stationary form $P_{\text{st}}(r)$.

As a first example, we examine the steady planar elongational flow $\mathbf{v} = \gamma(x, -y)$, turning our attention to random flows in the second part of this Letter. By assuming that the polymer extension in the x -direction is much greater than in the y -direction, it is easy to derive from Eq. (1) a Fokker-Planck equation for the probability density function of r :

$$\partial_t P = -\partial_r(D_1(r)P) + \partial_r D_2(r)\partial_r P, \quad (2)$$

where $D_1(r) = Wi r - \hat{f}(r)r/[2\hat{\nu}(r)]$, $D_2(r) = [2b\hat{\nu}(r)]^{-1}$, $\hat{f}(r) = f(rL)$, $\hat{\nu}(r) = \nu(rL)$, $Wi = \gamma\tau$, and $t' = t/\tau$. The stationary solution to Eq. (2) takes the potential form $P_{\text{st}}(r) = N \exp[-E(r)/K_B T]$, where N is the normalization constant and $E(r) = -K_B T \int_0^r D_1(\rho)/D_2(\rho) d\rho$. For large enough ζ_s/ζ_c , there is a narrow range of Wi around the critical value for the coil-stretch transition, $Wi_{\text{crit}} = 1/2$, where $E(r)$ has a double well structure.

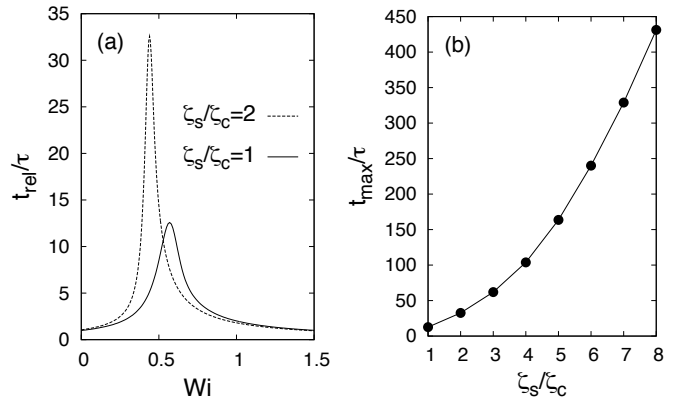


Figure 1: Elongational flow: (a) rescaled relaxation time vs. Wi for $b = 400$. The entropic force is given by the Warner law; (b) Rescaled maximum relaxation time vs. ζ_s/ζ_c ($b = 400$).

This property gives rise to a conformation hysteresis characterized by a multivalued mean molecular extension [18]. Strictly speaking, this is a finite-time effect since $P_{\text{st}}(r)$ is unique. However, the barrier height separating the coiled and the stretched state is much greater than thermal energy (E is of the order of $10K_B T$) and therefore the polymer remains trapped in its initial configuration for an exceptionally long time [18]. Conformation hysteresis has a clear counterpart in the time dependence of $P(r, t')$, as we shall see from the analysis of Eq. (2).

The probability density function of the extension admits the expansion

$$P(r, t') = P_{\text{st}}(r) + \sum_{n=1}^{\infty} a_n p_n(r) e^{-t'/\sigma_n}, \quad (3)$$

where $p_n(r)$ are the eigenfunctions of the Fokker-Planck operator and σ_n the reciprocals of its (strictly positive) eigenvalues, arranged in descending order ($\sigma_n > \sigma_{n+1}$). The coefficients a_n are fixed by $P(r, 0)$. The relaxation time is thus defined as $t_{\text{rel}} \equiv \sigma_1 \tau$. For $\zeta_s = \zeta_c$, t_{rel} can be computed by solving a central two-point connection problem for a generalized spheroidal wave equation [16]. In the general case, $\zeta_s > \zeta_c$, we resorted to a numerical computation based on the variation-iteration method of quantum mechanics [24]. For very small Wi , the dynamics is dominated by the entropic force, and therefore t_{rel} is approximately equal to the Zimm time. With increasing Wi , t_{rel}/τ grows as $1/(1 - 2Wi)$, as can be seen by replacing $\hat{f}(r)$ with 1 in Eq. (2) (Fig. 1). For $Wi \gg Wi_{\text{crit}}$, the thermal noise is negligible and the only role of the restoration force is to prevent extensions greater than L ; the time needed to reach the asymptotic regime is therefore set by the time scale of the flow, γ^{-1} , and t_{rel}/τ decreases as Wi^{-1} . In the vicinity of the coil-stretch transition t_{rel} shows a sharp peak (Fig. 1). In this range of Wi there is a critical competition between the entropic force

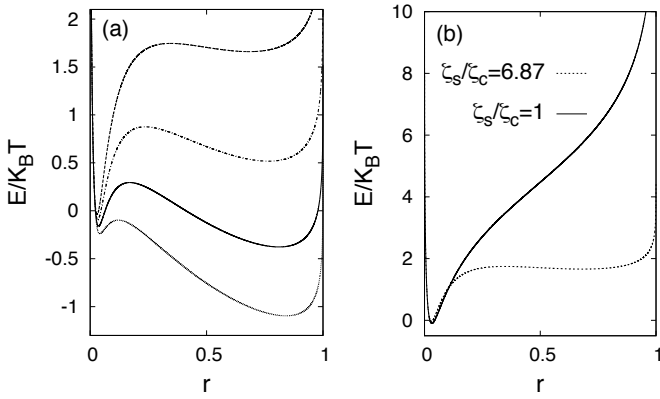


Figure 2: 3D Batchelor–Kraichnan flow: (a) effective energy for polyacrylamide (PAM), $b = 3953$, $\zeta_s/\zeta_c = 6.87$. From top to bottom: $Wi = 0.28, 0.33, 0.38, 0.43$; (b) comparison with a dumbbell polymer with same b , but conformation-independent drag coefficient ($Wi = 0.28$).

and the velocity gradient that makes the convergence time to the steady state extremely long. This effect is strongly enhanced by the conformation-dependent drag. The peak t_{\max} indeed increases with ζ_s/ζ_c (Fig. 1). Those extremely long relaxation times are intimately connected with the observation of conformation hysteresis.

More relevant to viscoelastic turbulence is the case of a random smooth flow (see, e.g., [25]). To make analytical progress, we initially assume that the flow obeys the Batchelor–Kraichnan statistics [26]. The velocity gradient is then a statistically isotropic and parity invariant Gaussian process with zero mean and correlation function: $\langle \partial_j v_i(t) \partial_k v_l(s) \rangle = 2\lambda \delta(t-s)[(d+1)\delta_{ik}\delta_{jl} - \delta_{ij}\delta_{kl} - \delta_{il}\delta_{jk}]/[d(d-1)]$, where d is the dimension of the flow and λ denotes the maximum Lyapunov exponent, that is the average logarithmic separation rate of nearby fluid trajectories. In this context, we indicate by $P(r, t')$ the probability density function of the extension both with respect to thermal noise and the realizations of the velocity field. The Fokker–Planck equation for $P(r, t')$ takes the form (2) with $D_1(r) = (d-1)/d Wi r - \hat{f}(r)r/[2\hat{\nu}(r)] + (d-1)/[2b\hat{\nu}(r)r]$, $D_2(r) = Wi r^2/d + [2b\hat{\nu}(r)]^{-1}$ with $Wi = \lambda\tau$. The stationary probability density function admits once more a potential form. For $\zeta_s > \zeta_c$, the potential $E(r)/K_B T$ displays a very wide well, the effect of the conformation-dependent drag being to increase the probability of large extensions and hence make the potential flatter (Fig. 2). There is no evidence of pronounced double wells. Near the coil–stretch transition, the effective barrier heights separating the coiled and stretched states are indeed at most comparable to thermal energy. As a result, for realistic ζ_s/ζ_c , no conformation hysteresis is expected to be observed in random flows. The behavior of t_{rel} as a function of Wi is however analogous to the one encountered in the elongational flow. The rescaled relaxation time in-

creases as $[1 - Wi(d+2)/d]^{-1}$ at small Wi , and decreases as Wi^{-1} at large Wi . A peak near the coil–stretch transition is present, that becomes more and more pronounced with increasing ζ_s/ζ_c as shown in Fig. 3, attaining values as large as about thirty times the Zimm time. The reason for this behavior is the breadth of $P_{\text{st}}(r)$ and the consequent large heterogeneity of accessible polymer configurations.

To corroborate the results obtained in the context of the short-correlated flow, we performed Brownian Dynamics simulations of Eq. (1) with the random flow introduced by Brunk et al. [27]. This model reproduces the small scale structure of a turbulent flow by means of a statistically isotropic Gaussian velocity gradient. The autocorrelation times of components of the strain and rotation tensors are set to be multiple of the Kolmogorov time τ_η by comparison with direct numerical simulations of 3D isotropic turbulence ($\tau_S = 2.3\tau_\eta$, $\tau_R = 7.2\tau_\eta$) [28]. The Lyapunov exponent of this flow is $\lambda \simeq 10\tau_\eta$. We computed t_{rel} as the time of convergence of the moments $\langle r^n(t) \rangle$ to their stationary value $\langle r^n \rangle_{\text{st}}$: $t_{\text{rel}}^{-1} = -\lim_{t \rightarrow \infty} \ln[\langle r^n(t) \rangle - \langle r^n \rangle_{\text{st}}]/t$, where the averages were taken over an ensemble of realizations of Eq. (1), all with the same initial extension $r(0)$. The numerical difficulty arising from the singularity of the entropic force at $R = L$ has been overcome by exploiting the algorithm introduced in Ref. [29]. The results shown in Fig. 4 confirm the scenario depicted in the context of the short-correlated flow. It is worth noticing that the

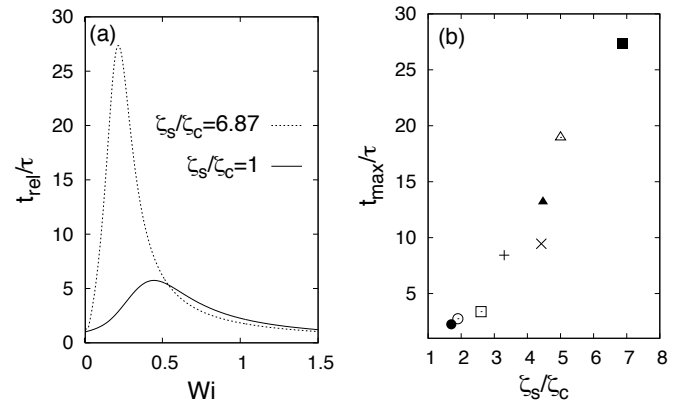


Figure 3: 3D Batchelor–Kraichnan flow: (a) rescaled relaxation time t_{rel}/τ vs. Wi for a PAM molecule ($b = 3953$); (b) rescaled maximum relaxation time t_{\max}/τ for the following polymers: DNA (\bullet , $b = 191.5$; \circ , $b = 260$; \square , $b = 565$; $+$, $b = 2250$), polystyrene (\times , $b = 673$), polyethyleneoxide (PEO) (\blacktriangle , $b = 1666$), Escherichia Coli DNA (Δ , $b = 9250$), PAM (\blacksquare). Measures of b and ζ_s/ζ_c can be found in [18, 22]. Synthetic polymers are modeled by the Warner law, whereas biological molecules are described by the Marko–Siggia law. Relaxation time were computed by means of the variation–iteration method [24]. For $\zeta_s = \zeta_c$ they can be obtained by solving an eigenvalue problem for a Heun differential equation [15].

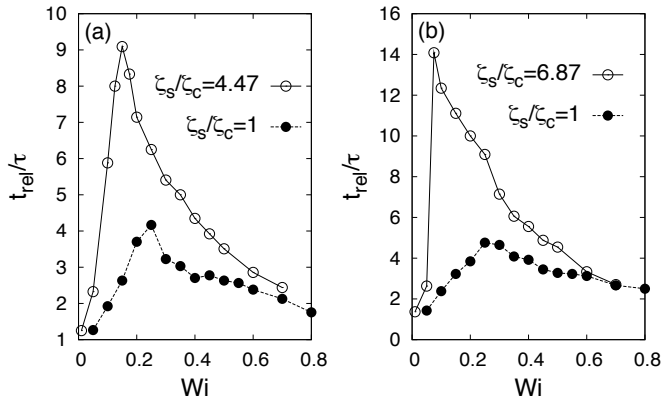


Figure 4: Brunk–Koch–Lion flow: rescaled relaxation time vs. $Wi = \lambda\tau$ from Brownian Dynamics simulations; (a) PEO; (b) PAM.

above definition provides an operational method to measure t_{rel} that can be implemented in experiments.

In summary, we have shown that the equilibrium configuration of a polymer in a flow, as well as the time a deformed molecule takes on average to recover that configuration, depend sensitively on the properties of the flow. In the vicinity of the coil–stretch transition the characteristic relaxation time is much longer than the Zimm time τ , both in elongational and random flows. In other words, the effective Weissenberg number differs considerably from the “bare” one. This effect is strongly amplified when the drag coefficient depends on the conformation of the polymer, and may play an important role in drag-reducing turbulent flows, where the strain rate often fluctuates around values typical of the coil–stretch transition [30]. Our conclusions thus suggest that the conformation-dependent drag should be included as a basic ingredient of continuum models of polymer solutions, calling for further theoretical, experimental and numerical study.

Inspiring discussions with M. Chertkov, S. Gerashchenko and V. Steinberg are gratefully acknowledged. This work has been partially supported by the EU under the contract HPRN-CT-2002-00300.

-
- [1] S. Chu, *Phil. Trans. R. Soc. Lond. A* **361**, 689 (2003).
 [2] R. G. Larson, *J. Rheol.* **49**, 1 (2005).
 [3] E. S. G. Shaqfeh, *J. Non-Newtonian Fluid Mech.* **130**, 1 (2005).
 [4] A. Gyr and H. W. Bewersdorff, *Drag reduction of Turbulent Flows by Additives* (Kluwer Academic, Dordrecht,

- Boston, 1995)
 [5] S. Gerashchenko, C. Chevillard, and V. Steinberg, *Europhys. Lett.* **71**, 221 (2005).
 [6] P. E. Rouse, Jr., *J. Chem. Phys.* **21**, 1272 (1953).
 [7] B. H. Zimm, *J. Chem. Phys.* **24**, 269 (1956).
 [8] S. R. Quake, H. Babcock, and S. Chu, *Nature* **388**, 151 (1997).
 [9] T. T. Perkins *et al.*, *Science* **264**, 822 (1994).
 [10] S. Manneville *et al.*, *Europhys. Lett.* **36**, 413 (1996).
 [11] Y. Marciano and F. Brochard-Wyart, *Macromolecules* **28**, 985 (1995).
 [12] R. Rzehak and W. Zimmermann, *Europhys. Lett.* **59**, 779 (2002).
 [13] P.-G. de Gennes, *J. Chem. Phys.* **60**, 5030 (1974).
 [14] A. Celani, S. Musacchio, and D. Vincenzi, *J. Stat. Phys.* **118**, 531 (2005).
 [15] M. Martins Afonso and D. Vincenzi, *J. Fluid Mech.* **540**, 99 (2005).
 [16] D. Vincenzi and E. Bodenschatz, *Q. J. Mech. Appl. Math.* (submitted).
 [17] V. Tirtaatmadja, G. H. McKinley, and J. J. Cooper-White, *Phys. Fluids* (submitted).
 [18] C. M. Schroeder *et al.*, *Science* **301**, 1515 (2003); C. M. Schroeder, E. S. G. Shaqfeh, and S. Chu, *Macromolecules* **37**, 9242 (2004); C.-C. Hsieh and R. G. Larson, *J. Rheol.* **49**, 1081 (2005).
 [19] R. B. Bird, C. F. Curtiss, R. C. Armstrong, and O. Hassager, *Dynamics of Polymeric Liquids*, 2nd edition (Wiley, New York, 1987).
 [20] J. W. Hatfield and S. R. Quake, *Phys. Rev. Lett.* **82**, 3548 (1999).
 [21] E. J. Hinch, *Colloques Internationaux du C.N.R.S.*, n. 233, “Polymères et lubrification” (1974).
 [22] R. G. Larson *et al.*, *Phys. Rev. E* **55**, 1794 (1997).
 [23] P. S. Doyle *et al.*, *Journal of Non-Newtonian Fluid Mechanics* **76**, 79 (1998).
 [24] P. M. Morse and H. Feshbach, *Methods of Theoretical Physics* (McGraw–Hill, New York, 1953).
 [25] M. Chertkov, *Phys. Rev. Lett.* **84**, 4761 (2000); E. Balkovsky, A. Fouxon, and V. Lebedev, *Phys. Rev. Lett.* **84**, 4765 (2000); J.-L. Thiffeault, *Phys. Lett. A* **308**, 445 (2003); M. Chertkov *et al.*, *J. Fluid Mech.* **531**, 251 (2005); A. Puliafito and K. Turitsyn, *Physica D* **211**, 9 (2005); J. Schumacher and J. Davoudi, *Phys. Fluids* **18**, 025103 (2006).
 [26] R. H. Kraichnan, *Phys. Fluids* **11**, 945 (1968).
 [27] B. K. Brunk, D. L. Koch, and L. W. Lion, *Phys. Fluids* **9**, 2670 (1997); *J. Fluid Mech.* **364**, 81 (1998).
 [28] S. S. Girimaji and S. Pope, *Phys. Fluids A* **2**, 242 (1990).
 [29] A. Celani, A. Puliafito, and K. Turitsyn, *Europhys. Lett.* **70**, 464 (2005).
 [30] K. R. Sreenivasan and C. M. White, *J. Fluid Mech.* **409**, 149 (2000); E. Balkovsky, A. Fouxon, and V. Lebedev, *Phys. Rev. E* **64**, 056301 (2001); G. Boffetta, A. Celani, and S. Musacchio, *Phys. Rev. Lett.* **91**, 034501 (2003); V. S. L’vov *et al.*, *ibid.* **92**, 244503 (2004).

Bibliography

- [1] Perkins T.-T., Quake S.-R., Smith D.-E., Chu S., *Relaxation of a single DNA molecule observed with optical microscopy*, *Science*, **264**, (1994), 822.
- [2] de Gennes P.-G., *Coil-stretch-transition of dilute flexible polymers under ultra-high velocity gradients*, *J. Chem. Phys.*, **60**, (1974), 5030.
- [3] Hinch E.-J. Mechanical models of dilute polymer solutions for strong flows with large polymer deformations. In *Proc. Symp. Polymer Lubrification*, 1974.
- [4] Fuller G.-G., Leal L.-G., *Flow birefringence of dilute polymer solutions in two-dimensional flows*, *Rheol. Acta*, **19**, (1980), 580.
- [5] Dunlap P.-N., Leal L.-G., *Dilute polystyrene solutions in extensional flows: birefringence and flow modification*, *J. Non-Newtonian Fluid Mech.*, **23**, (1986), 5.
- [6] Babcock H.-P., Teixeira R.-E., Hur J.-S., Shaqfeh E.-S.-G, Chu S., *Visualization of molecular fluctuations near the critical point of the coil-stretch transition in polymer elongation*, *Macromol.*, **36**, (2003), 4544–4548.
- [7] Gerashchenko S., Chevillard C., Steinberg V., *Single-polymer dynamics: Coil-stretch transition in a random flow*, *Europhys. Lett.*, **71**, (2005), 221.
- [8] Schroeder C.-M., Babcock H.-P., Shaqfeh E.-S.-G., Chu S., *Observation of polymer conformation hysteresis in extensional flow*, *Science*, **301**, (2003), 1515–1519.

- [9] Liu S., Ashok B., Muthukumar M., *Brownian dynamics simulations of bead-rod chain in simple shear flow and elongational flow*, *Polymer*, **45**, (2004), 1383–1389.
- [10] Smith D.-E., Babcock H.-P., Chu S., *Single polymer dynamics in steady shear flow*, *Science*, **283**, (1999), 1724.
- [11] Gerashchenko S., Steinberg V., *Statistics of tumbling of a single polymer molecule in shear flow*, *Phys. Rev. Lett.*, **96**, (2006), 038304.
- [12] Groisman A., Steinberg V., *Elastic turbulence in a polymer solution flow*, *Nature*, **405**, (2000), 53.
- [13] Groisman A., Steinberg V., *Elastic turbulence in curvilinear flows of polymer solutions*, *New J. Phys.*, **6**, (2004), 29.
- [14] Perkins T.-T., Smith D.-E., Chu S., *Single polymer dynamics in an elongational flow*, *Science*, **276**, (1997), 2016–2021.
- [15] Flory P. *Principles of Polymer Chemistry*. Cornell University Press, 1971.
- [16] Rouse P.-E., *A theory of the linear viscoelasticity properties of dilute solutions of coiling polymers*, *J. Chem. Phys.*, **21**, (1953), 1272–1280.
- [17] Doi M., Edwards S.-F. *The theory of polymer dynamics*. Clarendon Press, 1986.
- [18] Bird R.-B., Armstrong R.-C., Hassager O., Curtiss C.-F. *Dynamics of polymeric liquids*. John Wiley, 1987.
- [19] de Gennes P.-G. *Scaling concepts in polymer physics*. Cornell University Press, 1979.
- [20] Oettinger H.-C. *Stochastic Processes in Polymeric Fluids*. Springer Verlag, 1996.
- [21] Zimm B.-H., *Dynamics of polymer molecules in dilute solution: viscoelasticity, flow birefringence and dielectric loss*, *J. Chem. Phys.*, **24**, (1956), 269–278.
- [22] Bustamante C., Smith S.-B., Liphardt J., Smith D., *Single-molecule studies of DNA mechanics*, *Current opinion in structural biology*, **10**, (2000), 279–285.

- [23] Warner H.-R., *Kinetic theory and rheology of dilute suspensions of finitely extensible dumbbells*, Ind. Eng. Chem. Fundam., **11**, (1972), 379.
- [24] Marko J.-F., Siggia E.-D., *Stretching DNA*, Macromolecules, **28**, (1995), 8759–8770.
- [25] Hinch E.-J., Leal L.-G., *The effect of brownian motion on the rheological properties of a suspension of non-spherical particles*, J. Fluid Mech., **52**, (1972), 683–712.
- [26] Keller S.-R., Skalak R., *Motion of a tank-treading ellipsoidal particle in a shear flow*, J. Fluid Mech., **120**, (1982), 27–47.
- [27] Biben T., Kassner K., Misbah C., *Phase-field approach to three-dimensional vesicle dynamics*, Phys. Rev. E, **72**, (2005), 041921.
- [28] Kantsler V., Steinberg V., *Orientation and dynamics of a vesicle in tank-treading motion in shear flow*, Phys. Rev. Lett., **95**, (2005), 258101.
- [29] Seifert U., *Fluid vesicles in shear flow*, Phys. Rev. Lett., **77**, (1996), 3685–3688.
- [30] Chertkov M., Kolokolov I., Lebedev V., Turitsyn K., *Polymer statistics in a random flow with mean shear*, J. Fluid Mech., **531**, (2005), 251–260.
- [31] Celani A., Musacchio S., Vincenzi D., *Polymer transport in random flow*, Journal of Statistical Physics, **118**, (2005), 531.
- [32] Jeffery G.-B., *The motion of ellipsoidal particles immersed in a viscous fluid*, Proc. R. Soc. Lond. A, **102**, (1922), 161.
- [33] Kraichnan R.-H., *Small-scale structure of a scalar field convected by turbulence*, Phys. Fluids, **11**, (1968), 945–953.
- [34] Balkovsky E., Fouxon A., Lebedev V., *Turbulent dynamics of polymer solutions*, Phys. Rev. Lett., **84**, (2000), 4765.
- [35] Chertkov M., *Polymer stretching by turbulence*, Phys. Rev. Lett., **84**, (2000), 4761.

- [36] Boffetta G., Celani A., Musacchio S., *Two-dimensional turbulence of dilute polymer solutions*, Phys. Rev. Lett., **91**, (2003), 034501.
- [37] Turitsyn K.-S., *Polymer dynamics in chaotic flows with strong shear component*, submitted to Phys. Rev. E (2005).
- [38] Eckhardt B., Kronjager J., Schumacher J., *Stretching of polymers in a turbulent environment*, Comp. Phys. Comm., **147**, (2002), 538.
- [39] Ermak D.-L., McCammon J.-A., *Brownian dynamics with hydrodynamic interactions*, J. Chem. Phys., **69**, (1978), 1352–1360.
- [40] Doyle P.-S., Shaqfeh E.-S.-G., McKinley G.-H., Spiegelberg S.-H., *Relaxation of dilute polymer solutions following extensional flow*, J. Non Newtonian Fluid Mech., **76**, (1998), 79.
- [41] Larson R.-G., Perkins T.-T., Smith D.-E., Chu S., *Hydrodynamics of a DNA molecule in a flow field*, Phys. Rev. E, **55**, (1997), 1794–1797.
- [42] Groisman A., Steinberg V., *Efficient mixing at low Reynolds numbers using polymer additives*, Nature, **410**, (2001), 905.
- [43] Martins Afonso M., Vincenzi D., *Nonlinear elastic polymers in random flow*, J. Fluid Mech., **540**, (2005), 99–108.
- [44] Schroeder C.-M., Shaqfeh E.-S.-G., Chu S., *Effect of Hydrodynamic Interactions on DNA Dynamics in Extensional Flow: Simulation and Single Molecule Experiment*, Macromolecules, **37**, (2004), 9242–9256.
- [45] Hsieh C.-C., Larson R.-G., *Prediction of coil-stretch hysteresis for dilute polystyrene molecules in extensional flow*, J. Rheol., **49**, (2005), 1081–1089.
- [46] Brunk B.-K., Koch D.-L., Lion L.-W., *Turbulent coagulation of colloidal particles*, J. of Fluid Mech., **364**, (1998), 81–113.

Part II

**Dynamics of dilute polymer
solutions**

Introduction

Polymer solutions belong to the class of viscoelastic fluids, i.e. they behave both like viscous and elastic materials. The dynamics of polymeric liquids is a long-standing research subject in rheology and fluid mechanics due to the numerous industrial applications and to its challenging theoretical aspects.

It is known that the mechanical properties of a viscoelastic fluid can be dramatically different from those of a pure Newtonian solvent. One of the most striking differences is encountered in flow stability. It is well-established, indeed, that the properties of the laminar-to-turbulent transition are significantly altered by the presence of polymers, often resulting in the occurrence of novel types of instability mechanisms.

Here I will focus on the stability of a polymer solution in the Kolmogorov flow, where analytical perturbative methods can be applied, and I will present a numerical investigation on the dynamics of the turbulent viscoelastic Kolmogorov flow.

Chapter 5 is dedicated to the brief introduction to the stability analysis of fluid flows, and the Newtonian and viscoelastic cases are compared. The occurrence of elasticity driven turbulent-like states, and the dynamics of turbulent polymer solutions are also addressed.

In chapter 6 I will present the most used polymer solution models, focusing on their efficacy and on the correspondence between the phenomenology of the solution and microscopic description of polymer molecules.

In chapter 9 I will report the results of numerical simulations of a polymer solution in a turbulent Kolmogorov flow. These results suggest that the basic physical mechanisms of the drag reduction phenomenon can be studied in the absence of material boundaries.

Chapter 5

Dynamics of polymer solutions

Flow stability analysis is a formidably difficult problem in fluid dynamics. Even more challenging is the study of the stability of polymer solutions, due to their rich phenomenology. In general, the difficulties arising from the complexity of the laminar-to-turbulent transition and from the dynamics of viscoelastic fluids hinder the analytical approach, and numerical simulations are often the only suitable method of investigation.

In this chapter I will report some recent observations on the stability of polymer solutions [1, 2], which demonstrate that instabilities can develop in the limit of very small Reynolds numbers. These are called elastic instabilities. Moreover, I will present the results on the emergence of a novel turbulent-like state occurring at small Reynolds numbers, that has been called elastic turbulence [3, 4]. Finally I will briefly recall the major features of the drag reduction phenomenon [5, 6].

5.1 Flow stability analysis

5.1.1 The Newtonian case

The transition of fluid flows from a laminar to turbulent state is a matter of everyday experience. The flow of an incompressible fluid is a solution of the well known Navier-Stokes equations:

$$\begin{aligned}\partial_t v_\alpha + v_\beta \partial_\beta v_\alpha &= -\partial_\alpha p + \nu \partial^2 v_\alpha + f_\alpha \\ \partial_\alpha v_\alpha &= 0\end{aligned}\tag{5.1}$$

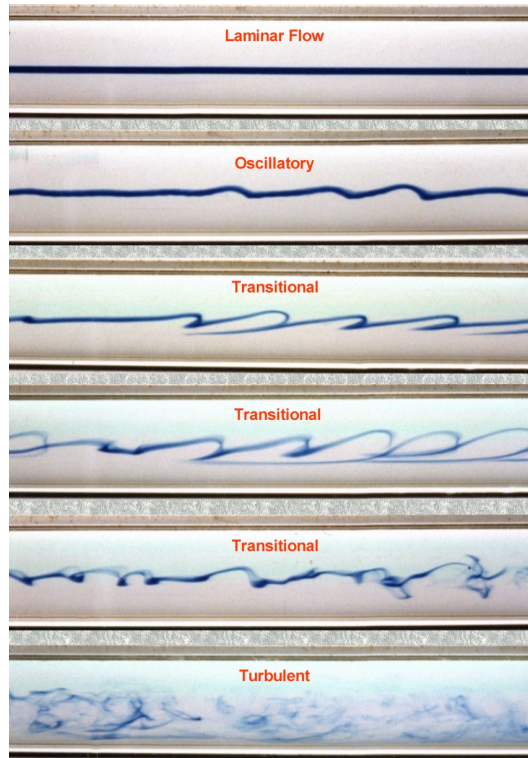


Figure 5.1: The laminar-to-turbulent transition in a Reynolds tank. The Reynolds number increases from top to bottom. Above the laminar regime transverse perturbations develop, eventually leading to a turbulent state. Picture taken from www.eng.man.ac.uk.

where v is the velocity field, p is the pressure, ν is the kinematic viscosity and f is a forcing term. The ratio of inertial effects to viscous forces is expressed by the Reynolds number:

$$\text{Re} = \frac{VL}{\nu} \quad (5.2)$$

where V is the typical velocity and L is a typical length scale. For small Re the dynamics is dominated by the viscosity, flows are regular and externally induced perturbations decay in time (see fig. 5.1).

With increasing Re , inertial effects take over, flows become essentially irregular in space and time, and “fully developed turbulence” is eventually achieved.

The study of the transition to turbulence is a longstanding problem in fluid dynamics for both its theoretical interest and technological applications. The basic idea of a stability analysis is the

following: a basic flow \vec{U} is perturbed by a superimposed velocity field \vec{w} . Such a flow is stable if the perturbation \vec{w} diminishes in time, whereas it is unstable if the perturbation grows and gives rise to an irregular (and eventually turbulent) state.

The perturbed flow is described by the velocity and pressure fields:

$$\begin{cases} v_\alpha = U_\alpha + w_\alpha \\ p = P + q \end{cases} \quad (5.3)$$

the evolution equation of which can be written by imposing that the flow (\vec{U}, P) satisfies the Navier-Stokes equations:

$$\partial_t w_\alpha + U_\beta \partial_\beta w_\alpha + w_\beta \partial_\beta U_\alpha + w_\beta \partial_\beta w_\alpha = -\partial_\alpha q + \nu \partial^2 w_\alpha \quad (5.4)$$

$$\partial_\alpha w_\alpha = 0 \quad (5.5)$$

This problem is even more complicated than the starting one, as there are two more terms which describes the coupling between the basic flow and the perturbation. To date a fully analytical approach to this problem is not available, except for few very simple cases.

A simplification of the problems (5.4), (5.5) is obtained if the perturbations amplitude is assumed to be slow with respect to the basic flow. This permits to neglect the nonlinear term in eq. (5.4), arriving to a linear equation for \vec{w} . The stability analysis performed under this simplification is called *linear stability analysis*. Although linear stability analysis represents a suitable approach to the problem, there are flows that are linearly stable but in fact unstable. In these cases a fully nonlinear analysis or a *weakly nonlinear analysis* should be performed. The latter is a perturbative approach in the small parameter obtained by the ratio between the perturbation amplitude and the basic flow amplitude.

Stability of a parallel flow

In the case of a plane parallel flow $\vec{U} = (U(y), 0, 0)$, eq. (5.4) simplifies to:

$$\begin{aligned} \partial_t w_x + U \partial_x w_x + w_y \partial_y U &= -\partial_x q + \nu \partial^2 w_x \\ \partial_t w_y + U \partial_x w_y &= -\partial_y q + \nu \partial^2 w_y \\ \partial_t w_z + U \partial_x w_z &= -\partial_z q + \nu \partial^2 w_z \end{aligned} \quad (5.6)$$

A normal mode expansion can be performed in x, z, t and the stability is related to the evolution in time of each mode.

A further simplification is introduced by the Squire's theorem [7], which for a parallel flow assures that *to each unstable three-dimensional disturbance there corresponds a more unstable two-dimensional one*. With this simplification we can describe everything in terms of the stream function and of its normal modes:

$$w_x = \partial_y \psi \quad (5.7)$$

$$w_y = -\partial_x \psi \quad (5.8)$$

$$\psi \longrightarrow \phi e^{ik(x-ct)} \quad (5.9)$$

where ϕ is the Fourier transform of ψ . Plugging these identities in eqs. (5.6) we can derive an evolution equation for the stream function:

$$(U - c)(\partial_y^2 \phi - k^2 \phi) - (\partial_y^2 U)\phi = \frac{\nu}{ik}(\partial_y^4 \phi - 2k^2 \partial_y^2 \phi + k^4 \phi) \quad (5.10)$$

that is called the *Orr-Sommerfeld* equation (see for example [8]). The analytical approach to eq. (5.10) is almost prohibitive, except for a few cases, and numerical studies are necessary to solve the problem.

5.1.2 The viscoelastic case

Conceptually, the same analysis can be repeated for viscoelastic flows. Practically (see chapter 6) the main additional difficulty arises from the description of viscoelasticity. The stresses in a viscoelastic fluid are modified by the presence of polymers and their evolution should be modeled accurately. This adds to eqs. (5.6) new unknowns and possibly terms of coupling between the polymeric stress and the velocity field.

The parameter that describes the relative importance of viscous effects over elastic effects is usually the non-dimensional Weissenberg number Wi (or Deborah number De). In principle we expect that the critical point above which instabilities can grow will be characterized by a critical Re and a critical Wi .

In the regime of small Re and small Wi flows are laminar and no instabilities take place. With increasing Re , inertial instabilities develop: these instabilities are those occurring in the Newtonian

case, possibly altered by the presence of polymers. In the limit of small Re and large Wi purely elastic instabilities can appear. These have no equivalence with the Newtonian case, and are generated by the viscoelasticity of the fluid.

In the past years a number of important experiments and numerical simulations have been performed to investigate the stability of viscoelastic flows. The instabilities that can arise in viscoelastic fluids are different according to the properties of the solution: dilute unentangled or moderately entangled solutions show altered hydrodynamic instabilities with respect to the Newtonian case, whereas concentrated entangled solutions show a different class of instabilities, namely fracture. Nevertheless, in all kinds of viscoelastic flows purely elastic instabilities are likely to appear.

Larson and coworkers [9] and then Steinberg and coworkers [10] studied experimentally the effect of elasticity on the stability of a Couette-Taylor flows by varying the ratio between Re and Wi . They found the existence of inertial and purely elastic instabilities, and they characterized these two regions and the crossover between them. A detailed analysis can be found in refs. [1, 2, 11, 12].

5.2 Elastic turbulence

In a series of recent papers by Steinberg and coworkers [3, 4, 10, 13] it has been noted that a turbulent like state can be generated at vanishingly small Reynolds number, yet relatively large Weissenberg numbers in polymer solution flows. The emergence of a “small- Re turbulence” is very important in all mixing related applications, as this implies that it is not necessary to excite a flow at large Reynolds numbers to obtain an efficient mixing. For example this could be exploited to improve drug mixing in micro-devices, where is typically difficult to reach large Re .

In polymer solutions an elasticity parameter measuring the relative importance of elasticity and viscosity can be defined as $El = Wi/Re$. When $El \lesssim 1$ and Re is small, the flow behaves like a laminar Newtonian flow. For large enough El , elastic instabilities develop, giving rise to a state exhibiting some features of developed turbulence. Steinberg and coworkers have identified a principal measure of elastic turbulence by measuring the ratio between the average shear stress and its corresponding value for a laminar flow.

For a flow between two rotating circular plates, this ratio has been

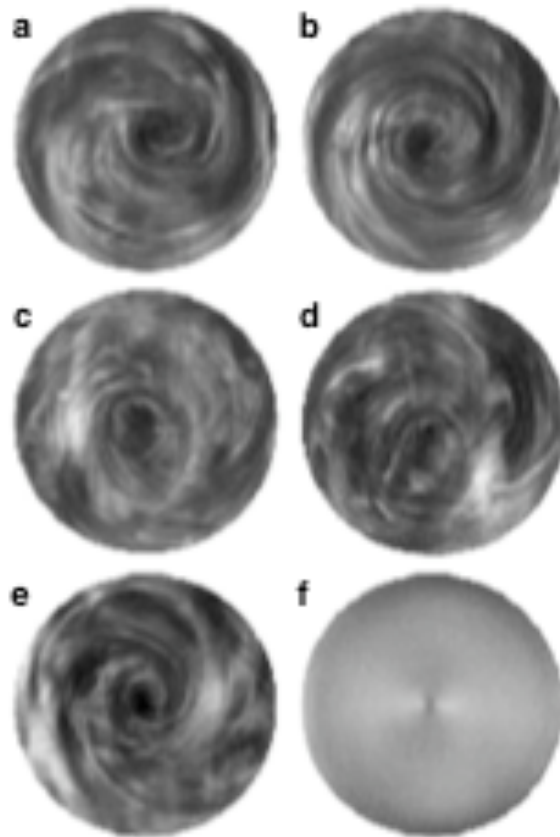


Figure 5.2: Representative snapshots of elastic turbulence in a flow generated between two rotating coaxial plates [4]. (a, b) Polymer solution at $Wi = 6.5$, $Re = 0.35$; (c, d, e) polymer solution at $Wi = 13$, $Re = 0.7$; (f) pure solvent at $Re = 1$.

measured (see ref. [3]). When the relative angular velocity between the two plates is increased the average rescaled shear stress grows significantly, showing a sharp transition. The same maximum stress value is found in a corresponding flow of a Newtonian fluid for $Re \sim 10^4$, whereas the measurements were taken at $Re < 1$, showing that these effects are due to the fluid elasticity. The spatial spectra of the velocity field have been measured, and a power law tail has been observed. This flow is irregular in time and in space, essentially at large scales.

Qualitatively the polymers are stretched by the shear flow thus triggering elastic instabilities. These instabilities give rise to a secondary flow that stretches further the molecules until the system reaches a stationary state. A theoretical analysis of elastic turbu-

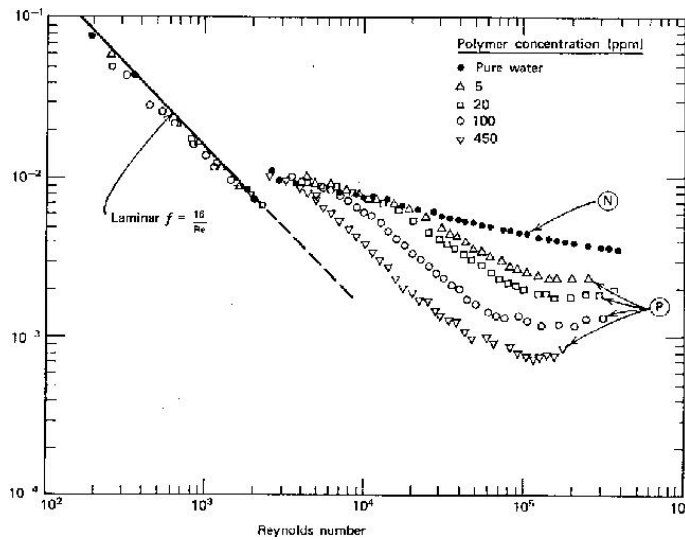


Figure 5.3: The friction coefficient as a function of the Reynolds number [5]. Black dots represent the Newtonian case, whereas the other symbols correspond to different concentrations of polymers. For small Re the typical dependence Re^{-1} is observed. After the transition from laminar to turbulent the friction coefficient notably reduces, and is a function of the concentration.

lence has been proposed in refs. [14–16].

5.3 The drag reduction phenomenon

The case of elastic turbulence concerns the regime $Re \ll 1$ and $El \gg 1$. In the opposite regime, $Re \gg 1$ and $El \ll 1$, inertial instabilities lead to a turbulent state with phenomenology different from the Newtonian one.

Since the seminal work by Toms it is known that the addition of a few parts per million of long chain polymers in a pipe flow can reduce the skin friction of a factor near 80%. The fundamental aspects related to the drag reduction phenomenon in a pipe flow have been reviewed by Virk [5] and are briefly explained hereafter. The friction coefficient can be defined as:

$$f = \frac{\Delta p}{\rho V^2} \frac{R}{L} \quad (5.11)$$

where Δp is the pressure drop across a length L of the pipe of radius R , ρ is the density and V is the mean-stream velocity. This coefficient is related to the frictional loss in pumping the fluid

through the pipe. For a turbulent pipe flow of a polymer solution the friction coefficient can be dramatically reduced in comparison to the Newtonian case, as shown in fig. 5.3, i.e. drag reduction occurs. In plain words the pressure drop that should be imposed to maintain a given throughput in the pipe is smaller for a polymer solution than for a Newtonian flow.

Many theories have been proposed to explain what is the basic physical mechanism of the drag reduction phenomenon. Lumley [17] proposed a quantitative approach based on the phenomenology of the channel flow. Another approach is due to de Gennes [18], who suggested an elasticity-based criterion. More recently Moin, Shaqfeh and collaborators proposed a mechanism based on the interaction of coherent structures (see for example [19, 20]). Much effort in understanding the mechanism of drag reduction in wall flows has been dedicated also by Piva, Casciola and coworkers (see [21] and refs. therein), by Procaccia and coworkers (see [22] and refs. therein), by Benzi and coworkers (see [23] and refs. therein), by Chertkov [24], Lebedev and coworkers [14, 15]. Collins, Sureshkumar, Beris and their respective collaborators have devoted a lot of attention to the numerical algorithms to simulate polymer solutions [25, 26]. Finally, recent experimental results are reported in refs. [6, 27–31]. A list of references updated to 1997 can be found in ref. [32].

Despite the considerable number of studies, a quantitative, fully satisfactory, explanation of drag reduction is not available yet, and the phenomenological theories are not universally accepted [33]. The experimental and theoretical studies of drag reduction have been performed in wall bounded flows, due to technological and industrial applications. We remark here that this effect can take place also without material boundaries (see chapter 9).

Chapter 6

Viscoelastic fluid models

Much effort has been dedicated in the past years to the formulation of polymer solution models able to reproduce experimental observations, yet simple enough to be simulated numerically or even treated analytically. This endeavor is motivated on the one hand by the diversity of phenomenological behaviors of polymer solutions, and on the other hand by the fact that numerical simulations of viscoelastic flows are exceptionally expensive from a computational point of view.

In this chapter I will present the most common models of viscoelastic fluids and show how these can be connected with the description of the polymer dynamics at the microscopic level.

6.1 Constitutive equations for viscoelastic fluids

A fluid is characterized by a constitutive equation that describes its mechanical response. This express the stress \mathcal{T} in a fluid element due to an external deformation rate \mathcal{D} :

$$\mathcal{T} = \mathcal{T}(\mathcal{D}) \tag{6.1}$$

where $\mathcal{D} = (\partial v + \partial v^T)/2$.

For a Newtonian fluid the stress is proportional to the rate of deformation via the viscosity of the fluid. The mechanical response of a fluid can be characterized for example in viscometric flows (see e.g. [34]), where a constant shear rate is imposed and the correspondingly produced stress can be measured. For example such

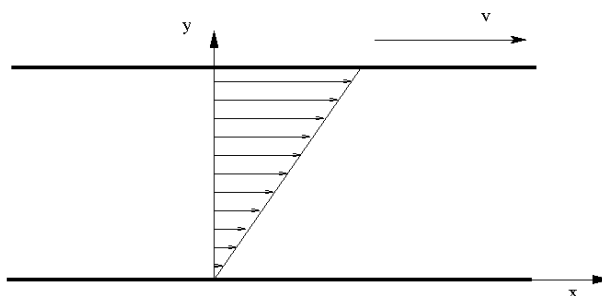


Figure 6.1: A sketch of a shearing flow used to measure the stress opposing an externally imposed deformation.

a flow can be generated as in fig. 6.1, where a fluid lies between two plates and one of them is displaced at constant velocity \vec{v} . This produces a pure shear flow with constant rate s , $v_x = sy$. A shear stress is generated by this deformation, whose components are:

$$\mathcal{T}_{xy} = \mathcal{T}_{yx} = \eta s \quad (6.2)$$

$$\mathcal{T}_{xx} = \mathcal{T}_{yy} = \mathcal{T}_{zz} = 0 \quad (6.3)$$

where η is the dynamics viscosity of the solvent, and the following relations hold:

$$N_1 = \mathcal{T}_{xx} - \mathcal{T}_{yy} = 0 \quad N_2 = \mathcal{T}_{yy} - \mathcal{T}_{zz} = 0 \quad (6.4)$$

where N_1 and N_2 are called the first and second normal stress differences, respectively.

For non-Newtonian fluids there is in general no proportionality between the stress and the rate of deformation, and the relation between them is more complicated.

Viscoelastic fluids are a class of non-Newtonian fluids that can be obtained for example by adding a few parts per million of long chain polymer to a Newtonian solvent. Chewing gum and polyurethane memory foam are other examples of viscoelastic materials.

In the case of viscoelastic fluids, the stress in a fluid element depends in general on the deformation history of that element. For example, in the experiment of fig. 6.1, if one stops the plate suddenly after the application of the external deformation, a time-dependent shear stress would be observed.

In eq. (6.2) the viscosity is replaced by a function of the local shear rate (called the shear viscosity) and of time. Usually this is a monotonically decreasing function of the shear rate, and the behavior of

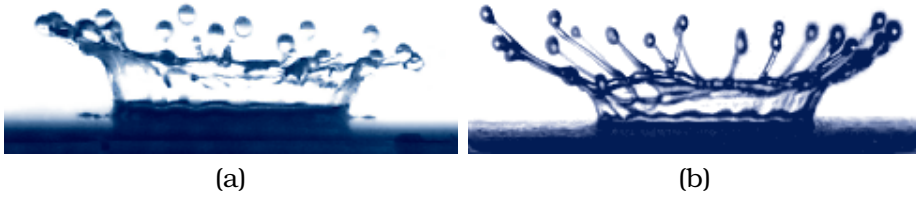


Figure 6.2: (a) A falling Newtonian fluid drop. (b) A non-Newtonian fluid drop. Due to the presence of altered normal stresses, the adhering part of the drop is smaller than for the Newtonian fluid, and the filaments are thinner.

the fluid is said to be “shear-thinning”. However, in some cases, the viscosity can increase with the shear rate, and the fluid is called “shear thickening”.

The first normal stress difference N_1 , which also depends on the local shear rate, is positive for polymeric liquids, giving rise to the most typical demonstrations of non-Newtonian behaviors, such as the rod-climbing (or Weissenberg) effect, the very large extrudate swelling at the exit of a die or the example given in fig. 6.2. The second normal stress difference N_2 is negative.

A review of the most common constitutive equations for polymeric liquids can be found in ref. [35] whereas a complete treatment can be found for example in ref. [36]. In the following subsections I will present the constitutive equations on which some of the most accepted polymer solution models are based.

6.1.1 The Maxwell model

An intuitive one-dimensional model for a viscoelastic fluid is sketched in fig. 6.3. The viscous behavior is reproduced by a dashpot, while the elastic behavior is represented by a spring. The tension T of the system would satisfy the following differential equation:

$$T + \tau \dot{T} = \eta D \quad (6.5)$$

where D is the strain rate of this system, and $\tau = \eta/k$ is the relaxation time of the dashpot. This is called the Maxwell model [36]. Other simple one-dimensional models can be realized by combining differently the spring and the dashpot: for example the so called Kelvin (or Voigt) model is obtained by a spring and a dashpot in parallel.

The generalization of the Maxwell model to the case of fluids yields

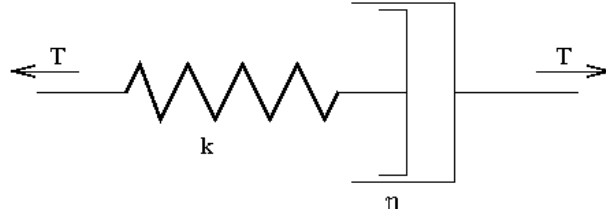


Figure 6.3: A representation of the Maxwell model as a superposition of a spring of elastic constant k and a dashpot corresponding to the viscosity η .

the constitutive equation:

$$\mathcal{T} + \tau \overset{\nabla}{\mathcal{T}} = 2\eta \mathcal{D} \quad (6.6)$$

where \mathcal{T} is the total stress tensor, and the symbol $\overset{\nabla}{\mathcal{T}}$ describes the time evolution of the tensor in a velocity field v [37] and is called upper-convected derivative:

$$\overset{\nabla}{\mathcal{T}} = \partial_t \mathcal{T} + v \cdot \partial \mathcal{T} - \partial v \cdot \mathcal{T} - \mathcal{T} \cdot \partial v^T \quad (6.7)$$

This model is also called upper convected Maxwell model.

The Maxwell model shows constant shear viscosity η , a first normal stress difference quadratic in the local shear rate, whereas the second normal stress difference is zero.

The drawback of the Maxwell model is that the so called extensional viscosity (the analogous of the shear viscosity for an elongational flow) is meaningful only for small stretching rates, and is negative for larger values.

6.1.2 The Oldroyd-B model

A more refined model is the Oldroyd-B model [36–39]. Its basic ingredient is that the stress is decomposed into two parts: a Newtonian contribution \mathcal{T}^n and a polymer contribution \mathcal{T}^p . Each of these components obeys a constitutive equation:

$$\mathcal{T}^n = 2\eta^n \mathcal{D} \quad (6.8)$$

$$\mathcal{T}^p + \tau \overset{\nabla}{\mathcal{T}}^p = 2\eta^p \mathcal{D} \quad (6.9)$$

where η^n is the solvent viscosity and η^p is the polymer contribution to the total viscosity. In the Oldroyd-B model the shear viscosity is

$\eta = \eta^n + \eta^p$, the first normal stress difference N_1 is quadratic in the local shear rate and $N_2 = 0$.

The main difference between the Oldroyd-B model and the Maxwell model is in the emergence of a second typical timescale. Indeed the constitutive equation for the total stress is:

$$\mathcal{T} + \tau \overset{\nabla}{\mathcal{T}} = 2\eta \left(\mathcal{D} + \tau_R \overset{\nabla}{\mathcal{D}} \right) \quad (6.10)$$

where $\tau_R = \eta^n \tau / \eta$ is called the retardation time. It is worth noticing that physically the relaxation time expresses the property of the fluid to have non zero stress even when no rate of deformation is applied, whereas the retardation time is related to the fact that the reaction to a deformation is not immediately followed by a corresponding stress. Note that the Oldroyd-B model recovers the Maxwell model for $\tau_R = 0$. Within this model the extensional viscosity is meaningful in a wider range of stretching rates.

6.1.3 The Giesekus model

In the Giesekus model [40], as in the Oldroyd-B model, the total stress is decomposed into solvent and polymer contributions, where the solvent contribution obeys eq. (6.8). Starting from considerations on the behavior of the solution at the molecular level, Giesekus developed a nonlinear evolution equation for \mathcal{T} that depends on three parameters:

$$\mathcal{T}^p + \tau \overset{\nabla}{\mathcal{T}}^p + \frac{\alpha_G \tau}{\eta^p} \mathcal{T}^p \cdot \mathcal{T}^p = 2\eta^p \mathcal{D} \quad (6.11)$$

This model has gained prominence because it accurately describes normal-stresses and gives a reasonable description of the behavior of a viscoelastic fluid in elongational flows. The third parameter α_G formally corresponds to the introduction of a stress-dependent relaxation time, that is also responsible for the emergence of a nonlinear term. The Giesekus model recovers the Oldroyd-B model for $\alpha_G = 0$ and the Maxwell model for $\alpha_G = 0$ and $\tau_R = 0$.

6.2 From the dumbbell to the constitutive equation

Simple theories that connect the dynamics of the dissolved molecules and the macroscopic behavior can be developed by exploiting the following assumptions [34, 36]:

- the solution is dilute, so that polymer-polymer interactions are negligible
- the concentration is uniform
- the solution is mono-disperse, i.e. there is only one kind of polymers.

Particularly simple is the case of the dumbbell model. The evolution equation of the end-to-end vector of a polymer described with the linear dumbbell model is:

$$\dot{R}_\alpha = -\frac{1}{2\tau}R_\alpha + R_\beta\partial_\beta v_\alpha + \sqrt{\frac{R_0^2}{\tau}}\xi_\alpha(t) \quad (6.12)$$

The average end-to-end vector of the polymers can be expressed in terms of the so called conformation tensor $\sigma_{\alpha\beta} = \langle R_\alpha R_\beta \rangle$, where the average is taken over the realizations of the thermal noise. The evolution equation for the conformation tensor can be derived from eq. (6.12):

$$\partial_t \sigma + v \cdot \partial \sigma - \partial v \cdot \sigma - \sigma \cdot \partial v^T = \frac{\nabla}{\tau} \sigma = -\frac{1}{\tau}(\sigma - R_0^2 \mathbb{1}) \quad (6.13)$$

where $\mathbb{1}$ is the identity. The conformation tensor can be interpreted as the effective average elongation of uniformly distributed and non-interacting polymers, as a function of space and time. Eq. (6.13) describes polymer deformation due to the presence of a velocity gradient.

The polymer contribution to the total stress per unit volume is:

$$\mathcal{T}^p = -n\langle \mathbf{R} \mathbf{F} \rangle - nHR_0^2 \mathbb{1} = nH(\sigma - R_0^2 \mathbb{1}) \quad (6.14)$$

where n is the number of dumbbells per unit volume and $\mathbf{F} = -H\mathbf{R}$ is the recalling force.

From eq. (6.13) and eq. (6.14) it is easy to obtain the evolution equation for the polymer contribution to the total stress:

$$\mathcal{T}^p + \tau \overset{\nabla}{\mathcal{T}}^p = 2R_0^2 n H \tau \mathcal{D} \quad (6.15)$$

where $R_0^2 n H \tau \equiv \eta^p$ is the polymer contribution to the total viscosity. Therefore the Oldroyd-B model constitutive equations correspond to considering a dilute uniform solution of non-interacting linear dumbbells.

The evolution equation for the stress tensor in the Giesekus model can be derived by assuming that the relaxation time is an anisotropic function of the stress:

$$\tau_G = \tau \left(\mathbf{1} - \frac{\alpha_G}{n k_B T} \mathcal{T}^p \right) \quad (6.16)$$

6.2.1 Evolution equations for the Oldroyd-B model

Plugging the expression for the total stress $\mathcal{T} = \mathcal{T}^n + \mathcal{T}^p$ into eq. (5.1) we obtain:

$$\begin{aligned} \partial_t \mathbf{v} + \mathbf{v} \cdot \partial \mathbf{v} &= -\frac{1}{\rho} \partial p + \nu^n \partial^2 \mathbf{v} + \frac{\nu^p}{\tau} \partial \cdot \frac{\boldsymbol{\sigma}}{R_0^2} + \mathbf{f} \\ \partial_t \boldsymbol{\sigma} + \mathbf{v} \cdot \partial \boldsymbol{\sigma} &= \partial \mathbf{v} \cdot \boldsymbol{\sigma} + \boldsymbol{\sigma} \cdot (\partial \mathbf{v})^T - \frac{1}{\tau} (\boldsymbol{\sigma} - R_0^2 \mathbf{1}) \\ \partial \cdot \mathbf{v} &= 0 \end{aligned} \quad (6.17)$$

where $\nu^n = \eta^n / \rho$ and $\nu^p = \eta^p / \rho$.

The Oldroyd-B model has been recently used to successfully investigate thermal convection in viscoelastic fluids [41], the occurrence of vortex pairing in viscoelastic Taylor-Couette flows [42], and drag reduction in channel flows [43].

It is worth noticing that from a computational point of view the numerical simulation of eqs. (6.17) can be expensive both for the increased number of unknowns with respect to the Newtonian case and for computational problems related to the evolution equation for $\boldsymbol{\sigma}$. By definition $\boldsymbol{\sigma}$ is a positive defined tensor: nonetheless, due to numerical errors, its positive definiteness can be lost during the time evolution. Alternative numerical schemes have been proposed to prevent these instabilities such as adding an artificial diffusivity on the tensor $\boldsymbol{\sigma}$ [26] or by decomposing it appropriately [25].

6.2.2 The FENE-P models

A conceptually simple extension to the Oldroyd-B model is the FENE-P model. When the polymer extension approaches the contour length L , the linear dumbbell model fails and nonlinearity becomes important. In this case it is sufficient to replace the elastic Hookean force by the Warner law (see chapter 2 and ref. [44]):

$$\mathbf{F} = -H \frac{\mathbf{R}}{1 - \frac{R^2}{L^2}} \quad (6.18)$$

However this would yield a nonlinear evolution equation for $\boldsymbol{\sigma}$ which is not closed:

$$\overset{\nabla}{\boldsymbol{\sigma}} = -\frac{1}{\tau} \left(\left\langle \frac{\mathbf{R}\mathbf{R}}{1 - \frac{\text{tr}(\mathbf{R}\mathbf{R})}{L^2}} \right\rangle - R_0^2 \mathbf{1} \right) \quad (6.19)$$

A commonly accepted closure is the Peterlin approximation [45]: the average term of eq. (6.19) is replaced by:

$$\frac{\boldsymbol{\sigma}}{1 - \frac{\text{tr}(\boldsymbol{\sigma})}{L^2}} \quad (6.20)$$

This approximation leads to the following evolution equation:

$$\overset{\nabla}{\boldsymbol{\sigma}} = -\frac{1}{\tau} \left(\frac{\boldsymbol{\sigma}}{1 - \frac{\text{tr}(\boldsymbol{\sigma})}{L^2}} - R_0^2 \mathbf{1} \right) \quad (6.21)$$

The FENE-P model is generally more accurate than the Oldroyd-B model in reproducing the scaling behavior for the shear viscosity and the normal stress differences. The FENE-P model compares well to the experimental measurements of extensional viscosity and is shear-thinning.

Chapter 7

Linear stability analysis of the viscoelastic Kolmogorov flow

In this chapter I will present my results on the stability analysis of the viscoelastic Kolmogorov flow. In 1959 A.N. Kolmogorov suggested to study this flow, which is parallel and periodic, as a toy model for the analysis of the transition to turbulence [46]. Shortly after Meshalkin and Sinai [47] were able to show that the Kolmogorov flow is linearly unstable with respect to large-scale transverse perturbation, still nonlinearly stable with respect to small-scale disturbances.

We have studied the occurrence of instabilities in a viscoelastic Oldroyd-B fluid in the Kolmogorov flow. By means of a perturbative, analytical approach, the instabilities of the Kolmogorov flow can be captured (see refs. [48–50]). Here we aim at studying the stability of a Kolmogorov flow of an Oldroyd-B fluid. For small polymer elasticity the solution behaves like a Newtonian fluid, and the instabilities are the same of the Newtonian case. For large polymer elasticity we recover purely elastic instabilities that develop differently from inertial ones, and cannot be studied completely within the analytical framework. We have performed numerical simulations to better understand how linear elastic instabilities take place.

As an introductory case, the linear stability analysis of the Newtonian Kolmogorov flow [47] will be performed by means of a multi-scale approach [51]. The analysis can be repeated in the other cases with the same spirit, but it is longer and the detailed calcu-

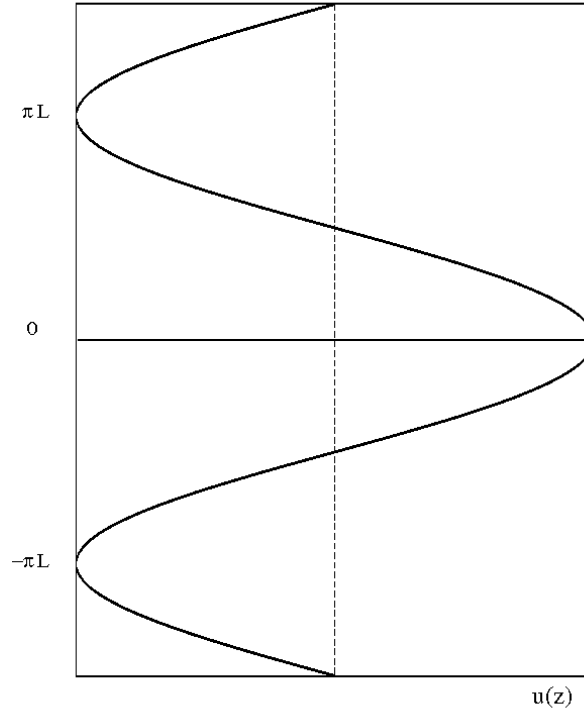


Figure 7.1: The Kolmogorov flow profile.

lations will not be reported.

7.1 The Newtonian case

As the Kolmogorov flow is a plane parallel flow, the Squire's theorem applies (see chapter 5 and ref. [7]). The two-dimensional Kolmogorov flow is obtained by imposing a sinusoidal forcing in the x direction, oscillating in the z direction, resulting in a sinusoidal profile for the velocity (see fig. 7.1):

$$\mathbf{f} = \left(\frac{\nu V}{L^2} \cos \frac{z}{L}, 0 \right) \quad \mathbf{u} = \left(V \cos \frac{z}{L}, 0 \right) \quad (7.1)$$

where $2\pi L$ is the periodicity box size.

The linearized evolution equations for the perturbations are:

$$\begin{aligned} \partial_\gamma w_\gamma &= 0 \\ \partial_t w_\gamma + \partial_\beta (u_\beta w_\gamma + w_\beta u_\gamma) &= -\partial_\gamma q + \nu \partial^2 w_\gamma \end{aligned} \quad (7.2)$$

Following ref. [51] we investigate the dynamics of perturbations with a characteristic length scale much larger than L . The ratio between the two scales will be denoted by ϵ . Therefore we introduce two classes of variables: the fast (x, t) and the slow $(\tilde{x} = \epsilon x, \tilde{t} = \epsilon^2 t)$ variables. The scaling of the slow time has been set to be quadratic as we expect to end up with a diffusive equation for the large-scale flow. With this spirit we introduce also the differential operators with respect to the fast and slow variables:

$$\partial_i \rightarrow \partial_i + \epsilon \tilde{\partial}_i, \quad \partial_t \rightarrow \partial_t + \epsilon^2 \tilde{\partial}_t, \quad (7.3)$$

The perturbation fields can then be expanded in power of ϵ as follows:

$$\mathbf{w} = \mathbf{w}^{(0)}(z, t, \tilde{x}, \tilde{z}, \tilde{t}) + \epsilon \mathbf{w}^{(1)}(z, t, \tilde{x}, \tilde{z}, \tilde{t}) + \epsilon^2 \mathbf{w}^{(2)}(z, t, \tilde{x}, \tilde{z}, \tilde{t}) + \dots, \quad (7.4)$$

$$q = q^{(0)}(z, t, \tilde{x}, \tilde{z}, \tilde{t}) + \epsilon q^{(1)}(z, t, \tilde{x}, \tilde{z}, \tilde{t}) + \epsilon^2 q^{(2)}(z, t, \tilde{x}, \tilde{z}, \tilde{t}) + \dots, \quad (7.5)$$

as we don't expect a dependence on the fast variable x . Substituting the expansions in eqs. (7.2) we end up with a hierarchy of equations at the various orders in ϵ . These must be solved together with the corresponding solvability conditions, obtained by averaging the equations at each order on the periodicity of the small scale. At order 0 we have:

$$\begin{aligned} w_x^{(0)} &= \frac{VL}{\nu} \langle w_z^{(0)} \rangle \sin\left(\frac{z}{L}\right) + \langle w_x^{(0)} \rangle \\ w_z^{(0)} &= \langle w_z^{(0)} \rangle \\ q^{(0)} &= 0 \end{aligned} \quad (7.6)$$

whereas at order ϵ we have:

$$\begin{aligned} w_x^{(1)} &= 3 \frac{VL^2}{\nu} \tilde{\partial}_z \langle w_z^{(0)} \rangle \cos\left(\frac{z}{L}\right) + \frac{VL}{\nu} \langle w_z^{(1)} \rangle \sin\left(\frac{z}{L}\right) + \langle w_x^{(1)} \rangle \\ w_z^{(1)} &= \frac{VL^2}{\nu} \tilde{\partial}_x \langle w_z^{(0)} \rangle V \cos\left(\frac{z}{L}\right) + \langle w_z^{(1)} \rangle \\ \tilde{\partial}_x \langle w_x^{(0)} \rangle + \tilde{\partial}_z \langle w_z^{(0)} \rangle &= 0 \end{aligned} \quad (7.7)$$

The solvability condition at order ϵ^2 gives a closed equation in the field $\mathbf{w}^{(0)}$:

$$\begin{aligned} \tilde{\partial}_t \langle w_x^{(0)} \rangle &= \frac{7V^2 L^2}{2\nu} \tilde{\partial}_x^2 \langle w_x^{(0)} \rangle - \tilde{\partial}_x \langle q^{(1)} \rangle + \nu \left(\tilde{\partial}_z^2 + \tilde{\partial}_x^2 \right) \langle w_x^{(0)} \rangle \\ \tilde{\partial}_t \langle w_z^{(0)} \rangle &= -\frac{1}{2} \frac{V^2 L^2}{\nu} \tilde{\partial}_x^2 \langle w_z^{(0)} \rangle - \tilde{\partial}_z \langle q^{(1)} \rangle + \nu \left(\tilde{\partial}_z^2 + \tilde{\partial}_x^2 \right) \langle w_z^{(0)} \rangle \end{aligned} \quad (7.8)$$

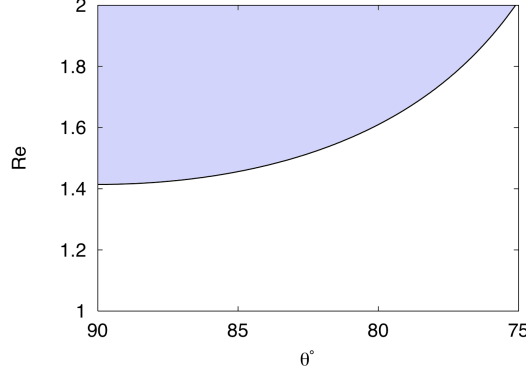


Figure 7.2: Stability diagram of the Kolmogorov flow as a function of the Reynolds number and the angle between the perturbation and the basic flow. The colored region is unstable and the white region is stable.

The field $w^{(0)}$ can be expressed in terms of a stream function:

$$\langle w_x^{(0)} \rangle = \frac{1}{V} \tilde{\partial}_z \psi \quad \langle w_z^{(0)} \rangle = -\frac{1}{V} \tilde{\partial}_x \psi \quad (7.9)$$

and eq. (7.8) can finally be rewritten as:

$$\tilde{\partial}_t (\tilde{\partial}_x^2 + \tilde{\partial}_z^2) \psi = \tilde{\nu}_{\alpha\beta} \tilde{\partial}_\alpha \tilde{\partial}_\beta \psi = \quad (7.10)$$

$$= \nu (\tilde{\partial}_z^2 + \tilde{\partial}_x^2)^2 \psi + \frac{7V^2 L^2}{2\nu} \tilde{\partial}_z^2 \tilde{\partial}_x^2 \psi - \frac{V^2 L^2}{2\nu} \tilde{\partial}_x^4 \psi \quad (7.11)$$

The stability of the Kolmogorov flow is given by the sign of the operator $\tilde{\nu}_{\alpha\beta} \tilde{\partial}_\alpha \tilde{\partial}_\beta$, where the tensor $\tilde{\nu}$ is called eddy viscosity. Introducing the Reynolds number $Re = VL/\nu$, and expressing the stream function in terms of normal modes we have:

$$\begin{aligned} \psi &= e^{ik\tilde{x} + im\tilde{z}} \\ \frac{k}{m} &= \tan(\theta) \\ (2 - Re^2) \tan^4(\theta) + (4 + 7Re^2) \tan^2(\theta) + 2 &\geq 0 \end{aligned} \quad (7.12)$$

where θ is the angle between w and u . The sign of this quadratic form is reported in fig. 7.2 as a function of θ and Re . The Kolmogorov flow is always linearly stable with respect to large-scale perturbations below a critical value $Re_c = \sqrt{2}$ [47, 52]. For $Re_c > \sqrt{2}$ the flow is stable only with respect to perturbation with a certain angle, as shown in fig. 7.2.

7.2 The viscoelastic case

The multi-scale analysis performed in the previous section can be repeated in the viscoelastic case. A generalization of the Squire's theorem to the case of viscoelastic flows is given in the appendix of the article following chapter 8. To perform the stability analysis, a perturbation on the velocity w , the pressure q and the conformation tensor ζ must be imposed. The corresponding linearized evolution equations are:

$$\begin{aligned}
 \partial_\alpha w_\alpha &= 0 \\
 \partial_t w_\alpha + \partial_\beta (u_\alpha w_\beta + w_\alpha u_\beta) &= -\partial_\alpha q + \nu\beta\partial^2 w_\alpha + \frac{(1-\beta)\nu}{\tau}\partial_\beta\zeta_{\beta\alpha} \\
 \partial_t\zeta_{\alpha\beta} + \partial_\gamma (u_\gamma\zeta_{\alpha\beta} + w_\gamma\sigma_{\alpha\beta}) &= \partial_\gamma u_\alpha\zeta_{\gamma\beta} + \partial_\gamma w_\alpha\sigma_{\gamma\beta} \\
 &+ \partial_\gamma w_\alpha\zeta_{\gamma\beta} + \zeta_{\alpha\gamma}\partial_\gamma w_\beta + \zeta_{\alpha\gamma}\partial_\gamma u_\beta + \sigma_{\alpha\gamma}\partial_\gamma w_\beta - \frac{1}{\tau}\zeta_{\alpha\beta}
 \end{aligned} \tag{7.13}$$

where we have indicated with $\nu\beta$ the solvent viscosity and with $(1-\beta)\nu$ the viscosity contribution of the polymers, and ζ is adimensionalized with R_0^2 . The basic state here is defined by (see chapter 6):

$$\begin{aligned}
 \mathbf{u} &= (V \cos \frac{z}{L}, 0) \\
 \boldsymbol{\sigma} &= \begin{pmatrix} 1 + 2\tau^2 (\partial_z U)^2 & \tau \partial_z U \\ \tau \partial_z U & 1 \end{pmatrix} = \\
 &= \begin{pmatrix} 1 + 2\tau^2 \frac{V^2}{L^2} \sin^2(\frac{z}{L}) & -\frac{V\tau}{L} \sin(\frac{z}{L}) \\ -\frac{V\tau}{L} \sin(\frac{z}{L}) & 1 \end{pmatrix}
 \end{aligned} \tag{7.14}$$

The analysis follows the one of the previous section: slow and fast variables are introduced both for space and time. For the slow time a diffusive behavior is expected and the same scalings of the Newtonian case are assumed. With these hypotheses the perturbation fields can be expanded as:

$$\begin{aligned}
 \mathbf{w} &= \mathbf{w}^{(0)}(z, t, \tilde{x}, \tilde{z}, \tilde{t}) + \epsilon \mathbf{w}^{(1)}(z, t, \tilde{x}, \tilde{z}, \tilde{t}) + \epsilon^2 \mathbf{w}^{(2)}(z, t, \tilde{x}, \tilde{z}, \tilde{t}) + \dots, \\
 q &= q^{(0)}(z, t, \tilde{x}, \tilde{z}, \tilde{t}) + \epsilon q^{(1)}(z, t, \tilde{x}, \tilde{z}, \tilde{t}) + \epsilon^2 q^{(2)}(z, t, \tilde{x}, \tilde{z}, \tilde{t}) + \dots, \\
 \boldsymbol{\zeta} &= \boldsymbol{\zeta}^{(0)}(z, t, \tilde{x}, \tilde{z}, \tilde{t}) + \epsilon \boldsymbol{\zeta}^{(1)}(z, t, \tilde{x}, \tilde{z}, \tilde{t}) + \epsilon^2 \boldsymbol{\zeta}^{(2)}(z, t, \tilde{x}, \tilde{z}, \tilde{t}) + \dots,
 \end{aligned} \tag{7.15}$$

With the same procedure of the Newtonian case we end up with an effective equation for the large scale stream function:

$$\tilde{\partial}_t \tilde{\partial}^2 \Psi = \tilde{\nu}_{\alpha\beta} \tilde{\partial}_\alpha^2 \tilde{\partial}_\beta^2 \Psi, \tag{7.16}$$

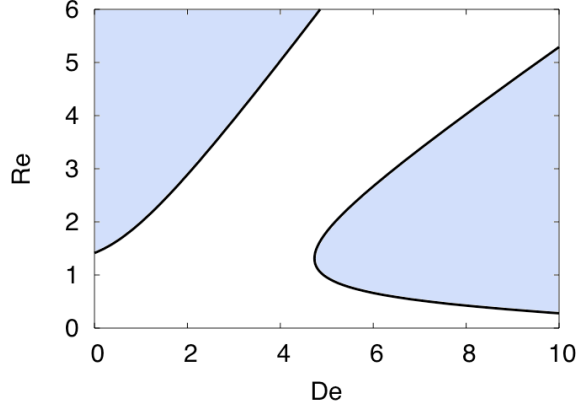


Figure 7.3: The stability diagram for the viscoelastic Kolmogorov flow obtained by means of multiple-scale analysis. Colored regions correspond to linear instability, whereas white region to linear stability. Here $\beta = 0.769$.

where $\tilde{\nu} = \nu \mathbf{1} + \nu^e$, and:

$$\begin{aligned} \nu_{xx}^e &= \frac{V^2 \{-L^2 + \nu(1 - \beta)\tau[3 + (1 + 2\beta)(\nu\tau/L^2)]\}}{2\nu} \\ \nu_{zz}^e &= 0 \\ \nu_{xz}^e = \nu_{zx}^e &= \frac{V^2 \{7L^2 + \nu(1 - \beta)\tau[-17 + (7 - 10\beta)(\nu\tau/L^2)]\}}{2\nu} + \nu. \end{aligned} \quad (7.17)$$

The basic state (7.14) is linearly stable if the operator $\tilde{\nu}_{\alpha\beta} \tilde{\partial}_\alpha^2 \tilde{\partial}_\beta^2$ is negative defined. Introducing the adimensional numbers Re and $\text{De} = V\tau/L$ (which is the equivalent of the Weissenberg number) and the angle between the basic flow and the perturbation, θ , we can rewrite the stability condition on eq. (7.16) as:

$$\begin{aligned} &\left(2 - \text{Re}^2 \beta^2 + 3(1 - \beta) \text{De} \text{Re} + (2\beta + 1)(1 - \beta) \text{De}^2\right) \tan^4 \theta + \left(4 + 7 \text{Re}^2 + \right. \\ &\left. + 17(\beta - 1) \text{De} \text{Re} + (10\beta - 7)(\beta - 1) \text{De}^2\right) \tan^2 \theta + 2 \geq 0 \end{aligned} \quad (7.18)$$

The resulting stability diagram is shown in fig. 7.3. For $\text{De} = 0$ we recover the Newtonian value $\text{Re}_c = \sqrt{2}$ above which the flow is linearly unstable. The curve of the diagram starting at $\text{Re} = \sqrt{2}$ in the region $\text{De} \sim 0$ defines the region of the so called inertial instabilities. Here the elasticity of the polymers is very small and the stability/instability mechanism is the same of the Newtonian case, i.e. the most unstable perturbations are transverse with respect

to the basic flow. However, the significant difference is that the critical value above which the flow is unstable is increased. For a given small De the critical Reynolds number is larger than $\sqrt{2}$. Thus polymers have a stabilizing effect in this range.

The instabilities present in the right-hand side of fig. 7.3 are generated for Re smaller than the inertial linear stability threshold $Re_c = \sqrt{2}$ and for large De , and are thus purely elastic instabilities. The occurrence of elastic instabilities has been investigated in the past in flows with curvilinear streamlines (see for example [1, 2, 4] and references therein), but has never been studied before in flows (like the Kolmogorov flow) with rectilinear streamlines. The instabilization mechanism here is different from the previous case, as the most unstable perturbations appear at small angles, i.e. for nearly parallel perturbations.

7.3 The validity of the scale separation hypothesis

The stability diagram shown in fig. 7.3 refers to instabilities that evolve at large scales. In the Newtonian case the hypothesis of scale separation between basic flow and leading instabilities is well verified, and within the multiple-scale approach the fastest instabilities can be found. However we have no clue that for elastic instabilities the same hypothesis holds. To check the validity of this approach we have simulated numerically eqs. (7.13). Performing the Fourier transform of the stream function and of the field ζ , a set of linear algebraic equations with non constant coefficients for the spectral amplitudes of the vorticity $(k_x^2 + k_z^2)\hat{\Psi}$ and of the conformation tensor perturbation $\hat{\zeta}$ can be derived. This problem can be reconducted to a generalized eigenvalue problem, which can be solved by a standard Arnoldi method [53].

The results of the simulations are shown in fig. 7.4. For inertial instabilities there is a perfect agreement between numerical simulations and analytical calculations. For larger De the two curves detach and the stability portrait obtained by numerical simulations is more restrictive. For even larger De there is a small region where the two curves are close, but for very small Re the two curves are again different. The light colored regions correspond to values of the parameter for which the system is unstable. The multiple-scale

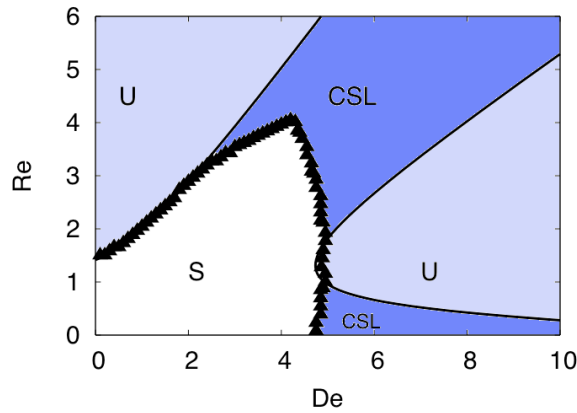


Figure 7.4: The stability diagram of the viscoelastic Kolmogorov flow obtained by means of numerical simulations (black triangles) compared to the results of multiple-scale analysis (lines). Colored regions are unstable, whereas white regions are stable. For the explanation see the text.

analysis predicts stability with respect to large-scale perturbations for the dark regions. Nevertheless, these regions are unstable with respect to small-scale perturbations and are not covered by the multiple-scale approach.

7.4 Generalization to finite Schmidt numbers

The numerical implementation of the Oldroyd-B model for direct numerical simulations presents several challenges, not only for the introduction of additional unknowns but also for the remarkable changes in the structure of the governing equations. Particularly critical is the fact that the conformation tensor (which by definition represents the second order moment of the end-to-end vector of polymers) can lose the positive definiteness, thus leading to numerical instabilities.

In ref. [26] it has been demonstrated that the addition of an artificial diffusivity term on the evolution equation for the conformation tensor can reduce considerably these problems, but for high values of the diffusivity parameter can lead to substantial changes in the dynamics. Here we want to investigate what is the effect of the artificial stress diffusivity on the stability of the Kolmogorov flow.

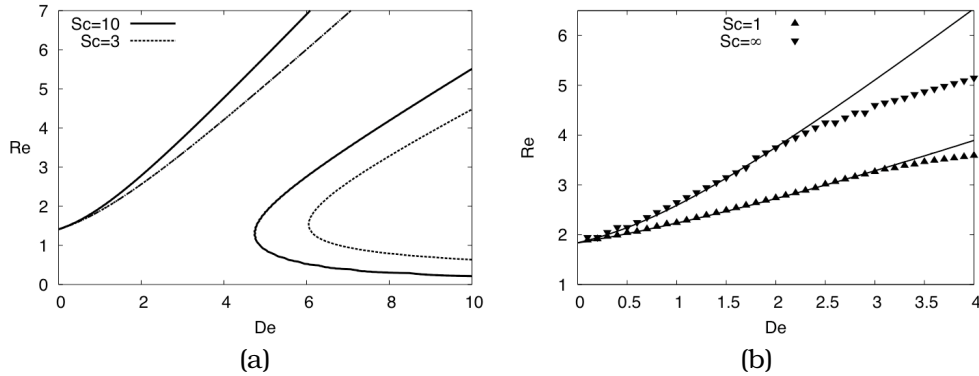


Figure 7.5: (a) The stability diagram for two different values of Sc . (b) The comparison of the stability diagram obtained from analytical perturbative methods (lines) with the one obtained from numerical simulations (triangles) for the case with and without diffusivity.

The stability analysis performed by means of multiple-scale techniques can be extended to this case with the only addition of the extra term $\kappa \partial^2 \sigma$ in the evolution equation for the conformation tensor. An additional complication arises in the resolution of the equations at different orders due to the fact that those coming from the evolution of the conformation tensor become differential rather than algebraic. The relative strength of the artificial diffusivity is measured by the adimensional Schmidt number $Sc = \beta \nu / \kappa$. The results of the multiple-scale approach are shown in fig. 7.5a. The effect of the artificial diffusivity is to move the elastic instabilities towards larger De and to reduce the stabilizing effect of polymers in the inertial stability region. This effect is an evidence that the action of the artificial diffusivity is to hinder polymer elongation. It is worth noticing that this observation suggests that no spurious drag reduction should be introduced in turbulence of Oldroyd-B fluids by the addition of this extra diffusivity. The results of the perturbative approach have been checked in the inertial region by numerical simulations, and are shown in fig. 7.5b. These results confirm quantitatively the previous conclusions.

7.5 Perspectives

It would be interesting to analyze the development of inertial instabilities as a function of the properties of the solvent that cannot be addressed within the context of the Oldroyd-B model (e.g. concentration, length of the dissolved molecules, molecular mass), and to extend the stability analysis to more refined models such as the Giesekus model. Furthermore, it is known that, in high concentration regimes, different kinds of instabilities take place such as fracture. A next step toward the understanding of instability of viscoelastic fluids would be to analyze the stability properties of more concentrated solutions where entanglement takes place.

Finally it would be interesting to perform a detailed analysis of the purely elastic instabilities and on the possible emergence of elastic turbulence.

The viscoelastic Kolmogorov flow: eddy viscosity and linear stability

By G. BOFFETTA¹, A. CELANI², A. MAZZINO³,
A. PULIAFITO² AND M. VERGASSOLA⁴

¹Dipartimento di Fisica Generale, Università di Torino and Istituto Nazionale di Fisica Nucleare, Sez. di Torino, V. Giuria 1, 10125 Torino, Italy

²CNRS, INLN, 1361 Route des Lucioles, 06560 Valbonne, France

³INFM – Dipartimento di Fisica, Università di Genova, and Istituto Nazionale di Fisica Nucleare, Sez. di Genova, Via Dodecaneso 33, 16146 Genova, Italy

⁴CNRS URA 2171, Inst. Pasteur, 28 rue du Dr. Roux, 75724 Paris Cedex 15, France.

(Received 25 May 2004 and in revised form 6 October 2004)

The stability properties of the laminar Kolmogorov flow of a viscoelastic Oldroyd-B fluid are investigated both analytically and numerically. Linear stability with respect to large-scale perturbations is studied by means of multiple-scale analysis. This technique yields an effective diffusion equation for the large-scale perturbation where the effective (eddy) viscosity can be computed analytically. Stability amounts to the positive definiteness of the eddy-viscosity tensor as a function of the Reynolds and the Deborah numbers. Two main results emerge from our analysis: (i) at small fluid elasticity, the flow is more stable than in the Newtonian case; (ii) at high elasticity, the flow is prone to elastic instabilities, occurring even at vanishing Reynolds number. The hypothesis of scale separation is verified up to moderate elasticity, as checked by numerical integration of the exact linearized equations by the Arnoldi method. Finally, it is shown that the addition of a stress diffusivity counteracts the effect of elasticity, in agreement with simple physical arguments.

1. Introduction

Flow instabilities are a classical subject in fluid dynamics (Drazin & Reid 1981) and the theoretical study of their occurrence in polymer solutions and melts is of paramount importance for several industrial applications (see e.g. Petrie & Denn 1976; Larson 1992; Shaqfeh 1996). A satisfactory understanding of these flow transitions entails taking account of the viscoelastic behaviour of such fluids.

A spectacular consequence of viscoelasticity is the drag reduction effect: addition of minute amounts (a few tenths of p.p.m. in weight) of long-chain soluble polymers to water leads to a strong reduction (up to 80%) of the power necessary to maintain a given throughput in a channel (Toms 1949; Lumley 1969; Virk 1975). Despite the vast number of studies on the subject, the understanding of drag reduction by polymers is still incomplete (Lumley 1969; Virk 1975; Nadolink & Haigh 1995; Sureshkumar, Beris & Handler 1997; Sreenivasan & White 2000).

Recently, some theoretical works have been aimed at establishing a link between drag reduction and the stability properties of the flow (Govindarajan, L'vov & Procaccia 2001; Stone, Waleffe & Graham 2002). Our goal here is to give further evidence that the seed of drag reduction is found at the very initial stage of the

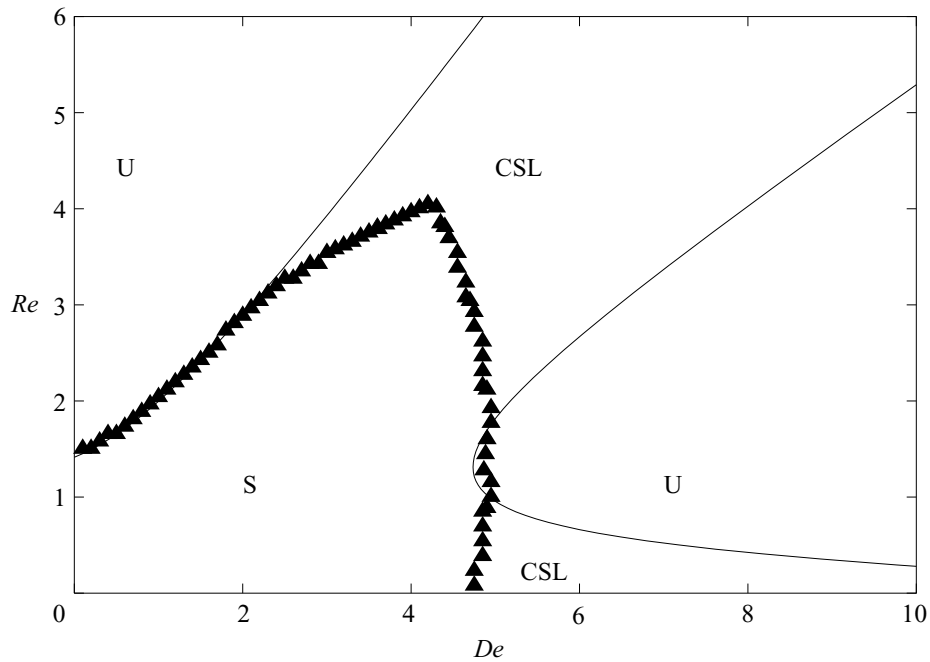


FIGURE 1. The stability portrait as predicted by multiple-scale analysis (solid line) and computed by numerical solution of the exact linearized equations (triangles). In the region denoted by U the flow is unstable, in that denoted by S it is stable. Inside the area denoted by CSL the flow is stable with respect to large-scale perturbations, but unstable with respect to generic perturbations.

successive instabilities which lead to a fully developed turbulent regime. In this framework, the possible occurrence of drag reduction can be detected by investigating how the stability of the flow changes upon polymer injection.

The basic flow we focus on is the extension to viscoelastic fluids of the well-known Kolmogorov flow (Arnold & Meshalkin 1960). Boffetta, Celani & Mazzino (2004) have shown that the fully developed turbulent regime of this flow displays drag reduction. Similarly to the Newtonian case (Meshalkin & Sinai 1961), the evolution of large-scale perturbations – the most unstable ones for moderate fluid elasticity – can be formally described by an effective viscous dynamics. Instabilities are thus associated with the loss of positive definiteness of the eddy-viscosity tensor, whose analytical expression can be explicitly derived from the equations of motion by means of multiple-scale analysis (Bensoussan, Lions & Papanicolaou 1978). In the Newtonian case, the eddy-viscosity tensor is a function of the Reynolds number, Re , and long-wave transverse instabilities occur above the threshold $Re_c = \sqrt{2}$ (Meshalkin & Sinai 1961). In the viscoelastic case studied here, the effective viscosity depends on both the Reynolds and the Deborah, De , numbers. (The latter is related to the typical polymer relaxation time.) The boundary between stable and unstable regions in the $Re-De$ phase space is determined by the parameter values such that the viscosity tensor loses its positive definiteness.

We anticipate our main result in figure 1, showing the phase-space portrait obtained by multiple-scale methods (see §4). For moderate De , the critical Reynolds number is an increasing function of the Deborah number: this demonstrates the stabilization of the flow field induced by the polymers (Govindarajan *et al.* 2001; Stone *et al.* 2002). The asymptotic result obtained for large-scale perturbations is confirmed by the numerical solution of the full linear stability problem (see §6). Discrepancies in figure 1 between perturbative and numerical results are due to lack of scale separation,

i.e. instabilities occurring at small or moderate scales, which cannot be captured by multiple-scale methods.

2. The Oldroyd-B model

The Oldroyd-B model is based on the assumption that a polymer solution can be treated as a dilute suspension of elastic dumbbells, i.e. pairs of microscopic beads connected by harmonic springs (Bird *et al.* 1987). The elastic constant of the spring is inversely proportional to the typical polymer relaxation time τ , controlling the response of the polymers to the stretching effects exerted by the local shear in the flow.

The distance between the two beads, here denoted by \mathbf{R} , evolves according to the stochastic equation

$$\dot{\mathbf{R}} = (\mathbf{R} \cdot \partial) \mathbf{u} - \frac{1}{2\tau} \mathbf{R} + \sqrt{\frac{R_0^2}{\tau}} \boldsymbol{\xi}. \quad (2.1)$$

On the right-hand side, the first term is the stretching/compression term, originating from the spatial variation of the flow experienced at \mathbf{R} . The second is a relaxation contribution, where one considers only the largest – and thus the most effective in the interaction with the flow – characteristic time τ . The last term, $\boldsymbol{\xi}$, is a white-in-time random process mimicking the effect of thermal noise on the polymers. R_0 denotes the equilibrium spring length, in the absence of advecting flow. This description remains valid and no other physical effects (such as the nonlinearity of the springs) need to be taken into account as long as we consider moderate polymer elongations.

Averaging (2.1) over the statistics of the thermal noise $\boldsymbol{\xi}$, the following evolution equation for the conformation tensor $\boldsymbol{\sigma} \equiv \langle \mathbf{R}\mathbf{R} \rangle / R_0^2$ is obtained:

$$\partial_t \boldsymbol{\sigma} + (\mathbf{u} \cdot \partial) \boldsymbol{\sigma} = (\partial \mathbf{u})^T \cdot \boldsymbol{\sigma} + \boldsymbol{\sigma} \cdot (\partial \mathbf{u}) - \frac{1}{\tau} (\boldsymbol{\sigma} - \mathbb{1}), \quad (2.2)$$

where $(\partial \mathbf{u})_{\alpha\beta} \equiv \partial_\alpha u_\beta$ and $\text{tr} \partial \mathbf{u} = \partial \cdot \mathbf{u} = 0$.

The dynamical effect of the polymers on the flow is due to the elastic contribution to the stress tensor. In the Oldroyd-B model (see e.g. Bird *et al.* 1987), that is for Hookean springs, this contribution per unit density is

$$\boldsymbol{\tau} = \frac{\nu(1-\beta)}{\tau} (\boldsymbol{\sigma} - \mathbb{1}), \quad (2.3)$$

where ν is the total kinematic viscosity of the solution, $\nu\beta$ and $\nu(1-\beta)$ are the contribution of the solvent and of the polymers to the total viscosity, respectively. Here we have introduced the dimensionless parameter $\beta = \eta_s / (n_p k_B \Theta \tau + \eta_s)$, n_p being the polymer concentration, k_B denoting the Boltzmann constant, Θ the temperature and η_s the dynamic viscosity of the solvent. The resulting momentum equations are

$$\partial_t \mathbf{u} + (\mathbf{u} \cdot \partial) \mathbf{u} = -\partial p + \nu \beta \partial^2 \mathbf{u} + \frac{\nu(1-\beta)}{\tau} \partial \cdot (\boldsymbol{\sigma} - \mathbb{1}) + \mathbf{f}. \quad (2.4)$$

3. Basic equilibrium state

As a first step in investigating the effect of polymers on the stability of the flow, we need to find a basic equilibrium state that will then be perturbed and the resulting perturbation growth evaluated exploiting a multiple-scale analysis.

Finding a basic equilibrium state for a generic forcing \mathbf{f} is already a formidable problem for the Navier–Stokes equations without polymers. The task is further complicated here by the additional term in (2.4) and the coupling with (2.2).

The problem simplifies for $\mathbf{f} \equiv (f(z), 0, 0)$ that induces a parallel flow $\mathbf{U} = (U(z), 0, 0)$, trivially annihilating the nonlinear term in (2.4). A further substantial simplification is introduced by the viscoelastic version of Squire's theorem (Squire 1933), which states that for parallel flows the most unstable perturbations are two-dimensional. We shall therefore restrict consideration to the two-dimensional flow (u_x, u_z) , without prejudicing generality. We further specialize by assuming $f(z) = F_0 \cos(z/L)$, producing the well-known Kolmogorov flow (Arnold & Meshalkin 1960) $U(z) \equiv u_x(z) = V \cos(z/L)$, $u_z = 0$.

The conformation tensor at equilibrium has then the form

$$\boldsymbol{\sigma} = \begin{pmatrix} 1 + 2\tau^2(\partial_z U)^2 & \tau \partial_z U \\ \tau \partial_z U & 1 \end{pmatrix} = \begin{pmatrix} 1 + 2\tau^2 \frac{V^2}{L^2} \sin^2\left(\frac{z}{L}\right) & -\tau \sin\left(\frac{z}{L}\right) \\ -\tau \frac{V}{L} \sin\left(\frac{z}{L}\right) & 1 \end{pmatrix}, \quad (3.1)$$

and $F_0 = \nu V/L^2$.

4. Multiple-scale analysis

Let us now consider the linearized equations for the system of perturbations $(\mathbf{w}, q, \boldsymbol{\zeta})$ of the basic state $(\mathbf{u}, p, \boldsymbol{\sigma})$. Equations (2.2) and (2.4), together with the incompressibility condition, lead to

$$\boldsymbol{\partial} \cdot \mathbf{w} = 0, \quad (4.1)$$

$$\partial_t \mathbf{w} + \boldsymbol{\partial} \cdot (\mathbf{u}\mathbf{w} + \mathbf{w}\mathbf{u}) = -\partial q + \nu\beta \partial^2 \mathbf{w} + \nu(1 - \beta)\tau^{-1} \boldsymbol{\partial} \cdot \boldsymbol{\zeta}, \quad (4.2)$$

$$\partial_t \boldsymbol{\zeta} + \boldsymbol{\partial} \cdot (\mathbf{u}\boldsymbol{\zeta} + \mathbf{w}\boldsymbol{\sigma}) = (\boldsymbol{\partial}\mathbf{u})^T \cdot \boldsymbol{\zeta} + (\boldsymbol{\partial}\mathbf{w})^T \cdot \boldsymbol{\sigma} + \boldsymbol{\zeta} \cdot (\boldsymbol{\partial}\mathbf{u}) + \boldsymbol{\sigma} \cdot (\boldsymbol{\partial}\mathbf{w}) - \tau^{-1} \boldsymbol{\zeta}. \quad (4.3)$$

We shall study the behaviour of perturbations with a characteristic length scale much larger than L , the periodicity of the basic flow. The ratio of small to large scales will be denoted by ϵ . In the spirit of multiple-scale expansions (Bensoussan *et al.* 1978), we introduce a set of *slow variables* ($\tilde{\mathbf{x}} = \epsilon \mathbf{x}$, $\tilde{t} = \epsilon^2 t$) in addition to the *fast variables* (\mathbf{x}, t) of evolution of the basic flow. The scaling of the slow time \tilde{t} is suggested by physical reasons: we are expecting a diffusive behaviour at large scales and the relation between space and time is thus assumed to be quadratic.

The multiple-scale technique (Bensoussan *et al.* 1978) treats slow and fast variables as independent, in order to capture the secular effects shaping the macroscopic dynamics. The differential operators appearing in (4.1)–(4.3) transform according to the chain rule as

$$\partial_i \rightarrow \partial_i + \epsilon \tilde{\partial}_i, \quad \partial_t \rightarrow \partial_t + \epsilon^2 \tilde{\partial}_t, \quad (4.4)$$

where $i = 1, 2$ denotes x and z . In the following, we assume that the amplitude of the fields in (4.1)–(4.3) are small enough to neglect nonlinear effects (their analysis will be reported elsewhere). The amplitudes can then be rescaled out so that the fields \mathbf{w} , q and $\boldsymbol{\zeta}$ are expanded as

$$\left. \begin{aligned} \mathbf{w} &= \mathbf{w}^{(0)}(z, t, \tilde{x}, \tilde{z}, \tilde{t}) + \epsilon \mathbf{w}^{(1)}(z, t, \tilde{x}, \tilde{z}, \tilde{t}) + \epsilon^2 \mathbf{w}^{(2)}(z, t, \tilde{x}, \tilde{z}, \tilde{t}) + \dots, \\ q &= q^{(0)}(z, t, \tilde{x}, \tilde{z}, \tilde{t}) + \epsilon q^{(1)}(z, t, \tilde{x}, \tilde{z}, \tilde{t}) + \epsilon^2 q^{(2)}(z, t, \tilde{x}, \tilde{z}, \tilde{t}) + \dots, \\ \boldsymbol{\zeta} &= \boldsymbol{\zeta}^{(0)}(z, t, \tilde{x}, \tilde{z}, \tilde{t}) + \epsilon \boldsymbol{\zeta}^{(1)}(z, t, \tilde{x}, \tilde{z}, \tilde{t}) + \epsilon^2 \boldsymbol{\zeta}^{(2)}(z, t, \tilde{x}, \tilde{z}, \tilde{t}) + \dots, \end{aligned} \right\} \quad (4.5)$$

where all the functions have the same periodicity as the basic state.

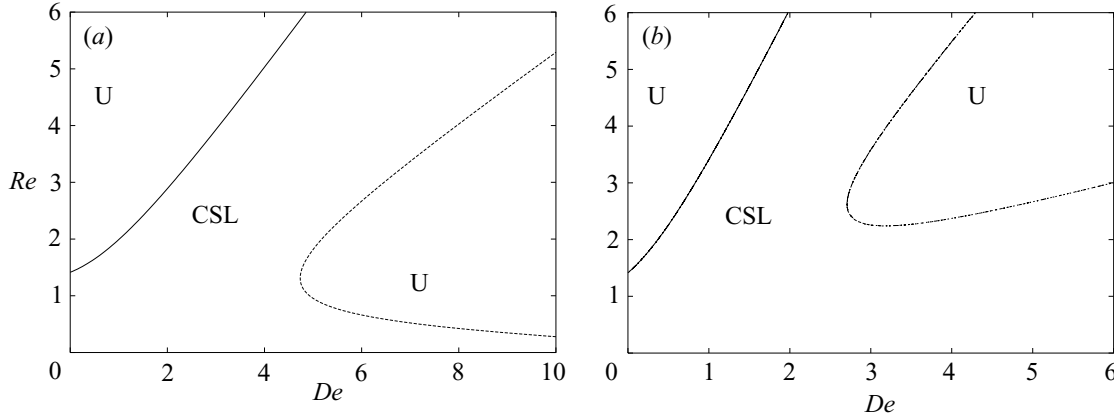


FIGURE 2. The stability diagram obtained by multiple-scale analysis for (a) $\beta = 0.77$ and (b) $\beta = 0.167$, with the notation of figure 1. Higher β corresponds to very low polymer concentrations while lower β means high concentrations.

Inserting (4.5) into (4.1)–(4.3) and exploiting (4.4), we end up with equations in which both fast and slow variables appear. By a further average over z , we obtain a set of equations involving large-scale fields only, i.e. depending on \tilde{x} and \tilde{t} .

Using incompressibility, the large-scale velocity perturbations $\langle \mathbf{w}^{(0)} \rangle$ can be described via the large-scale stream function $\Psi(\tilde{x}, \tilde{z}, \tilde{t})$ as

$$\langle w_x^{(0)} \rangle = \tilde{\partial}_z \Psi, \quad \langle w_z^{(0)} \rangle = -\tilde{\partial}_x \Psi. \quad (4.6)$$

The evolution equation for Ψ is obtained as a solvability condition (Fredholm alternative) at order ϵ^2 . After lengthy, but straightforward, algebra we obtain

$$\tilde{\partial}_t \tilde{\Delta} \Psi = \nu_{\alpha\beta} \tilde{\partial}_\alpha^2 \tilde{\partial}_\beta^2 \Psi, \quad (4.7)$$

where $\mathbf{v} = \nu \mathbb{1} + \mathbf{v}^e$, and

$$\begin{aligned} \nu_{xx}^e &= \frac{V^2 \{-L^2 + \nu(1-\beta)\tau[3 + (1+2\beta)(\nu\tau/L^2)]\}}{2\nu}, & \nu_{zz}^e &= 0, \\ \nu_{xz}^e = \nu_{zx}^e &= \frac{V^2 \{7L^2 + \nu(1-\beta)\tau[-17 + (7-10\beta)(\nu\tau/L^2)]\}}{2\nu} + \nu. \end{aligned}$$

The perturbations in (4.7) decay if the operator $\nu_{\alpha\beta} \tilde{\partial}_\alpha^2 \tilde{\partial}_\beta^2$ is negative. The condition of stability of the system is obtained by introducing the Reynolds number $Re = VL/\nu$, the Deborah number $De = V\tau/L$ and rewriting (4.7) in Fourier space:

$$\begin{aligned} (2 - Re^2 \beta^2 + 3(1-\beta) De Re + (2\beta+1)(1-\beta) De^2) s^2 + (4 + 7 Re^2 + 17(\beta-1) De Re \\ + (10\beta-7)(\beta-1) De^2) s + 2 > 0 \quad \forall s \geq 0. \end{aligned} \quad (4.8)$$

Here, $s^{1/2} = \tan \theta$, and θ is the angle between the perturbation and the basic flow, i.e. $\theta = 0$ corresponds to longitudinal perturbations, $\theta = \pi/2$ to transverse perturbations. The stability diagram in the Re – De plane is given in figure 2 (note that the topology of the phase space changes above $\beta_c \equiv 7/10$).

Two types of instabilities are predicted by our multiple-scale analysis:

(i) Hydrodynamic-like transverse instabilities take place for sufficiently large values of the Reynolds number, that is above the upper critical line in figure 2(a). In particular, we observe that the critical Reynolds number is an increasing function of the Deborah number: the elastic component tends to stabilize the flow. We can

interpret such behaviour as a prelude to the drag reduction effect observed in the fully turbulent regime (Boffetta *et al.* 2004). The lowest critical Reynolds number for such instabilities is attained for the Newtonian case ($De = 0$), where we recover the well-known result that the Kolmogorov flow is linearly stable below $Re_c = \sqrt{2}$ (Meshalkin & Sinai 1961).

(ii) Purely elastic instabilities emerge for sufficiently high values of the Deborah number and small Reynolds numbers (bottom-right region of figure 2a), that is instabilities that arise for purely elastic effects. Those instabilities were discussed in Shaqfeh (1996) and Groisman & Steinberg (1996, 1997, 1998a, b, 2004) for curvilinear streamlines. The present case is, to our knowledge, the first evidence of elastic instabilities for rectilinear streamlines.

Note that in this case the direction of the most unstable mode is at a small angle with respect to the basic flow, at variance with the purely hydrodynamic transverse instabilities.

5. Generalization to finite Schmidt numbers

Adding a stress diffusion term $\kappa \partial^2 \sigma$ to the equation of motion for the conformation tensor (2.2) was suggested by Sureshkumar & Beris (1995b) to avoid Hadamard instabilities which may emerge when (2.2) and (2.4) are integrated numerically. Such instabilities are triggered when the positive definiteness of the conformation tensor is lost due to the accumulation of numerical errors. How does the artificial diffusivity alter the stability portrait? We can address this question by exploiting the multiple-scale expansion to obtain an analytical answer.

The results shown in the previous section have been obtained for an infinite Schmidt number $Sc = \nu\beta/\kappa$, where we recall that $\nu\beta$ is the solvent viscosity and κ the stress diffusivity. The latter appears on the right-hand side of (4.3) as an extra term $\kappa \partial^2 \zeta$. The analysis proceeds exactly as in the case $\kappa = 0$. A source of technical difficulty is that the equations stemming from (4.3) now have a differential character, rather than algebraic as for $\kappa = 0$, making the computation more cumbersome and tedious. However, the final result is still a diffusion equation like (4.7), with an eddy-viscosity tensor dependent on the Schmidt number. The resulting stability portrait for the hydrodynamic regime is shown in figure 3 for two different values of Sc . The case $Sc = \infty$ (i.e. $\kappa = 0$) has been treated in the previous section, where it has been shown that the multiple-scale expansion provides reliable predictions up to Deborah numbers of order unity.

From figure 3 it is evident that the presence of the diffusivity reduces the stabilizing action of the polymers. In plain words, a non-zero stress diffusion in the equation of motion for the conformation tensor brings the system back toward the Newtonian behaviour. The physical reason is quite intuitive: the presence of a non-vanishing diffusivity tends to destroy the alignment between the stretching directions and the polymers, wiping out their capability to interact with the flow by selecting preferential orientations and making them behave, in practice, as point particles. The tendency to reach this limit for $Sc \ll 1$ has been observed in our computations and simulations (not shown).

6. Numerical analysis

For a plane parallel flow such as the basic flow of §3 it is possible to compute the exact, linear, rate of growth of a perturbation with arbitrary wavenumber, by

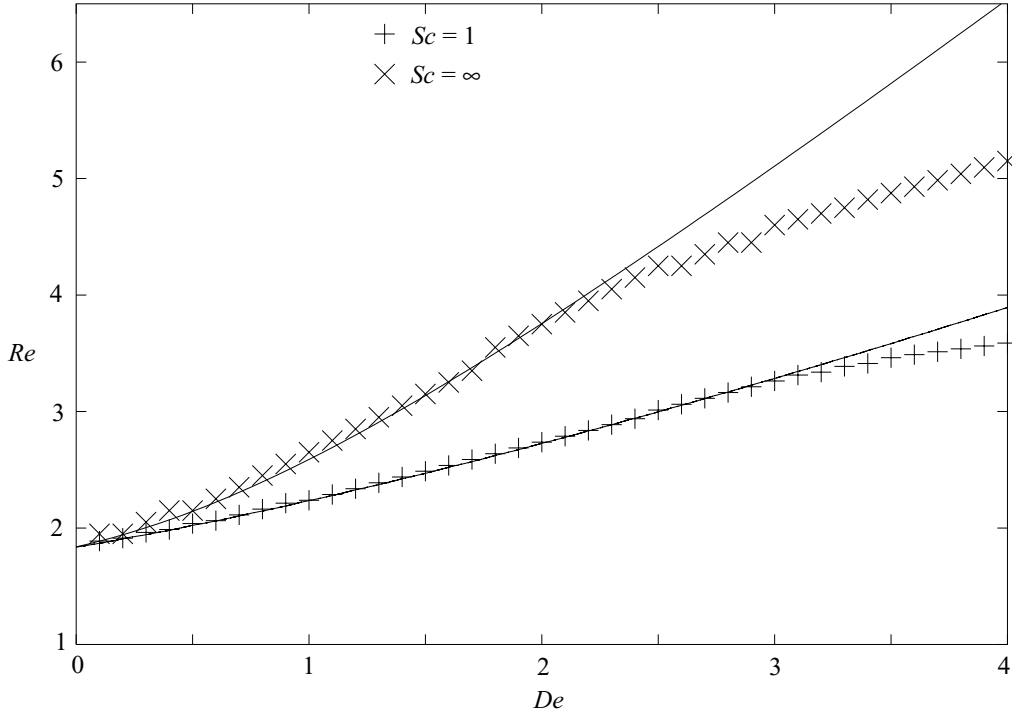


FIGURE 3. The stability portrait for finite Schmidt numbers. Symbols represent the numerical result based on the Arnoldi method, whereas solid lines are the prediction for large-scale instabilities.

means of a procedure that closely resembles the derivation of the Orr–Sommerfeld equations. Additionally, this will allow us to check if the first unstable modes are localized at the large scales and the onset of the instability of the laminar flow can be captured by the multiple-scale analysis developed in §4.

The starting point is again the set of equations (4.1)–(4.3). Neglecting the nonlinear terms we have to deal with a set of linear partial differential equations with periodic boundary conditions. The first step is to take the Fourier transform of the perturbations \mathbf{w} and ζ (denoted, respectively, by $\hat{\mathbf{w}}$ and $\hat{\zeta}$), e.g.

$$w_x = \partial_z \psi \mapsto \hat{w}_x = ik_z e^{i(k \cdot x - ct)} \hat{\psi}(k_x, k_z), \quad (6.1)$$

$$w_z = -\partial_x \psi \mapsto \hat{w}_z = -ik_x e^{i(k \cdot x - ct)} \hat{\psi}(k_x, k_z), \quad (6.2)$$

$$\zeta_{ij} \mapsto e^{i(k \cdot x - ct)} \hat{\zeta}_{ij}(k_x, k_z). \quad (6.3)$$

Accordingly, the equation for the vorticity, $\hat{\omega} \equiv (k_x^2 + k_z^2) \hat{\psi}$, and for $\hat{\zeta}$ are easily derived from (4.1)–(4.3). For the sake of brevity, we report here the equation for $\hat{\omega}$ only:

$$\begin{aligned} & -\frac{iV k_x}{2L^2} [L^2 k_x^2 + (L k_z - 1)^2 - 1] \hat{\psi}(k_x, k_z - 1/L) - \nu \beta (k_x^2 + k_z^2)^2 \hat{\psi}(k_x, k_z) \\ & - \frac{iV k_x}{2L^2} [L^2 k_x^2 + (L k_z + 1)^2 - 1] \hat{\psi}(k_x, k_z + 1/L) + \frac{\nu(1-\beta) k_x k_z}{\tau} \hat{\zeta}_{xx}(k_x, k_z) \\ & - \frac{\nu(1-\beta)}{\tau} ((k_x^2 - k_z^2) \hat{\zeta}_{xz}(k_x, k_z) - k_x k_z \hat{\zeta}_{zz}(k_x, k_z)) = -ic(k_x^2 + k_z^2) \hat{\psi}(k_x, k_z). \end{aligned} \quad (6.4)$$

Equations with a similar structure hold for $\hat{\zeta}$ as well. The complete set of equations constitutes an infinite hierarchy of linear algebraic equations with non-constant coefficients, which shows a foliation in terms of k_x . Upon truncating all modes $|k_z| > k_{max}$, for each k_x , we end up with a closed linear system of $4(2k_{max} + 1)$ equations

of the form

$$\mathbf{A}\boldsymbol{\phi} = c\mathbf{B}\boldsymbol{\phi}, \quad (6.5)$$

where $\boldsymbol{\phi} = \phi_p(k_x)$ ($p \in [1, 2k_{max} + 1]$) is a vector constructed from $\hat{\psi}$ and $\hat{\zeta}$ and \mathbf{A} and \mathbf{B} are two $(2k_{max} + 1) \times (2k_{max} + 1)$ matrices. A particularly convenient choice is to arrange the fields in the form

$$\phi_{4k_z+4k_{max}+1}(k_x) = \hat{\psi}(k_x, k_z), \quad (6.6)$$

$$\phi_{4k_z+4k_{max}+2}(k_x) = \hat{\zeta}_{xx}(k_x, k_z), \quad (6.7)$$

$$\phi_{4k_z+4k_{max}+3}(k_x) = \hat{\zeta}_{xz}(k_x, k_z), \quad (6.8)$$

$$\phi_{4k_z+4k_{max}+4}(k_x) = \hat{\zeta}_{zz}(k_x, k_z), \quad (6.9)$$

for k_z integer and $k_z \in [-k_{max}, k_{max}]$. With this choice, the matrix \mathbf{B} turns out to be diagonal and \mathbf{A} is band diagonal: only $(8/L) - 1$ upper-diagonal and $(8/L) + 2$ sub-diagonal survive. Note that these numbers do not depend on k_{max} . The matrix \mathbf{B} has no null diagonal elements, and can be inverted:

$$\mathbf{B}^{-1}\mathbf{A}\boldsymbol{\phi} = c\boldsymbol{\phi}. \quad (6.10)$$

To obtain non-trivial solutions for $\boldsymbol{\phi}$, we are thus reduced to a standard eigenvalue problem, whose eigenvalues, $c(k_x)$, give the dispersion relation.

An effective solution to our eigenvalue problem is to use Krylov subspace methods for computing a subset of the eigenvalues. Here, we use the Arnoldi method, which has been successfully applied to the linear stability of Newtonian coating flows by Cristodoulou & Scriven (1988) and for viscometric viscoelastic flows by Sureshkumar & Beris (1995a). This method consists of the generation, via a Krylov sequence, of a system of reduced dimension whose eigenvectors approximate those of the whole system. The Arnoldi method is the generalization to asymmetric eigenvalue problems of the Lanczos algorithm for symmetric matrices, which is proved convergent (see e.g. Parlett 1980). This procedure yields the whole spectrum of eigenvalues $c(k_x)$ for every k_x . The stability region for a given set of parameters is defined by the condition $\max\{\text{Im}[c(k_x)]\} < 0$ for every k_x .

To obtain the results reported in figures 1 and 3 (triangles) we worked in a bi-periodic square box of side 2π with $L = 2\pi/64$ and $k_{max} = 512$. Larger values of both L^{-1} and k_{max} did not produce appreciable differences in the results.

Some remarks on figure 1 are useful. Up to $De \simeq 2.3$ (for $\beta = 0.77$), the marginal curve obtained by the multiple-scale expansion is practically indistinguishable from the one obtained by the numerical solution of the full linearized equations. For larger Deborah numbers, multiple-scale analysis fails; this is the fingerprint of the lack of scale separation between the basic Kolmogorov flow and the perturbations. For large elasticity the leading instabilities do not occur at large scales: this is the realm of elastic instabilities, the first step toward the elastic turbulence regime (Groisman & Steinberg 2000).

7. Conclusions

We have investigated the linear stability of a viscoelastic fluid flowing in a channel with periodic boundary conditions. The flow is maintained by an external source and, for the particular choice $\mathbf{f} = (F_0 \cos(z/L), 0)$, it gives rise to the well-known Kolmogorov flow. Under the hypothesis that the most unstable perturbations evolve on scales much larger than L , we exploited an asymptotic perturbative strategy (the

multiple-scale expansion) to obtain an effective equation for the temporal evolution of the large-scale perturbation. The stability problem is thus reduced to the study of the sign of the eddy viscosity appearing in the large-scale equation.

Two different kinds of instabilities are captured by the multiple-scale expansion: (i) hydrodynamic-like instabilities that, in the limit of small elasticity, give the well-known $Re_c = \sqrt{2}$ corresponding to the Newtonian limit of the theory; (ii) purely elastic instabilities occurring for large values of the elasticity. The major effect of elasticity on hydrodynamic instabilities is to increase their critical Reynolds number. In plain words, polymers stabilize the flow, a prelude to drag reduction (Govindarajan *et al.* 2001; Stone *et al.* 2002).

Our results hold for finite Schmidt numbers as well. On decreasing Sc , the effect of stabilization reduces and for $Sc \rightarrow 0$ polymers behave as a suspension of spherical particles. Finally, our perturbative predictions have been corroborated by numerical analysis carried out on the original differential equations for the perturbations, by means of the Arnoldi method. The hypothesis of scale separation is verified up to Deborah numbers of order unity. For larger De , scale separation does not hold and multiple-scale methods fail. Nonetheless, at least qualitatively, the occurrence of purely elastic instabilities is captured by the asymptotic expansions.

This work has been supported by Cofin 2003 “Sistemi Complessi e Problemi a Molti Corpi” (AM), and by the European Networks “Stirring and Mixing” HPRN-CT2002-00300 (AC) and “Non-ideal turbulence” HPRN-CT-2000-00162 (MV). Numerical simulations have been performed at CINECA (INFM parallel computing initiative).

REFERENCES

- ARNOLD, V. I. & MESHALKIN, L. 1960 A. N. Kolmogorov’s seminar on selected problems of analysis (1958–1959). *Uspekhi Mat. Nauk* **15**, 247–250.
- BENSOUSSAN, A., LIONS, J.-L. & PAPANICOLAOU, G. 1978 *Asymptotic Analysis for Periodic Structures*. North-Holland.
- BIRD, R. B., HASSAGER, O., ARMSTRONG, R. C. & CURTISS, C. F. 1987 *Dynamics of Polymeric Liquids*. Wiley-Interscience.
- BOFFETTA, G., CELANI, A. & MAZZINO, A. 2004 Drag reduction in the turbulent Kolmogorov flow. *Phys. Rev. E* (submitted).
- CRISTODOULOU, K. N. & SCRIVEN, L. E. 1988 Finding leading modes of a viscous free surface flow: an asymmetric generalized eigenproblem. *J. Sci. Comput.* **3**, 355–406.
- DRAZIN, P. G. & REID, W. D. 1981 *Hydrodynamic Stability*. Cambridge University Press.
- GOVINDARAJAN, R., L’VOV, V. S. & PROCACCIA, I. 2001 Retardation of the onset of turbulence by minor viscosity contrasts. *Phys. Rev. Lett.* **87**, 174501-1–4
- GROISMAN, A. & STEINBERG, V. 1996 Couette-Taylor flow in a dilute polymer solution. *Phys. Rev. Lett.* **77**, 1480–1483.
- GROISMAN, A. & STEINBERG, V. 1997 Solitary vortex pairs in viscoelastic Couette flow. *Phys. Rev. Lett.* **78**, 1460–1463.
- GROISMAN, A. & STEINBERG, V. 1998a Elastic vs. inertial instability in a polymer solution flow. *Europhys. Lett.* **43**, 165–170.
- GROISMAN, A. & STEINBERG, V. 1998b Mechanism of elastic instability in Couette flow of polymer solutions: experiment. *Phys. Fluids* **10**, 2451–2463.
- GROISMAN, A. & STEINBERG, V. 2000 Elastic turbulence in a polymer solution flow. *Nature* **405**, 53–55.
- GROISMAN, A. & STEINBERG, V. 2004 Elastic turbulence in curvilinear flows of polymer solutions. *New J. Phys.* **6**, 29–48.
- LARSON, R. G. 1992 Instabilities in viscoelastic flows. *Rheol. Acta* **31**, 213–263.
- LUMLEY, J. 1969 Drag reduction by additives. *Annu. Rev. Fluid Mech.* **1**, 367–384.

- MESHALKIN, L. & SINAI, YA G. 1961 Investigation of the stability of a stationary solution of a system of equations for the plane movement of an incompressible viscous fluid. *J. Appl. Math. Mech.* **25**, 1700–1705.
- NADOLINK, R. H. & HAIGH, W. W. 1995 Bibliography on skin friction reduction with polymers and other boundary-layer additives. *ASME Appl. Mech. Rev.* **48**, 351–460.
- PARLETT, B. N. 1980 *The Symmetric Eigenvalue Problem*. Prentice-Hall.
- PETRIE, C. J. S. & DENN, M. M. 1976 Instabilities in polymer processing. *AIChE J.* **22**, 209–236.
- SHAQFEH, E. S. G. 1996 Purely elastic instabilities in viscometric flows. *Annu. Rev. Fluid Mech.* **28**, 129–185.
- SQUIRE, H. B. 1933 On the stability of a three-dimensional disturbances of viscous flow between parallel walls. *Proc. R. Soc. Lond. A* **142**, 621–628.
- SREENIVASAN, K. R. & WHITE, C. M. 2000 The onset of drag reduction by dilute polymer additives, and the maximum drag reduction asymptote. *J. Fluid Mech.* **409**, 149–164.
- STONE, P. A., WALEFFE, F. & GRAHAM, M. D. 2002 Toward a structural understanding of turbulent drag reduction: nonlinear coherent states in viscoelastic shear flow. *Phys. Rev. Lett.* **89**, 208301-1–4
- SURESHKUMAR, R. & BERIS, A. N. 1995a Linear stability analysis of viscoelastic Poiseuille flow using an Arnoldi-based orthogonalization algorithm. *J. Non-Newtonian Fluid Mech.* **56**, 151–182.
- SURESHKUMAR, R. & BERIS, A. N. 1995b Effect of artificial stress diffusivity on the stability of numerical calculations and the flow dynamics of time-dependent viscoelastic flows. *J. Non-Newtonian Fluid Mech.* **60**, 53–80.
- SURESHKUMAR, R., BERIS, A. N. & HANDLER, R. A. 1997 Direct numerical simulation of polymer-induced drag reduction in turbulent channel flow. *Phys. Fluids* **9**, 743–755.
- TOMS, B. A. 1949 Observation on the flow of linear polymer solutions through straight tubes at large Reynolds numbers. *Proc. 1st International Congress on Rheology* **2**, 135–141.
- VIRK, P. S. 1975 Drag reduction fundamentals. *AIChE Journal* **21**, 625–656.

Chapter 8

Nonlinear stability analysis of the viscoelastic Kolmogorov flow

The linear stability analysis for the Newtonian Kolmogorov flow predicts the occurrence of instabilities for transverse perturbations above the critical Reynolds number. The dynamics of these instabilities should be investigated by means of a weakly nonlinear analysis. It is known that the weakly nonlinear dynamics displays a particularly rich behavior already for Newtonian fluids [52,54,55], showing a Cahn-Hilliard dynamics (see [56] or [57] for a recent review) for the large-scale transverse perturbation. Cahn-Hilliard dynamics can be found in the theory of phase-ordering kinetics as well as in the context of fluid dynamics [58,59].

In this chapter I will present my results on the weakly nonlinear analysis of the viscoelastic Kolmogorov flow, starting from the well known Newtonian case as an example. I will show that in the vicinity of the marginal stability curve presented in the previous chapter, the transverse large-scale perturbation obeys a Cahn-Hilliard equation, and that when the flow becomes strong enough, higher order nonlinearities should be accounted for, leading to a generalized Cahn-Hilliard dynamics. Analytical (perturbative) as well as numerical results will be presented.

Furthermore the linear stability analysis of the viscoelastic Kolmogorov flow has shown that the effect of polymers is stabilizing, suggesting that drag reduction can be found in the turbulent state. In the last section of this chapter I will introduce the results on the analysis of the friction coefficient, confirming the qualitative pic-

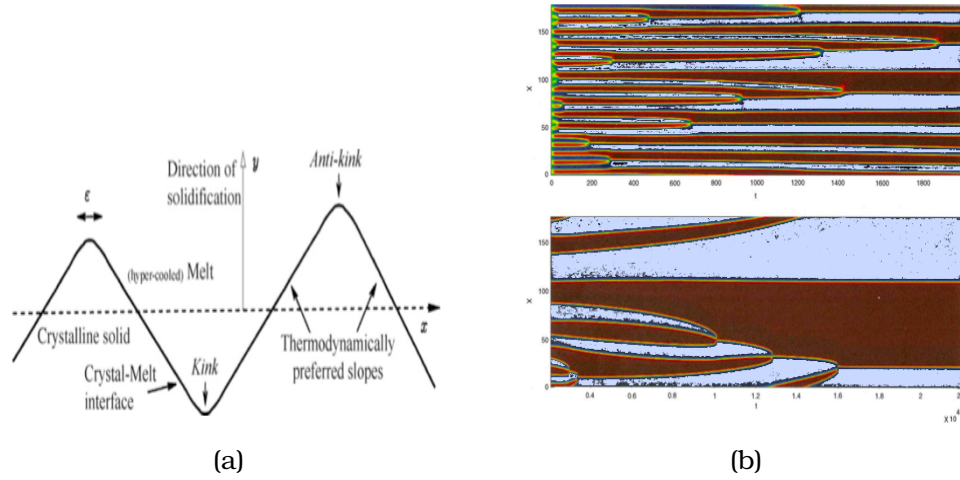


Figure 8.1: (a) Sketch of crystal growth, regulated by the Cahn-Hilliard equation. Kinks and anti-kinks are interface structures that annihilate, giving rise to larger ones. (b) Annihilation of structures in Cahn-Hilliard dynamics extracted from numerical simulations. The pictures are taken from ref. [60].

ture of the linear case.

8.1 Weakly nonlinear analysis: the standard Cahn-Hilliard dynamics

The complete nonlinear evolution equation for the perturbations in the Newtonian case are:

$$\begin{aligned} \partial \cdot \mathbf{w} &= 0 \\ \partial_t \mathbf{w} + \partial \cdot (\mathbf{u}\mathbf{w} + \mathbf{w}\mathbf{u} + \mathbf{w}\mathbf{w}) &= -\partial q + \nu \partial^2 \mathbf{w} \end{aligned} \quad (8.1)$$

As the most unstable direction in the linear case is the transverse direction, it can be assumed that this will hold for the nonlinear case too. Thus we will focus on a one-dimensional dynamics for the perturbation w_z . For Re smaller than the linear stability threshold we have:

$$\tilde{\partial}_t \langle w_z \rangle \sim -A \tilde{\partial}^2 \langle w_z \rangle - C \tilde{\partial}^4 \langle w_z \rangle. \quad (8.2)$$

where the coefficients A and C are known functions of Re . When we move slightly above Re_c , the coefficient A changes sign and the corresponding growth of the perturbation, if a stationary state exists, must be saturated by another term. Physical constraints (momentum conservation and space-inversion symmetries) set this term to

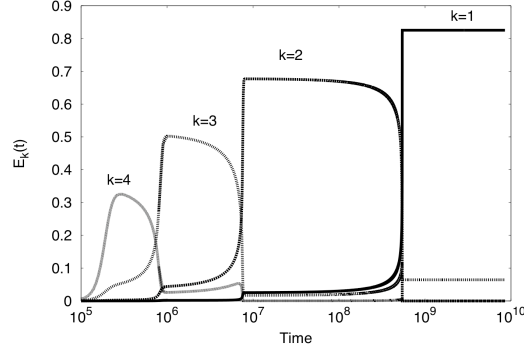


Figure 8.2: The energy spectrum of the lowest modes in the Cahn-Hilliard equation, obtained from numerical integration of eq. (8.7)

have the form:

$$B\tilde{\partial}_x \left(\langle w_z \rangle^2 \tilde{\partial}_x \langle w_z \rangle \right) \quad (8.3)$$

To derive the large-scale equation for the perturbation with a multiple-scale approach, we introduce the slow and fast space-derivative operators, as in the previous chapter. Note that here we should find how to expand the fields in the scale separation parameter and the scaling relation for the slow time. The prescription comes from the balance between the three terms of the equation. Performing a Taylor expansion in the vicinity of the marginal curve yields:

$$A \simeq \left. \frac{\partial A}{\partial \text{Re}} \right|_{\text{Re}_c} (\text{Re} - \text{Re}_c) \quad (8.4)$$

and the balance, expressed in terms of ϵ reads:

$$B\epsilon^2 \epsilon_w^3 \sim \left. \frac{\partial A}{\partial \text{Re}} \right|_{\text{Re}_c} (\text{Re} - \text{Re}_c) \epsilon^2 \epsilon_w, \quad \left. \frac{\partial A}{\partial \text{Re}} \right|_{\text{Re}_c} (\text{Re} - \text{Re}_c) \epsilon^2 \epsilon_w \sim C\epsilon^4 \epsilon_w. \quad (8.5)$$

where ϵ_w is the scaling of the velocity perturbation. These two relations set the scaling $\epsilon_w = \epsilon$, the distance from the marginal curve $\text{Re} = \text{Re}_c(1 + \epsilon^2)$. The scaling of the pressure perturbation is equal to the one of the velocity perturbation. The balance of any of these terms with the large-scale time derivative gives $\tilde{t} = \epsilon^4 t$.

The field expansion is thus:

$$\begin{aligned} \mathbf{w} &= \epsilon \mathbf{w}^{(1)}(z, \tilde{x}, \tilde{t}) + \epsilon^2 \mathbf{w}^{(2)}(z, \tilde{x}, \tilde{t}) + \dots, \\ q &= \epsilon q^{(1)}(z, \tilde{x}, \tilde{t}) + \epsilon^2 q^{(2)}(z, \tilde{x}, \tilde{t}) + \dots \end{aligned} \quad (8.6)$$

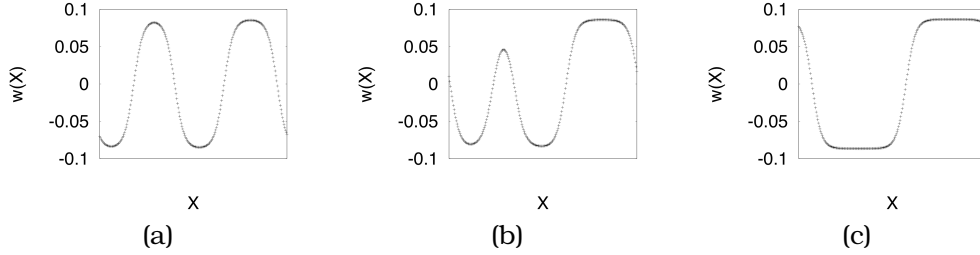


Figure 8.3: The velocity perturbation profile w_z at different times obtained by the same simulation of fig. 8.2. An annihilation process between small modes occurs, leading to a transition from a $k = 2$ -dominated state to a $k = 1$ -dominated state.

Substituting these expansions into the nonlinear evolution equations (8.1), solving the equations at the different orders and the corresponding solvability conditions, yields a closed equation in the perturbation obtained as the solvability condition at order 5:

$$\tilde{\partial}_t \langle w_z^{(1)} \rangle = \tilde{\partial}_x \left\{ (-A + B \langle w_z^{(1)} \rangle^2) \tilde{\partial}_x \langle w_z^{(1)} \rangle \right\} - C \tilde{\partial}_x^4 \langle w_z^{(1)} \rangle \quad (8.7)$$

This is a “standard” Cahn-Hilliard equation and its dynamics and phenomenology are known [57].

The existence of a stationary state is related to the existence of an extremal formulation for eq. (8.7). In this case a so called Lyapunov functional exists and the evolution of the perturbation profile can be described as a superposition of so called kink and anti-kink structures which correspond to local minima of the Lyapunov functional. As qualitatively shown in fig. 8.1, kinks and anti-kinks are structures of the described field that interact with each other leading to a coarsening dynamics.

The energy associated to each wavenumber for a Cahn-Hilliard equation is shown in fig. 8.2: a sequence of metastable states appears, where the amplitude of each mode grows abruptly, lasts for a certain time and then gives way to the following smaller mode, until a stationary state is reached, where only the smallest possible mode is excited.

The dynamics of the transverse velocity perturbation is presented in fig. 8.3, where the field w_z containing initially the harmonic $k = 2$ evolves in time arriving at a stationary state containing only the mode $k = 1$. This dynamics corresponds to small counter-rotating vortices that interact and give rise to larger structures [55].

In the viscoelastic case, for small polymer elasticity, the same

procedure can be applied. The evolution equations for the perturbations are:

$$\begin{aligned} \partial \cdot \mathbf{w} &= 0 \\ \partial_t \mathbf{w} + \partial \cdot (\mathbf{u}\mathbf{w} + \mathbf{w}\mathbf{u} + \mathbf{w}\mathbf{w}) &= -\partial q + \nu\beta\partial^2 \mathbf{w} + \frac{(1-\beta)\nu}{\tau} \partial \cdot \boldsymbol{\zeta} \\ \partial_t \boldsymbol{\zeta} + \partial \cdot (\mathbf{u}\boldsymbol{\zeta} + \mathbf{w}\boldsymbol{\sigma} + \mathbf{w}\boldsymbol{\zeta}) &= (\partial \mathbf{u})^T \cdot \boldsymbol{\zeta} + (\partial \mathbf{w})^T \cdot \boldsymbol{\sigma} + (\partial \mathbf{w})^T \cdot \boldsymbol{\zeta} + \\ &+ \boldsymbol{\zeta} \cdot (\partial \mathbf{u}) + \boldsymbol{\sigma} \cdot (\partial \mathbf{w}) + \boldsymbol{\zeta} \cdot (\partial \mathbf{w}) - \tau^{-1} \boldsymbol{\zeta}, \end{aligned} \quad (8.8)$$

where as usual $\nu\beta$ is the solvent viscosity and $(1-\beta)\nu$ is the polymer effective viscosity. The reasoning on the scaling of the fields in ϵ is almost identical to the Newtonian case and yields the same scaling of \mathbf{w} for the perturbation $\boldsymbol{\zeta}$. Expansions (8.6) hold together with the one for the conformation tensor perturbation $\boldsymbol{\zeta}$:

$$\boldsymbol{\zeta} = \epsilon \boldsymbol{\zeta}^{(1)}(z, \tilde{x}, \tilde{t}) + \epsilon^2 \boldsymbol{\zeta}^{(2)}(z, \tilde{x}, \tilde{t}) + \dots \quad (8.9)$$

This must be plugged together with the other expansions in eqs. (8.8) to yield a hierarchy of equations at different orders in ϵ which can be solved together with the corresponding solvability conditions.

Following this procedure we obtain a large-scale evolution equation for the perturbation w_z which is analogous to eq. (8.7), where the coefficient A , B and C are known complicated functions of De and β and will not be derived here (see the following article, p. 133). The phenomenology is the same as in the Newtonian case, except that the dynamics is slowed down by the presence of polymers.

It is worth noting that in this equation the growth of the perturbation is saturated if two conditions are met (see fig. 8.4a):

- (i) The coefficient C must be positive, to ensure the saturation of small scale instabilities (still at larger scale with respect to the basic flow)
- (ii) As the coefficient A is non-negative because we are slightly above the marginal curve, the coefficient B must be positive so that when the perturbation becomes $O(\sqrt{A/B})$ the growth in eq. (8.7) can be saturated.

8.2 A novel Cahn-Hilliard dynamics

When the two conditions on the sign of the coefficient are not satisfied a next-order nonlinearity must be introduced, to stabilize

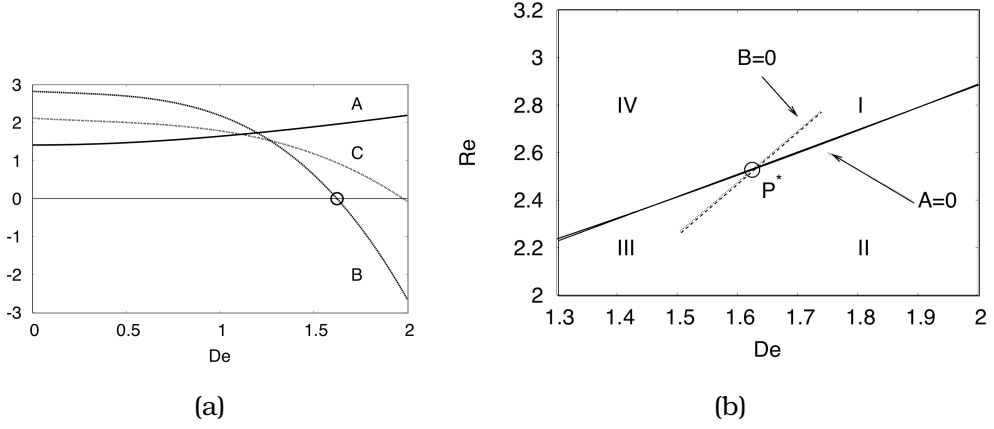


Figure 8.4: (a) The sign of the coefficients of the Cahn-Hilliard equation computed by a multiple-scale analysis. The coefficient B changes sign at De^* (circled point). (b) The stability portrait around the point P^* where the lines $A = 0$ crosses the line $B = 0$: the regions I, II, III and IV are all characterized by different dynamics.

eq. (8.7). The situation is sketched in fig. 8.4b. Region I is linearly unstable and the condition (ii) is not satisfied, so that a fifth order nonlinearity should be accounted for. Region II is linearly stable, nevertheless condition (ii) is not satisfied, and a fifth order nonlinearity must be introduced to stabilize the third order term which is unstable in this regime. Zone III is linearly and nonlinearly stable and in region IV a fifth order nonlinearity must be introduced approaching the line $B = 0$.

Expanding around De^* (see fig. 8.4a) we can repeat the reasoning performed in the previous section to find the scaling for the expansions of velocity, pressure and conformation tensor perturbation ($\epsilon^{1/2}$) and for the slow time scaling (ϵ^4). With the same spirit of the previous section, the solvability condition at order $9/2$ gives (for regions I and II):

$$\tilde{\partial}_t \langle w_z^{(1/2)} \rangle = \tilde{\partial}_x \left[(-A + B \langle w_z^{(1/2)} \rangle^2 + D \langle w_z^{(1/2)} \rangle^4) \tilde{\partial}_x \langle w_z^{(1/2)} \rangle \right] - C \tilde{\partial}_x^4 \langle w_z^{(1/2)} \rangle, \quad (8.10)$$

where the coefficients A , B , C and D are known analytical functions of the parameters of the system. In region IV the same equation holds except that the cubic nonlinearity is assumed to be negligible.

Equation (8.10) belongs to the class of Cahn-Hilliard equations as defined by Bray [57]. Nevertheless, the dynamics is significantly slowed down with respect to a standard Cahn-Hilliard dynamics,

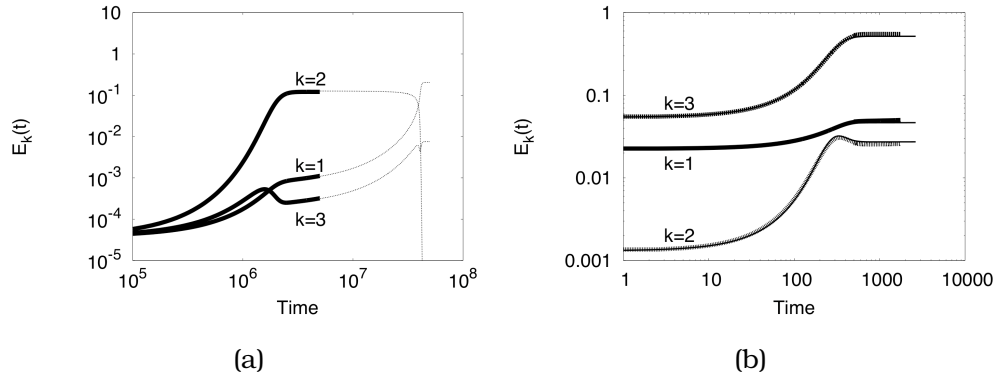


Figure 8.5: Direct numerical simulations (points or thicker lines) compared with numerical integration of the respective Cahn-Hilliard equations ($\beta = 0.769$). (a) The spectral energy of each mode for the standard Cahn-Hilliard dynamics: $De = 1.4$ and $Re/Re_c = 1.14$. (b) Spectral energy of each mode for the generalized Cahn-Hilliard equation around P^* : $De = 1.62$ and $Re = 2.5159$.

due to the presence of the fifth order nonlinearity. Note also that a fully analytical (perturbative) approach can be applied only provided that $Re \sim Re_c$ and $De \sim De_c$. The general case should be treated by means of numerical simulations.

8.3 Numerical simulations

The perturbative analytical results have been checked by means of direct numerical simulations of eqs. (6.17), via a pseudo-spectral method in a two-dimensional rectangle of dimensions $L_x \times 64L_x$. The growth rates of the perturbations have been numerically measured by imposing an initially small white noise in space as a perturbation. The direct numerical simulations have also been compared to numerical integration of eqs. (8.7) and (8.10). The validity of the scale separation hypothesis assumed in the studied range, $Re \simeq Re_c$ and $De \simeq De^*$, can be checked.

The comparison between the standard Cahn-Hilliard dynamics and direct numerical simulations of the whole system of equations have been performed. The agreement is perfect, as shown in fig. 8.5a. The results of the comparison of direct numerical simulations and numerical integration of the generalized Cahn-Hilliard equation (8.10) are presented in fig. 8.5b also showing a perfect agreement. In these simulations a major technical difficulty emerges because the position of P^* needs to be determined precisely, a very difficult task

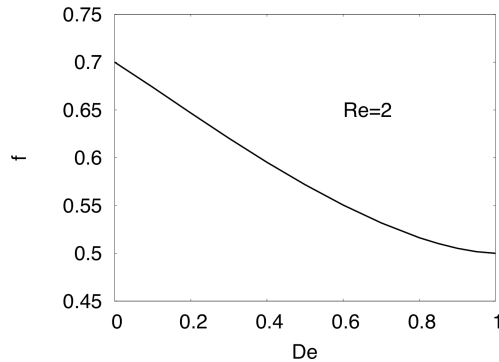


Figure 8.6: The drag coefficient in the weakly nonlinear regime ($Re \simeq Re_c$, $De < De^*$) computed within the multiple-scale approach.

in direct numerical simulations.

Clues of “drag reduction”

Following ref. [61] we have computed the drag coefficient f , defined as follows:

$$f = \frac{F_0 L}{U^2} \quad (8.11)$$

where F_0 is the forcing amplitude, L is the forcing periodicity scale and U is the mean flow amplitude. In the laminar regime we have $f = Re^{-1}$. For the regime $Re \simeq Re_c$ and $De < De^*$ the drag coefficient can be computed analytically, yielding the results shown in fig. 8.6. As predicted by direct numerical simulations of ref. [61] the drag coefficient decreases as De increases, even if the flow is barely in the nonlinear regime. This indication is confirmed by the numerical data (not shown).

8.4 Perspectives

This research suggests that polymers can generate non trivial effects even in the absence of material boundaries, and hints at the existence of a rich phenomenology of the turbulent case. This issue is addressed within the next chapter.

Furthermore it would be interesting to investigate the nonlinear dynamics of purely elastic instabilities, and to analyze the possible emergence of elastic turbulence.

Nonlinear dynamics of the viscoelastic Kolmogorov flow

By **A. BISTAGNINO**¹, **G. BOFFETTA**¹,
A. CELANI², **A. MAZZINO**^{3,5}, **A. PULIAFITO**^{2,3}
 AND **M. VERGASSOLA**⁴

¹ Dipartimento di Fisica Generale, Università di Torino and Istituto Nazionale di Fisica Nucleare, Sez. di Torino, V. Giuria 1, 10125 Torino, Italy

² CNRS, INLN, 1361 Route des Lucioles, 06560 Valbonne, France

³ Dipartimento di Fisica, Università di Genova, Via Dodecaneso 33, 16146 Genova, Italy

⁴ CNRS URA 2171, Inst. Pasteur, 25 rue du Dr. Roux, 75724 Paris Cedex 15, France.

⁵ Istituto Nazionale di Fisica Nucleare, Sez. di Genova, Via Dodecaneso 33, I-16146 Genova, Italy

(Received 2 February 2006)

The weakly nonlinear regime of a viscoelastic Navier–Stokes fluid is investigated. For the purely hydrodynamic case, it is known that large-scale perturbations tend to the minima of a Ginzburg–Landau free-energy functional with a double-well (fourth-order) potential. The dynamics of the relaxation process is ruled by a one-dimensional Cahn–Hilliard equation that dictates the hyperbolic tangent profiles of kink–antikink structures and their mutual interactions. For the viscoelastic case, we found that the dynamics still admits a formulation in terms of a Ginzburg–Landau free-energy functional. For sufficiently small elasticities, the phenomenology is very similar to the purely hydrodynamic case: the free-energy functional is still a fourth-order potential and slightly perturbed kink–antikink structures hold. For sufficiently large elasticities, a critical point sets in: the fourth-order term changes sign and the next-order nonlinearity must be taken into account. Despite the double-well structure of the potential, the one-dimensional nature of the problem makes the dynamics sensitive to the details of the potential. We analysed the interactions among these generalized kink–antikink structures, demonstrating their role in a new, elastic instability. Finally, consequences for the problem of polymer drag reduction are presented.

1. Introduction

The derivation of coarse-grained equations of motion, averaging out microscopic degrees of freedom and retaining only those features relevant to the process of interest, is a major goal in many different scientific domains. A first classical example is the dynamics of celestial bodies, the physical problem which motivated the introduction of asymptotic techniques to systematically average over rapidly rotating, angular degrees of freedom. More recently, many interesting phenomena in biological contexts (e.g. related to domain formation in lipid membrane, bilayer fusion, and cooperative motions associated with phase changes) have been found to occur on times and length scales much larger than the typical times and scales where the classical molecular-dynamics methods are applicable (Vattulainen & Karttunen 2005). To reach those larger length-scales, one re-

sorts to coarse-grained models that employ effective interaction potentials (Karttunen *et al.* 2004).

Another relevant example of coarse-grained model comes from climatology. The current numerical models for prediction of weather and climate involve general circulation models. They consist of coupled, nonlinear partial differential equations, discretized in space and time for the purpose of numerical simulations. The current generation of supercomputers supports mesh spacing of the order of 200 km for short-term climate simulations. However, many important physical processes occur on smaller scales (e.g. the cloud cover in the boundary layer) and they significantly affect the large-scale dynamics of resolved fields. A powerful way to incorporate the unresolved dynamics is provided by suitable coarse-grained stochastic models (Khouider *et al.* 2003).

Finally, in the framework of phase-ordering kinetics, the concept of coarse-grained description plays a crucial role for the order-parameter dynamics. Coarsening is intimately related to the fact that domain growth is a scaling phenomenon: domain patterns at different times differ solely by a global scale factor (see the review by Bray 2002). A suitable coarse-grained description for systems where the order parameter is not conserved (e.g. for anti-ferromagnetic ordering) is provided by the time-dependent Ginzburg–Landau equation. When the order parameter is conserved, as in phase separation, the coarse-grained dynamics is ruled by the Cahn–Hilliard equations (Bray 2002):

$$\frac{\partial w}{\partial t} = \partial_x^2 \frac{\delta F}{\delta w}, \quad (1.1)$$

where $w(\mathbf{x}, t)$ is a suitable coarse-grained order-parameter and F a Landau free-energy functional:

$$F[w] = \int d\mathbf{x} \left[\frac{\lambda}{2} |\nabla w|^2 + I(w) \right]. \quad (1.2)$$

The potential $I(w)$ typically has a double-well structure, whose minima correspond to two equilibrium states. λ is a positive constant related to the distance between the equilibrium states and thus the size of the interface between them.

In fluid mechanics, the Cahn–Hilliard equations (1.1) play a fundamental role in the stability analysis of large-scale perturbations. In a variety of situations, it turns out that the evolution of large-scale perturbations is governed by equation (1.1), with a fourth-order potential $I(w)$ (see Nepomnyashchy 1976; Sivashinsky 1985; Pedlosky 1987; Manfroi & Young 1999). The structure of the potential controls the profile and the interactions of the so-called kink-antikink structures observed in snapshots of the flow (She 1987).

In the present paper, we focus our attention on a simple model of viscoelastic flows, the so-called viscoelastic Kolmogorov flow. Its linear stability analysis has been recently investigated by Boffetta *et al.* (2005a), while the turbulent regime and its massive drag reduction effects have been studied by Boffetta *et al.* (2005b). Here, we analyse the weakly nonlinear dynamics, intermediate between the linear stage of evolution and the fully turbulent regime.

The starting points of our analysis are three results obtained by Boffetta *et al.* (2005a) for the linearized stage: i) The most unstable perturbation has a long wavelength (large-scale) compared to the period of the basic Kolmogorov flow; ii) Its linear evolution is captured by asymptotic multiscale methods, at least up to moderate elasticities of the flow; iii) The most unstable perturbation is transverse with respect to the basic flow.

Multiscale asymptotic methods can be applied, as in the Newtonian case, to show that the evolution in the presence of polymers obeys a one-dimensional Cahn–Hilliard equation of the form (1.1). The point demonstrated here is that there exists a critical

value of the elasticity, where the potential $I(w)$ passes from the fourth to the sixth order in the field w . This corresponds to a triple critical point. Due to the one-dimensional character of the nonlinear dynamics, the transition strongly impinges on the dynamics of the large-scale perturbation.

Above the critical elasticity, “hydrodynamic” kink-antikink structures are replaced by generalized kinks and anti-kinks and their annihilation processes are shown to be severely slowed down. Moreover, below the critical value of the elasticity, the mechanism of instability is linear and nonlinear terms stabilize the flow. Conversely, above the critical value, we show that a sub-critical, nonlinear mechanism of instability takes place, provided the initial amplitude of the perturbation be sufficiently strong.

The paper is organized as follows. In §2 and 3, we describe the viscoelastic model considered in the sequel and briefly review the results by Boffetta *et al.* (2005a) needed here. In §4, we use multiscale methods to derive the coarse-grained equations for the perturbations. In §5, we study the system around the triple critical point and work out the evolution equations in its neighborhood. In §6 and 7, we reformulate the asymptotic behaviour of the coarse-grained equations in terms of variational analysis and present the numerical results that corroborate our analytical predictions. Finally, in §8 we address the problem of drag reduction and show that, even for the weakly unstable regime considered here, the injection of polymers induces an enhancement of the mean flow amplitude.

2. The viscoelastic Navier–Stokes equations

Several models have been introduced (see e.g. Hinch 1977) to describe viscoelastic fluids. A powerful class describes the fluid as non-Newtonian, accounting for the reaction of the polymers onto the flow via an extra-term in the stress tensor. A popular and often employed model within this class is the Oldroyd-B (Oldroyd 1950), which is the one considered in the sequel. We briefly review it here for the sake of completeness.

In the Oldroyd-B model, it is assumed that viscoelastic flows can be treated as a dilute suspension of elastic dumbbells, i.e. identical pairs of microscopic beads connected by Hookean springs. The flow is considered “external” to the molecule, neglecting the effects of the finite size of the polymers on the flow. Furthermore, the polymer concentration is supposed to be uniform and low enough to neglect polymer-polymer interactions.

The reaction of the dumbbells on the fluid is treated at a mean-field level and the study of the dynamics is limited to scales much larger than the inter-polymer distance. The polymer solution is regarded as a continuous medium, whose reaction on the flow is described by an elastic contribution \mathbf{T} to the total stress tensor of the fluid. Its value per unit density depends on the free energy of the molecule and the thermal noise as (see e.g. Bird *et al.* 1987):

$$\mathbf{T} = -n_p \langle \mathbf{R}\mathbf{F} \rangle - n_p k_B \Theta \mathbf{1}, \quad (2.1)$$

where n_p is the polymer density, $k_B \Theta$ is the energy associated with thermal noise, F_i is the dumbbell relaxation force and R_i its elongation vector. The average is taken over the statistics of the thermal noise. Assuming the force between the beads to be Hookean with dynamical coefficient K_0 , the average in the elastic stress reduces to $\langle \mathbf{R}\mathbf{F} \rangle = -K_0 \langle \mathbf{R}\mathbf{R} \rangle$. The latter is proportional to the conformation tensor $\boldsymbol{\sigma} \equiv \langle \mathbf{R}\mathbf{R} \rangle / R_0^2$, where R_0 denotes the equilibrium spring length. The inclusion of the extra elastic stress term in the Navier–Stokes equations leads to the following equation for the viscoelastic flow:

$$\partial_t \mathbf{v} + (\mathbf{v} \cdot \boldsymbol{\partial}) \mathbf{v} = -\boldsymbol{\partial} p + \nu \beta \partial^2 \mathbf{v} + \frac{\nu(1-\beta)}{\tau} \boldsymbol{\partial} \cdot (\boldsymbol{\sigma} - \mathbf{1}) + \mathbf{f}. \quad (2.2)$$

Here, ν is the total kinematic viscosity of the solution, while $\nu\beta$ and $\nu(1-\beta)$ are the sepa-

rate contributions by the solvent and the polymers, respectively, and we have introduced the dimensionless parameter $\beta = \eta_s / (n_p k_B \Theta \tau + \eta_s)$, η_s being the dynamic viscosity of the solvent. τ is a parameter depending on K_0 and R_0 , representing the typical relaxation time of the polymers. A more precise definition of τ and σ comes in the following. Throughout the paper, it is understood that $(\partial \mathbf{v})_{\alpha\beta} \equiv \partial_\alpha v_\beta$ and $\text{tr}(\partial \mathbf{v}) = \partial \cdot \mathbf{v} = 0$.

An equation for the dynamics of the polymer conformation tensor σ is needed to close the system of equations. Simple physical reasoning by Bird *et al.* (1987) gives the following stochastic equation for the separation \mathbf{R} between two beads:

$$\dot{\mathbf{R}} = (\mathbf{R} \cdot \partial) \mathbf{v} - \frac{1}{2\tau} \mathbf{R} + \sqrt{\frac{R_0^2}{\tau}} \boldsymbol{\xi}. \quad (2.3)$$

On the right-hand side, the first term is the stretching/compression term, originating from the spatial variation of the flow experienced by \mathbf{R} , and the last one, $\boldsymbol{\xi}$, is a white-in-time random process mimicking the effect of thermal noise on the polymers. The second is the relaxation due to the force between the beads, proportional to the elongation derivative of the dumbbell free energy $-\partial E / \partial R_i = -\partial(1/2K_0 R^2) / \partial R_i$. A quadratic form of the potential, and thus a linear Hookean force, is an approximation valid for moderate polymer elongations. The dynamical coefficient τ is the same as the one appearing in (2.2). Considering it constant amounts to assume that the polymers have only one relaxation time. Numerical and theoretical studies point out that this hypothesis is reasonable (Geraschenko *et al.* 2005). Experiments (see Lumley 1969; Virk 1975; Nadolink & Haigh 1995) show that polymers have a spectrum of typical relaxation times, but they also show that interactions with the fluid mostly depend on the largest one, that is the one we are retaining.

Multiplying (2.3) by \mathbf{R} and averaging over the statistics of the thermal noise $\boldsymbol{\xi}$, the following evolution equation for the conformation tensor $\sigma = \langle \mathbf{R}\mathbf{R} \rangle / R_0^2$ is obtained (see Bird *et al.* 1987):

$$\partial_t \sigma + (\mathbf{v} \cdot \partial) \sigma = (\partial \mathbf{v})^T \cdot \sigma + \sigma \cdot (\partial \mathbf{v}) - \frac{1}{\tau} (\sigma - \mathbf{1}). \quad (2.4)$$

Summarizing, the set of equations (2.2) and (2.4) constitutes the Oldroyd-B model that we shall be considering in the sequel.

Our first step in the investigation of the effect of polymers onto the stability of the flow will be to find out the basic equilibrium state. The state will then be perturbed and the resulting equations analysed using multiscale methods.

2.1. A basic equilibrium state

Finding analytically the basic equilibrium state for a generic forcing \mathbf{f} is a hopeless task already for the Navier–Stokes equations without polymers. The problem is further complicated here by the additional term in (2.2) and the coupling with (2.4).

The problem simplifies for $\mathbf{f} \equiv (f(z), 0, 0)$, inducing a parallel flow $\mathbf{U} = (U(z), 0, 0)$, which trivially annihilates the advective nonlinear term in (2.2). A further substantial simplification comes from the viscoelastic version of Squire’s theorem (see Appendix A), stating that, for parallel flows, the most unstable perturbations are two-dimensional. We shall therefore restrict to a two-dimensional flow (u_x, u_z) , without any lack of generality (see also Boffetta *et al.* 2005a). We further assume $f(z) = F_0 \cos(z/L)$, producing the well-known Kolmogorov flow (Arnold & Meshalkin 1960) $U(z) \equiv (V \cos(z/L), 0)$, where $V = F_0 L^2 / \nu$. The corresponding conformation tensor at equilibrium is:

$$\sigma = \begin{pmatrix} 1 + 2\tau^2 (\partial_z U)^2 & \tau \partial_z U \\ \tau \partial_z U & 1 \end{pmatrix} = \begin{pmatrix} 1 + 2\tau^2 \frac{V^2}{L^2} \sin^2(\frac{z}{L}) & -\tau \frac{V}{L} \sin(\frac{z}{L}) \\ -\tau \frac{V}{L} \sin(\frac{z}{L}) & 1 \end{pmatrix}. \quad (2.5)$$

This choice also allows to precisely define the Reynolds number of the flow as $Re = VL/\nu$. In this model the elasticity of the polymers is taken into account by the relaxation time τ only. We can thus introduce an adimensional parameter, the Deborah number $De = \tau V/L$, to characterize the elastic properties of the flow.

3. Some previous results on the linear stability analysis

It has long been known that the Newtonian Kolmogorov flow becomes unstable for Reynolds numbers $Re > \sqrt{2}$ (Meshalkin & Sinai 1961): the evolution of large-scale perturbations is formally described by an effective diffusive dynamics and instabilities are associated to the loss of positive-definiteness of the eddy-viscosity tensor.

In the presence of polymers, performing a multiscale analysis (Bensoussan *et al.* 1978; Bayly *et al.* 1988) on the linearized Oldroyd-B model, one obtains an explicit expression for the eddy-viscosity tensor, valid for sufficiently low elasticity (Boffetta *et al.* 2005a). The resulting stability curve in terms of the Reynolds and the Deborah number is reported in figure 1.

3.1. Multiscale analysis

Substituting $\mathbf{v} = \mathbf{u} + \mathbf{w}$ into (2.2,2.4), the equations for the perturbation fields read:

$$\boldsymbol{\partial} \cdot \mathbf{w} = 0, \quad (3.1)$$

$$\partial_t \mathbf{w} + \boldsymbol{\partial} \cdot (\mathbf{u}\mathbf{w} + \mathbf{w}\mathbf{u} + \mathbf{w}\mathbf{w}) = -\boldsymbol{\partial}q + \nu\beta\partial^2\mathbf{w} + \nu(1-\beta)\tau^{-1}\boldsymbol{\partial} \cdot \boldsymbol{\zeta}, \quad (3.2)$$

$$\begin{aligned} \partial_t \boldsymbol{\zeta} + \boldsymbol{\partial} \cdot (\mathbf{u}\boldsymbol{\zeta} + \mathbf{w}\boldsymbol{\sigma} + \mathbf{w}\boldsymbol{\zeta}) &= (\boldsymbol{\partial}\mathbf{u})^T \cdot \boldsymbol{\zeta} + (\boldsymbol{\partial}\mathbf{w})^T \cdot \boldsymbol{\sigma} + (\boldsymbol{\partial}\mathbf{w})^T \cdot \boldsymbol{\zeta} + \\ &+ \boldsymbol{\zeta} \cdot (\boldsymbol{\partial}\mathbf{u}) + \boldsymbol{\sigma} \cdot (\boldsymbol{\partial}\mathbf{w}) + \boldsymbol{\zeta} \cdot (\boldsymbol{\partial}\mathbf{w}) - \tau^{-1}\boldsymbol{\zeta}, \end{aligned} \quad (3.3)$$

where q and $\boldsymbol{\zeta}$ are the perturbations associated to the pressure term p and the basic stress tensor $\boldsymbol{\sigma}$. In the linear stability analysis, the nonlinear terms containing the product of two perturbation fields are supposed to be negligible (see Boffetta *et al.* 2005a).

As in the Newtonian case, it is assumed that the first unstable perturbations have periodicity much larger than that of the basic flow. The validity of this assumption has already been investigated by Boffetta *et al.* (2005a) and is satisfied in the range of parameters considered here.

In addition to the usual “fast” space/time variables \mathbf{x}, t , describing the basic flow, multiscale techniques introduce “slow” variables $\tilde{\mathbf{x}} = \epsilon\mathbf{x}$, $\tilde{t} = \epsilon^2 t$, to describe the large-scale flow, and prescribe to treat the two sets as independent. This leads to the expansion of the differential operators:

$$\partial_i \rightarrow \partial_i + \epsilon\tilde{\partial}_i, \quad \partial_t \rightarrow \partial_t + \epsilon^2\tilde{\partial}_t, \quad (3.4)$$

and of the fields:

$$\begin{aligned} \mathbf{w} &= \mathbf{w}^{(0)}(z, t, \tilde{x}, \tilde{z}, \tilde{t}) + \epsilon\mathbf{w}^{(1)}(z, t, \tilde{x}, \tilde{z}, \tilde{t}) + \epsilon^2\mathbf{w}^{(2)}(z, t, \tilde{x}, \tilde{z}, \tilde{t}) + \dots, \\ q &= q^{(0)}(z, t, \tilde{x}, \tilde{z}, \tilde{t}) + \epsilon q^{(1)}(z, t, \tilde{x}, \tilde{z}, \tilde{t}) + \epsilon^2 q^{(2)}(z, t, \tilde{x}, \tilde{z}, \tilde{t}) + \dots, \\ \boldsymbol{\zeta} &= \boldsymbol{\zeta}^{(0)}(z, t, \tilde{x}, \tilde{z}, \tilde{t}) + \epsilon\boldsymbol{\zeta}^{(1)}(z, t, \tilde{x}, \tilde{z}, \tilde{t}) + \epsilon^2\boldsymbol{\zeta}^{(2)}(z, t, \tilde{x}, \tilde{z}, \tilde{t}) + \dots. \end{aligned} \quad (3.5)$$

All of the functions have the periodicity of the basic flow and are independent of x .

Inserting (3.5) into (3.1)-(3.3) and collecting terms of the same order in ϵ , the coarse-grained equation for a large-scale perturbation is obtained as the solvability condition at the order ϵ^2 . In terms of the stream function Ψ , the perturbation evolves according to the non-isotropic diffusion equation:

$$\tilde{\partial}_t \tilde{\Delta} \Psi = \nu_{\alpha\beta} \tilde{\partial}_\alpha^2 \tilde{\partial}_\beta^2 \Psi, \quad (3.6)$$

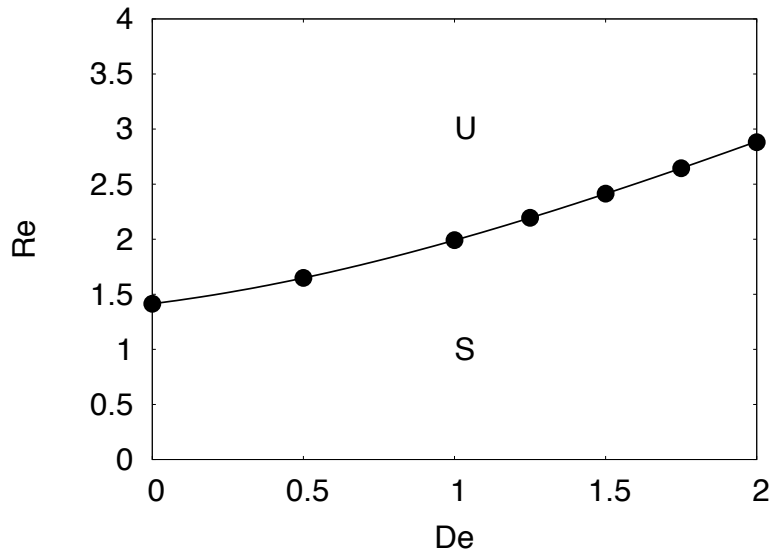


FIGURE 1. The linear stability diagram for $\beta = 0.769$. Stable and unstable regions are denoted by S and U, respectively. The bullets represent direct numerical simulations (DNS) of the complete Oldroyd-B system of equations, confirming theoretical predictions for this window of parameters.

where the eddy-viscosity tensor $\nu_{\alpha\beta}$ is not positive-definite for $Re > \sqrt{2}$ (in the absence of polymers). In general, there exist critical values of Re and De where perturbations start growing in time.

The phase-space (Re, De) is thus divided in regions where the eddy-viscosity tensor is positive-definite (the system is linearly stable with respect to any small perturbation) and where there exists at least one unstable mode, as shown in figure 1 for low Deborah numbers. The diagram reveals two kinds of instabilities. When the Deborah number is sufficiently low, the flow experiences hydrodynamic-like large-scale transverse instabilities, captured by multiscale analysis. In this region, the critical Reynolds number where the flow becomes unstable, grows with De : polymers stabilize the flow. This has been interpreted by Boffetta *et al.* (2005a), and will be shown in § 8, to be a prelude to the drag reduction effect observed in the turbulent regime.

For high values of the Deborah number (not shown in figure 1) the multiscale analysis predicts the flow to be unstable, even for very low Reynolds numbers. However, numerical simulations show that the assumption of scale separation does not hold and multiscale techniques are not applicable. This region, possibly characterized by purely elastic instabilities, will not be the concern of the present investigation which focuses on $0 \leq De \leq 2$.

If the amplitude of the large-scale perturbation is strong enough and/or the eddy-viscosity is negative, nonlinear effects are important and should be taken into account. These two situations correspond to different scalings of the fields and will be treated separately in the next sections.

4. Nonlinear dynamics: the standard Cahn–Hilliard equation

Linear stability analyses, by their very definition, are not able to capture the full-time dynamics of unstable perturbations: as perturbations grow in time, their magnitude becomes large and nonlinearities ought to be taken into account. In the Newtonian case

(Sivashinsky 1985; She 1987), the lowest-order nonlinearity (third-order) is sufficient to stabilize the linear exponential growth and lead to a steady state. Here, we show how this occurs and generalize it first to the viscoelastic case. The next section will then be devoted to the case where the lowest-order nonlinearity does not stabilize the flow and higher-order nonlinearities become relevant.

A careful analysis of the linear eddy-viscosity tensor $\nu_{\alpha\beta}$ derived in (3.6) ensures that for low enough Deborah numbers the first modes to become linearly unstable are the large-scale transverse ones. For barely unstable flows we may expect that the perturbations involved in the nonlinear dynamics will be confined to these modes. This suggests that the result will be a one-dimensional diffusion equation for the averaged transverse modes, linearly stable for small-scale modes, involving at least one nonlinear term.

Assume now that the initial amplitude of the large-scale perturbation is sufficiently small and the system we consider is in the surroundings of a point of the critical curve. According to (3.6), the average transverse velocity perturbation $\langle w_z \rangle$ linearly evolves according to a diffusion equation:

$$\tilde{\partial}_t \langle w_z \rangle \sim -A \tilde{\partial}^2 \langle w_z \rangle, \quad (4.1)$$

where A is a positive coefficient representing the linear eddy-viscosity tensor of (3.6), restricted to low Deborah numbers (as explained in the end of §3). It vanishes on the stability curve, being positive above it and negative below it.

In this equation, all modes are linearly unstable. It needs to be modified to keep track of the multiscale hypothesis, which requires small-scale modes to be stable. This is done introducing a bi-Laplacian term into (4.2) to stabilize the small scales (the fourth-order derivative ensures that this term will be dominant on the small-scale perturbations only):

$$\tilde{\partial}_t \langle w_z \rangle \sim -A \tilde{\partial}^2 \langle w_z \rangle - C \tilde{\partial}^4 \langle w_z \rangle. \quad (4.2)$$

In general, close to the linear instability threshold, where the coefficient A changes sign, we do not expect C to vanish. To comply with the stability requirements, we will request it to have a finite, positive value in the region of interest.

We expect to find the presence of a nonlinear term, eventually stabilizing this growth. This part cannot be played by the advective nonlinearity because of the one-dimensional character of the equation. The next-order nonlinearity is cubic and must contain at least two space derivatives: one before the whole term, to ensure momentum conservation, and an additional one to respect space-inversion symmetries. This yields a nonlinear term: $B \tilde{\partial}_x \left(\langle w_z^{(1)} \rangle^2 \tilde{\partial}_x \langle w_z^{(1)} \rangle \right)$, where B is some constant related to the (nonlinear) eddy-viscosity.

We can now introduce, as in §3, the “slow” variables $\tilde{\mathbf{x}} = \epsilon \mathbf{x}$ and \tilde{t} (notice that we still do not know the scaling between t and \tilde{t}). The space derivatives must again be expanded as $\partial_i \rightarrow \partial_i + \epsilon \tilde{\partial}_i$. We now have to look for a prescription on how to expand the different fields in terms of ϵ .

In the vicinity of the marginal eddy-viscosity curve $A \approx 0$, and a Taylor expansion gives $A \sim \frac{\partial A}{\partial \nu} \Big|_{\nu_c} (\nu - \nu_c)$, where ν_c indicates the critical viscosity. Balances between the term $A \tilde{\partial}^2 \langle w_z \rangle$ and both the cubic nonlinearity and $C \tilde{\partial}^4 \langle w_z \rangle$ yield:

$$B \epsilon^2 \epsilon_w^3 \sim \frac{\partial A}{\partial \nu} \Big|_{\nu_c} (\nu - \nu_c) \epsilon^2 \epsilon_w, \quad \frac{\partial A}{\partial \nu} \Big|_{\nu_c} (\nu - \nu_c) \epsilon^2 \epsilon_w \sim C \epsilon^4 \epsilon_w. \quad (4.3)$$

Here, ϵ_w is the scaling of the amplitude of the velocity perturbation \mathbf{w} .

Equations (4.3) completely define the scaling for the velocity perturbation and the

distance from the critical viscosity:

$$\epsilon = \epsilon_w, \quad \frac{\nu - \nu_c}{\nu} \sim \epsilon^2 \Rightarrow \nu = \nu_c(1 - \epsilon^2). \quad (4.4)$$

It follows from (4.4) that the Reynolds number $Re = Re_c(1 + \epsilon^2)$. The comparison of any of the previous terms with the (slow) time derivative of \mathbf{w} gives the scaling $\tilde{t} = \epsilon^4 t$. As for the scaling of the polymer conformation tensor, balancing ζ/τ and $(\partial w_z) \cdot \sigma$, we obtain that the scaling of ζ coincides with ϵ_w . The same equality holds for the pressure field.

Summarizing, the fields are expanded as:

$$\begin{aligned} \mathbf{w} &= \epsilon \mathbf{w}^{(1)}(z, \tilde{x}, \tilde{t}) + \epsilon^2 \mathbf{w}^{(2)}(z, \tilde{x}, \tilde{t}) + \dots, \\ q &= \epsilon q^{(1)}(z, \tilde{x}, \tilde{t}) + \epsilon^2 q^{(2)}(z, \tilde{x}, \tilde{t}) + \dots, \\ \zeta &= \epsilon \zeta^{(1)}(z, \tilde{x}, \tilde{t}) + \epsilon^2 \zeta^{(2)}(z, \tilde{x}, \tilde{t}) + \dots \end{aligned} \quad (4.5)$$

The next step to obtain a coarse-grained equation for the large-scale dynamics is to plug (4.5) into (3.1)-(3.3). Exploiting the chain rule, the definitions of \tilde{x} and \tilde{t} and averaging along z , we end up with a set of equations involving solely the large-scale fields. The equation for the large-scale transverse perturbation $\langle w_z^{(1)} \rangle(\tilde{x}, \tilde{t})$ is obtained from the solvability condition at order ϵ^5 . For details on the Newtonian case and solvability conditions, see Gama *et al.* (1994).

We can summarize the whole procedure in the following schematic way:

- (a) Solve the continuity equation. The explicit expression of $w_z^{(n)}$ is thus obtained in terms of known functions of z .
- (b) Solve the equation for $\zeta_{zz}^{(n)}$; this can always be done algebraically as $\zeta_{zz}^{(n)}$ is slaved to the $w_z^{(n)}$ field.
- (c) Solve the evolution equation for $w_z^{(n)}$. This field is obtained from (a); we are then able to obtain the expression for the pressure field perturbation q .
- (d) Solve the system for $\zeta_{xz}^{(n)}$ and $w_x^{(n)}$ by direct integration.
- (e) Algebraically obtain the explicit expression for $\zeta_{xx}^{(n)}$.
- (f) Impose solvability condition at order $n + 1$ on the continuity and the velocity field equations. Such condition is automatically fulfilled by the polymer conformation tensor, as it is slaved to the velocity field at the previous order.

The final equation has the form of a ‘‘standard’’ Cahn–Hilliard equation:

$$\tilde{\partial}_t \langle w_z^{(1)} \rangle = \tilde{\partial}_x \left[\left(-A + B \langle w_z^{(1)} \rangle^2 \right) \tilde{\partial}_x \langle w_z^{(1)} \rangle \right] - C \tilde{\partial}_x^4 \langle w_z^{(1)} \rangle. \quad (4.6)$$

‘‘Standard’’ is meant to stress that the structure of (4.6) (including the cubic non-linearity) emerges in a variety of hydrodynamic situations (see Nepomnyashchy 1976; Sivashinsky 1985; Pedlosky 1987; Manfroi & Young 1999). The parameters A, B, C are known functions of the parameters De and β , as shown in figure 2. It is worth noting that A is non-negative as the system is supposed to be slightly above the threshold of instability and we have explicitly incorporated a negative sign in (4.6).

The saturation of the instability requires two conditions. First, C must be positive to ensure that the instability be saturated at sufficiently high wave-numbers (still much smaller than those of the basic flow, of order unity). Second, B ought to be positive to ensure that, as $\langle w_z^{(1)} \rangle$ becomes $O(\sqrt{A/B})$, the nonlinear eddy-viscosity $-A + B \langle w_z^{(1)} \rangle^2$ change sign and the growth be again saturated. Both these conditions are satisfied up to a critical value of the Deborah number, De^* (see figure 2).

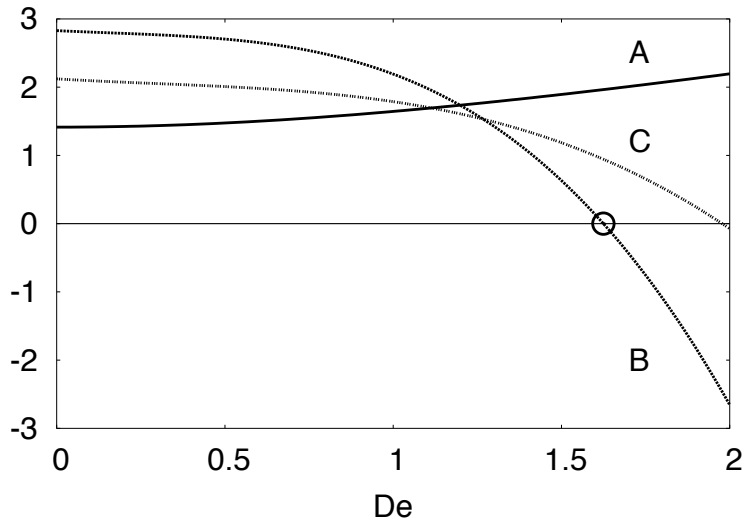


FIGURE 2. The parameters A, B and C appearing in the coarse-grained Cahn-Hilliard equation (4.6) as a function of the Deborah number (for $\beta = 0.769$).

Up to the critical Deborah number De^* , the equation (4.6) for the large-scale perturbations has the same structure as in the Newtonian case and the only difference is in the numerical value of the parameters A, B, C . As we shall see in the next sections, this property ceases to be true above De^* .

To conclude, we stress the fact that all the fields up to order four are expressed in terms of explicit functions of the fast variables and of the large-scale field $\langle w_z^{(1)} \rangle$, obeying the Cahn-Hilliard equation (4.6).

5. Generalized Cahn-Hilliard dynamics

We have observed in the previous section that, along the marginal linear stability curve, there exists a critical value of the Deborah number, De^* , where the cubic nonlinear term becomes negative. Furthermore, the change of sign is taking place in the region where the small-scale operator is stable. The problem is thus well-posed and lends to multiscale methods.

For $De > De^*$, the field keeps growing at sufficiently large scales, until it reaches amplitudes where the next-order nonlinearity becomes important. Its structure is dictated by the conservation of momentum and the symmetries of the basic flow: $\tilde{\partial}_x \left(\langle w_z \rangle^4 \tilde{\partial}_x \langle w_z \rangle \right)$, with a regular coefficient D in the neighborhood of the critical point P^* , where both the eddy-viscosity and the coefficient of the third-order nonlinearity change sign.

Four regions can be identified around P^* (see figure 3). The eddy-viscosity $A = 0$ curve has been obtained by means of the linear stability analysis (§ 3). The linear approximation of the curve $B = 0$ in the vicinity of P^* is obtained from the analytic expression of B on the marginal curve and the marginal curve itself.

Zone I is linearly unstable ($A > 0$), has a third-order destabilizing term ($B < 0$) and we can guess that a fifth-order term will enter into play to stabilize the growth. Zone II is particularly interesting as it is linearly stable ($A < 0$), but has a third-order destabilizing contribution ($B < 0$). Perturbing with a field of sufficiently strong amplitude, the system

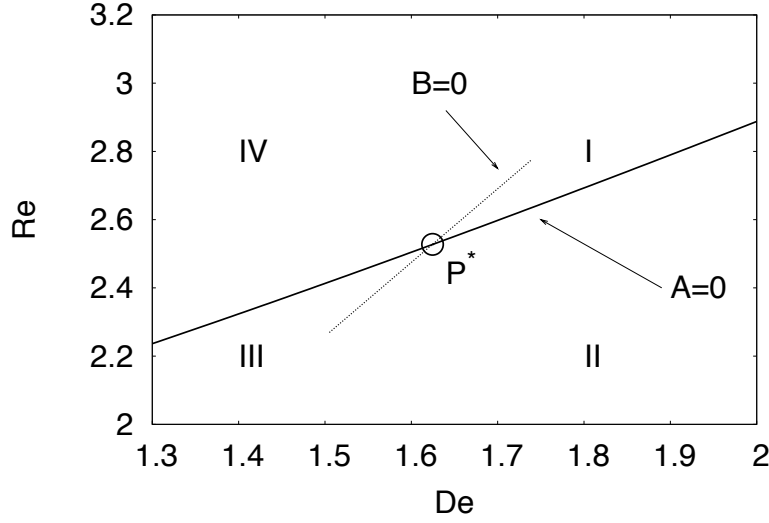


FIGURE 3. The phase-space around the critical point P^* where both the eddy-viscosity and the coefficient of the third-order nonlinearity change sign. The region is divided in four regions schematically sketched here by the two critical curves $A = 0$ and $B = 0$. The former is found from the linear stability analysis in section 3. The latter is found locally, around the $A = 0$ curve, by solving (5.5), and is linearly extrapolated for graphical purposes as a dashed line. For $\beta = 0.769$, the curve $B = 0$ is inclined at approximately 60° with respect to the De axis.

jumps to the asymptotic steady state where the two nonlinear terms (third and fifth-order) balance each other. Zone III is completely stable ($A < 0, B > 0$). In the last region, IV, as De approaches the critical value, the coefficient B goes to zero and cannot saturate the exponential growth from the linear instability. The fifth-order nonlinearity, which is negligible far from the critical point, must enter again into play.

5.1. Zone I

When both the Reynolds and the Deborah numbers exceed their critical values, previous considerations suggest the following structure for the coarse-grained equation:

$$\tilde{\partial}_t w = -A \tilde{\partial}_x^2 w - |B| \tilde{\partial}_x (w^2 \tilde{\partial}_x w) - C \tilde{\partial}_x^4 w + D \tilde{\partial}_x (w^4 \tilde{\partial}_x w). \quad (5.1)$$

Confining the analysis to the surroundings of the critical point P^* , we may represent the position in phase space as:

$$\nu = \nu^* (1 - K_1 \epsilon_\nu - K_2 \epsilon_\nu^2), \quad (5.2)$$

$$De = De^* (1 + \epsilon_{De}). \quad (5.3)$$

Adequately choosing the K_1 and K_2 parameters, any point around P^* can be reached as ϵ varies. The reason why we need to incorporate in (5.2) the additional contribution of order ϵ^2 will be clear shortly.

In the neighborhood of P^* , the coefficients A and B are expanded as:

$$A = \frac{\partial A}{\partial De} (De - De^*) + \frac{\partial A}{\partial \nu} (\nu - \nu^*), \quad (5.4)$$

$$B = \frac{\partial B}{\partial De} (De - De^*) + \frac{\partial B}{\partial \nu} (\nu - \nu^*), \quad (5.5)$$

where all derivatives are computed at P^* .

The scaling in ϵ of the velocity field amplitude, ϵ_w , and the parameters ϵ_ν , ϵ_{De} is found by requiring that all terms in (5.1) be of the same order in the scale-separation small parameter ϵ .

The comparison between the last two terms in (5.1) fixes the relation between ϵ and ϵ_w :

$$D \epsilon^2 \epsilon_w^5 \sim C \epsilon^4 \epsilon_w \Rightarrow \epsilon_w = \epsilon^{1/2}. \quad (5.6)$$

The parameters ϵ_ν and ϵ_{De} are found by comparing the terms associated to A , B and D in (5.1). Using (5.2)-(5.6), we obtain:

$$D \epsilon^2 \epsilon^{5/2} \sim \left[\frac{\partial A}{\partial De} (\epsilon_{De} De^*) - \frac{\partial A}{\partial \nu} (K_1 \epsilon_\nu \nu^*) \right] \epsilon^2 \epsilon^{1/2} \quad (5.7)$$

$$D \epsilon^2 \epsilon^{5/2} \sim \left[\frac{\partial B}{\partial De} (\epsilon_{De} De^*) - \frac{\partial B}{\partial \nu} (K_1 \epsilon_\nu \nu^*) \right] \epsilon^2 \epsilon^{3/2}. \quad (5.8)$$

Choosing $\epsilon_\nu = \epsilon_{De} = \epsilon$ and setting K_1 to ensure $\left[\frac{\partial A}{\partial De} De^* - \frac{\partial A}{\partial \nu} K_1 \nu^* \right] = 0$, both equations (5.7) and (5.8) are satisfied. Equation (5.7) is balanced by the second-order term of the ν expansion (5.2), dependent on K_2 . The scalings of time, pressure and polymer conformation tensor perturbation, ϵ^4 , $\epsilon^{1/2}$ and $\epsilon^{1/2}$, respectively, are derived as in § 4.

Once the scalings have been determined we can proceed as in § 4 to obtain the large-scale equation for $\langle w_z^{(1/2)} \rangle(\tilde{t}, \tilde{x})$. The evolution equation emerges now from the solvability condition at the order $\epsilon^{9/2}$:

$$\tilde{\partial}_t \langle w_z^{(1/2)} \rangle = \tilde{\partial}_x \left[\left(-A + B \langle w_z^{(1/2)} \rangle^2 + D \langle w_z^{(1/2)} \rangle^4 \right) \tilde{\partial}_x \langle w_z^{(1/2)} \rangle \right] - C \tilde{\partial}_x^4 \langle w_z^{(1/2)} \rangle, \quad (5.9)$$

where the coefficients are explicit functions of β . For $\beta = 0.769$, they read:

$$\left\{ \begin{array}{l} A = 0.5106 + 1.965K_2, \quad B = -8.979, \\ C = 0.9439, \quad D = 23.11, \quad K_1 = 0.594. \end{array} \right\} \quad (5.10)$$

Although (5.9) belongs to the class of the Cahn–Hilliard equations (1.1), the emergence of the new, sixth-order nonlinearity will be responsible for new dynamical aspects, not present for $De < De^*$, which will be discussed in detail in § 6.

5.2. Zone II

For Deborah numbers above the critical value, perturbations are nonlinearly unstable: $B < 0$. This is true regardless of the sign of the linear term and strong enough perturbations may then grow even if the system is linearly stable.

Let us then consider systems with $\nu > \nu^*$ and $De > De^*$. No major difference with respect to case I is expected. At zero-th order, the coefficients A and B vanish and equations (5.4)-(5.5) hold. Again, we define the position in phase-space via the two parameters ϵ_ν and ϵ_{De} . As the viscosity is now larger than the critical value, a positive sign appears in the expansion of the viscosity:

$$\nu = \nu^* (1 + K_1 \epsilon_\nu - K_2 \epsilon_\nu^2), \quad (5.11)$$

while (5.3) holds. The parameter K_2 , as we shall point out later, can take any value compatible with the condition $A > 0$.

The same calculations discussed in the previous subsection can be carried out to derive the coarse-grained equation for the transverse velocity. As one might expect, its form is exactly the same as (5.9), a generalized Cahn–Hilliard equation. The only difference is

in the value of the parameters. For $\beta = 0.769$, they read:

$$\left\{ \begin{array}{l} A = -0.2202 + 1.965K_2, \quad B = -35.62, \\ C = 0.9439, \quad D = 23.11, \quad K_1 = 0.5974. \end{array} \right\} \quad (5.12)$$

Only A and B have changed with respect to (5.10), as expected since they are the only parameters which depend on ϵ (and thus on Re and De) in physical coordinates. Notice that there is an upper bound on the values we can choose for K_2 , reflecting the linear stability requirement.

5.3. Zone IV

What happens when the Deborah number is barely smaller than the critical value De^* ? Sufficiently close to it, the third-order instability can be made subdominant with respect to the fifth-order and our aim here is to work out the scaling coefficients corresponding to such situation.

For this purpose, let us assume that the cubic nonlinearity is negligible. At leading order, the terms associated to A , C and D must be of the same order. This means:

$$\epsilon^4 \epsilon_w \sim \epsilon^2 \epsilon_w \left[\frac{\partial A}{\partial De} (De - De^*) + \frac{\partial A}{\partial \nu} (\nu - \nu^*) \right], \quad (5.13)$$

$$\epsilon^2 \epsilon_w^5 \sim \epsilon^2 \epsilon_w \left[\frac{\partial A}{\partial De} (De - De^*) + \frac{\partial A}{\partial \nu} (\nu - \nu^*) \right], \quad (5.14)$$

and implies:

$$\nu = \nu^* (1 - K_2 \epsilon^2), \quad De = De^* (1 - \epsilon^2). \quad (5.15)$$

Additionally, the velocity field scales as $\epsilon^{1/2}$, as the pressure and polymer fields do. The time derivative scales as ϵ^4 .

To be consistent, we are left to check that the third-order nonlinearity is negligible. Using the previous scalings and the ensuing fact that $B \sim O(\epsilon^2)$, we have to verify that:

$$O(B \partial^2 w^3) \ll O(D \partial^2 w^5) \Rightarrow O(\epsilon^{11/2}) \ll O(\epsilon^{9/2}), \quad (5.16)$$

which holds true. It is now possible to apply the strategy discussed in §4 to derive the large-scale equation and obtain (at order ϵ^5):

$$\tilde{\partial}_t \langle w_z^{(1/2)} \rangle = \tilde{\partial}_x \left[\left(-A + D \langle w_z^{(1/2)} \rangle^4 \right) \tilde{\partial}_x \langle w_z^{(1/2)} \rangle \right] - C \tilde{\partial}_x^4 \langle w_z^{(1/2)} \rangle, \quad (5.17)$$

where C and D have the same value as before and $A = 1.1740 + 1.965K_2$.

6. Variational formulation

It is well-known that the “standard” Cahn–Hilliard equation admits a variational formulation in terms of a Ginzburg–Landau potential (Cahn & Hilliard 1958). Equation (4.6), after appropriate rescalings, $w \rightarrow (A/B)^{1/2} w$, $t \rightarrow A^{-1} t$, $\lambda = C/A$, is recast in the form (1.1) with the Lyapunov functional:

$$F[w] = \int \left[\frac{\lambda}{2} (\partial_x w)^2 + I(w) \right] dx, \quad I(w) = -\frac{w^2}{2} + \frac{w^4}{12}. \quad (6.1)$$

Note that mean fields only are considered, that is w must be read as the rescaled leading contribution $\langle w_z^{(1)} \rangle(\tilde{x}, \tilde{t})$.

The existence of a Lyapunov functional implies the existence of an asymptotic state

for w , if boundary conditions are periodic and stationary. Such state corresponds to a minimum of the Lyapunov functional and it is calculated by the following equations:

$$I'(w) = \lambda \partial_x^2 w \leftrightarrow \partial_x I = \frac{\lambda}{2} \partial_x (\partial_x w)^2. \quad (6.2)$$

When w is a maximum (or a minimum), $I(w_{max})$ is constant and w_{max} is obtained solving $I' = 0$ as $w_{max} = \pm\sqrt{3}$. Considering this boundary condition, equation (6.2) can be easily solved. Its solutions are the well-known *kink* and *anti-kink* structures, namely:

$$w = \pm\sqrt{3} \tanh \left[\sqrt{\frac{1}{2\lambda}} x \right]. \quad (6.3)$$

The issue now is whether or not a Lyapunov extremal formulation exists in the generalized Cahn–Hilliard case (5.1) as well, and how it relates to the standard one. In particular, a Painlevé test (Ablowitz & Clarkson 1991) can be performed on the equation to check its integrability. The calculation consists in checking that all movable singularities (whose location depends on initial and/or boundary conditions) are poles (see for details Ablowitz & Clarkson 1991). The test is based on a well-known connection between the integrability property of a nonlinear differential equation and its analytic structure for complex values of the independent variable (Kowalesvki 1889, 1890; Painlevé 1897). The explicit calculation is performed in Appendix B. The generalized Cahn–Hilliard equation indeed enjoys the Painlevé property and is thus integrable.

Let us then write the equation (5.1) after the rescalings $w \rightarrow (A/B)^{1/2}w$, $t \rightarrow A^{-1}t$, $\lambda = C/A$, $\gamma = AD/B^2$:

$$\partial_t w = -\partial_x^2 w - \frac{1}{3} \partial_x^2 w^3 - \lambda \partial_x^4 w + \frac{\gamma}{5} \partial_x^2 w^5. \quad (6.4)$$

Integrability of this equation is related to the existence of the following Lyapunov functional, similar to that of the standard case, yet with a sixth-order potential:

$$F[w] = \int \left[\frac{\lambda}{2} (\partial_x w)^2 + I(w) \right] dx, \quad I(w) = -\frac{w^2}{2} - \frac{w^4}{12} + \frac{\gamma}{30} w^6. \quad (6.5)$$

The calculation of the function corresponding to its minimum is performed using again (6.2).

All solutions tend to final steady states which minimize F . The approach to the solution is however nontrivial and the structure is made of plateaux having velocity $\pm W_0$ ($I'(W_0) = 0$), separated by positive and negative kinks (see figure 4). The amplitude of the velocity w in the plateaux is:

$$W_0^2 = \frac{5 + \sqrt{25 + 180\gamma}}{6\gamma}. \quad (6.6)$$

Note that, at small γ 's, the asymptotic velocity W_0 diverges as $1/\sqrt{\gamma}$. This is quite intuitive: the field amplitude equilibrating the third and the fifth-order nonlinearities increases as the coefficient of the fifth-order nonlinearity reduces.

The explicit expression of the profiles for kinks and anti-kinks is obtained from the integration of equations (6.2), (6.5). For the sake of example, when $\lambda = 1/2$ and $\gamma = 10/9$ the profiles read:

$$w = \pm\sqrt{15} \frac{e^{2\sqrt{3}x} - 1}{\sqrt{5e^{4\sqrt{3}x} + 26e^{2\sqrt{3}x} + 5}}. \quad (6.7)$$

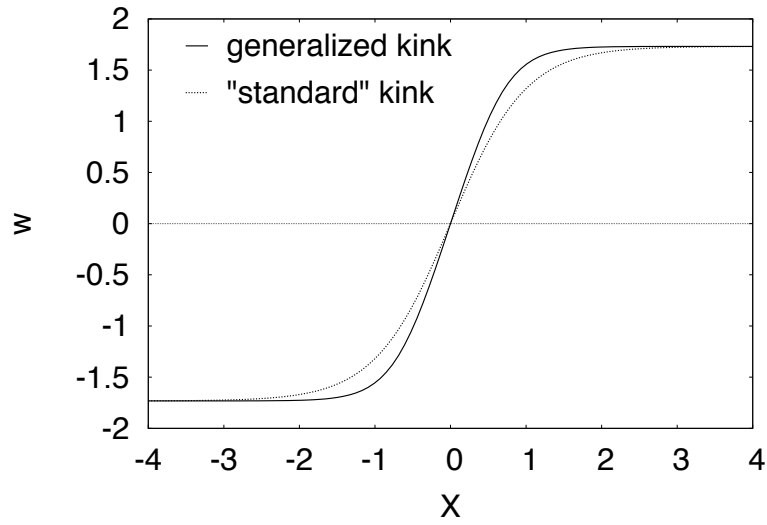


FIGURE 4. The “generalized” (solid) and “standard” (dotted) kinks for $\lambda = 1/2$ and $\gamma = 10/9$. The former has a manifestly shorter range. It is shown in the body of the text that this entails longer time-scales for their annihilation with the corresponding anti-kinks.

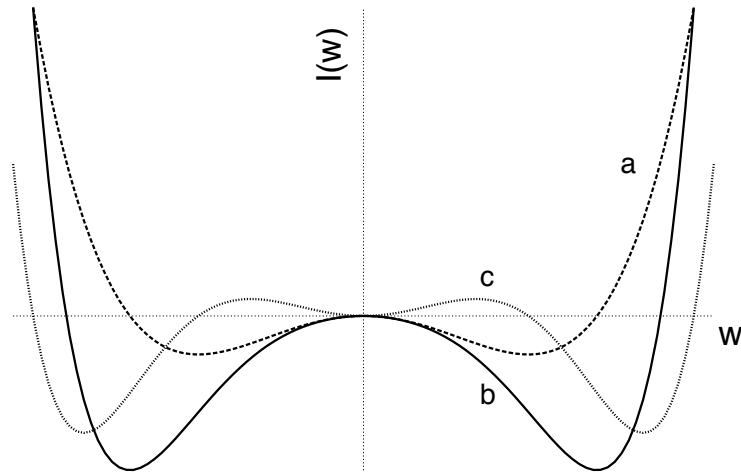


FIGURE 5. The potentials associated to the different evolution equation. Curve *a* is related to the standard Cahn–Hilliard equation (fourth-order potential); curve *b* represents the generalized Cahn–Hilliard equation (sixth-order potential). Curve *c* is the characteristic triple-well potential of the purely nonlinearly unstable case. The plots are in arbitrary units, to ease the comparison between the curves.

The generalized kink-antikink structures, e.g. those given by equation (6.7), will be dubbed “generalized” kinks and anti-kinks.

6.1. Dynamics of generalized kink/antikink annihilation and approach to equilibrium

Detailed calculations are performed following Legras & Villone (2003), who in turn based theirs on Kawasaki & Ohta (1982). They are lengthy, yet quite simple in their basic idea, sketched hereafter.

During metastable transitions, the kinks do not satisfy (6.2) exactly, due to the presence of other kinks and/or anti-kinks. The deviation of the amplitude in the plateau is proportional to $e^{-s\Lambda}$, where $\Lambda = 4|x|$ and x denotes the distance to the point where $w = 0$. Here, s is the inverse of the typical length scale of this deviation (for details, see Appendix A of Legras & Villone 2003). The quantity s turns out to be crucial as neighboring kinks and anti-kinks attract proportionally to $e^{-s\Delta x}$, where Δx is the distance between neighbouring kinks and anti-kinks (for details, see Appendix B of Legras & Villone 2003).

The behavior of the kink size s is grasped as follows. Consider a metastable state of the Cahn–Hilliard equation. The potential felt by a kink $w(x)$ close to the plateau $w = W_0$ is estimated by the Taylor expansion:

$$I(w - W_0) \simeq I(W_0) + I'(W_0)(w - W_0) + I''(W_0)\frac{(w - W_0)^2}{2}, \quad (6.8)$$

where we know that $I'(W_0) = 0$. Note also that the dynamics of w does not change if we add an arbitrary constant to the potential I , so that we can set $I(W_0) \equiv 0$.

Let us now calculate the shape of the profile between w and W_0 . For a metastable state, $\partial_t(w - W_0) = 0$, that implies:

$$\frac{\lambda}{2}(\partial_x(w - W_0))^2 + [I''(W_0)\frac{(w - W_0)^2}{2}] = 0. \quad (6.9)$$

Interpreting ∂_x as the inverse of the typical length scale s for $(w - W_0)$, one easily obtains $s = \sqrt{\lambda/I''(W_0)}$. The second-order derivative can be explicitly calculated using (6.6):

$$I''(W_0) = 4 + \frac{2}{3}W_0^2. \quad (6.10)$$

Qualitative properties of s are easy to grasp. At large γ 's, the size of the kinks tends to a constant, independent of γ . At small γ 's, the kinks get steeper and steeper, their size scaling as $\gamma^{1/2}$. This implies that the convergence to equilibrium will be slower and slower as γ is reduced (recall that the kinks attract proportionally to $e^{-s\Delta x}$).

For the same band of unstable modes, i.e. keeping λ fixed, it holds that the convergence to equilibrium is slower for the generalized than for the standard Cahn–Hilliard equation. Indeed, for the Cahn–Hilliard potential $I_{CH} = -w^2/2 + w^4/12$, the second-order derivative $I''_{CH}(W_0) = 2$. As for (6.10), we can use the identity $1 + W_0^2/3 = \gamma W_0^4/5$, following from the very definition $I'(W_0) = 0$, to obtain $I''(W_0) > 2$. This implies that the interactions for the generalized kink-antikink structures have a shorter range and their dynamics of annihilation is thus slower.

A special remark applies to the linearly stable case (zone II). In this case, the equation is associated to an uncommon triple-well potential. The typical nonlinear kink-antikink dynamics appears only if the initial perturbation will be energetic enough to let the system “jump” out of the central well and fall into one of the side wells.

7. Numerical results

The analytical results presented in this work have been obtained by multiscale techniques. Their basic assumption is the strong scale separation between the basic flow and

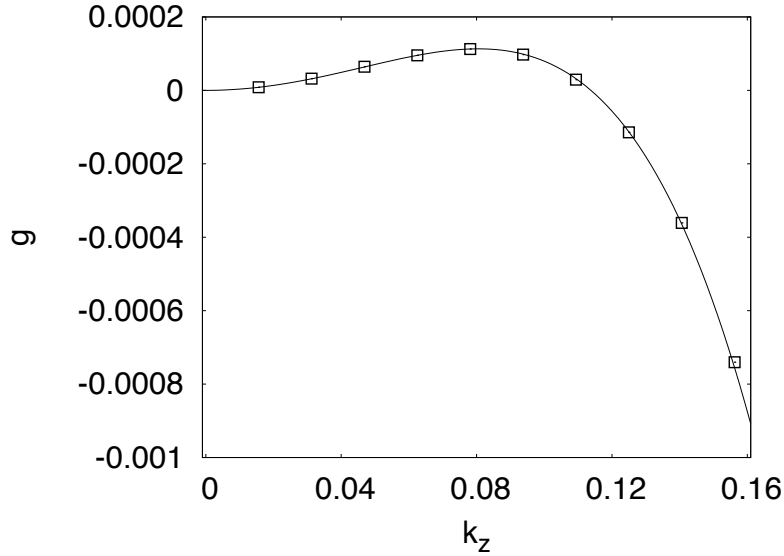


FIGURE 6. Growth rates g of the transverse Fourier modes k for a simulation with $De = 1.4$ and $\beta = 0.769$. The simulations are performed in a rectangular domain with aspect ratio $1/64$. The distance to the critical point $Re/Re_c - 1$ is 0.28 . The solid line represents the linear prediction (7.1). The circles representing the numerically computed growth rates have been obtained with a DNS simulation by a linear fit of the logarithm of the energy for each mode versus time, in the early stages of their exponential growth.

the most unstable perturbations. In this section, we shall present the numerical simulations performed to check the validity of this assumption.

The linear analysis results have already been checked in Boffetta *et al.* (2005a) by reducing the original linear partial differential equation to a generalized eigenvalue problem and computing its eigenvalues/eigenvectors. The scale separation hypothesis is found to be well verified up to Deborah numbers of order unity ($De \approx 2.3$ for the value $\beta = 0.769$ used in this study). For larger De , scale separation does not hold and multiscale methods are not applicable.

To check the nonlinear results derived here, we have numerically simulated the complete Oldroyd-B model equations (2.2)-(2.4) via a pseudospectral algorithm (see Canuto *et al.* 1988, for details on the numerical method). In the following, we will refer to these as to Direct Numerical Simulations (DNS), while numerical integration of the one-dimensional Cahn–Hilliard equation (4.6) will be referred to as CH simulations.

To enforce a transverse perturbation, we integrated the equations on a rectangular slab with $L = L_x = 2\pi$ and $L_z = 64L_x$. The aspect ratio r is then fixed at $1/64$. The simplest check of our results concerns the growth rates of the instability which, in the linear regime, can be obtained by the Cahn–Hilliard equation. Neglecting the nonlinear term, the dispersion relation for the transverse Fourier modes k reads:

$$g = A \left(\frac{Re}{Re_c} - 1 \right) k^2 - Ck^4 \quad (7.1)$$

In figure 6, we report the growth rates of the first modes for a (white-noise in space) small initial perturbation. We are then able to observe also negative g (stable modes). The comparison with the linear prediction is excellent, even for modes whose scale separation is not very small.

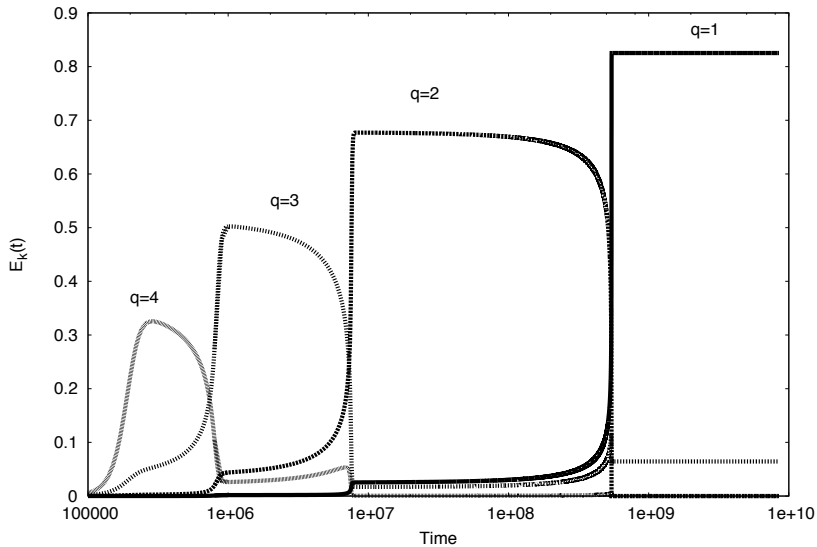


FIGURE 7. The energy associated to the lowest wavenumber modes resulting from a CH simulation. The values of the coefficients have been arbitrarily chosen for convenience of display. The quasi-stationary states can be clearly seen up to the asymptotic one corresponding to the largest periodicity. In this simulation, $De = 1.4$ and $Re/Re_c - 1 = 0.28$.

Let us now consider the nonlinear stage of the perturbation growth. It is well known that the time evolution of the Cahn–Hilliard equation shows a succession of long-lasting metastable states characterized by a well defined periodicity. For sufficiently small initial perturbations, the wave-number k associated to the maximum growth-rate g will be the first to reach the balance between the destabilizing linear term $A\tilde{\partial}^2\langle w_z \rangle$ and the stabilizing non-linear one $B\tilde{\partial}^2\langle w_z \rangle^3$. When such equilibrium is reached, the energy associated to that mode is constant and the system is quasi-stable. In the meanwhile the other modes $k_{max} - 1, k_{max} - 2, \dots$ keep growing. When the mode $k_{max} - 1$ balances the two terms, the energy associated to the mode k_{max} drops. This new state is again quasi-stationary and has a well-defined periodicity $k_{max} - 1$.

The process continues until a state with the box periodicity is reached (see figure 7); such a state is stationary and corresponds to the asymptotic behaviour in § 6. The kink structures described there, are characteristic of all of these stages. Indeed, any transition between two quasi-stationary states can be seen as a kink-antikink annihilation, yielding a decrease in periodicity, as in figure 8 (She 1987).

To check the results obtained in § 4, we have performed a DNS simulation for a particularly long lapse of time. The excellent agreement between the DNS and the prediction of the Cahn-Hilliard equation is shown in figure 9.

The same comparison can be realized in the neighborhood of the critical point P^* . This kind of simulation is much harder than for the standard Cahn–Hilliard, because it involves a very precise knowledge of the position of the critical point, and there is no easy way to obtain this from the simulations. Moreover, any system we simulate will be at a finite distance from the critical point. The parameter that will mostly feel this difference will be D , as we have chosen it to be approximately constant around P^* . We have been able to overcome this weakness via a limited tweaking of the D parameter in the CH simulation. As shown in figure 10, an excellent agreement between the curves is again achieved.

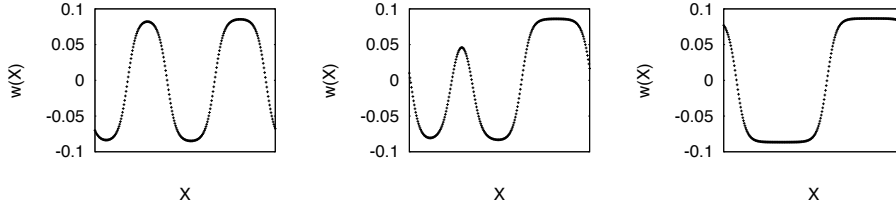


FIGURE 8. Instantaneous transverse velocity field at different times. The simulation is the same as in figure 7. The transition between two metastable states can be regarded as a kink-antikink annihilation. In this figure a transition from a $k = 2$ to a $k = 1$ state is represented, the x -axis being the physical x direction of the integration box and the y -axis being the amplitude of the w perturbation. The time figure set over the graphs refers to the evolution shown in figure 7.

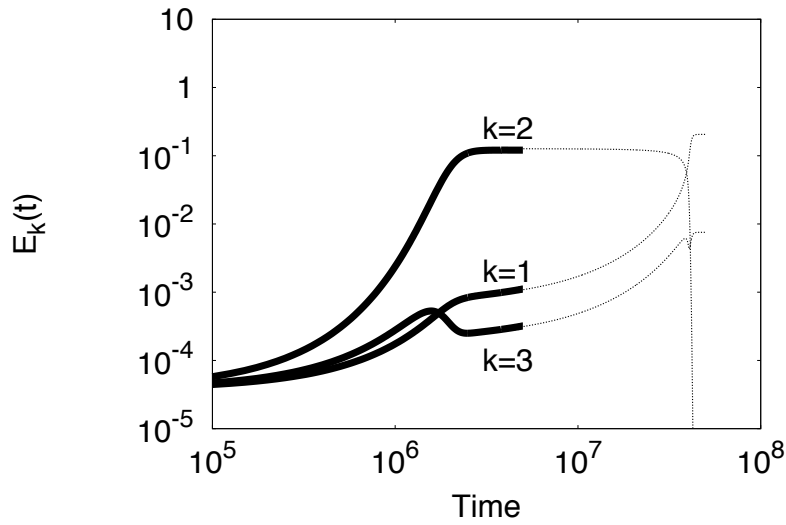


FIGURE 9. The comparison between DNS simulations of the Oldroyd–B model and the coarse-grained Cahn–Hilliard equation derived in the body of the text. The thicker lines represent the evolution of the lowest-energy modes in a DNS simulation, while the thinner lines are the result of a CH simulation. Its dynamical parameters have been set with the results obtained in section 4. This particular figure refers to a simulation with $De = 1.4$, $\beta = 0.769$ and $Re/Re_c - 1 = 0.14$.

8. Clues on drag reduction

One of the most striking properties of viscoelastic fluids is the drag reduction effect. In 1949, Toms found that the injection of minute amounts of polymers in turbulent fluids flowing in a channel was able to increase the mean flow by an amount soaring up to 80%. Even if this phenomenon has been known for over fifty years (Toms 1949; Lumley 1969; Virk 1975), a satisfactory understanding of its fundamental mechanisms is still lacking.

A large number of experiments has been performed to study this effect (see, e.g. Virk 1975; Nadolink & Haigh 1995; Sreenivasan & White 2000), but a burst in its theoretical analysis occurred after drag reduction was found in numerical simulations of viscoelastic fluids (Sureshkumar *et al.* 1997). The activity is being spurred both by fundamental interest and industrial applications (Larson 1992).

Drag reduction is commonly associated to channel flows and boundary effects. Still, it is now clear that the phenomenon is present even for free flows (Boffetta *et al.* 2005b).

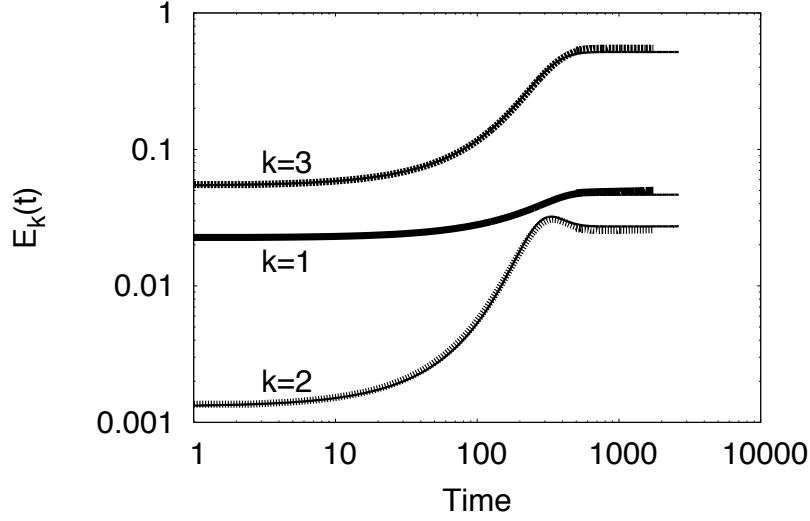


FIGURE 10. The generalized Cahn–Hilliard equation reproduces the dynamics of the Oldroyd-B model around the critical point P^* . As in figure 9, the thicker lines are DNS simulations while the thinner ones are CH simulations. This comparison was realized for $De = 1.62$ and $Re = 2.5159$.

What we show here is that, even at relatively small Reynolds numbers, an increase in the Deborah number produces an enhancement in the mean flow amplitude. Simply looking at the linear stability diagram (1) we may already conclude that, as the polymer elasticity grows, so does the critical Reynolds number and the flow is stabilized. Let us further investigate this effect analytically using the results of § 4.

A parameter that can be employed to study the mean flow properties in free flows is the drag coefficient f (Boffetta *et al.* 2005b):

$$f = \frac{F_0 L}{U^2}. \quad (8.1)$$

The drag coefficient can be seen as the ratio between the energy input (through the forcing F_0) and the mean energy of the flow. As we are interested in mean effects only, we will average U^2 over the basic flow periodicity. This will ensure that only mean effects will be taken into account.

When the state is linearly stable (low Reynolds numbers) we know that no perturbation can alter the basic flow, $U = V = F_0 L^2 / \nu$ and thus $f = Re^{-1}$.

In § 4, we have solved all the equations of motion up to the fourth order. They give the following form of the flow (up to the second order):

$$\begin{aligned} U_x(z) = & V \cos\left(\frac{z}{L}\right) + \frac{V(L^2 + (\beta - 1)\nu\tau)}{\nu L} \langle w_z^{(1)} \rangle \sin\left(\frac{z}{L}\right) + \\ & - \frac{De[L^4 + \nu\tau(\beta - 1)(2L^2 + \nu\tau\beta)]}{\nu^2 \tau L} \langle w_z^{(1)} \rangle^2 \cos\left(\frac{z}{L}\right) + \\ & + \frac{DeL(\beta - 1)}{2} (\tilde{\partial}_x \langle w_z^{(1)} \rangle) \sin\left(\frac{2z}{L}\right). \end{aligned} \quad (8.2)$$

The first term is the basic, stationary Kolmogorov flow. Averaging over all possible initial conditions, component proportional to $\sin(z/L)$ and $\sin(2z/L)$ disappear. The resulting

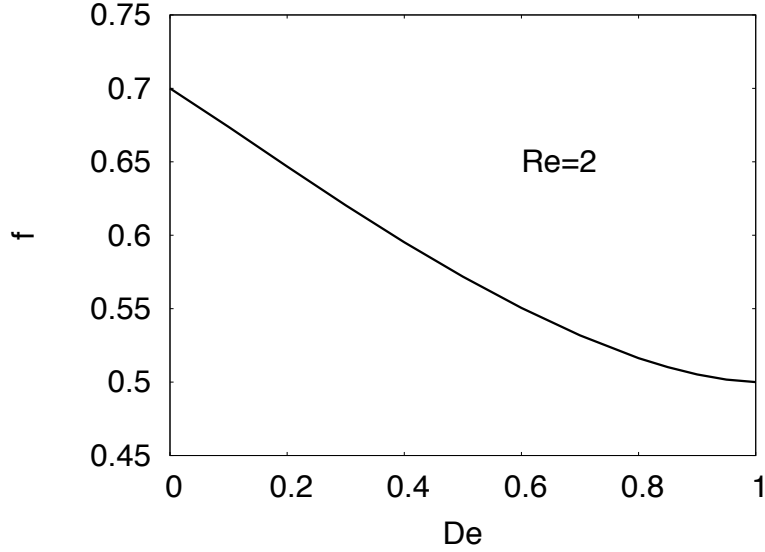


FIGURE 11. The drag coefficient f plotted versus the Deborah number De at constant Re . As the polymer elasticity grows, the drag coefficient diminishes. This implies that the mean flow grows with De .

expression for the mean flow in the x direction reads:

$$\overline{U_x(z)} = (V + h(De, \beta) \frac{\overline{\langle w_z^{(1)} \rangle^2}}{V}) \cos\left(\frac{z}{L}\right) = V_{eff} \cos\left(\frac{z}{L}\right), \quad (8.3)$$

where the quantity $\overline{\langle w_z^{(1)} \rangle^2}$ follows from the Cahn–Hilliard equation in the stationary state:

$$0 = -\partial_x^2 \overline{\langle w_z^{(1)} \rangle} A \epsilon^2 + \frac{B}{3} \partial_x^2 \overline{\langle w_z^{(1)} \rangle^3} - \partial_x^4 \overline{\langle w_z^{(1)} \rangle} C. \quad (8.4)$$

As $\overline{\langle w_z^{(1)} \rangle}$ is periodic, we can integrate twice over the domain and notice that, on the plateau, the last term is zero. The field amplitude must then satisfy:

$$0 = -A \epsilon^2 + \frac{B}{3} \overline{\langle w_z^{(1)} \rangle^2} \Rightarrow \overline{\langle w_z^{(1)} \rangle} = \sqrt{\frac{3 \epsilon^2 A}{B}} \quad (8.5)$$

Since the analytical expression of A and B is known, as well as how ϵ changes with De for a fixed Reynolds number, the analytical expression for f is obtained:

$$f = \frac{\nu FL}{V_{eff}^2} = \frac{V^2}{Re V_{eff}^2} = \frac{1}{Re \left(1 + h \frac{3A}{BV^2} \frac{Re - Re_c}{Re_c}\right)^2}, \quad (8.6)$$

where h , A , B and Re_c are explicit functions of the Deborah number and β .

As we want to investigate how the polymer elasticity affects the flow, a meaningful approach is to keep the Reynolds number fixed, while varying the Deborah number. This allows studying how the same flow reacts when different kinds of polymers are injected. Once β and Re are chosen, it is possible to plot f versus De on the basis of analytical results, as in figure 11. The drag coefficient is clearly decreasing with the Deborah number even though the flow is barely in its nonlinear regime.

Numerical simulations have been performed to check the consistency of these results

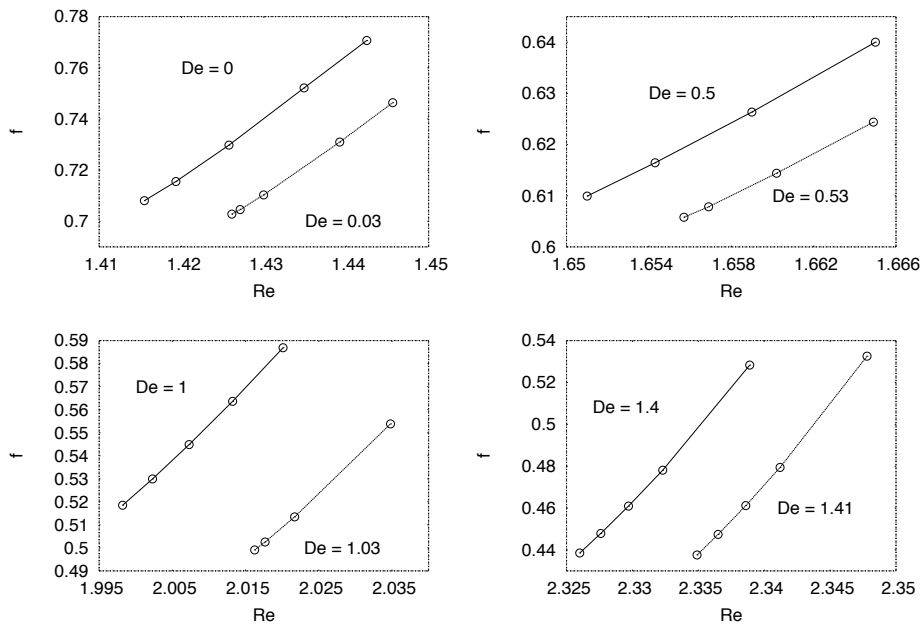


FIGURE 12. CH simulations at fixed De . the drag coefficient f is found to increase with the Reynolds number. The comparison between the various curves shows that the drag coefficient reduces with the Deborah number.

and their outcome is summarized in figure 12. Here, the Deborah number has been fixed at different values and the drag coefficient has been plotted versus the Reynolds number. While f increases with Re , as expected, larger Deborah numbers are always found to be associated to smaller drag coefficients.

9. Conclusions

The weakly nonlinear dynamics of a viscoelastic Kolmogorov flow has been analysed both analytically and numerically. The physical reasons for considering this flow are that, despite the fundamental difference consisting in the absence of material boundaries, it has several analogies with channel flows and is one of the few well-known exact solutions of the Oldroyd-B model.

The linear stability analysis for the Kolmogorov flow had already been developed by Boffetta *et al.* (2005a). No insights had however been given for the weakly nonlinear stage of evolution. This regime amounts to considering values of the Reynolds number close to the marginal stability curve separating stable from unstable regions of the phase-space. In the general nonlinear case (i.e. for arbitrarily large distances from the marginal curve), there is no way to solve the fully nonlinear equations. Conversely, close to the marginal curve, asymptotic perturbation techniques can be employed to capture the weakly nonlinear dynamics.

We found that the weakly nonlinear dynamics is described by Cahn–Hilliard-like equations, with coefficients dependent on the Deborah number. The behaviour of these coefficients with respect to De reveals that there exists a critical value of the Deborah number, where the system bifurcates to another regime. The resulting nonlinear equation still has a Cahn–Hilliard form, but contains a novel, fifth-order nonlinearity.

Above the critical De , the “hydrodynamic” kink-antikink structures are replaced by

generalized structures. We have shown that their processes of annihilation are slowed down with respect to the standard Cahn-Hilliard equation. We also found a purely nonlinear, subcritical mechanism of instability, which occurs for sufficiently large amplitudes of the initial perturbation.

Our results demonstrate that, for hydrodynamical systems governed by a standard Cahn-Hilliard equation, the presence of an additional parameter might lead to higher-order nonlinear dynamics. A system where similar phenomena are to be expected is the stratified Kolmogorov flow investigated by Balmforth & Young (2005), with the role of elasticity played by stratification.

Our results have been obtained both exploiting the multiscale expansion and via direct numerical simulations of the original equations and their coarse-grained version. The agreement between the Cahn-Hilliard dynamics and the full-resolved one is excellent even at large times. This is true for both the standard Cahn-Hilliard and the generalized one. The asymptotic analysis is thus able to capture all of the relevant features of the flow.

In the last part of the work, we have presented some consequences for the problem of drag reduction. Although it is not common to talk about this effect in non-turbulent flows, we have shown that, even in the weakly nonlinear case, the injection of polymers induces a reduction in the drag coefficient, via the stabilization of the basic flow. Using the results of the nonlinear analysis, we have been able to give an analytical expression for the flow enhancement due to the polymers. The main qualitative conclusion is that drag reduction stems from a stabilization of the flow and appears to be a phenomenon coupling large and small scales.

Acknowledgments

This work has been supported by the Italian MIUR COFIN 2005 project n. 2005027808 (GB,AM), by Fondazione CRT-Progetto Lagrange (AB) and by the European Networks “Stirring and Mixing” HPRN-CT2002-00300 (AC) and “Non-ideal turbulence” HPRN-CT-2000-00162 (MV).

Appendix A. Squire's theorem for Oldroyd-B

Consider a parallel flow $\mathbf{U} = (U(z), 0)$. To investigate its stability properties one writes the linearized, nondimensional equations

$$\begin{aligned} \partial_t \mathbf{w} + (\mathbf{u} \cdot \nabla) \mathbf{w} + (\mathbf{w} \cdot \nabla) \mathbf{u} = -\nabla q + \beta Re^{-1} \Delta \mathbf{w} + \\ + (1 - \beta) Re^{-1} De^{-1} \nabla \cdot \zeta \end{aligned} \quad (\text{A } 1)$$

$$\begin{aligned} \partial_t \zeta + (\mathbf{u} \cdot \nabla) \zeta + (\mathbf{w} \cdot \nabla) \boldsymbol{\sigma} = (\nabla \mathbf{u})^T \cdot \zeta + (\nabla \mathbf{w})^T \cdot \boldsymbol{\sigma} + \\ + \zeta \cdot (\nabla \mathbf{u}) + \boldsymbol{\sigma} \cdot (\nabla \mathbf{w}) - De^{-1} \zeta \end{aligned} \quad (\text{A } 2)$$

where \mathbf{w} is the perturbation of the basic profile \mathbf{u} , and ζ is the perturbation of the basic stress tensor $\boldsymbol{\sigma}$.

We now perform a Fourier transform in the directions x and y , and in time,

$$w_i(x, y, z, t) = \int d\omega dk_x dk_y e^{-i\omega t + k_x x + k_y y} \hat{w}_i(k_x, k_y, \omega, z) \quad (\text{A } 3)$$

$$\zeta_{ij}(x, y, z, t) = \int d\omega dk_x dk_y e^{-i\omega t + k_x x + k_y y} \hat{\zeta}_{ij}(k_x, k_y, \omega, z) \quad (\text{A } 4)$$

Introducing the notation

$$\begin{aligned} \mathbf{k} = \begin{pmatrix} k_x \\ k_y \end{pmatrix} \quad \mathbf{u} = \begin{pmatrix} U(z) \\ 0 \end{pmatrix} \quad \hat{\mathbf{w}} = \begin{pmatrix} \hat{w}_x \\ \hat{w}_y \end{pmatrix} \\ \hat{\mathbf{t}} = \begin{pmatrix} \hat{\zeta}_{xz} \\ \hat{\zeta}_{yz} \end{pmatrix} \quad \hat{\mathbf{z}} = \begin{pmatrix} \hat{\zeta}_{xx} & \hat{\zeta}_{xy} \\ \hat{\zeta}_{yx} & \hat{\zeta}_{yy} \end{pmatrix} \quad \mathbf{r} = \begin{pmatrix} \sigma_{xz} \\ \sigma_{yz} \end{pmatrix} \quad \mathbf{s} = \begin{pmatrix} \sigma_{xx} & \sigma_{xy} \\ \sigma_{yx} & \sigma_{yy} \end{pmatrix} \end{aligned} \quad (\text{A } 5)$$

the linearized equations in normal modes take the form

$$\begin{aligned} (-i\omega + i\mathbf{k}^T \cdot \mathbf{u}) \hat{\mathbf{w}} + \hat{w}_z \frac{d\mathbf{u}}{dz} = -i\mathbf{k}\hat{q} + \beta Re^{-1} (-\mathbf{k}^2 + \frac{d^2}{dz^2}) \hat{\mathbf{w}} + \\ + (1 - \beta) Re^{-1} De^{-1} \left(i\hat{\mathbf{z}}^T \cdot \mathbf{k} + \frac{d}{dz} \hat{\mathbf{t}} \right) \end{aligned} \quad (\text{A } 6)$$

$$\begin{aligned} (-i\omega + i\mathbf{k}^T \cdot \mathbf{u}) \hat{w}_z = -\frac{d\hat{q}}{dz} + \beta Re^{-1} (-\mathbf{k}^2 + \frac{d^2}{dz^2}) \hat{w}_z + \\ + (1 - \beta) Re^{-1} De^{-1} \left(i\mathbf{k}^T \cdot \hat{\mathbf{t}} + \frac{d}{dz} \hat{\zeta}_{zz} \right) \end{aligned} \quad (\text{A } 7)$$

$$\begin{aligned} (-i\omega + i\mathbf{k}^T \cdot \mathbf{u} + De^{-1}) \hat{\mathbf{z}} + \hat{w}_z \frac{d}{dz} \mathbf{s} = \hat{\mathbf{t}} \cdot \frac{d\mathbf{u}^T}{dz} + \frac{d\mathbf{u}}{dz} \cdot \hat{\mathbf{t}}^T + \\ + i(\mathbf{s} \cdot \mathbf{k}) \hat{\mathbf{w}}^T + i\hat{\mathbf{w}}(\mathbf{k}^T \cdot \mathbf{s}) + \mathbf{r} \frac{d}{dz} \hat{\mathbf{w}}^T + \frac{d\hat{\mathbf{w}}}{dz} \mathbf{r}^T \end{aligned} \quad (\text{A } 8)$$

$$\begin{aligned} (-i\omega + i\mathbf{k}^T \cdot \mathbf{u} + De^{-1}) \hat{\mathbf{t}} + \hat{w}_z \frac{d}{dz} \mathbf{r} = \hat{\zeta}_{zz} \frac{d\mathbf{u}}{dz} + \\ + i(\mathbf{s} \cdot \mathbf{k}) \hat{w}_z + i\hat{\mathbf{w}}(\mathbf{r}^T \cdot \mathbf{k}) + \mathbf{r} \frac{d}{dz} \hat{w}_z + \frac{d}{dz} \hat{\mathbf{w}} \end{aligned} \quad (\text{A } 9)$$

$$(-i\omega + i\mathbf{k}^T \cdot \mathbf{u} + De^{-1}) \hat{\zeta}_{zz} = 2i(\mathbf{r}^T \cdot \mathbf{k}) \hat{w}_z + 2\frac{d}{dz} \hat{w}_z \quad (\text{A } 10)$$

Consider the following transformation

$$\begin{aligned}\bar{k}_x &= |\mathbf{k}| & \bar{w}_x &= \frac{\mathbf{k}^T \cdot \hat{\mathbf{w}}}{|\mathbf{k}|} & \bar{w}_z &= \hat{w}_z & \bar{q} &= \frac{|\mathbf{k}|}{k_x} \hat{q} \\ \bar{Re} &= \frac{k_x}{|\mathbf{k}|} Re & \bar{De} &= \frac{k_x}{|\mathbf{k}|} De & \bar{\omega} &= \frac{|\mathbf{k}|}{k_x} \omega \\ \bar{t}_x &= \frac{k_x}{|\mathbf{k}|} \frac{\mathbf{k}^T \cdot \hat{\mathbf{t}}}{|\mathbf{k}|} & \bar{\zeta}_{xx} &= \frac{k_x}{|\mathbf{k}|} \frac{\mathbf{k}^T \cdot \hat{\boldsymbol{\zeta}} \cdot \mathbf{k}}{|\mathbf{k}|^2} & \bar{\zeta}_{zz} &= \frac{k_x}{|\mathbf{k}|} \hat{\zeta}_{zz}\end{aligned}\quad (\text{A } 11)$$

From (A 6)-(A 10) one can derive the equations for the overlined variables

$$\begin{aligned}[-i\bar{\omega} + i\bar{k}_x U(z)] \bar{w}_x + \bar{w}_z \frac{dU}{dz} &= -i\bar{k}_x \bar{q} + \beta \bar{Re}^{-1} \left(-\bar{k}_x^2 + \frac{d^2}{dz^2} \right) \bar{w}_x + \\ &+ (1 - \beta) \bar{Re}^{-1} \bar{De}^{-1} \left(i\bar{k}_x \bar{\zeta}_{xx} + \frac{d}{dz} \bar{t}_x \right)\end{aligned}\quad (\text{A } 12)$$

$$\begin{aligned}[-i\bar{\omega} + i\bar{k}_x U(z)] \bar{w}_z &= -\frac{d\hat{q}}{dz} + \beta \bar{Re}^{-1} \left(-\bar{k}_x^2 + \frac{d^2}{dz^2} \right) \bar{w}_z + \\ &+ (1 - \beta) \bar{Re}^{-1} \bar{De}^{-1} \left(i\bar{k}_x \bar{t}_x + \frac{d}{dz} \bar{\zeta}_{zz} \right)\end{aligned}\quad (\text{A } 13)$$

$$\left[-i\bar{\omega} + i\bar{k}_x U(z) + \bar{De}^{-1} \right] \bar{\zeta}_{xx} + \bar{w}_z \frac{d\bar{s}_{xx}}{dz} = 2\bar{t}_x \frac{dU}{dz} + 2i\bar{k}_x \bar{s}_{xx} \bar{w}_x + 2\bar{r}_x \frac{d\bar{w}_x}{dz} \quad (\text{A } 14)$$

$$\begin{aligned}\left[-i\bar{\omega} + i\bar{k}_x U(z) + \bar{De}^{-1} \right] \bar{t}_x + \bar{w}_z \frac{d}{dz} \bar{r}_x &= \bar{\zeta}_{zz} \frac{dU}{dz} + i\bar{s}_{xx} \bar{k}_x \bar{w}_z + i\bar{k}_x \bar{w}_x \bar{r}_x \\ &+ \bar{r}_x \frac{d\bar{w}_z}{dz} + \frac{d\bar{w}_x}{dz}\end{aligned}\quad (\text{A } 15)$$

$$\left[-i\bar{\omega} + i\bar{k}_x U(z) + \bar{De}^{-1} \right] \bar{\zeta}_{zz} = 2i\bar{k}_x \bar{r}_x \bar{w}_z + 2 \frac{d\bar{w}_z}{dz} \quad (\text{A } 16)$$

where we introduced the quantities

$$\bar{s}_{xx} = \frac{\mathbf{k}^T \cdot \mathbf{s} \cdot \mathbf{k}}{|\mathbf{k}|^2} = 1 + \bar{De}^2 [U'(z)]^2, \quad \bar{r}_x = \frac{\mathbf{k}^T \cdot \mathbf{r}}{|\mathbf{k}|} = \bar{De}^2 U'(z) \quad (\text{A } 17)$$

Equations (A 12)-(A 16) are exactly the same as (A 6)-(A 10) but with $k_y = 0$, $\hat{w}_y = 0$, $\zeta_{xy} = \zeta_{yy} = \zeta_{yz} = 0$. Therefore they describe a two-dimensional linear disturbance of the basic flow at smaller Reynolds and Deborah numbers. If the three-dimensional perturbation $\mathbf{w}, \boldsymbol{\zeta}$ is unstable at (Re, De) , then the two-dimensional disturbance $\bar{\mathbf{w}}, \bar{\boldsymbol{\zeta}}$ is unstable at (\bar{Re}, \bar{De}) and its rate of growth is larger ($\text{Im}(\bar{\omega}) \geq \text{Im}(\omega) > 0$).

Appendix B. Painlevé analysis

We perform a Painlevé analysis to ascertain whether the fifth-order equation (5.1) is integrable as the usual cubic Cahn–Hilliard equation (4.6).

After rescaling dependent and independent variables, the stationary equation takes the form:

$$-u - \frac{u^3}{3} - \lambda \partial_x^2 u + \frac{\gamma}{5} u^5 = 0. \quad (\text{B } 1)$$

The Painlevé test consists in checking whether the structure of the solution around singularities in the complex plane has the form of a Laurent series. A simple balance of

the last two terms in the equation indicates that the singularity has order $-1/2$. The putative Laurent series should then be sought as:

$$u(z) = z^{-1/2} [u_0 + u_1 z + u_2 z^2 + u_3 z^3 + \dots], \quad (\text{B } 2)$$

where z is the complex variable denoting the separation from the singularity z_* . When the series (B 2) is inserted into equation (B 1), a hierarchy of equations of the form $a_k u_k = b_k$ is obtained. The a_k 's and b_k 's can be calculated in terms of u_{k-1}, \dots, u_0 . The impossibility for an arbitrary equation to have a Laurent series expansion is due to resonances, i.e. values of k such that $a_k = 0$. Integrability is equivalent to checking that $b_k = 0$ for the orders corresponding to resonances. In our case, it is easy to check that

$$a_k = -\lambda \left(k - \frac{1}{2} \right) \left(k - \frac{3}{2} \right) + \gamma u_0^4; \quad u_0 = \left(\frac{15\lambda}{4\gamma} \right)^{1/4} \mapsto a_k = -\lambda(k+1)(k-3). \quad (\text{B } 3)$$

The resonance is therefore at the third order and we need to perform the explicit calculation up to that order to check whether or not $b_3 = 0$. The algebra is elementary and the coefficients are:

$$u_1 = \frac{u_0^3}{12\lambda}, \quad u_2 = \frac{u_0}{\lambda} \left[\frac{1}{3} + \frac{5}{128\gamma} \right]. \quad (\text{B } 4)$$

Using these values, one can verify that

$$b_3 = 2\gamma u_0^2 u_1^3 + 4\gamma u_0^3 u_1 u_2 - u_1 - u_0^2 u_2 - u_0 u_1^2 \quad (\text{B } 5)$$

vanishes and the Painlevé test is satisfied.

REFERENCES

- ABLOWITZ, M.J. & CLARKSON, P.A. 1991 *Solitons, Nonlinear Evolution Equations and Inverse Scattering*. Cambridge University Press.
- ARNOLD, V.I. & MESHALKIN, L. 1960 A.N. Kolmogorov's seminar on selected problems of analysis (1958–1959). *Uspekhi Mat. Nauk* **15**, 247–250.
- BALMFORTH, N.J., YOUNG, Y.-N. 2005 Stratified Kolmogorov flow. Part 2. *J. Fluid Mech.* **528**, 23–42.
- BAYLY, B.J., ORSZAG, S.A., HERBER, T. 1988 Instability mechanisms in shear-flow transition. *Annu. Rev. Fluid Mech.* **20**, 359–391.
- BENSOUSSAN, A., LIONS, J.-L. & PAPANICOLAOU, G. 1978 *Asymptotic Analysis for Periodic Structures*. North-Holland.
- BIRD, R.B., HASSAGER, O., ARMSTRONG, R.C. & CURTISS, C.F. 1987 *Dynamics of Polymeric Liquids*. Wiley-Interscience.
- BOFFETTA, G., CELANI, A., MAZZINO, A., PULIAFITO, A. & VERGASSOLA, M. 2005a The viscoelastic Kolmogorov flow: eddy viscosity and linear stability. *J. Fluid Mech.* **523**, 161–170.
- BOFFETTA, G., CELANI, A. & MAZZINO, A. 2005b Drag reduction in the turbulent Kolmogorov flow. *Phys. Rev. E* **71**, 036307.
- BRAY, A.J. 2002 Theory of phase-ordering kinetics. *Advances in Physics* **51**, 481–587
- CAHN, J.W. & HILLIARD, J.E. 1958 Free energy of a non uniform system. *J. Chem. Phys.* **28**, 258.
- CANUTO, C., HUSSAINI, M.Y., QUARTERONI, A. & ZANG, T. A. 1988 *Spectral Methods in Fluid Dynamics*. Springer-Verlag.
- GAMA, S., VERGASSOLA, M. & FRISCH, U. 1994 Negative eddy-viscosity in isotropically forced two-dimensional flow: linear and nonlinear dynamics. *J. Fluid Mech.* **260**, 95–126.
- GERASCHENKO, S., CHEVALLARD, C. & STEINBERG, V. 2005 Single-polymer dynamics: Coil-stretch transition in a random flow. *Europhys. Lett.* **71**(2), 221–227.
- HINCH, E.J. 1977 Mechanical models of dilute polymer solutions in strong flows. *Phys. Fluids* **20**, S22–S30.

- 26 A. Bistagnino, G. Boffetta, A. Celani, A. Mazzino, A. Puliafito, M. Vergassola
- KAWASAKI, K. & OHTA, T. 1982 Kink dynamics in one-dimensional nonlinear systems. *Physica A* **116** 573.
- KARTTUNEN, M., VATTULAINEN, I. & LUKKARINEN, A. 2004 *Novel Methods in Soft Matter Simulations*. Springer-Verlag.
- KHOUIDER, B., MAJDA, A.J. & KATSOULAKIS, M.A. 2003 Coarse-grained stochastic models for tropical convection and climate. *Proc. Natl. Acad. Sci* **100**, 11941-11946.
- KOWALESVKI, S. 1889 Sur le problème de la rotation d'un corps solide autour d'un point fixe. *Acta Math.* **12**, 177–232.
- KOWALESVKI, S. 1890 Sur une propriété du système d'équations différentielles qui définit la rotation d'un corps solide autour d'un point fixe. *Acta Math.* **14**, 81–93.
- LARSON, R.G. 1992 Instabilities in viscoelastic flows. *Rheol. Acta* **31**, 213–263.
- LEGRAS, B. & VILLONE, B. 2003 Dispersive and friction-induced stabilization of the Cahn–Hilliard inverse cascade. *Physica D* **175**, 139–166.
- LUMLEY, J. 1969 Drag reduction by additives. *Annu. Rev. Fluid Mech.* **1**, 367–384.
- MANFROI, A., & YOUNG, W. 1999 Slow evolution of zonal jets on the beta-plane. *J. Atmos. Science* **56**, 784–800.
- MESHALKIN, L. & SINAI, YA G. 1961 Investigation of the stability of a stationary solution of a system of equations for the plane movement of an incompressible viscous fluid. *J. Appl. Math. Mech.* **25**, 1700–1705.
- NADOLINK, R.H. & HAIGH, W.W. 1997 Bibliography on skin friction reduction with polymers and other boundary-layer additives. *ASME Appl. Mech. Rev.* **48**, 351–460.
- NEPOMNYASHCHYI, A.A. 1976 On the stability of the secondary flow of a viscous fluid in an infinite domain. *Appl. Math. Mech.* **40**, 886–891.
- OLDROYD, J.G. 1950 On the formulation of rheological equations of state. *Proc. Roy. Soc. London Ser A* **200**, 523–541.
- PAINLEVÉ, P. 1897 *Leçons sur la Théorie Analytique des Équations Différentielles*. Hermann, Paris.
- PEDLOSKY, J. 1987 *Geophysical fluid dynamics* 2nd edition. Springer.
- SHE, Z.S. 1987 Metastability and vortex pairing in the Kolmogorov flow. *Phys. Lett. A* **124**, 161–164.
- SIVASHINSKY, G.I. 1985 Weak turbulence in periodic flows. *Physica D* **17**, 243–255.
- SREENIVASAN, K.R. & WHITE, C.M. 2000 The onset of drag reduction by dilute polymer additives, and the maximum drag reduction asymptote. *J. Fluid Mech.* **409**, 149–164.
- SURESHKUMAR, R., BERIS, A.N., & HANDLER, R.A. 1997 Direct numerical simulation of polymer-induced drag reduction in turbulent channel flow. *Phys. Fluids* **9**, 743–755.
- TOMS, B.A. 1949 Observation on the flow of linear polymer solutions through straight tubes at large Reynolds numbers. *Proc. 1st International Congress on Rheology* **2**, 135–141.
- VATTULAINEN, I. & KARTTUNEN, M. 2005 *Computational Nanotechnology*, edited by M. Rieth and W. Schommers. American Scientific Press, in press.
- VIRK, P. S. 1975 Drag reduction fundamentals. *AIChE Journal* **21**, 625–656.

Chapter 9

The viscoelastic turbulent Kolmogorov flow

The results of the stability analysis presented in the previous chapters suggest that drag reduction by polymer additives can be found in the viscoelastic turbulent Kolmogorov flow. A recent breakthrough has been the observation of drag reduction in channel flows by means of viscoelastic fluids models [43, 62] in good agreement with experimental measurements.

In this chapter I will present my research result on the study of turbulence of a polymer solution in a Kolmogorov flow by means of two simple viscoelastic fluid models. Here we aim at simplifying as much as possible both the geometry of the problem and the viscoelastic model to isolate a physical mechanism yielding drag reduction. The first objective is met by considering the turbulent Kolmogorov flow [63], whereas the second is met by choosing both the Oldroyd-B model and a further simplification, the uniaxial model. The results of direct numerical simulations are presented, focusing on the comparison with the corresponding results obtained in the channel flow.

9.1 The Newtonian case

In the Newtonian case, below $Re_c = \sqrt{2}$, the Kolmogorov flow is laminar, the velocity profile being sinusoidal. Above the critical value the profile remains sinusoidal but it is independent of the Reynolds number [63]. The flow is highly turbulent and intermittent even at large-scales.

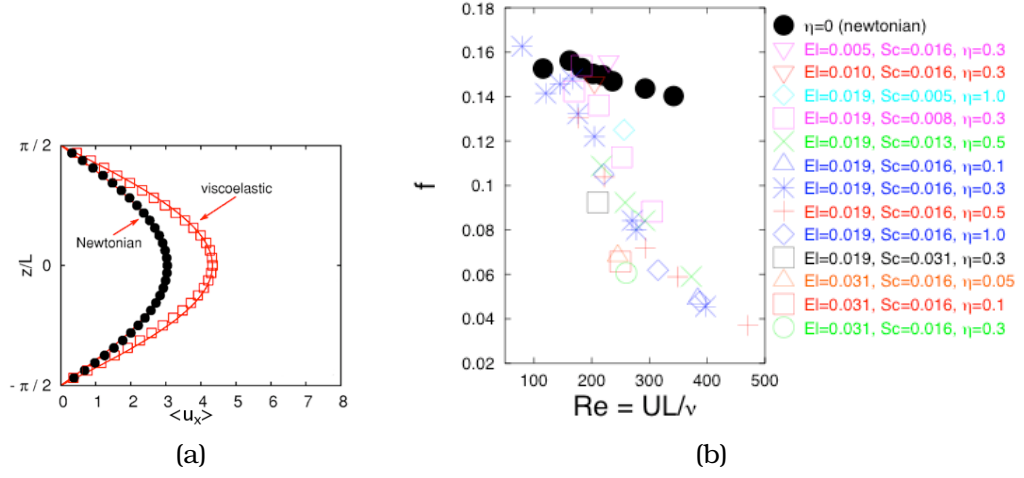


Figure 9.1: (a) The mean velocity profile for the Newtonian and viscoelastic cases fitted with two sinusoidal profiles. (b) The friction coefficient as a function of the Reynolds number for different values of El , Sc and $\eta = \nu^p/\nu$.

The velocity profile in the laminar case is:

$$\mathbf{v} = \left(\frac{FL^2}{\nu} \cos\left(\frac{z}{L}\right), 0, 0 \right) \quad (9.1)$$

At large Re the flow becomes turbulent and a fluctuating Reynolds stress $\langle v_x v_z \rangle$ is produced, which can be expressed as:

$$\langle v_z v_z \rangle = -\nu_{eff} \frac{d\langle v_x \rangle}{dz} \quad (9.2)$$

where ν_{eff} is a nearly constant effective viscosity. The r.m.s. values of the fluctuations are proportional to $a + b \cos(2z/L)$ where a and b are appropriate constants. The same holds for the total turbulent kinetic energy and for the averaged energy dissipation rate. The analogies between a channel flow and the Kolmogorov flow are the following:

- the forcing amplitude F plays the role of the pressure gradient, maintaining the flow rate
- the periodicity box width is the equivalent to the channel height
- the velocity amplitude U represents the centerline velocity.

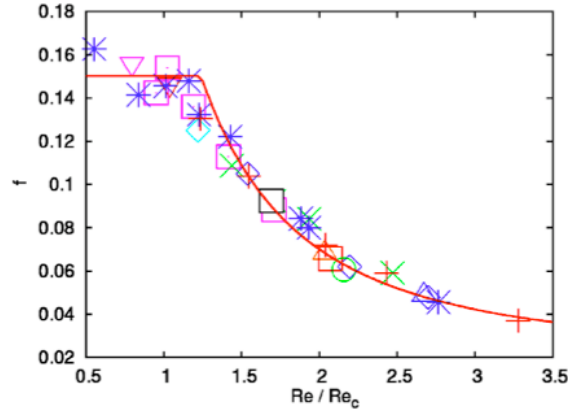


Figure 9.2: The drag coefficient as a function of the rescaled Reynolds number.

9.2 The viscoelastic case

9.2.1 Oldroyd-B model

Here I present the results for the viscoelastic Kolmogorov flow of the Oldroyd-B fluid. The evolution equations read:

$$\begin{aligned}
 \partial_t \mathbf{v} + \mathbf{v} \cdot \partial \mathbf{v} &= -\frac{1}{\rho} \partial p + \nu^n \partial^2 \mathbf{v} + \frac{\nu^p}{\tau} \partial \cdot \frac{\boldsymbol{\sigma}}{R_0^2} + \mathbf{F} \\
 \partial_t \boldsymbol{\sigma} + \mathbf{v} \cdot \partial \boldsymbol{\sigma} &= \partial \mathbf{v} \cdot \boldsymbol{\sigma} + \boldsymbol{\sigma} \cdot (\partial \mathbf{v})^T - \frac{1}{\tau} (\boldsymbol{\sigma} - R_0^2 \mathbf{1}) + \kappa \partial^2 \boldsymbol{\sigma} \\
 \partial \cdot \mathbf{v} &= 0
 \end{aligned} \tag{9.3}$$

where ν^n and ν^p are the solvent and polymer viscosity contribution respectively, and the artificial diffusivity κ is added to prevent numerical instabilities (see chapter 6 and 7).

We perform direct numerical simulations of equations (9.3) in a periodic cube of size 2π with 64^3 collocation points by a fully dealiased pseudo-spectral method. The averages are performed over a hundred to a thousand eddy-turnover times.

The measured mean velocity profile is increased with respect to the Newtonian case, due to the presence of polymers as shown in fig. 9.1a. The main difference with wall bounded flows is in the profile shape: in the channel flow, the region close to the wall (viscous sub-layer) is not altered by polymers, but the central region is characterized by the emergence of a so called elastic sub-layer, and the centerline velocity is enhanced. Here the profile is changed

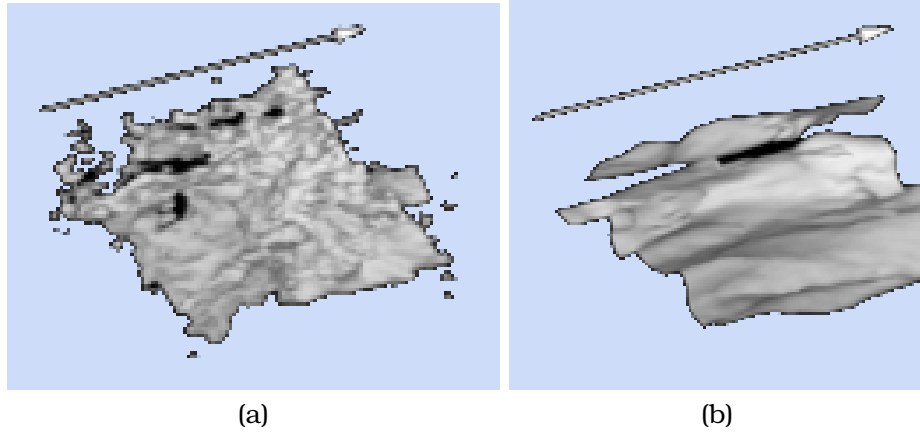


Figure 9.3: Representative snapshots of velocity component u_x for a Newtonian (a) and viscoelastic Kolmogorov flow (b). Here $Re \simeq 350$, $El = 0.019$, $Sc = 0.016$, $\eta = 0.5$.

by a uniform multiplication factor [61].

The friction coefficient in the Kolmogorov flow can be defined as follows:

$$f = \frac{FL}{U^2} \quad (9.4)$$

For the laminar Newtonian case we have $f = Re^{-1}$. At $Re \gtrsim 50$ the flow is turbulent and the friction coefficient becomes almost independent on Re as shown in fig. 9.1b (black dots). The friction coefficient for the viscoelastic case ($\eta \neq 0$) is shown in fig. 9.1b as a function of the polymer elasticity:

$$El = \frac{De}{Wi} = \frac{\nu\tau}{L^2} \quad (9.5)$$

and of the Schmidt number $Sc = \nu^n/\kappa$. For small El the behavior is almost identical to the Newtonian case, whereas large El are characterized by a notable reduction in the friction factor. For fixed El , smaller Sc correspond to higher reductions. The dependence on ν^p cannot be extracted from these simulations. Our data show a maximum drag reduction of 75%.

The dependence of the friction coefficient on the fluid parameter can be found following simple observations and a physical argument given in ref. [15]. For moderate Re the presence of polymers does not affect the drag coefficient, whereas for larger Re drag reduction occurs. Therefore there exists a critical Reynolds number

separating these two regimes, that can be estimated as [61]:

$$\text{Re}_c \sim \left(\frac{1}{\text{El}} + \frac{1}{\text{Sc}} \right)^{2/3} \quad (9.6)$$

Rescaling the Reynolds number with Re_c allows to collapse the data as shown in fig. 9.2. The curve can be fitted by the following relation:

$$f = \begin{cases} \beta & \text{Re} \lesssim \text{Re}_c \\ \gamma \left(\frac{\text{Re}}{\text{Re}_c} \right)^2 + \delta & \text{Re} \gtrsim \text{Re}_c \end{cases} \quad (9.7)$$

where the coefficients δ , γ and β can be extracted from the measurement of the stresses (see below).

The amplitude of the transverse fluctuations $\langle u_y^2 \rangle$ and $\langle u_z^2 \rangle$ is reduced with respect to the Newtonian case, whereas longitudinal fluctuations $\langle u_x^2 \rangle - \langle u_x \rangle^2$ are enhanced (see fig. 9.3).

The momentum balance of the first of eqs. (9.3) in the x direction gives:

$$F_x = -\nu^n \partial_z^2 \langle v_x \rangle + \partial_z \langle v_x v_z \rangle - \frac{\nu^p}{\tau} \langle \sigma_{xz} \rangle \quad (9.8)$$

and from numerical measurements we obtain:

$$\langle v_x v_z \rangle = S \sin \left(\frac{z}{L} \right) \quad (9.9)$$

$$\frac{\nu^p}{\tau} \langle \sigma_{xz} \rangle = -T \sin \left(\frac{z}{L} \right) \quad (9.10)$$

Therefore the balance (9.8) becomes:

$$F = \nu^n \frac{U}{L^2} + \frac{S}{L} + \frac{T}{L} \quad (9.11)$$

where the first term in the right hand side is relevant only for laminar flows, and can be neglected here.

The balance between these terms and the behavior as a function of the rescaled Re are shown in fig. 9.4.

9.2.2 Uniaxial model

A further simplification of the Oldroyd-B model has been proposed in ref. [15]. When polymer elongation is much larger than the equilibrium length R_0 , the tensor σ can be decomposed in the product

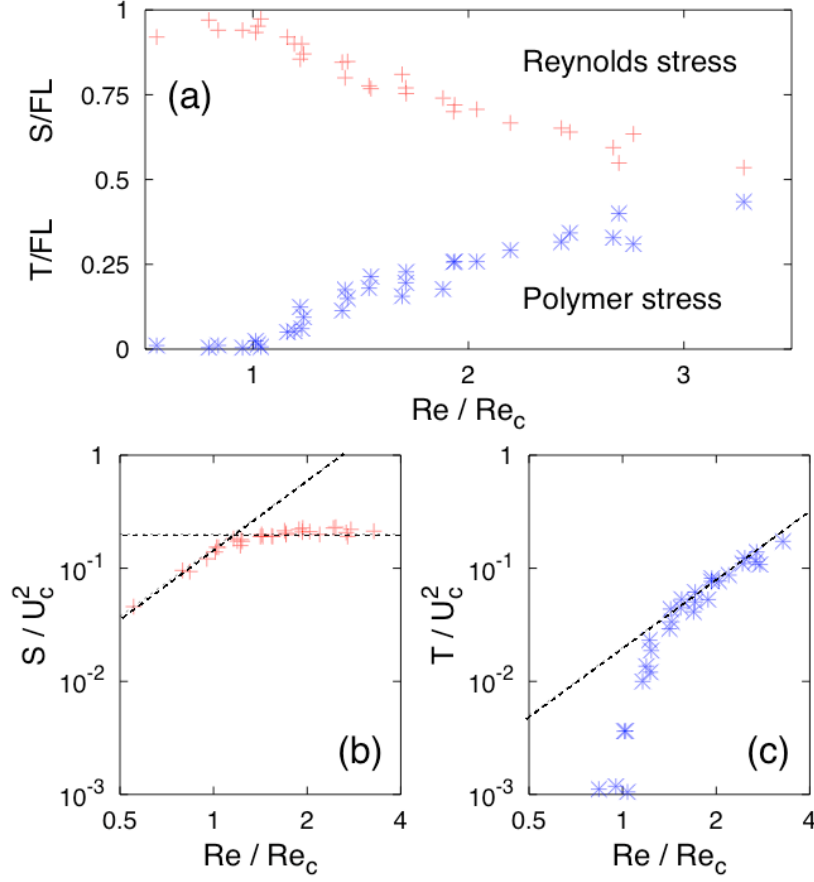


Figure 9.4: Oldroyd-B model: (a) Reynolds and polymer stress amplitudes rescaled with the total stress amplitude FL as a function of the rescaled Reynolds number. (b) The Reynolds stress: the oblique line is $S/U_c^2 = \beta(Re/Re_c)^2$ whereas the horizontal line is $S/U_c^2 = \gamma$. (c) The polymer contribution to the stress. The line is $T/U_c^2 = \delta(Re/Re_c)^2$. U_c is the critical velocity corresponding to the critical Reynolds number.

of two identical vectors $\mathbf{B} = \mathbf{R}/R_0$, and the obtained model is called uniaxial. Its evolution equations read:

$$\begin{aligned} \partial_t \mathbf{v} + \mathbf{v} \cdot \partial \mathbf{v} &= -\frac{1}{\rho} \partial p + \nu^n \partial^2 \mathbf{v} + \frac{\nu^p}{\tau} \mathbf{B} \cdot \partial \mathbf{B} + \mathbf{F} \\ \partial_t \mathbf{B} + \mathbf{v} \cdot \partial \mathbf{B} &= \mathbf{B} \cdot \partial \mathbf{v} - \frac{1}{\tau} \mathbf{B} + \kappa \partial^2 \mathbf{B} \\ \partial \cdot \mathbf{v} &= 0 \end{aligned} \quad (9.12)$$

It has been noted that these equations are equivalent to those of magneto-hydrodynamics with magnetic diffusivity κ [64], except for

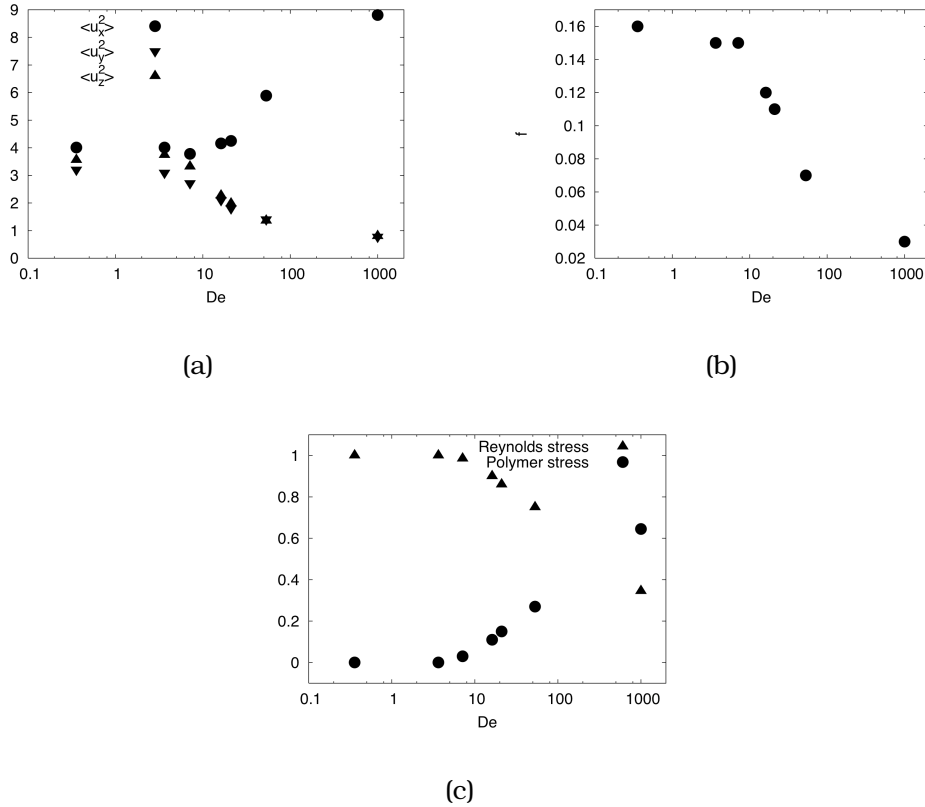


Figure 9.5: Uniaxial model: in these simulations the viscosity is kept fixed, $F = 2$ and $Sc = 100$. (a) The velocity fluctuations variance as a function of De . (b) The friction coefficient as a function of De . (c) The Reynolds and polymer stress as a function of De .

the dumping term B/τ .

The numerical investigation of the previous section can be repeated for the uniaxial model, with the only difference that here we use hyper-viscosity and hyper-diffusivity to stabilize the small-scale dynamics of eqs. (9.12), and to reduce the artificial diffusivity. Here we did not investigate the dynamics as a function of the Reynolds number. The results of the simulations are shown in fig. 9.5 and are qualitatively similar to the Oldroyd-B case, suggesting that the drag reduction mechanism can be studied within the simple uniaxial model as well.

9.3 Perspectives

It would be interesting to raise the numerical resolution of the simulations within the Oldroyd-B model. This could be useful to study the mechanism of transverse momentum transfer and to verify if this is a crucial mechanism in the occurrence of drag reduction in unbounded flows. Moreover, higher resolution simulations in the case of the uniaxial model would permit to compare the results of the two models more accurately, and to better establish the dynamical similarities with magneto-hydrodynamics.

Drag reduction without boundaries: the viscoelastic turbulent Kolmogorov flow

G. Boffetta¹, A. Celani², A. Mazzino³, A. Puliafito²

¹Dipartimento di Fisica Generale and INFN
Università degli Studi di Torino, Via Giuria 1, 10125, Torino, Italy

²Institut Nonlinéaire de Nice, CNRS
1361 Route des Lucioles, 06560 Valbonne, France

³Department of Physics and INFN
Università di Genova, Via Dodecaneso 33, 16146 Genova

Contact address: *antonio.celani@inln.cnrs.fr*

1 Introduction

In 1949 the British chemist Toms reported that the turbulent drag could be reduced by up to 80% through the addition of minute amounts (few tenths of p.p.m. in weight) of long-chain soluble polymers to water. This observation triggered an enormous experimental activity to characterize this phenomenon (see, e.g., [1][2][3][4][5]). In spite of these efforts, no fully satisfactory theory of drag reduction is available yet. However, a recent breakthrough has been the observation of drag reduction in numerical simulations of the turbulent channel flow of viscoelastic fluids [6]. Most of the features of experimental flows of dilute polymer solutions are successfully reproduced by these models, even at the quantitative level [7][8].

Here we present the results of an extensive numerical investigation of the viscoelastic turbulent Kolmogorov flow. This flow is realized by driving the fluid through a parallel force with a sinusoidal profile. We will show that drag reduction takes place notwithstanding the absence of material boundaries.

2 The viscoelastic turbulent Kolmogorov flow

To describe the dynamics of a dilute polymer solution we first consider the linear viscoelastic model (Oldroyd-B) [9]

$$\partial_t \mathbf{u} + (\mathbf{u} \cdot \nabla) \mathbf{u} = -\nabla p + \nu_0 \Delta \mathbf{u} + \frac{2\eta\nu_0}{\tau} \nabla \cdot \sigma + \mathbf{F} \quad (1)$$

$$\partial_t \sigma + (\mathbf{u} \cdot \nabla) \sigma = (\nabla \mathbf{u})^T \cdot \sigma + \sigma \cdot (\nabla \mathbf{u}) - 2 \frac{\sigma - \mathbf{1}}{\tau} + \kappa \Delta \sigma, \quad (2)$$

where σ is the conformation tensor of polymers $\sigma_{ij} = \langle R_i R_j \rangle / R_0^2$, being \mathbf{R} the end-to-end separation and R_0 the equilibrium gyration radius of the polymer molecule. The parameter τ is the (slowest) polymer relaxation time. $(\nabla \mathbf{u})_{ij} =$

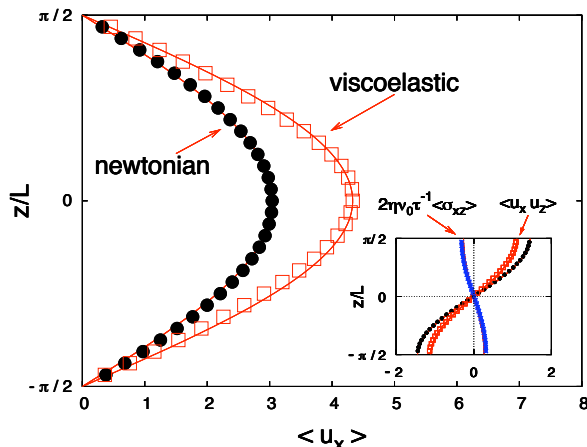


Figure 1: Mean velocity profiles for a Newtonian ($\eta = 0$) and a viscoelastic simulation ($\eta = 0.3$, $El = 0.019$) at given forcing amplitude $F = 1.5$. The measured profiles are undistinguishable from $\langle u_x \rangle = U \cos(z/L)$ (full lines) in both cases. The effect of elasticity is to increase the peak value U with respect to the Newtonian case: in the present case this corresponds to a reduction of the drag coefficient, defined in eq. (3), of about 40%. In the inset, the profiles of the Reynolds stress $\langle u_x u_z \rangle = S \sin(z/L)$ and the mean polymer stress $2\nu_0 \eta \tau^{-1} \langle \sigma_{xz} \rangle = -T \sin(z/L)$. In this case the Reynolds stress is reduced upon polymer addition to approximately 70% of its Newtonian value, consistently with experimental results at comparable drag reduction. The "missing" turbulent shear stress is compensated by the contribution of the polymer stress: the sum of S and T is equal to F in both the Newtonian and viscoelastic case. Data result from the numerical integration of eqs. (1) and (2) in a periodic cube of side 2π by means of a fully dealiased pseudospectral code with 64^3 collocation points. The mean flow lengthscale is $L = 1$ and the viscosity is $\nu = 0.015625$. Starting from an initial configuration with a small amount of energy on the smallest modes, after the system evolved into a statistically stationary state, time averages over 100 to 1000 eddy-turnover times have been performed to obtain the mean velocity profiles.

$\partial_i u_j$ and $\mathbf{1}$ is the unit tensor. The solvent viscosity is denoted by ν_0 and η is the zero-shear contribution of polymers to the total solution viscosity $\nu = \nu_0(1 + \eta)$. The diffusive term $\kappa \Delta \sigma$ is added to prevent numerical instabilities [10]. The forcing \mathbf{F} maintains the system in a statistically stationary state and has the form $F_x = F \cos(z/L)$, $F_y = F_z = 0$.

As shown in Fig. 1 the mean velocity profile measured in numerical experiments is $\langle u_x \rangle = U \cos(z/L)$, $\langle u_y \rangle = \langle u_z \rangle = 0$, where $\langle \dots \rangle$ denotes the time average. The drag coefficient is thus defined in terms of the centerline mean

velocity as

$$f = \frac{FL}{U^2}. \quad (3)$$

As shown in Fig. 2 the viscoelastic flow is characterized by drag reduction for several values of fluid parameters (for further details see Ref. [11])

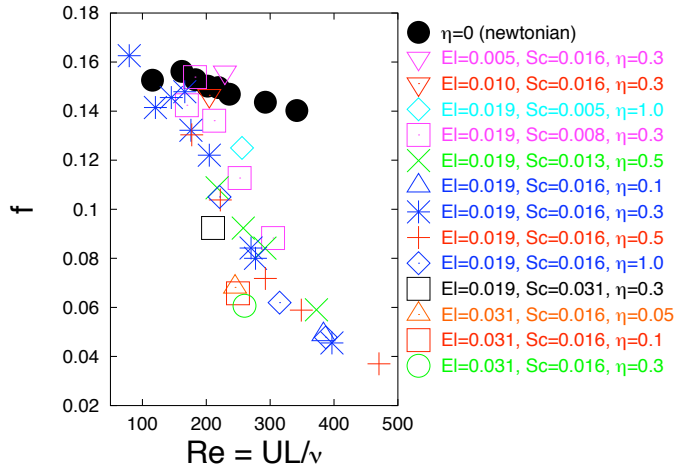


Figure 2: The drag coefficient for different viscoelastic fluid parameters.

3 The limit of strong polymer elongation

An even simpler model of viscoelastic flow is obtained by taking the limit of strong polymer elongation, or, equivalently, of vanishingly small equilibrium gyration radius [12]. In this case the governing equations take the following form:

$$\partial_t \mathbf{u} + (\mathbf{u} \cdot \nabla) \mathbf{u} = -\nabla p + \nu_0 \Delta \mathbf{u} + \frac{2\eta \nu_0}{\tau} \mathbf{R} \cdot \nabla \mathbf{R} + \mathbf{F} \quad (4)$$

$$\partial_t \mathbf{R} + (\mathbf{u} \cdot \nabla) \mathbf{R} = \mathbf{R} \cdot \nabla \mathbf{u} - \frac{\mathbf{R}}{\tau} + \kappa \Delta \mathbf{R} \quad (5)$$

where \mathbf{R} denotes the typical end-to-end separation of a polymer molecule.

In spite of the crude approximation, drag reduction is observed in this system as well, as shown in the table below. These results point to the conclusion that the basic mechanism for drag reduction does not depend neither on boundary conditions nor on the particular choice of the model.

τ	$\langle u_x'^2 \rangle$	$\langle u_y'^2 \rangle$	$\langle u_z'^2 \rangle$	U	DR[%]	f	\tilde{f}	$-\tau_R$	$-\tau_P$	ν_e	μ_e
0.1	4.01	3.21	3.56	3.57	0	0.16	0.1	2.0	0	0.57	0
1	4.01	3.1	3.74	3.64	3.8	0.15	0.1	2.0	0	0.55	0
2	3.78	2.72	3.32	3.61	2.2	0.15	0.12	1.97	0.06	0.55	0.02
4	4.16	2.11	2.27	4.04	28.1	0.12	0.16	1.80	0.22	0.45	0.05
5	4.25	1.81	1.98	4.25	29.4	0.11	0.19	1.72	0.3	0.40	0.07
10	5.89	1.41	1.36	5.31	54.8	0.07	0.21	1.5	0.54	0.28	0.10
∞	8.81	0.78	0.80	8.66	83	0.03	0.26	0.69	1.29	0.08	0.15

Table 1: Results from the integration of Eqs. (4) and (5) at $Sc = 100$ and $F = 2$. The columns are: the polymer relaxation time τ , the velocity variance in the three directions, the centerline mean velocity U , the drag reduction DR , the friction factor f , the ratio between energy input and velocity fluctuations $\tilde{f} = (FU/2)/u_{rms}^3$, the peak Reynolds stress $\tau_R = -\langle u_x u_z \rangle$, the peak polymer stress $\tau_P = 2\eta\nu\tau^{-1}\langle R_x R_z \rangle$, the eddy viscosity defined by $\tau_R = \nu_e \partial_z \langle u_x \rangle$, and the effective polymer viscosity defined by $\tau_P = \mu_e \partial_z \langle u_x \rangle$.

References

- [1] J. Lumley, *Annu. Rev. Fluid Mech.* **1**, 367 (1969).
- [2] P. S. Virk, *AICHE Journal* **21**, 625 (1975).
- [3] W. D. D. Mc Comb, *The physics of fluid turbulence*, Oxford University Press (1992).
- [4] R. H. Nadolink and W. W. Haigh, *ASME Appl. Mech. Rev.* **48**, 351 (1995).
- [5] K. R. Sreenivasan and C. M. White, *J. Fluid Mech.* **409**, 149 (2000).
- [6] R. Sureshkumar, A. N. Beris, and R. A. Handler, *Phys. Fluids* **9**, 743 (1997).
- [7] Ptasinski, P.K., Boersma, B.J., Nieuwstadt, F.T.M., Hulsen, M.A., van den Brule, B.H.A.A., and Hunt J.C.R. *J. Fluid Mech.* **490**, 251 (2003).
- [8] T., Min, J. Y. Yoo, H. Choi, and D. D. Joseph, *J. Fluid. Mech.* **486**, 213 (2003).
- [9] R. B. Bird, C. F. Curtiss, R. C. Armstrong, and O. Hassager, *Dynamics of polymeric fluids* Vol.2, Wiley, New York (1987).
- [10] R. Sureshkumar and A. N. Beris, *J. Non-Newtonian Fluid Mech.* **60**, 53 (1995).
- [11] G. Boffetta, A. Celani, and A. Mazzino, <http://arxiv.org/nlin.CD/0309036> (2003).
- [12] E. Balkovsky, A. Fouxon, and V. Lebedev, *Phys. Rev. E* **64**, 056301 (2001).

Bibliography

- [1] Larson R.-G., *Instabilities in viscoelastic flows*, Rheologica Acta, **31**, (1992), 213–263.
- [2] Shaqfeh E.-S.-G., *Fully elastic instabilities in viscometric flows*, Ann. Rev. of Fluid Mech., **28**, (1996), 129–185.
- [3] Groisman A., Steinberg V., *Elastic turbulence in a polymer solution flow*, Nature, **405**, (2000), 53.
- [4] Groisman A., Steinberg V., *Elastic turbulence in curvilinear flows of polymer solutions*, New J. Phys., **6**, (2004), 29.
- [5] Virk P.-S., *Drag reduction fundamentals*, AiChe J., **21 (4)**, (1975), 625.
- [6] Gyr A., Bewersdorff H.W. *Drag Reduction of Turbulent Flows by Additives*. Kluwer Academic Publishers, 1995.
- [7] Squire H.-B., *On the stability of three-dimensional disturbances of viscous flow between parallel walls*, Proc. R. Soc. London A, **142**, (1933), 621.
- [8] Herron I.-H., *The Orr-Sommerfeld Equations on Infinite Intervals*, SIAM Rev., **29**, (1987), 597–620.
- [9] Larson R.-G., Shaqfeh E.-S.-G., Muller S.-J., *A purely elastic instability in Taylor-Couette flow*, J. Fluid Mech., **218**, (1990), 573–600.
- [10] Groisman A., Steinberg V., *Elastic vs. inertial instability in a polymer solution flow*, Europhys. Lett., **43**, (1998), 165–170.
- [11] Pakdel P., McKinley G.-H., *Elastic instability and curved streamlines*, Phys. Rev. Lett., **77**, (1996), 2459–2462.

- [12] Bonn D., Meunier J., *Viscoelastic free-Boundary problems: non-Newtonian viscosity vs normal stress effects*, Phys. Rev. Lett., **79**, (1997), 2662–2665.
- [13] Groisman A., Steinberg V., *Efficient mixing at low Reynolds numbers using polymer additives*, Nature, **410**, (2001), 905.
- [14] Balkovsky E., Fouxon A., Lebedev V., *Turbulent dynamics of polymer solutions*, Phys. Rev. Lett., **84**, (2000), 4765.
- [15] Balkovsky E., Fouxon A., Lebedev V., *Turbulence of polymer solutions*, Phys. Rev. E, **64**, (2001), 056301.
- [16] Fouxon A., Lebedev V., *Spectra of turbulence in dilute polymer solutions*, Phys. Fluids, **15**, (2003), 2060–2072.
- [17] Lumley J.-J., *Drag reduction by additives*, Ann. Rev. Fluid Mech., **1**, (1969), 367–383.
- [18] Tabor M., de Gennes P.-G., *A cascade theory of drag reduction*, Europhys. Lett., **2**, (1986), 519.
- [19] Dubief Y., Terrapon V.-E., White C.-M., Shaqfeh E.-S.-G., Moin P., Lele S.-K., *New answers on the interaction between polymers and vortices in turbulent flows*, Flow, Turbulence and Combustion, **74**, (2005), 311–329.
- [20] Dimitropoulos C.-D., Dubief Y., Shaqfeh E.-S.-G., Moin P., Lele S.-K., *Direct numerical simulation of polymer-induced drag reduction in turbulent boundary layer flow*, Phys. of Fluids, **17**, (2005), 011705.
- [21] De Angelis E., Casciola C.-M., L'vov V.-S., Piva R., Procaccia I., *Drag reduction by polymers in turbulent channel flows: Energy redistribution between invariant empirical modes*, Phys. Rev. E, **67**, (2003), 056312.
- [22] L'vov V.-S., Pomyalov A., Procaccia I., Tiberkevich V., *Drag reduction by polymers in wall bounded turbulence*, Phys. Rev. Lett., **92**, (2004), 244503.
- [23] Benzi R., L'vov V.-S., Procaccia I., Tiberkevich V., *Saturation of turbulent drag reduction in dilute polymer solutions*, Europhys. Lett., **68**, (2004), 825–831.

- [24] Chertkov M., *Polymer stretching by turbulence*, Phys. Rev. Lett., **84**, (2000), 4761.
- [25] Vaithianathan T., Collins L.-R., *Numerical approach to simulating turbulent flow of a viscoelastic polymer solution*, J. Comp. Phys., **187**, (2003), 1–21.
- [26] Sureshkumar R., Beris A.-N., *Effect of artificial stress diffusivity on the stability of numerical calculations and the flow dynamics of time-dependent viscoelastic flows*, J. Non-Newtonian Fluid Mech., **60**, (1995), 53–80.
- [27] Bonn D., Amarouchene Y., Wagner C., Douady S., Cadot O., *Turbulent drag reduction by polymers*, J. Phys.: Condens. Matter, **17**, (2005), S1195–S1202.
- [28] Jovanović J., Pashtrapanska M., Frohnapfel B., Durst F., Koskinen J., Koskinen K., *On the Mechanism Responsible for Turbulent Drag Reduction by Dilute Addition of High Polymers: Theory, Experiments, Simulations, and Predictions*, Journal of Fluids Engineering, **128**, (2006), 118.
- [29] Wagner C., Amarouchene Y., Doyle P., Bonn D., *Turbulent-drag reduction of polyelectrolyte solutions: Relation with the elongational viscosity*, Europhysics Letters, **64**, (2003), 823–829.
- [30] Cadot O., Bonn D., Douady S., *Turbulent drag reduction in a closed flow system: Boundary layer versus bulk effects*, Physics of Fluids, **10**, (1998), 426.
- [31] Amarouchene Y., Kellay H., *Polymers in 2D turbulence: suppression of large scale fluctuations*, Phys. Rev. Lett., **89**, (2002), 104502.
- [32] Nadolink R.-H., Haigh W.-W., *Bibliography on skin friction reduction with polymers and other boundary-layer additives*, ASME Appl. Mech. Rev., **48**, (1997), 351–460.
- [33] Sreenivasan K.-R., White C.-M., *The onset of drag reduction by polymer additives, and the maximum drag reduction asymptote*, J. Fluid Mech., **409**, (2000), 149–164.

- [34] Larson R.-G. *The Structure and Rheology of Complex Fluids*. Oxford University Press, 1999.
- [35] Bird R.-B., Wiest J.-M., *Constitutive equations for polymeric liquids*, Annu. Rev. of Fluid Mech., **27**, (1995), 169–193.
- [36] Bird R.-B., Armstrong R.-C., Hassager O., Curtiss C.-F. *Dynamics of polymeric liquids*. John Wiley, 1987.
- [37] Oldroyd J.-G., *On the formulation of rheological equations of state*, Proc. R. Soc. London Ser. A, **200**, (1950), 523–541.
- [38] Oldroyd J.-G., *Non-Newtonian effects in steady motion of some idealized elastico-viscous fluids*, Proc. R. Soc. London Ser. A, **245**, (1958), 278–297.
- [39] Oldroyd J.-G., *An approach to non-Newtonian fluid mechanics*, J. Non-Newtonian Fluid Mech., **14**, (1964), 9–16.
- [40] Giesekus H., *A simple constitutive equation for polymer fluids based on the concept of deformation-dependent tensorial mobility*, J. Non-Newtonian Fluid Mech., **11**, (1982), 69–109.
- [41] Li Z., Khayat R.-E., *Three-dimensional thermal convection of viscoelastic fluids*, Phys. Rev. Lett., **71**, (2005), 066305.
- [42] Lange M., Eckhardt B., *Vortex pairs in viscoelastic Couette-Taylor flow*, Phys. Rev. E, **64**, (2001), 027301.
- [43] Min T., Yul Yoo J., Choi H., Joseph D.D., *Drag reduction by polymer additives in a turbulent channel flow*, Journal of Fluid Mechanics, **486**, (2003), 213–238.
- [44] Warner H.-R., *Kinetic theory and rheology of dilute suspensions of finitely extensible dumbbells*, Ind. Eng. Chem. Fundam., **11**, (1972), 379.
- [45] Peterlin A., *Hydrodynamics of macromolecules in a velocity field with longitudinal gradient*, J. Poly. Sci. B., Poly. Lett., **B4**, (1966), 287–291.
- [46] Arnold V.-I., Meshalkin L., *A. N. Kolmogorov's seminar on selected problems of analysis (1958-1959)*, Uspekhi Mat. Nauk., **15**, (1960), 247–250.

- [47] Meshalkin L., Sinai Y.-G., *Investigation of the stability of a stationary solution of a system of equations for the plane movement of an incompressible viscous fluid*, J. Appl. Math. Mech., **25**, (1961), 1700–1705.
- [48] Balmforth N.-J., Young Y.-N.-A.-N., *Stratified Kolmogorov flow*, Journal of Fluid Mechanics, **450**, (2002), 131–167.
- [49] Manfroi A., Young W., *Stability of β -plane Kolmogorov flow*, Physica D, **162**, (2002), 208–232.
- [50] Balmforth N.-J., Young Y.-N., *Stratified Kolmogorov flow. Part 2*, Journal of Fluid Mechanics, **528**, (2005), 23–42.
- [51] Bensoussan A., Lions J.-L., Papanicolau G. *Asymptotic analysis for periodic structures*. North Holland, 1978.
- [52] Nepomnyashchy A.-A., *On the stability of the secondary flow of a viscous fluid in an infinite domain*, Appl. Math. Mech., **40**, (1976), 886–891.
- [53] Golub G., Van Loan C.-V. *Matrix computation*. The Johns Hopkins University Press, Baltimore, 1996.
- [54] Sivashinsky G.-I., *Weak turbulence in periodic flows*, Physica D, **17**, (1985), 243–255.
- [55] She Z.-S., *Metastability and vortex pairing in the Kolmogorov flow*, Phys. Lett., **124**, (1987), 161–164.
- [56] Cahn J.-W., Hilliard J.-E., *Free energy of a non uniform system*, J. Chem. Phys., **28**, (1958), 258.
- [57] Bray A.-J., *Theory of phase-ordering kinetics*, Adv. in Phys., **51**, (2002), 481–587.
- [58] Manfroi A., Young W., *Slow evolution of zonal jets on the beta-plane*, J. Atmos. Science, **56**, (1999), 784–800.
- [59] Pedlosky J. *Geophysical fluid dynamics*. Springer, 2nd edition, 1987.
- [60] Watson S.-J., Otto F., Rubinstein B.-Y., Davis S.-H., *Coarsening dynamics of the convective Cahn-Hilliard equation*, Physica D, **178**, (2003), 127–148.

- [61] Boffetta G., Celani A., Mazzino A., *Drag reduction in the turbulent Kolmogorov flow*, Phys. Rev. E, **71**, (2005), 036307.
- [62] R. Sureshkumar, *Direct numerical simulation of the turbulent channel flow of a polymer solution*, Physics of Fluids, **9**, (1997), 743.
- [63] Borue V., Orszag S.-A., *Numerical study of three-dimensional Kolmogorov flow at high Reynolds numbers*, J. Fluid Mech., **306**, (1996), 293–324.
- [64] Ogilvie G.-I., Proctor M.-R.-E., *On the relation between viscoelastic and magnetohydrodynamic flows and their instabilities*, Journal of Fluid Mechanics, **476**, (2003), 389–409.

Abstract

Résumé

Cette thèse regroupe des travaux numériques et théoriques s'inscrivant dans le cadre général de la dynamique des polymères en écoulement. La première partie est dédiée à l'étude de la dynamique de molécules isolées dans des écoulements, situation d'intérêt pour la rhéologie et la biophysique. Le mouvement individuel d'une molécule a été analysé en détail grâce à des méthodes stochastiques et à de nouveaux algorithmes numériques. Ces études ont permis d'obtenir les distributions de probabilité de l'élongation et de l'orientation des molécules et de caractériser les temps dynamiques du système dans des écoulements laminaires et aléatoires.

La deuxième partie de la thèse porte sur les solutions diluées de polymères, qui jouent un rôle essentiel dans les applications industrielles et pour l'étude de la dynamique des fluides complexes en général. La stabilité de l'écoulement de Kolmogorov viscoélastique a été étudiée à l'aide d'une approche perturbative multi-échelles. On a ainsi montré que les polymères peuvent stabiliser l'écoulement mais aussi générer des instabilités purement élastiques. L'état turbulent correspondant a été analysé par des simulations numériques, qui mettent en évidence les différences entre les cas viscoélastique et newtonien.

Sinossi

Questa tesi contiene uno studio teorico e numerico della dinamica di polimeri in flussi. La prima parte è dedicata allo studio del moto di un singolo polimero in flussi esterni, argomento di interesse nella caratterizzazione delle proprietà meccaniche di biomolecole e in reologia. Il moto di una singola molecola e le quantità statistiche relative sono state analizzate in dettaglio grazie a metodi stocastici e a nuovi algoritmi numerici. Tali strumenti permettono di accedere alla distribuzione di probabilità della lunghezza e dell'orientamento della molecola e di studiare i tempi dinamici del problema in flussi laminari e aleatori.

Nella seconda parte della tesi affronterò il problema della dinamica di soluzioni diluite di polimeri, tematica di grande interesse per le sue applicazioni industriali nonché nello studio della meccanica di fluidi complessi in generale. Ho studiato la stabilità del flusso di Kolmogorov di una soluzione polimerica con metodi perturbativi a scale multiple. La presenza di polimeri può aumentare la stabilità, ma può dare anche luogo a instabilità di tipo puramente elastico. Ho analizzato il corrispondente regime turbolento per mezzo di simulazioni numeriche, che mettono in evidenza come tale stato sia differente dal caso newtoniano.

Abstract

This thesis encompasses numerical and theoretical work within the general framework of polymers in fluid flows. The first part concerns the study of single polymer dynamics and statistics, a subject of interest in the research on mechanical properties of biomolecules and in rheology. By means of stochastic methods and of new numerical algorithms the motion of a single molecule in an external flow has been analyzed in detail, and its statistics has been studied. In particular the probability distribution functions of extension and orientation of the molecule, as well as the dynamical timescales of the system, can be derived both in laminar and random flows.

The second part of the thesis refers to the dynamics of dilute polymer solutions which appears in technological and industrial applications as well as in complex fluid dynamics. The stability properties of a polymer solution in a Kolmogorov flow have been inferred by means of multiple-scale perturbation techniques. The presence of polymers results in a stabilization of the flow, but can also generate purely elastic instabilities. The corresponding turbulent dynamics is analyzed via direct numerical simulations, and the viscoelastic and the Newtonian cases are compared.